NANOSCALE COORDINATION POLYMERS FOR ANTICANCER DRUG DELIVERY

Rachel Huxford Phillips

A dissertation submitted to the faculty of the University of North Carolina at Chapel Hill in partial fulfillment of the requirements for the degree of Doctor of Philosophy in the Department of Chemistry.

Chapel Hill
2013

Approved by:

Dr. Wenbin Lin

Dr. Cynthia Schauer

Dr. Joseph Templeton

Dr. Wei You

Dr. Sohrab Habibi

ABSTRACT

RACHEL HUXFORD PHILLIPS: Nanoscale Coordination Polymers for Anticancer Drug Delivery
(Under the direction of Wenbin Lin)

This dissertation reports the synthesis and characterization of nanoscale coordination polymers (NCPs) for anticancer drug delivery. Nanoparticles have been explored in order to address the limitations of small molecule chemotherapeutics. NCPs have been investigated as drug delivery vehicles as they can exhibit the same beneficial properties as the bulk metal-organic frameworks as well as interesting characteristics that are unique to nanomaterials.

Gd-MTX (MTX = methotrexate) NCPs with a MTX loading of 71.6 wt% were synthesized and stabilized by encapsulation within a lipid bilayer containing anisamide (AA), a small molecule that targets sigma receptors which are overexpressed in many cancer tissues. Functionalization with AA allows for targeted delivery and controlled release to cancer cells, as shown by enhanced efficacy against leukemia cells. The NCPs were doped with $Ru(bpy)_3^{2+}$ (bpy = 2,2'-bipyridine), and this formulation was utilized as an optical imaging agent by confocal microscopy.

NCPs containing the chemotherapeutic pemetrexed (PMX) were synthesized using different binding metals. Zr-based materials could not be stabilized by encapsulation with a lipid bilayer, and Gd-based materials showed that PMX had degraded during synthesis. However, Hf-based NCPs containing 19.7 wt% PMX were stabilized by a lipid coating and

showed *in vitro* efficacy against non-small cell lung cancer (NSCLC) cell lines. Enhanced efficacy was observed for formulations containing AA.

Additionally, NCP formulations containing the cisplatin prodrug disuccinatocisplatin were prepared; one of these formulations could be stabilized by encapsulation within a lipid layer. Coating with a lipid layer doped with AA rendered this formulation an active targeting agent. The resulting formulation proved more potent than free cisplatin in NSCLC cell lines. Improved NCP uptake was demonstrated by confocal microscopy and competitive binding assays.

Finally, a Pt(IV) oxaliplatin prodrug was synthesized and incorporated in different NCPs using various binding metals. A moderate drug loading of 44.9 wt% was determined for Zr-based NCPs. This drug loading, along with a diameter less than 200 nm, make these particles promising candidates for further stabilization via lipid encapsulation.

ACKNOWLEDGEMENTS

First and foremost, I would like to thank my doctorate advisor, Dr. Wenbin Lin for supporting my research and providing me with invaluable insight and direction for my projects. Additionally, I thank the members of my dissertation committee, Dr. Cynthia Schauer, Dr. Joseph Templeton, Dr. Wei You, and Dr. Sohrab Habibi for their guidance and for considering my dissertation.

Many people have directly aided in the projects presented in this dissertation. Dr. Kathryn deKrafft helped tremendously in providing the foundation for the methotrexate project through nanoparticle synthesis, characterization, and stabilization attempts. Demin Liu contributed by synthesizing many of the materials needed for these projects, conducting powder X-ray diffraction and transmission electron microscopy imaging experiments, and providing helpful insight. Dr. Juan Vivero-Escoto helped in the magnetic resonance imaging of methotrexate- and pemetrexed-based materials as well as in iodine assays for poly(ethylene glycol) content. I also recognize the efforts of three undergraduates in the synthesis and characterization of nanomaterials: Will Boyle, Shane Russell, and Parth Majmudar. I would like to thank other members of the Lin Lab nanomedicine subgroup, past and present, for their experimental help and insightful conversations: Dr. Joseph Della Rocca, Stephanie Kramer, Kuangda Lu, and Chris Poon. Additionally, I owe many thanks to Joseph Falkowski, Marcela Wanderley, and Seth Barrett for their guidance and support.

Additionally, I thank those whom have helped in obtaining and interpreting data on instrumentation. This includes Amar Kumbhar, Carrie Donley, and Wallace Ambrose of the Chapel Hill Analytical and Nanofabrication Laboratory, Sohrab Habibi of the Department of Chemistry Mass Spectrometry Facility, and Robert Bagnell of the UNC Microscopy Service Laboratory.

Finally, this journey would not have been made possible if not for the endless support and guidance of my parents, Harry and Betty Huxford. My parents have aided in my every endeavor and I could not possibly show my gratitude enough. I also am thankful for the love and encouragement of my husband, Robert Phillips, who has been by my side for the entirety of my time at the University of North Carolina at Chapel Hill. I am truly looking forward to beginning our life together.

TABLE OF CONTENTS

LIST OF TABLES

Table

LIST OF FIGURES

Figure

LIST OF ABBREVIATIONS AND SYMBOLS

°	degrees
@	denotes one component inside of another
$\alpha_v\beta_3$	an integrin that is overexpressed in some cancer tissues
μ	micro-
θ	angle
ζ	zeta
Å	angstroms
A549	human non-small cell lung carcinoma cell line
AA	anisamide
ALL	acute lymphoblastic leukemia
aq.	aqueous
As	arsenic
Bodipy	boron dipyrromethane
bpy	2,2'-bipyridine
BSA	bovine serum albumin
CCRF-CEM	human acute lymphoblastic leukemia cell line
$CDCl_3$	deuterated chloroform
Co	cobalt
Cr	chromium
c(RGDfk)	small cyclic peptide known to target the $\alpha_v\beta_3$ integrin
DACH	R,R-diaminocyclohexane
DIC	differential interference contrast
DLS	dynamic light scattering

DMF	N,N-dimethylformamide
DMSO	dimethylsulfoxide
DNA	deoxyribonucleic acid
DOPA	1,2-dioleoyl-*sn*-glycero-3-phosphate
DOPC	1,2-dioleoyl-*sn*-glycero-3-phosphocholine
DOPE	L-α-phosphatidylethanolamine, dioleoyl
DOTAP	1,2-dioleoyl-3-trimethylammonium propane
DSCP	disuccinatocisplatin
DSOX	disuccinato oxaliplatin
DSPE-Peg	1,2-distearoyl-*sn*-glycero-3-phosphoethanolamine-N-(polyethylene glycol)
DSTAP	1,2-stearoyl-3-trimethylammonium propane
EDS	energy dispersive X-ray spectroscopy
EPR	enhanced permeability and retention
eq.	equivalents
ESCP	ethoxysuccinatocisplatin
Et_2O	diethylether
EtOH	ethanol
FBS	fetal bovine serum
FDA	Food and Drug Administration
Fe	iron
FITC	fluorescein isothiocyanate
g	grams
Gd	gadolinium
h	hours
HeLa	human cervical adenocarcinoma cell line

Hf	hafnium
HPLC	high performance liquid chromatography
HT-29	human colorectal adenocarcinoma cell line
IC_{50}	inhibitory concentration 50%
ICP-MS	inductively-coupled plasma mass spectrometry
IR	infrared
Jurkat	human acute lymphoblastic leukemia cell line
K_{sp}	solubility product
L	liters
La	lanthanum
m	milli-
M	molar
MeOH	methanol
MIL	Materials of Institut Lavoisier
min	minutes
Mn	manganese
MOF	metal-organic framework
mol	moles
MR	magnetic resonance
MRI	magnetic resonance imaging
MTX	methotrexate
n	nano-
NCI-H460	human non-small cell lung carcinoma cell line
NCP	nanoscale coordination polymer
NCP-1	terbium disuccinatocisplatin nanoscale coordination polymer

Ni	nickel
NMOF	nanoscale metal-organic framework
NMR	nuclear magnetic resonance
NSCLC	non-small cell lung cancer
OEt	ethoxy
PBS	phosphate buffered saline
PDI	polydispersity index
PEG	poly(ethylene glycol)
PMX	pemetrexed
Pr	praseodymium
Pt	platinum
PVP	polyvinylpyrrolidone
PXRD	powder x-ray diffraction
r_1	longitudinal relaxivity
r_2	transverse relaxivity
Ru	ruthenium
SBF	simulated body fluid
SEM	scanning electron microscopy
Suc	succinate
$t_{1/2}$	half-life
T_1	longitudinal relaxation time
T_2	transverse relaxation time
Tb	terbium
TEA	triethylamine
TEM	transmission electron microscopy

TEOS	tetraethyl orthosilicate
TGA	thermogravimetric anaylsis
THF	tetrahydrofuran
UV	ultraviolet
vis	visible
W	water to surfactant molar ratio
wt	weight
Zn	zinc
Zr	zirconium

CHAPTER 1

An Overview of Anticancer Chemotherapy with Nanoscale Coordination Polymers

(Portions of this chapter were adapted with permission from Huxford, R.C.; Della Rocca, J.; Lin, W. *Curr. Opin. Chem. Biol.* **2010**, *14*, 262. Copyright 2010 Elsevier)

1.1. Introduction

Despite remarkable progress in the fundamental biology behind many diseases, we have yet to achieve comparable advances in the treatment of these diseases, particularly cancer. Current therapeutics, small molecule drugs, are limited by their nonspecific distribution throughout the body and rapid clearance, resulting in poor pharmacokinetics, high doses, high side effects, and narrow therapeutic windows.[1,2] In the effort to alleviate these drawbacks of small molecule chemotherapeutics, nanoparticle-based therapeutics have received an increasing amount of attention over the past 25 years. These novel systems are typically composed of an active agent (e.g., chemotherapy drug or prodrug) incorporated within the nanoparticle carrier. A variety of nanocarriers have been designed for this purpose, such as polymeric nanoparticles, micelles, liposomes, iron oxide, and gold.[3,4] Nanomaterials display several beneficial characteristics that make them adept at drug delivery such as small size, high drug loadings, surface functionality, favorable drug release kinetics and pharamacokinetics, and intrinsic biocompatibility.[5-9] Nanoparticles are unique as they take advantage of the enhanced permeability and retention (EPR) effect (Figure 1.1).[1] This effect arises from the ability of small particles to permeate through the leaky vasculature of tumor tissue and be retained due to poor lymphatic drainage present in the tumor. The EPR effect is

considered a mode of passive targeting as nanoparticles are too large to enter the highly ordered vasculature of normal, healthy tissue. Thus, nanoparticles, if remaining in circulation long enough, eventually will accumulate in the tumor region.

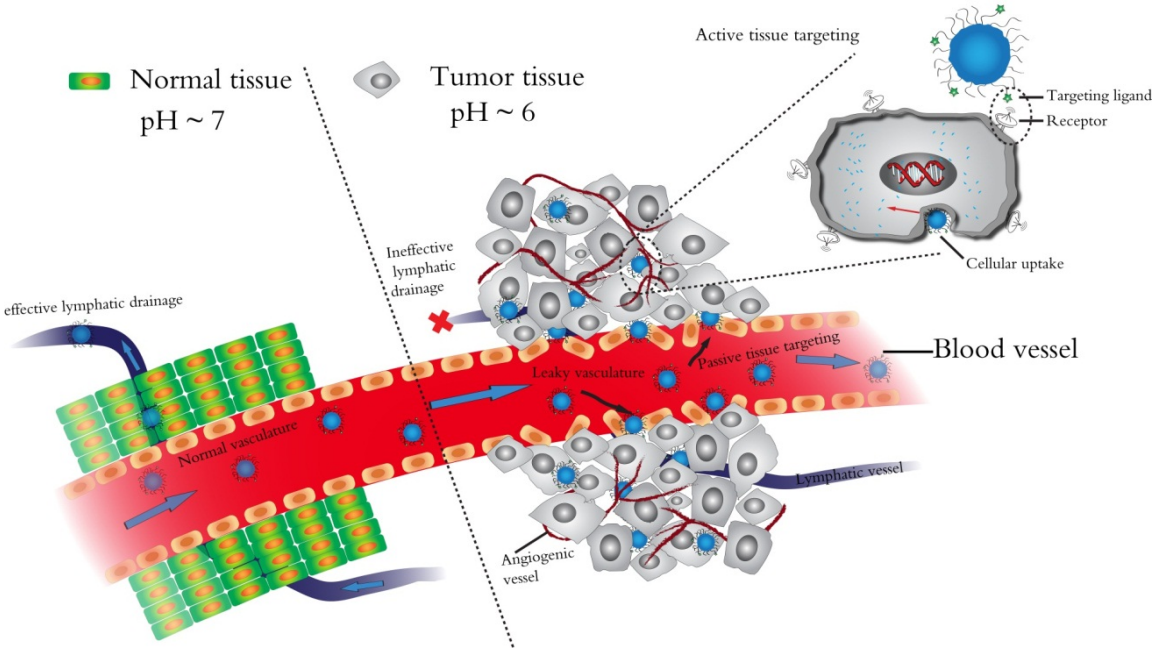

Figure 1.1. Illustration of the EPR effect in which nanoparticles are too large to penetrate the ordered vasculature of normal tissue but can permeate through the leaky vasculature of diseased tissue and are retained there due to poor lymphatic drainage. Courtesy of Demin Liu.

Additionally, nanoparticles can be actively targeted to diseased tissues (e.g., tumor regions) by conjugation with targeting ligands and can be engineered to contain multiple agents (e.g., imaging and therapeutic agents for both imaging and therapy), both of which are much more difficult to achieve with conventional therapeutics. The clinical success of nanoparticle therapies such as Abraxane and Doxil illustrates the power of this approach. A large number of promising nanoparticle-drug conjugates are currently in different stages of clinical development.[1,3,4]

Metal-organic frameworks (MOFs) are a new class of highly tunable hybrid materials crafted from metal-connecting points and organic polydentate ligands.[10] They are typically synthesized under mild conditions via coordination-directed self-assembly processes (Figure 1.2), and are also called coordination polymers or coordination networks.[11-15] Known for their large porosities with tunable pore sizes, shapes, and functionalities, MOFs are well studied among the scientific community for many applications such as nonlinear optics, gas storage, catalysis, chemical sensing, and separations.[10,11,14-21] MOFs exhibit many desirable characteristics as drug carriers, including exceptionally high surface areas and large pore sizes for drug encapsulation, intrinsic biodegradability as a result of relatively labile metal-ligand bonds, and versatile functionality for post-synthetic grafting of drug molecules.

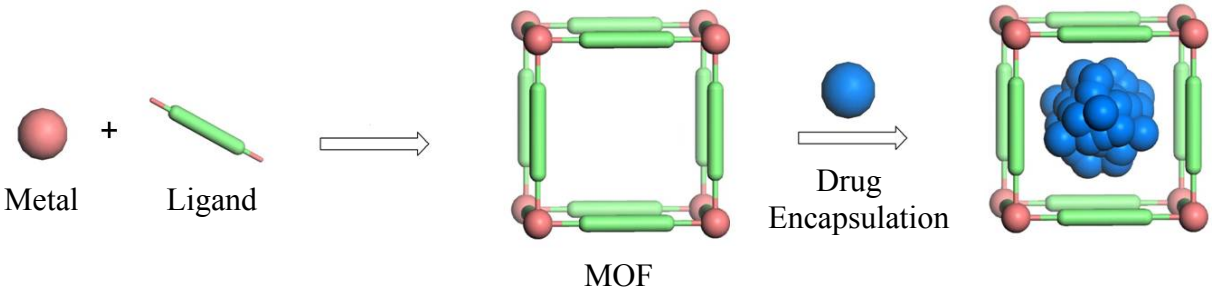

Figure 1.2. Formation of MOFs by coordination-directed self-assembly processes and the loading of drugs into MOFs via physical encapsulation. Only one unit of an infinite MOF framework is shown for clarity.

Recently, MOFs have been investigated for applications in loading and release of several drug molecules. When scaled down to the nano-regime to form nanoscale metal-organic frameworks (NMOFs), or nanoscale coordination polymers (NCPs), these materials exhibit the same beneficial properties as their bulk counterparts but also possess interesting characteristics that are unique to nanomaterials. NCPs can be formed from a number of self-assembly processes, each of which is illustrated in Figure 1.3.[22-24] The most straightforward

of these methods is a solvothermal synthesis in which the metal and ligand molecules are heated in a solvent, which can lead to amorphous or crystalline products. NCPs can also be synthesized in reverse (water-in-oil) microemulsions in which the reactants are suspended in surfactant-stabilized aqueous droplets in an organic phase. These droplets behave as nanoreactors, facilitating the assembly of the NCP material. This strategy can also be utilized in a surfactant-templated heating method in which a reverse microemulsion is heated to facilitate the reaction. Finally, NCPs can be formed via rapid precipitation, in which a solution of reactants is precipitated with a solvent, usually resulting in the formation of amorphous particles.

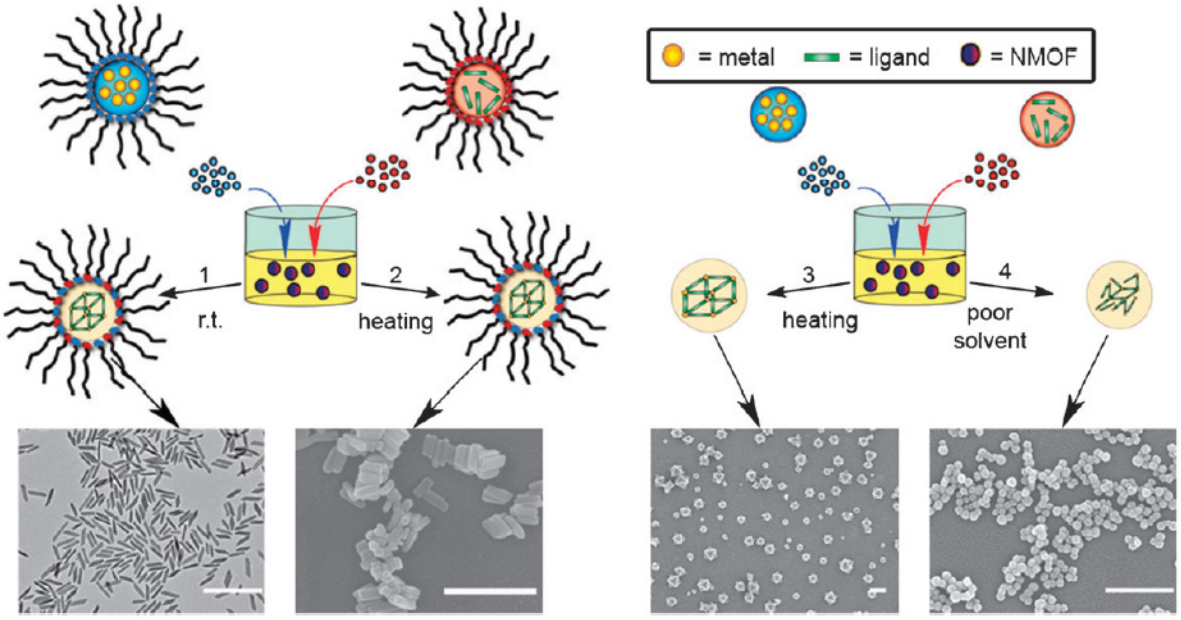

Figure 1.3. Synthetic techniques for NCPs. (1) Reverse microemulsion, (2) Surfactant-templated synthesis, (3) solvothermal synthesis, (4) rapid precipitation.

NCPs are potential nanovectors for delivering therapeutic agents to targeted areas of the body, as drug release can be controlled with their large surface areas, high porosities, and

presence of functional groups to interact with loaded moieties. Our group has recently reported NCPs as important delivery vehicles for contrast enhancement agents for magnetic resonance imaging, computed tomography, and optical imaging;[25-31] however, this chapter will focus on applications of MOFs and NCPs as potential drug delivery vehicles. Although their drug delivery applications are still in their infancy, NCPs exhibit many desired characteristics as nanocarriers. Intrinsic tunability and biodegradability, as well as exceptionally high drug loading capacity, of this emerging class of hybrid nanomaterials should make these systems promising candidates for further development as nanotherapeutics.

1.2. Proof of Concept: Drug Release from MOFs

In developing MOFs for drug delivery, the goal is to design carriers that possess minimal toxicity in the body; biocompatibility of both the metal and bridging ligand must be considered. While chromium and other metals are highly toxic, some metals exist in appreciable amounts in the body. For example, iron is a component of hemoglobin and has a concentration of approximately 22 μM in blood plasma. Tissues also contain various metals, such as copper (68 μM), manganese (180 μM), nickel (2 μM), and zinc (180 μM).[32] Since this is an emerging class of drug carriers, there are very limited data on the biological fate of NCP platforms. Iron oxide nanoparticles are clinically approved as MRI contrast agents, and *in vitro* assays have shown that these particles are not cytotoxic.[33]

The first group of MOFs to be investigated as a potential drug delivery system is the MIL (Materials of Institut Lavoisier) family, pioneered by Férey and co-workers.[34] This investigation occurred as the Lin group first explored the applications of NCPs as potential

MRI contrast agents.[26] The MIL family of MOFs is crafted from trivalent metal centers and carboxylic acid bridging ligands and holds great promise in drug delivery for their attractive characteristics: large pores (25-34 Å), outstanding surface areas (3100-5900 m^2/g), and the ability to incorporate functional groups into the framework.

Férey and co-workers studied the storage and release of Ibuprofen with chromium-based MIL-101 (Figure 1.4) and MIL-100.[35] Both materials showed high Ibuprofen loadings, with 0.347 g Ibuprofen/g MOF for MIL-100 and 1.376 g Ibuprofen/g MOF for MIL-101. The drastic difference in drug loading between the two materials is attributed to the pore sizes of the materials; MIL-101 has larger pore volumes of 12700 and 20600 Å (8200 and 12700 Å for MIL-100). The kinetics of Ibuprofen release was investigated by suspending the Ibuprofen-loaded materials in simulated body fluid (SBF) at 37 °C. There is an initial release of weakly-bound drug molecules within the first 2 h for MIL-100, and the entire cargo is released within 3 days. For MIL-101, steady release is observed for the first 8 h, with complete release after 6 days. These MOFs contain toxic chromium, and thus, the use of these materials for drug delivery is limited. A less toxic analog, MIL-101(Fe) has been developed as a biocompatible alternative.[36]

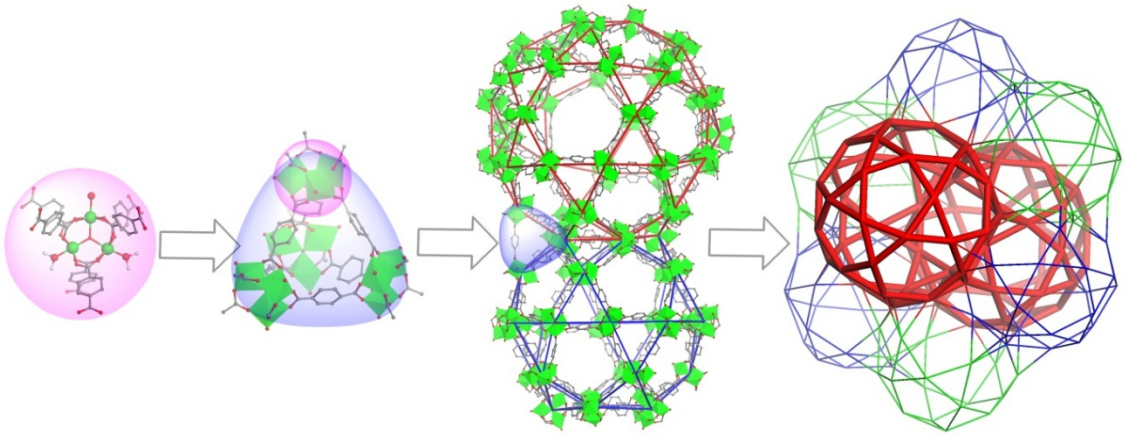

Figure 1.4. The structure of MIL-101. The tetrahedra are assembled from trivalent metal centers (Cr or Fe) and 1,4-benzenedicarboxylate. MIL-101 possesses larger pores than MIL-100, which facilitates Ibuprofen loading.

The Férey group has also reported controlled drug release for MIL-53, a more flexible MOF in the MIL family.[37] Both MIL-53(Cr) and the less toxic MIL-53(Fe) achieved loadings of 0.220 g Ibuprofen/g MOF and 0.210 g Ibuprofen/g MOF, respectively. The delivery kinetics were investigated in SBF at 37 °C; complete drug delivery occurred in 3 weeks, a long release time attributed to the flexibility of the MIL-53 framework and strong drug-framework interactions. This prolonged drug release gives MIL-53 the potential of being used for sustained release and drug delivery. The drug loadings achievable with the MIL family are much higher than any material previously studied for drug encapsulation (through non-covalent interactions). Given the ability to construct highly porous MOFs with tunable hydrophobicity from practically any metal center, the possibilities are unlimited.

MOFs with hydrophobic pores such as the MIL family are ideal for encapsulating drug molecules that possess poor aqueous solubility. MOFs can also be designed to have hydrophilic pores that can carry either positive or negative charges, and such MOFs can be

used to encapsulate drugs that contain opposing charges to the MOFs. Rosi and co-workers recently developed an anionic MOF composed of Zn(II) ions, adenine, and *para*-biphenyldicarboxylic acid that can be cationically-triggered to release its cargo.[38] The MOF is anionic, so its use for storage and release of cationic drugs via exchange with cations in biological fluid was investigated. The MOF was loaded with 0.22g/g of hydrochloride salt of procainamide, an antiarrythmia drug. Procainamide therapy is currently limited by its rapid clearance from the body, requiring dosing every 3 to 4 h. The drug release behavior of the MOF was monitored by HPLC; complete release was observed at 72 h in phosphate buffered saline (PBS). In contrast, the drug-loaded MOF was also dialyzed against pure water, with only 20% of the drug released, suggesting that the majority of procainamide is released by the cations present in PBS. In addition, the authors demonstrated that the framework remained intact under these conditions.

MOFs have also been studied as carriers for gaseous therapeutics which represent a significant challenge for drug delivery. Nitric oxide (NO) has several applications in therapy, including antibacterial, antithrombotic, and wound-healing applications.[39,40] The storage and release of nitric oxide (NO) in a MOF was investigated by Morris and co-workers.[41] Two MOFs were synthesized by a previously reported procedure,[42] from either cobalt or nickel and 2,5-dihydroxyterephthalic acid. These MOFs can absorb 7 times the amount of NO than any previously reported material on a per gram basis via ligation to coordinatively unsaturated metal centers, with little background release.[43] Figure 1.5 depicts the activation, loading, and release of NO by these MOFs.

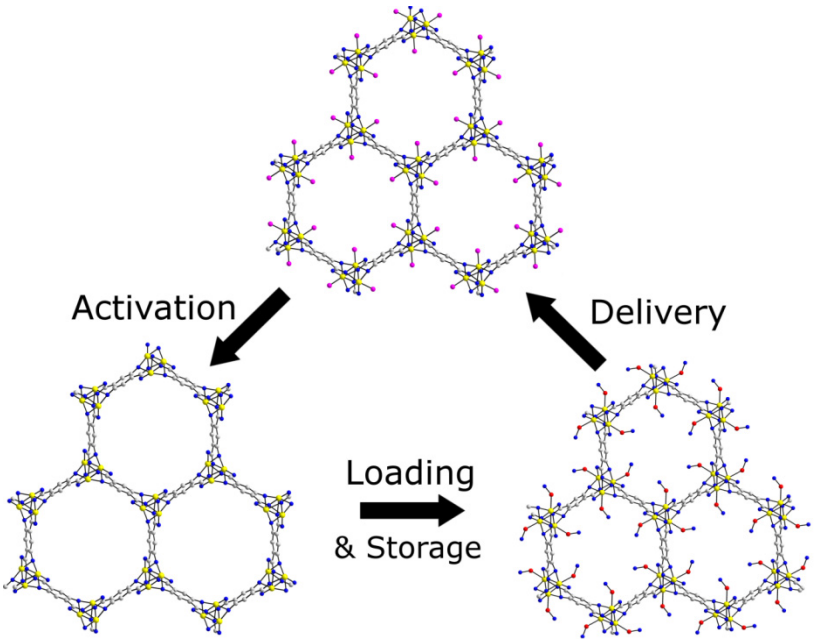

Figure 1.5. Absorption, storage, and release of nitric oxide (NO) in a Co or Ni MOF. Activation occurs by dehydration of the MOF at 110 °C, followed by NO loading at room temperature. Finally, delivery (release) of NO is triggered when the MOF was exposed to 11% relative humidity. (Pink spheres indicate water molecules, red and blue spheres indicate nitric oxide.)

The effect of the NO-loaded MOFs on precontracted pig coronary arteries was investigated; the MOFs resulted in more vessel relaxation than the NO-free control. While Ni and Co are too toxic to be used for biological applications, the work discussed thus far shows the ability of MOF materials to absorb and release large amounts of therapeutic cargo. The ability to deliver significant doses of NO is also relevant to cancer therapy since NO has shown anticancer activity in high concentrations, but shows tumorigenic properties at lower concentrations. The concentration at which this switch occurs is unknown.[44,45]

1.3. Drug Delivery with Nano-MOFs

While the systems discussed above illustrate the promise of MOFs as drug delivery vehicles, *in vivo* applications of the bulk MOFs are however limited because they are not suitable for systemic circulation due to their large sizes or toxicity. The bulk MOFs thus

need to be scaled down to the nano-regime so that the resulting NCPs can circulate systemically while maintain the advantageous properties of bulk MOFs for drug delivery. NCPs can improve the pharmacokinetic properties of the encapsulated drugs.[1,5,7]

Not only can small molecule agents be encapsulated within a MOF framework, the drug can also be incorporated within the framework directly as the bridging ligand. The Lin group was able to fabricate an NCP (designated as NCP-1) from Tb(III) ions and *c*,*c*,*t*-$[PtCl_2(NH_3)_2(O_2CCH_2CH_2CO_2H)_2]$ (disuccinatocisplatin, DSCP), a Pt(IV) cisplatin prodrug.[46] The NCP-1 nanoparticles were 58.3 ± 11.3 nm in diameter by dynamic light scattering (DLS), and were encapsulated with silica to enhance stability (half-life, $t_{1/2}$, of 9 h in HEPES buffer at 37°C, compared to 1 h for as-synthesized NCPs). Silica-coated NCP-1 particles were further functionalized with c(RGDfk), a cyclic peptide that targets the $\alpha_v\beta_3$ integrin, which is overexpressed in many epithelial cancers. The cytotoxicity of the nanoparticles was investigated against HT-29 human colon adenocarcinoma cells. These particles displayed a lower IC_{50} (Inhibitory Concentration, 50%) than that of free cisplatin (9.7 μM vs. 13.0 μM for cisplatin), while the untargeted particle did not exhibit significant cell death. The improved cytotoxicity of the c(RGDfk)-functionalized particles suggests that these particles are taken up by receptor-mediated endocytosis, followed by reduction to the active Pt(II) species by the reducing environment inside the cell (Figure 1.6). The ability to transform from a relatively nontoxic prodrug to a highly potent anticancer drug in such a delivery scheme is quite attractive since it facilitates selective delivery of anticancer drugs to cancerous cells, which can in turn lower the dose-limiting side effects that plague most anticancer chemotherapeutics.

Additionally, small molecule anticancer agents can be incorporated into a MOF framework by post-synthetic grafting of a prodrug into the framework. The Lin group reported loading and release of biomedical agents in nanoMIL-101(Fe).[47] This is the first report of the synthesis of an NCP and subsequent loading of a fluorophore and anticancer agent via post-synthetic modification (Figure 1.7). The NCP particles of MIL-101(Fe) were octahedral particles of about 200 nm in diameter with impressive porosity, a Langmuir surface area of 3700-4535 m^2/g. Amino-functionalized nanoMIL-101 was synthesized by incorporating 2-aminoterephthalic acid in the synthesis. A Bodipy fluorophore was grafted on the NCP through a covalent amine bond with up to 11 wt% loading. Confocal microscopy of the Bodipy-loaded particles with HT-29 cells showed fluorescent signal only with those cells incubated with the particles, indicating that the particles are able to permeate the cell membrane and release their fluorescent cargoes. Additionally, a Pt(IV) prodrug, *c*,*c*,*t*-$[PtCl_2(NH_3)_2(OEt)(O_2CCH_2CH_2CO_2H]$ (ethoxysuccinatocisplatin, ESCP) was grafted on amino-functionalized nanoMIL-101, with an overall drug loading of 12.8 wt%.

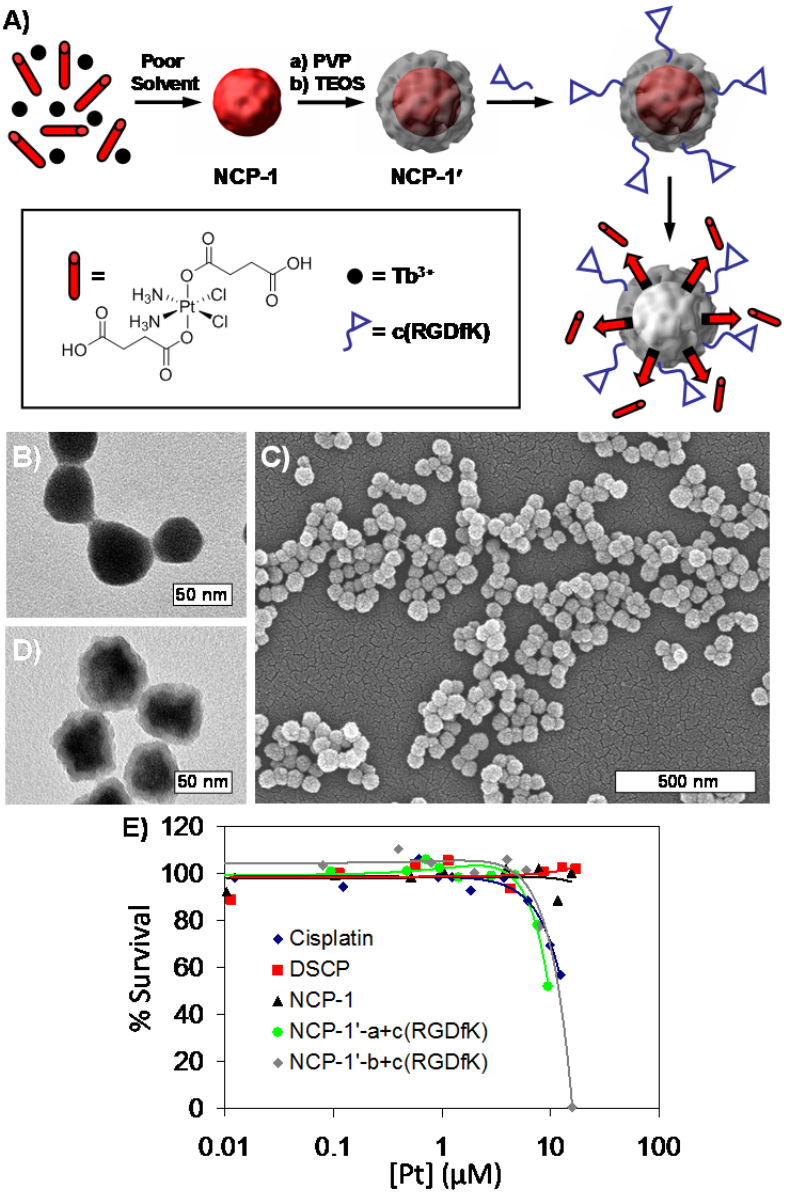

Figure 1.6. A) Schematic showing the synthesis of Tb-DSCP NCP (NCP-1) and its subsequent coating with a silica shell (NCP-1′) and conjugation with a cyclic peptide. (PVP = polyvinylpyrollidone, TEOS = tetraethylorthosilicate) B) TEM micrograph for as-synthesized NCP-1. C) TEM and D) SEM micrographs for NCP-1′. E) *In vitro* cytotoxicity assay curves for HT-29 cells obtained by plotting the % cell viability against the Pt concentration of various samples and free cisplatin control.

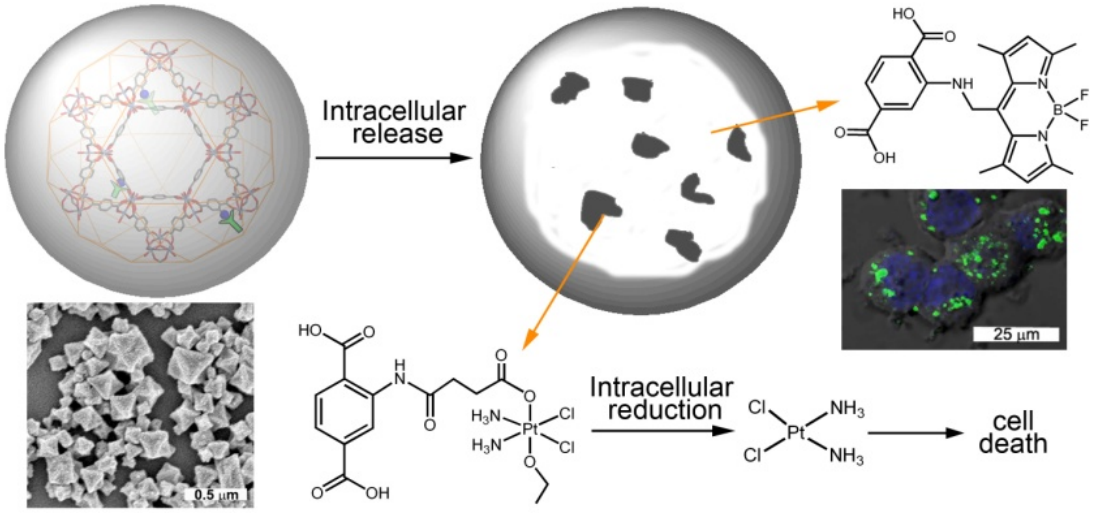

Figure 1.7. NanoMIL-101 can be loaded both with an optical imaging agent and a cisplatin prodrug. Simultaneous release of the fluorophore and cisplatin prodrug allows real-time monitoring of drug delivery by optical imaging.

The particles were coated with silica to enhance stability *in vitro*, giving a $t_{1/2}$ of 14 h in PBS at 37 °C, compared to 1.2 h for the uncoated particles. Silica-coated particles were grafted with the cyclic peptide c(RGDfk) and studies with the functionalized particles against HT-29 cells showed that the particles had comparable cytotoxicity to that of free cisplatin (IC_{50} = 21 µM for the particles, IC_{50} = 20 µM for cisplatin, IC_{50} = 29 µM for silica-coated, untargeted particles). Grafting of both an optical imaging agent and a cisplatin prodrug into the nanoMIL-101 system suggests the potential of using such a platform for theranostic (both diagnosis and therapy with a single nanoparticle) applications that allow real-time monitoring of therapeutic responses of an anticancer drug.

It is worth noting that several related inorganic nanoparticle systems have also been developed as potential anticancer therapeutics. O'Halloran and co-workers were able to improve efficacy of the leukemia agent, As_2O_3, by formation of insoluble metal-arsenate

complexes inside liposomes.[48,49] As_2O_3 is a potent therapy for leukemia, limited by its severe side effects and poor pharmacokinetics. Salts of nickel, cobalt, copper, and zinc were incorporated into liposomes, followed by loading of $As(OH)_3$ to form insoluble M(II) complexes of As_2O_3. Folate-targeted liposomes with Ni/As_2O_3 showed high cytotoxicity against HeLa cervical cancer cells with an IC_{50} of 1.8 ± 0.6 μM (IC_{50} = 4.3 ± 0.3 μM for free As_2O_3). Recently, O'Halloran and co-workers were able to co-encapsulate As_2O_3 and a cisplatin-like drug (acetate salt of diaqua-cisplatin) inside a liposome using the same strategy.[50] This formulation exhibited comparable cytotoxicity to As_2O_3 and diaqua-cisplatin alone, with several different cancer cell lines. Adair and coworkers were able to successfully encapsulate organic fluorophores and hydrophobic chemotherapeutics within calcium phosphate nanoparticles.[51,52] Calcium phosphate nanoparticles provide a pH-tunable way to deliver encapsulated molecules to targeted cells with minimal background release. Ceramide, an apoptosis inducer, was encapsulated into the nanoparticles during synthesis. Preliminary *in vitro* cell assays against breast cancer and melanoma cell lines revealed that the nanoparticle conjugate showed highly effective induction of apoptosis, while the nanoparticle carrier displayed little toxicity. Additionally, the Ceramide-containing calcium phosphate conjugate showed activity in resistant cell lines. Although these systems are not NCPs, they share some of the same design principles as NCP-based nanotherapeutics.

1.4. Conclusion

Significant progress has been made in adapting MOFs and NCPs for drug delivery. With these hybrid systems, a multitude of metal centers and organic building blocks can be pieced together and specifically tailored to form new materials with desirable characteristics as drug delivery vehicles. Since NCPs represent an infinitely tunable material platform, many

other drugs can be incorporated into them in a foreseeable future. The ability to carry both imaging and therapeutic agents in NCPs should greatly facilitate the efficacy studies of this promising class of nanotherapeutics. The future for MOFs and NCPs in drug delivery is bright, although many more improvements are needed before these materials can be considered for clinical applications.

1.5. References

(1) Davis, M. E.; Chen, Z.; Shin, D. M. *Nat. Rev. Drug Discov.* **2008**, *7*, 771.

(2) Dyson, P. J.; Sava, G. *Dalton Trans.* **2006**, 1929.

(3) Cho, K.; Wang, X.; Nie, S.; Chen, Z.; Shin, D. M. *Clin. Cancer Res.* **2008**, *15*, 1310.

(4) Peer, D.; Karp, J. M.; Hong, S.; Farokzhad, O. C.; Margalit, R.; Langer, R. *Nat. Nanotechnol.* **2007**, *2*, 751.

(5) Alexis, F.; Pridgen, E.; Molinar, L. K.; Farokzhad, O. C. *Mol. Pharm.* **2008**, *5*, 505.

(6) Ferrari, M. *Nat. Rev. Cancer* **2005**, *5*, 161.

(7) Li, S. D.; Huang, L. *Mol. Pharm.* **2008**, *5*, 496.

(8) Sanhai, W. R.; Sakamoto, J. H.; Canady, R.; Ferrari, M. *Nat. Nanotechnol.* **2008**, *3*, 242.

(9) Parveen, S.; Misra, R.; Sahoo, S. K. *Nanomedicine* **2012**, *8*, 147.

(10) Li, H.; Eddaoudi, M.; O'Keeffe, M.; Yaghi, O. M. *Nature* **1999**, *402*, 276.

(11) Evans, O. R.; Xiong, R.-G.; Wang, Z.; Wong, G. K.; Lin, W. *Angew. Chem. Int. Ed.* **1999**, *38*, 536

(12) Moulton, B.; Zaworotko, M. J. *J. Chem. Rev.* **2001**, *101*, 1629.

(13) Kitagawa, S.; Kitaura, R.; Noro, S.-I. *Angew. Chem. Int. Ed.* **2004**, *43*, 2334.

(14) Oh, M.; Mirkin, C. A. *Nature* **2005**, *438*, 651.

(15) Evans, O. R.; Lin, W. *Acc. Chem. Res.* **2002**, *35*, 511.

(16) Seo, J. S.; Whang, D.; Lee, H.; Jun, S. I.; Oh, J.; Jeon, Y. J.; Kim, K. *Nature* **2000**, *404*, 982.

(17) Ferey, G.; Latroche, M.; Serre, C.; Millange, F.; Loiseau, T.; Percheron-Guegan, A. *Chem. Commun.* **2003**, 2976.

(18) B, C.; Wang, L.; Xiao, Y.; Fronczek, F. R.; Xue, M.; Cui, Y.; Qian, G. *Angew. Chem. Int. Ed.* **2009**, *48*, 500.

(19) Lan, A.; Li, K.; Wu, H.; Olsson, D. H.; Emge, T. J.; Ki, W.; Hong, M.; Li, J. *Angew. Chem. Int. Ed.* **2009**, *48*, 2334.

(20) Lin, W.; Wang, L.; Ma, L. *J. Am. Chem. Soc.* **1999**, *121*, 11249.

(21) Park, K. H.; Jang, K.; Son, S. U.; Sweigart, D. A. *J. Am. Chem. Soc.* **2006**, *128*, 8740.

(22) Lin, W.; Rieter, W. J.; Taylor, K. M. L. *Angew. Chem. Int. Ed.* **2009**, *48*, 650.

(23) Della Rocca, J.; Liu, D.; Lin, W. *Acc. Chem. Res.* **2011**, *44*, 957.

(24) Taylor-Pashow, K. M. L.; Della Rocca, J.; Huxford, R. C.; Lin, W. *Chem. Commun.* **2010**, *46*, 5832.

(25) Rieter, W. J.; Taylor, K. M. L.; Lin, W. *J. Am. Chem. Soc.* **2007**, *129*, 9852.

(26) Rieter, W. J.; Taylor, K. M. L.; An, H.; Lin, W.; Lin, W. *J. Am. Chem. Soc.* **2006**, *128*, 9024.

(27) Taylor, K. M. L.; Jin, A.; Lin, W. *Angew. Chem. Int. Ed.* **2008**, *47*, 7722.

(28) Taylor, K. M. L.; Rieter, W. J.; Lin, W. *J. Am. Chem. Soc.* **2008**, *130*, 14358.

(29) deKrafft, K. E.; Xie, Z.; Cao, G.; Tran, S.; Ma, L.; Zhou, O. Z.; Lin, W. *Angew. Chem. Int. Ed.* **2009**, *48*, 9901.

(30) deKrafft, K. E.; Boyle, W. S.; Burk, L. M.; Zhou, O. Z.; Lin, W. *J. Mater. Chem.* **2012**, *22*, 18139.

(31) Liu, D.; Huxford, R. C.; Lin, W. *Angew. Chem. Int. Ed.* **2011**, *50*, 3696.

(32) Bertini, I.; Gray, H. B.; Stiefel, E. I.; Valentine, J. S. *Biological Inorganic Chemistry: Structure and Reactivity*; University Science Books: Sausalito, CA, 2007.

(33) Park, J.; Yu, M. K.; Jeong, Y. Y.; Kim, J. W.; Lee, K.; Phan, V. N.; Jon, S. *J. Mater. Chem.* **2009**, *19*, 6412.

(34) Ferey, G.; Mellot-Draznieks, C.; Serre, C.; Millange, F.; Dutour, J.; Surble, S.; Matgiolaki, I. *Science* **2005**, *309*, 2040.

(35) Horcajada, P.; Serre, C.; Vallet-Regi, M.; Sebban, M.; Taulelle, F.; Ferey, G. *Angew. Chem. Int. Ed.* **2006**, *309*, 5974.

(36) Bauer, S.; Serre, C.; Deciv, T.; Horcajada, P.; Morrot, J.; Ferey, G. *Inorg. Chem.* **2008**, *47*, 7568.

(37) Horcajada, P.; Serre, C.; Maurin, G.; Ramsahye, N. A.; Balas, F.; Vallet-Regi, M.; Sebban, M.; Tailelle, F.; Ferey, G. *J. Am. Chem. Soc.* **2008**, *130*, 6774.

(38) An, J.; Geib, S. J.; Rosi, N. L. *J. Am. Chem. Soc.* **2009**, *131*, 8376.

(39) Miller, A. R.; Megson, I. L. *Br. J. Pharmacol.* **2007**, *151*, 305.

(40) Zhu, H. F.; Ka, B.; Murad, F. *World J. Surg.* **2007**, *31*, 624.

(41) McKinlay, A. C.; Ziao, B.; Wragg, D. S.; Wheatley, P. S.; Megson, I. L.; Morris, R. E. *J. Am. Chem. Soc.* **2008**, *130*, 10440.

(42) Dietzel, P. D. C.; Morita, Y.; Blom, R.; Fjellvag, H. *Angew. Chem. Int. Ed.* **2005**, *44*, 6354.

(43) Wheatley, P. S.; Butler, A. R.; Crane, M. S.; Fox, S.; Xiao, B.; Rossi, A. G.; Megson, I. L.; Morris, R. E. *J. Am. Chem. Soc.* **2006**, *128*, 502.

(44) Sonveaux, P.; Jordan, B. F.; Gallez, B.; Feron, O. *Eur. J. Cancer* **2009**, *45*, 1352.

(45) Huerta, S.; Chilka, S.; Bonavida, B. *Int. J. Oncol* **2008**, *33*, 909.

(46) Rieter, W. J.; Pott, K. M.; Taylor, K. M. L.; Lin, W. *J. Am. Chem. Soc.* **2008**, *130*, 11584.

(47) Taylor-Pashow, K. M. L.; Della Rocca, J.; Xie, Z.; Tran, S.; Lin, W. *J. Am. Chem. Soc.* **2009**, *131*, 14261.

(48) H, C.; MacDonald, R. C.; Li, S.; Krett, N. L.; Rosen, S. T.; O'Halloran, T. V. *J. Am. Chem. Soc.* **2006**, *128*, 13348.

(49) H, C.; Ahn, R.; Van den Bossche, J.; Thompson, D. H.; O'Halloran, T. V. *Mol. Cancer. Ther.* **2009**, *8*, 1955.

(50) Chen, H.; Pazicni, S.; Krett, N. L.; Ahn, R. W.; Penner-Hahn, J. E.; Rossen, S. T.; O'Halloran, T. V. *Angew. Chem. Int. Ed.* **2009**, *48*, 9295.

(51) Kester, M.; Heakal, Y.; Fox, T.; Sharma, A.; Robertson, G. P.; Morgan, T. T.; Altinoglu, E. I.; Tabakovic, A.; Parette, M. R.; Rouse, S. M. *Nano Lett.* **2008**, *8*, 4116.

(52) Morgan, T. T.; Muddana, H. S.; Altinoglu, E. I.; Rouse, S. M.; Tabakovic, A.; Tabouillot, T.; Russin, T. J.; Shanmugavelandy, S. S.; Butler, P. J.; Eklund, P. C. *Nano Lett.* **2008**, *8*, 4108.

CHAPTER 2

Lipid-Coated Nanoscale Coordination Polymers for Targeted Delivery of Methotrexate

(Portions of this chapter were adapted with permission from Huxford, R.C.;† deKrafft, K.E.;† Boyle, W.S.; Liu, D.; Lin, W. *Chem. Sci.* **2012**, *3*, 198. †Contributed equally to this work.

2.1. Introduction

2.1.1. Conventional Cancer Chemotherapy - Methotrexate

Conventional cancer chemotherapy regimens consist of a single small molecule agent or a combination of agents. Despite the high efficacy of these therapies, current treatments are limited by nonspecific distribution throughout the body leading to high doses, rapid clearance, narrow therapeutic windows, poor pharmacokinetics, and high side effects.[1] One such chemotherapeutic agent is methotrexate (MTX), shown in Figure 2.1.

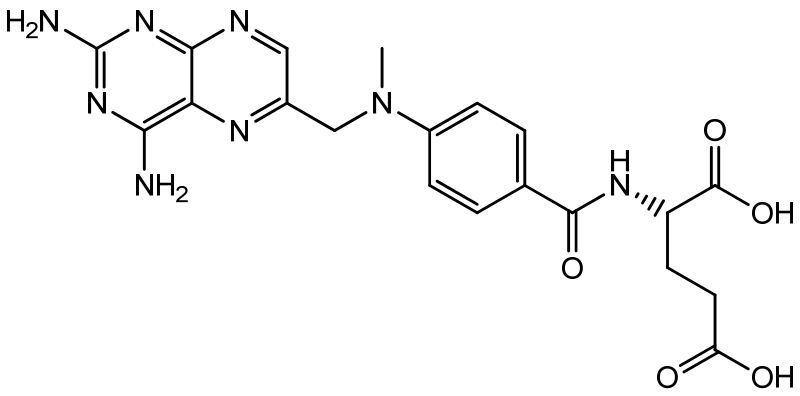

Figure 2.1. Structure of the antifolate methotrexate (MTX).

MTX belongs to a group of anticancer agents known as antifolates, small molecules

that are structurally similar to folic acid and can thus mimic this essential nutrient, causing havoc throughout the folic acid pathway. MTX works by inhibiting dehydrofolate reductase, thus preventing DNA synthesis and inducing apoptotic cell death. While MTX is quite efficacious and is the first-line treatment for acute lymphoblastic leukemia (ALL), this efficacy is compromised by the array of drawbacks associated with conventional small molecule chemotherapeutics.[2] Large doses of MTX are required as a result of its nonspecific distribution and rapid renal clearance, which often leads to systemic toxicity. Prolonged MTX treatment results in numerous side effects such as mucositis, hematological toxicity, and secondary cancer. In the attempt to alleviate the therapeutic drawbacks, a few MTX-containing nanoparticle systems (polymer conjugates and liposomes) have been developed; however, these vehicles contain relatively low drug loadings.[3-8] Thus, we hypothesized incorporation of MTX directly into an NCP framework by coordination of the two carboxylate groups of MTX to metal centers. This chapter highlights the use of NCPs to deliver the antifolate chemotherapeutic, MTX; very high loadings of MTX can be achieved in such formulations (up to 79.1 wt%). This chapter includes the synthesis and characterization of MTX-based NCPs, their stabilization and cancer targeting with a lipid bilayer, and *in vitro* efficacy against Jurkat ALL cells (Figure 2.2). A carboxylic acid derivative of the phosphor $Ru(bpy)_3^{2+}$ (bpy = 2,2'-bipyridine) was also incorporated into the NCPs to allow the monitoring of MTX uptake by cancer cells via confocal microscopy.

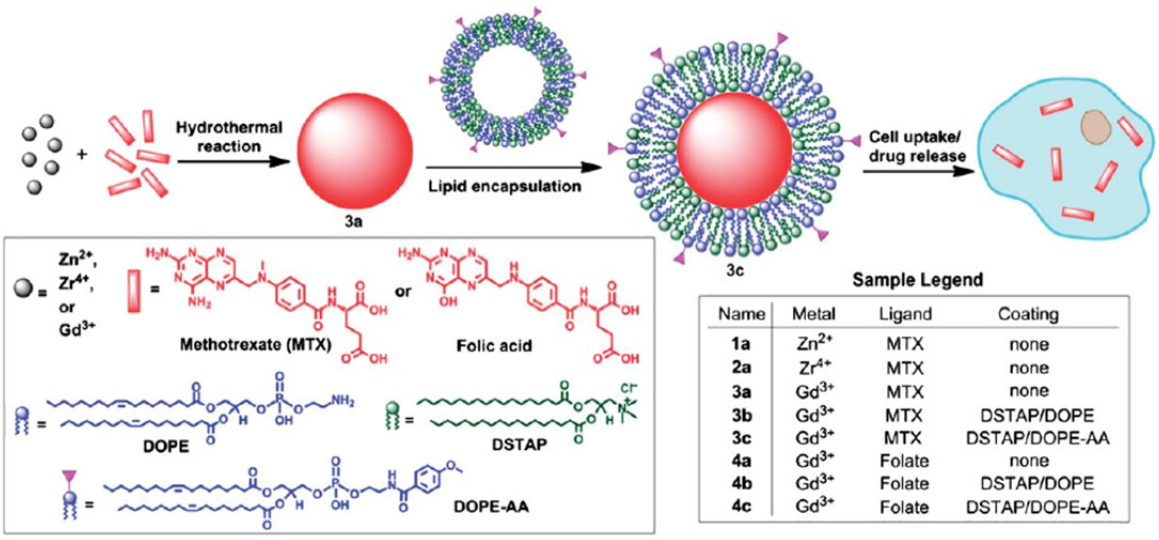

Name	Metal	Ligand	Coating
1a	Zn^{2+}	MTX	none
2a	Zr^{4+}	MTX	none
3a	Gd^{3+}	MTX	none
3b	Gd^{3+}	MTX	DSTAP/DOPE
3c	Gd^{3+}	MTX	DSTAP/DOPE-AA
4a	Gd^{3+}	Folate	none
4b	Gd^{3+}	Folate	DSTAP/DOPE
4c	Gd^{3+}	Folate	DSTAP/DOPE-AA

Figure 2.2. Schematic showing the solvothermal synthesis of MTX- and folate-containing NCPs, encapsulation with a lipid bilayer containing a targeting ligand, and cell uptake and release.

2.1.2. Previous Methotrexate-Based Nanoscale Coordination Polymers

Two generations of MTX-containing NCPs were reported previously and serve as the foundation for this work.[9] The first MTX-containing NCP, based on Zn(III) (Zn-MTX, Figure 2.3a and 2.3c), possessed a very high MTX loading by thermogravimetric analysis (TGA, 79.1 wt%, Figure 2.4), but were unstable in aqueous conditions due to the labile nature of the Zn-carboxylate bond. We hypothesized that Zr(IV) would build a more stable MTX-containing NCP due to the reported stability of the Zr-carboxylate bond in MOF frameworks.[10] Nanoparticles of Zr-MTX (78.2 wt% MTX by TGA, Figures 2.3b, 2.3d, and 2.5) were synthesized but could not be further stabilized ($t_{1/2}$ in PBS ~ 30 min) by coating with a biocompatible layer (silica or lipid coating). This instability can be explained by the high driving force of Zr(IV) to form phosphate salts ($Zr_3(PO_4)_4$, $k_{sp} = 10^{-134}$). The following work utilizes Gd(III) as the binding metal ($GdPO_4$, $k_{sp} = 10^{-23}$), stabilizes the resulting NCPs

by encapsulation in a lipid bilayer (liposome), and exhibits cytotoxicity and enhanced uptake in Jurkat ALL cells.

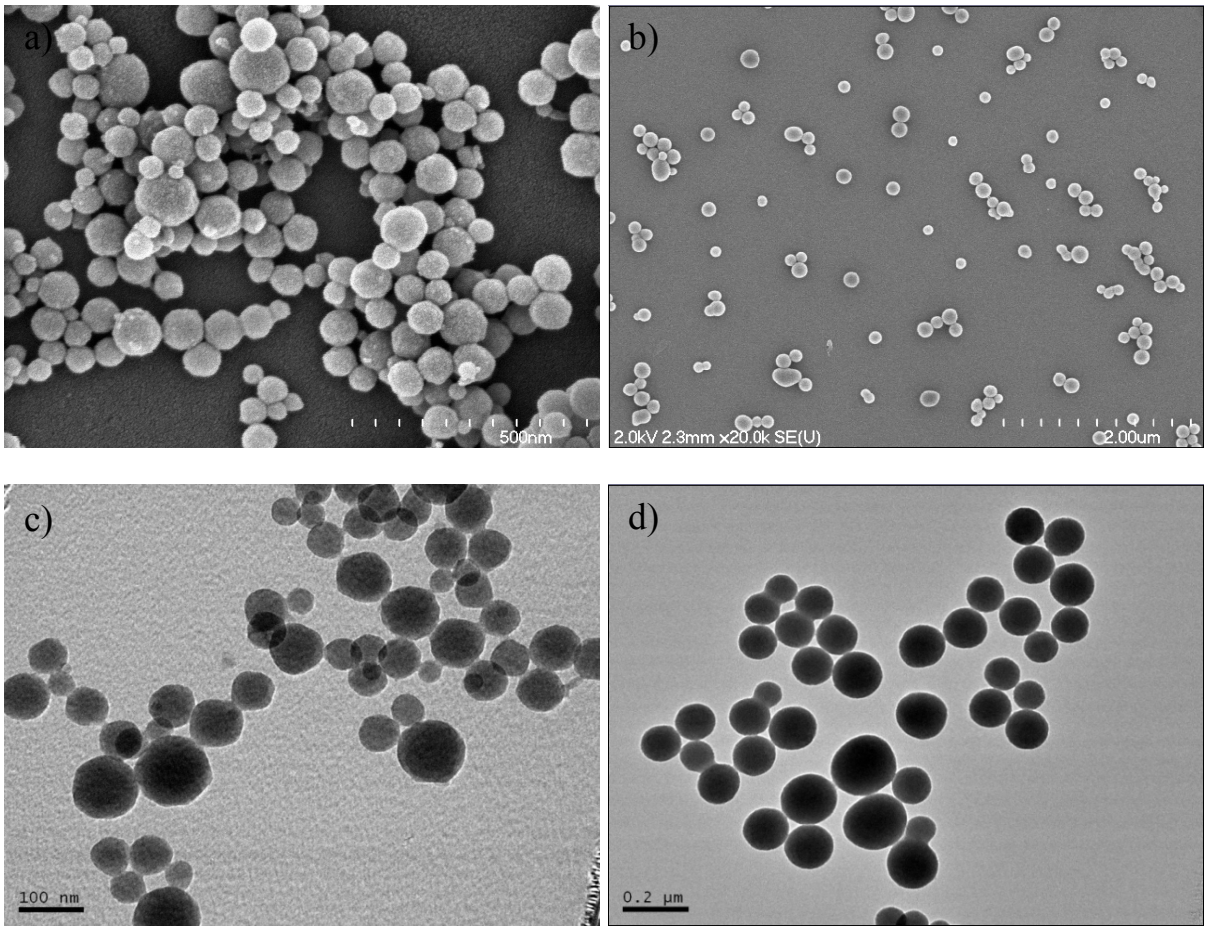

Figure 2.3. SEM micrographs of (a) Zn-MTX and (b) Zr-MTX. TEM micrographs of (c) Zn-MTX and (d) Zr-MTX.

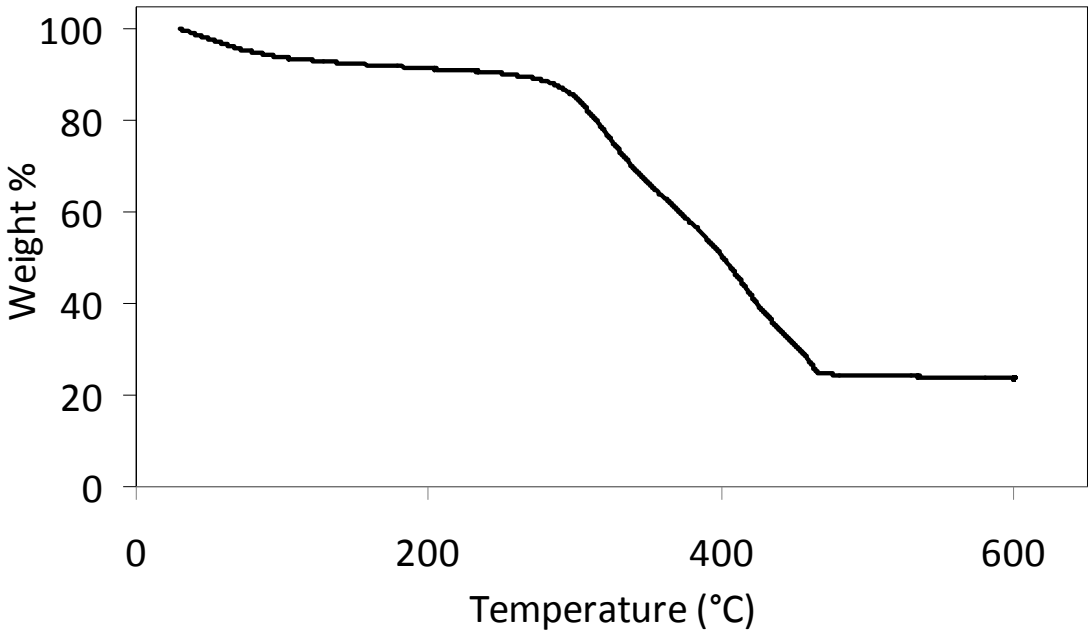

Figure 2.4. TGA plot of Zn-MTX, showing organic weight loss between 250 and 500 °C attributed to MTX (79.1 wt%).

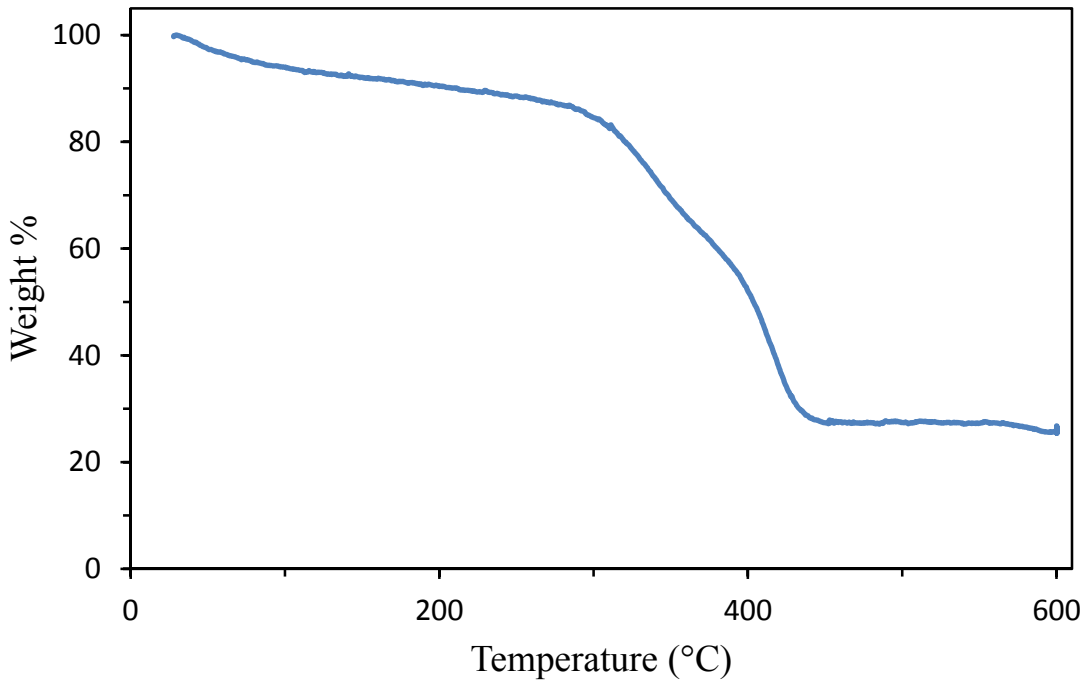

Figure 2.5. TGA plot of Zr-MTX, showing organic weight loss between 250 and 500 °C attributed to MTX (78.2 wt%).

2.1.3. Liposomes

Liposomes, bilayers of typically phospholipids, are known to stabilize nanomaterials.[11-14] The coating process presumably occurs via charge-charge interactions between oppositely-charged particles and liposomes.[15] Liposomes are formed by the self-assembly of lipids dispersed in aqueous solution, which forms liposomes that are multilamellar (containing concentric layers). The liposome diameter can be refined by development of multilamellar liposomes through an extruder to yield monodisperse liposomes containing one bilayer (unilamellar).[16] These liposomes can be mixed with an aqueous particle dispersion, and the liposomes rearrange to result in encapsulation of individual particles (Figure 2.6). The addition of a lipid bilayer to a particle surface can result in enhanced stability as liposomes are mostly impermeable to moieties such as salts and macromolecules, compounds known to rapidly degrade particles under biological conditions.[12,17,18]

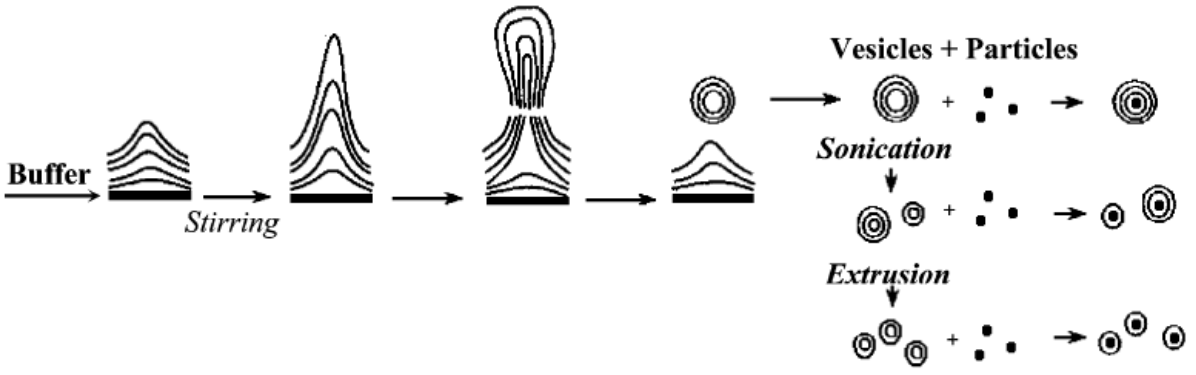

Figure 2.6. Illustration showing self-assembled liposome formation via hydration of a lipid film, followed by encapsulation of individual particles within lipid bilayers. Reproduced with permission from reference 15.

2.2. Results and Discussion

2.2.1. Lipid Coating of Zr-MTX NCP

Briefly, liposomes containing cationic lipids DOTAP (1,2-dioleoyl-3-trimethylammonium propane) or DSTAP/DOPE (DSTAP = 1,2-stearoyl-3-trimethylammonium propane, DOPE = L-α-phosphatidylethanolamine, dioleoyl) were prepared by reduction of lipids in chloroform to a lipid film, hydration in 1 mM aq. KCl, and extrusion through a series of polycarbonate filter membranes. For example, DOTAP liposomes with a Z average diameter of 51.9 nm, PDI of 0.105, and ζ potential of 68.3 mV were produced by this method (Figure 2.7).

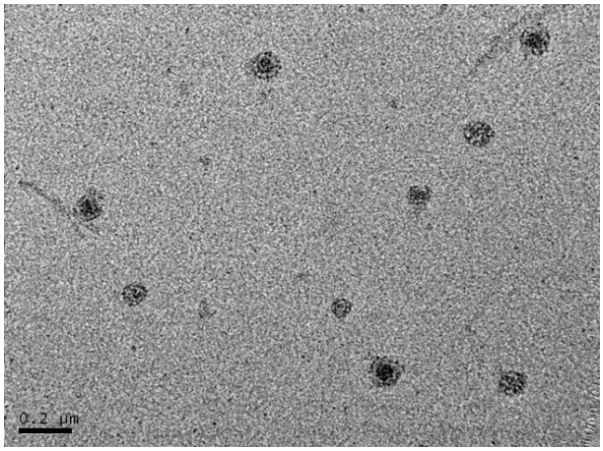

Figure 2.7. TEM micrograph of DOTAP liposomes using Pt(II) as a stain.

Several attempts were made to stabilize Zr-MTX by encapsulation within a lipid bilayer. Several formulations of liposomes were prepared (all molar ratios): 1:1 DOTAP/cholesterol, 5:62:33 DOTAP/DOPE/cholesterol, 100% DOTAP or DSTAP, and 1:1 DSTAP/DOPE. Lipid coatings using all of these formulations were evidenced by DLS size

and ζ potential plots, but encapsulation with a lipid bilayer did not result in stabilization of the Zr-MTX NCP. The following will illustrate an example: encapsulation of Zr-MTX with 1:1 (by mol) DOTAP/cholesterol liposomes. A dispersion of Zr-MTX in 1 mM aq. KCl was mixed with different amounts of 1:1 (by mol) DOTAP/cholesterol liposomes, resulting in different particle:liposome weight ratios. Monitoring the Z average diameter and ζ potential of the samples by DLS (Figure 2.8) can indicate successful lipid encapsulation. As liposomes are added to the NCP dispersion, aggregation is observed when some liposomes are added, followed by stabilization in Z average as the addition of more liposomes alleviates the aggregation. Encapsulation can also be monitored via changes in ζ potential; the potential increases from a negative value (non-coated particles = -26.2 mV) to a positive value that approaches that of the liposome dispersion (72.6 mV).

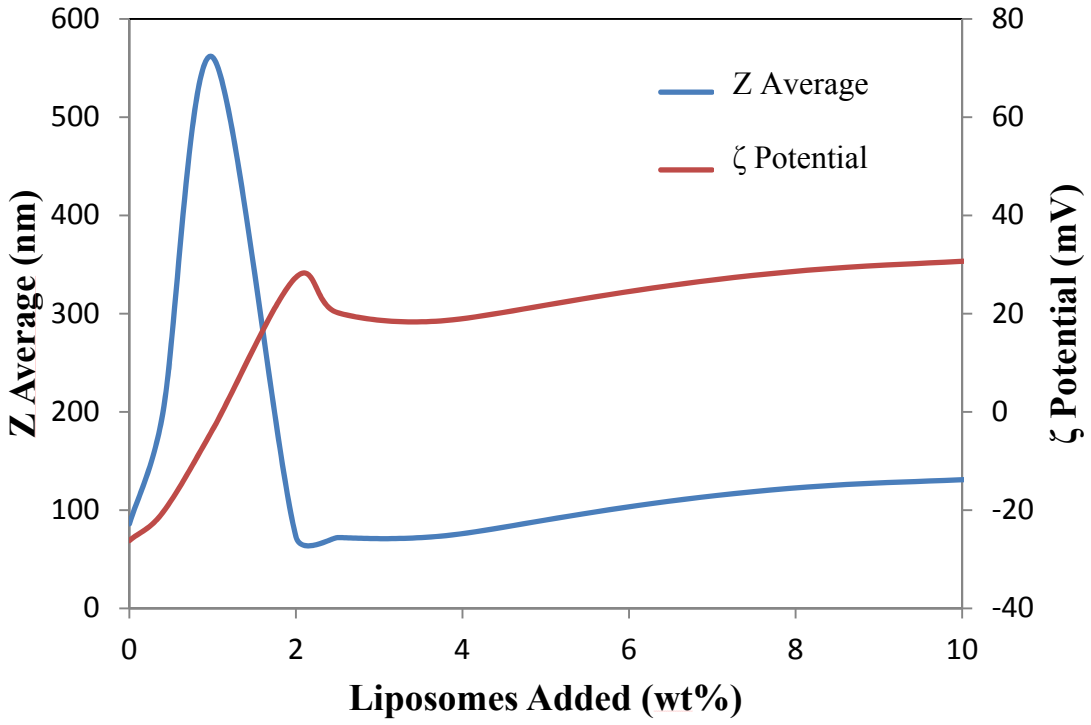

Figure 2.8. DLS plots of ζ potential and Z average of Zr-MTX NCPs given increasing amounts of 1:1 (by mol) DOTAP/cholesterol liposomes. As more liposomes are added to the formulation, ζ potential stabilizes at a positive value and aggregation dissipates.

By SEM, the lipid-coated Zr-MTX particles, Zr-MTX@Lipid, do not differ from the as-synthesized particles, but use of a uranyl acetate stain with TEM imaging shows evidence of the DOTAP/cholesterol lipid bilayer (Figure 2.9). Uranyl acetate produces a dark ring around as-synthesized Zr-MTX since uranyl ions bind preferentially to carboxylates on the NCP surface.[15] In lipid-coated particles, this dark ring is not present since the particles are lipid-coated and the uranyl acetate cannot permeate the lipid bilayer to bind with the particle. Despite the accumulating evidence of lipid encapsulation of Zr-MTX with DOTAP/cholesterol liposomes, the formulation did not stabilize the NCP, as shown by a release profile of Zr-MTX@Lipid in 8 mM PBS at 37 °C (Figure 2.10).

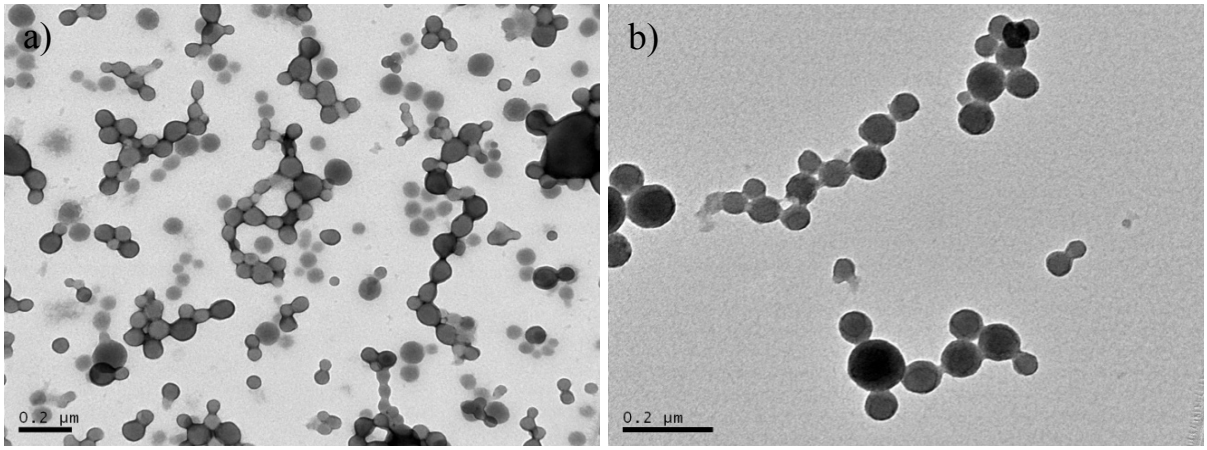

Figure 2.9. TEM micrographs of (a) Zr-MTX and (b) Zr-MTX@Lipid treated with uranyl acetate stain. Zr-MTX has a dark surface due to binding of uranyl acetate to surface carboxylates, a phenomenon not observed for Zr-MTX@Lipid due to shielding of the NCP surface by the lipid bilayer.

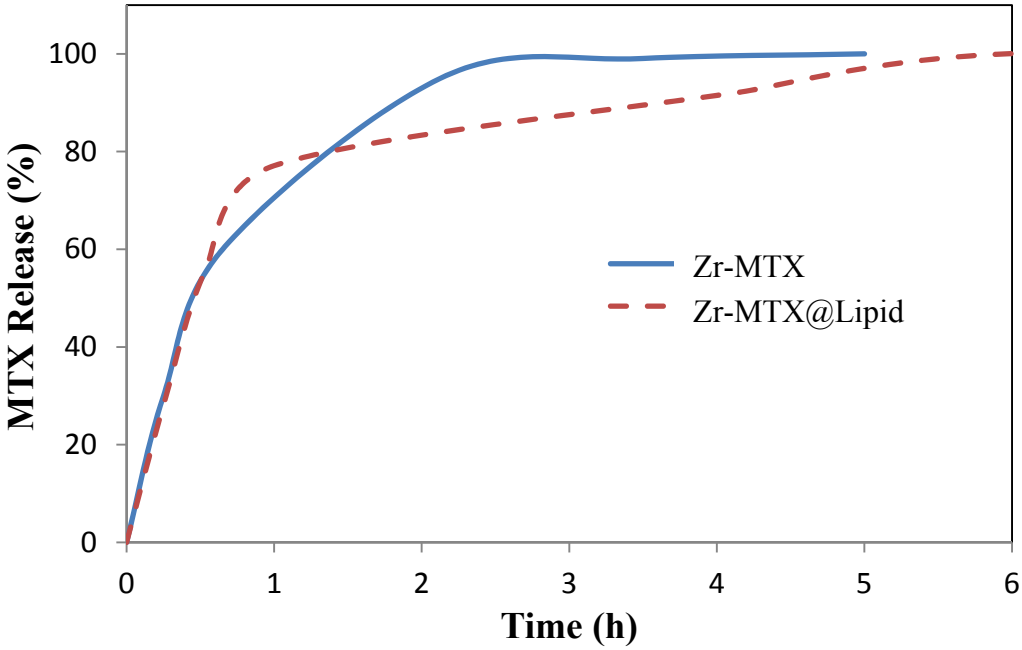

Figure 2.10. Release profile of Zr-MTX and Zr-MTX@Lipid in 8 mM PBS at 37 °C showing no enhanced stabilization for the lipid-coated formulation ($t_{1/2}$ ~ 30 min).

After several attempts to stabilize Zr-MTX via lipid encapsulation, we speculated that Zr-MTX could not be stabilized due to the great driving force of Zr(IV) to form $Zr_3(PO_4)_4$ ($k_{sp} = 10^{-134}$). Since phosphates of trivalent lanthanides have lower k_{sp} values, we sought to fabricate MTX-containing NCPs using lanthanide (III) metals.

2.2.2. Synthesis and Characterization of La-MTX and Pr-MTX NCPs

NCPs of La-MTX were synthesized by a solvothermal method in which MTX and $LaCl_3 \cdot 7H_2O$ were heated in DMF at 80 °C. The resulting spherical particles were 300-500 nm in diameter by SEM (Figure 2.11). The large size of these particles precluded their use in biological applications. Several attempts were made to reduce the diameter of this formulation, but all were unsuccessful.

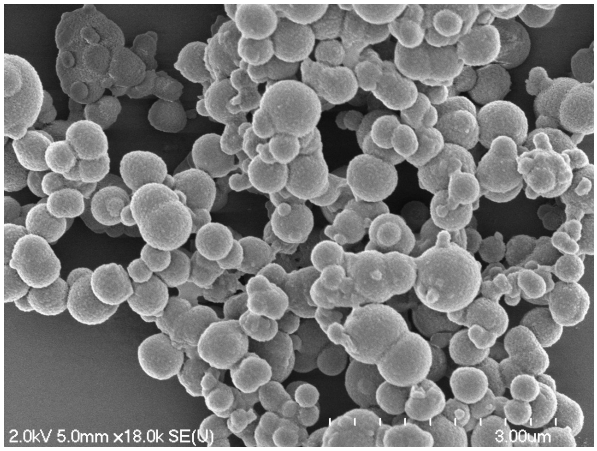

Figure 2.11. SEM micrograph of La-MTX NCPs.

NCPs using the trivalent lanthanide praseodymium were produced by a similar solvothermal method to La-MTX. These particles are spherical and between 150-300 nm in diameter by SEM (Figure 2.12), with a Z average diameter of 235.6 nm, PDI of 0.192, and ζ potential of -15.3 mV by DLS. Pr-MTX has an exceptionally high MTX drug loading of 63.7 wt% by TGA (Figure 2.13). These particles are too large for biomedical applications, and the effect of Pr in biological systems is unknown, so these particles were not explored further.

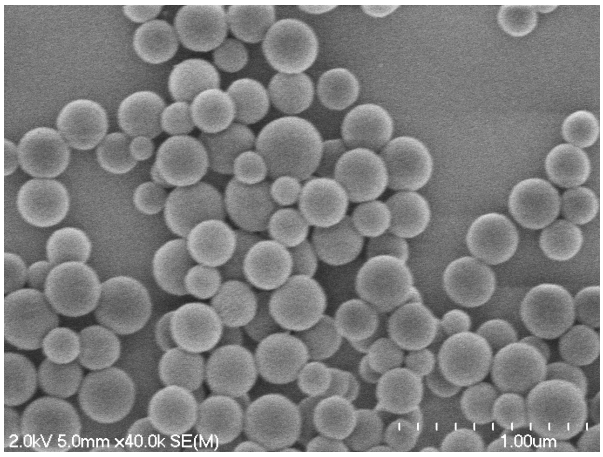

Figure 2.12. SEM micrograph of Pr-MTX NCPs.

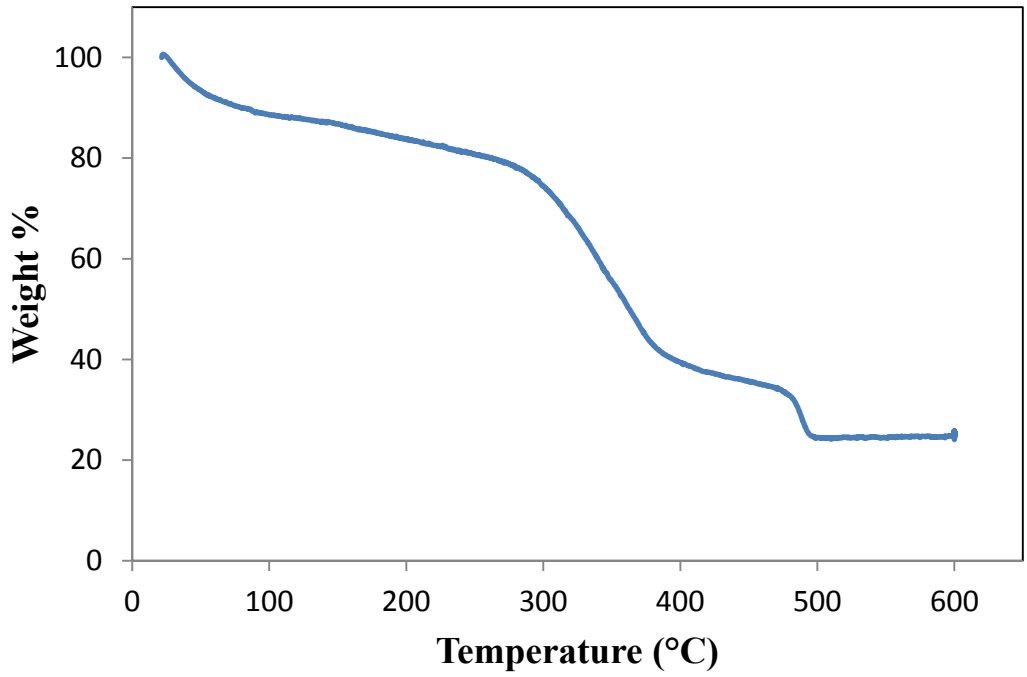

Figure 2.13. TGA of Pr-MTX, showing organic weight loss between 250 and 550 °C attributed to MTX.

2.2.3. Synthesis and Characterization of Gd-MTX NCP

Nanoparticles of Gd-MTX were produced by a solvothermal technique in which equal molar amounts of $Gd(NO_3)_3 \cdot 6H_2O$ and MTX were heated in DMF at 80 °C for 5 min. This reaction afforded a yellow product in ~85% yield. These NCPs are between 70-200 nm by both SEM and TEM with a diameter (number average) of 77.7 nm (Figure 2.14) and PDI of 0.040 by DLS, indicating a highly monodisperse sample. Gd-MTX possesses a high MTX drug loading of 71.6 wt% by TGA (Figure 2.15). Particles of Gd-MTX have a ζ potential of -10.0 mV, indicating that these particles can be encapsulated with a cationic lipid bilayer.

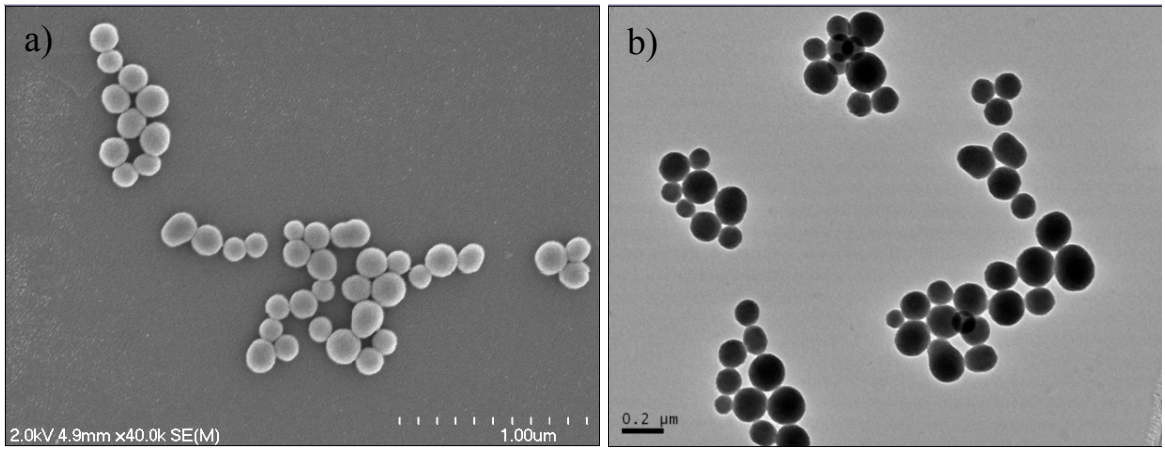

Figure 2.14. SEM (a) and TEM (b) micrographs of Gd-MTX NCPs.

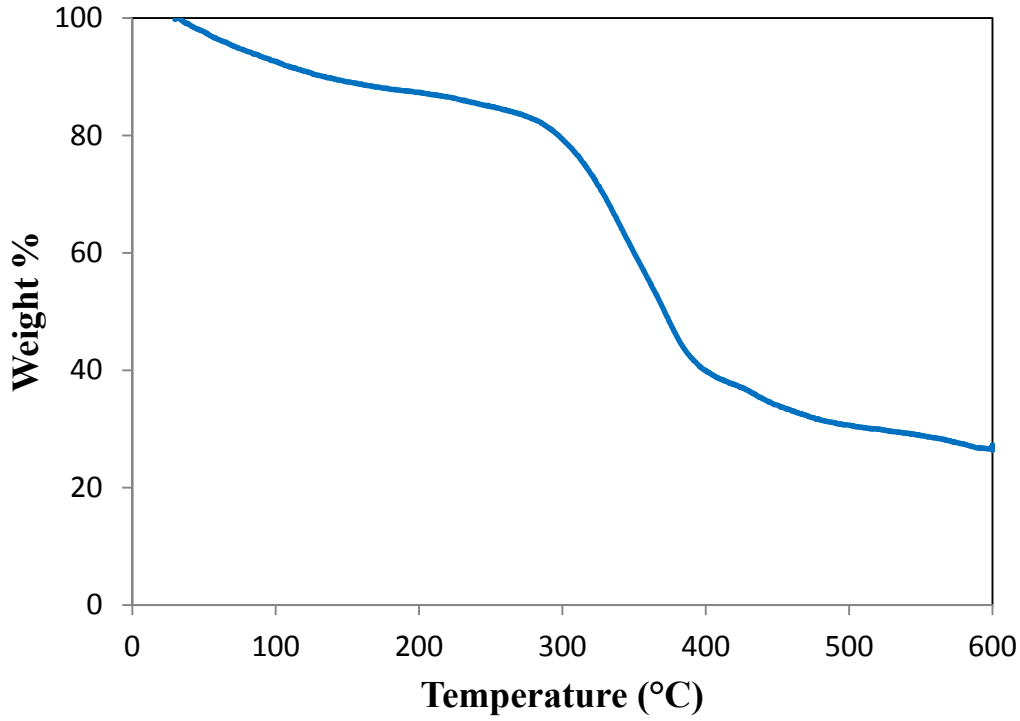

Figure 2.15. TGA of Gd-MTX showing organic weight loss between 250 and 500 °C attributed to MTX.

2.2.4. Lipid Coating of Gd-MTX NCP

As-synthesized Gd-MTX NCPs were encapsulated in a 1:1 (by mol) DSTAP/DOPE lipid bilayer by mixing dispersions of liposomes and particles in 1 mM aq. KCl to yield Gd-

MTX@Lipid. Successful lipid encapsulation was evidenced by monitoring the Z average diameter and ζ potential of the particle/liposome mixture with increasing liposome:particle weight ratios (Figure 2.16). Aggregation of the particles ceases and the ζ potential becomes positive with increased additions of liposomes, indicating successful lipid encapsulation. When Gd-MTX@Lipid is stained with uranyl acetate and imaged by TEM, a dark ring is evident presumably due to uranyl ions binding to the phosphates of the DOPE lipid,[15] a phenomenon that is not observed for Gd-MTX (Figure 2.17).

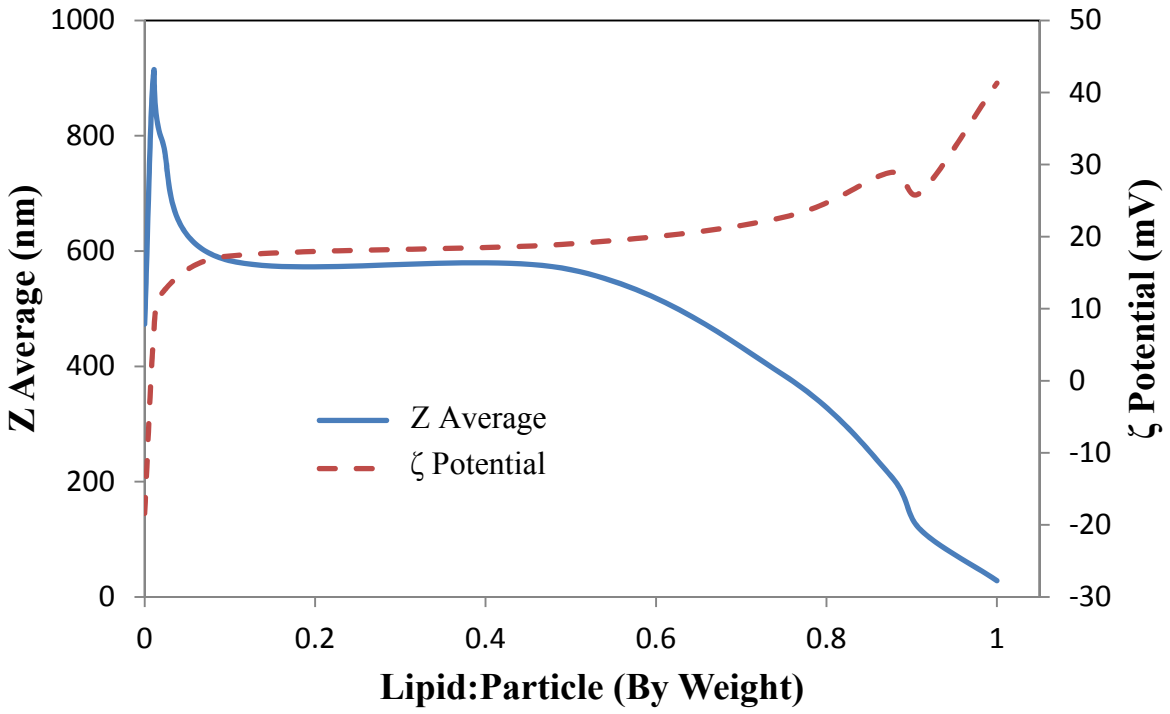

Figure 2.16. DLS plots of ζ potential and Z average of Gd-MTX NCPs with the addition of increasing amounts of 1:1 (by mol) DSTAP/DOPE liposomes. This plot shows that with increasing liposome amounts, the ζ potential becomes positive and the Z average diameter approaches that of free liposomes.

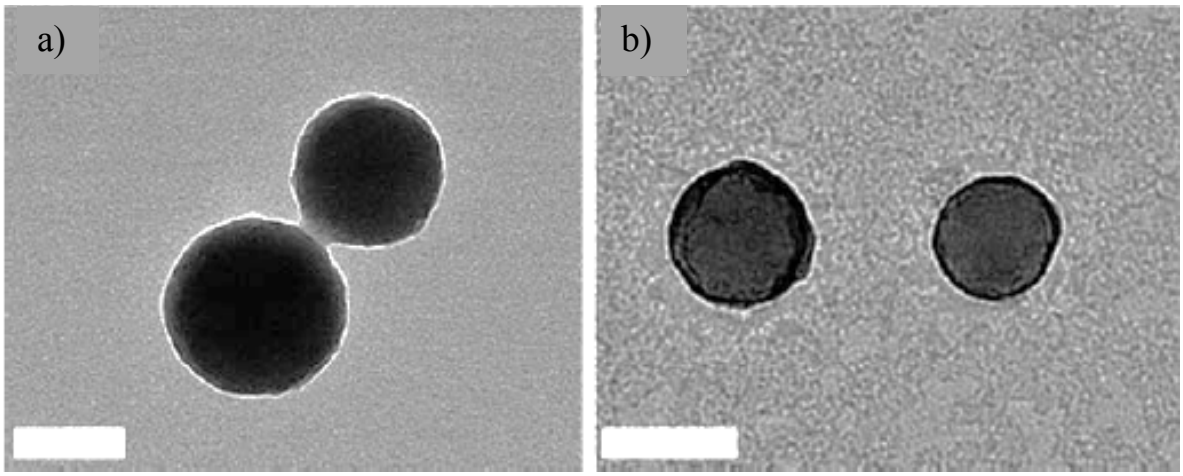

Figure 2.17. TEM micrographs of (a) Gd-MTX and (b) Gd-MTX@Lipid in the presence of uranyl acetate stain. Uranyl acetate forms dark rings on the surface of the lipid-coated formulation due to binding to the phosphates of the DOPE lipid.

Only a slight decrease in particle size from the as-synthesized particles is observed by DLS; particles of Gd-MTX@Lipid were 64.6 nm (number average) with a PDI of 0.240. The decrease in size can be attributed to a decrease in aggregation due to the lipid coating. The lipid-coated particles have a cationic ζ potential (32.6 mV) due to presence of the lipid bilayer on the particle surface. Further evidence of lipid encapsulation can be observed by laser scanning confocal microscopy. Gd-MTX particles doped with the optical imaging agent $Ru(bpy)_3^{2+}$ (discussed in section 2.2.7) were encapsulated with a 1:1 (by mol) DSTAP/DOPE bilayer containing 10 mol% DOPE-FITC, another optical imaging agent. When the particles are imaged by confocal microscopy, co-localization of the red channel (particles) with the green channel (FITC) indicates individual particles are associated with lipid bilayers (Figure 2.18). Encapsulation of Gd-MTX with a DSTAP/DOPE lipid bilayer results in significant stabilization of the material in a release profile in 8 mM PBS at 37 °C (Figure 2.19). The as-synthesized particles are quite unstable, with $t_{1/2} \sim 2$ h, but the lipid-coated formulation has a $t_{1/2} \sim 23$ h, with complete release at 192 h. The amount of MTX released was determined by UV-Vis spectroscopy. MTX absorbs in the 200-400 nm region (Figure 2.20), and a standard

curve was determined using the absorbance at ~305 nm ($Absorbance_{305\ nm}$ = 0.0222(μM MTX).

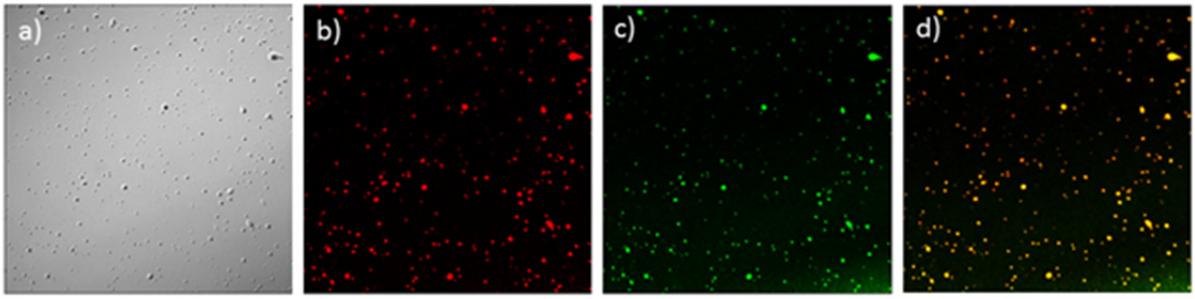

Figure 2.18. Confocal microscopy images of $Ru(bpy)_3$-doped Gd-MTX@Lipid in which the lipid bilayer has been doped with 10 mol% DOPE-FITC. This experiment was conducted to show co-localization of NCP fluorescence with the fluorescence of the lipid bilayer. a) DIC image, b) red fluorescence due to NCPs, c) green fluorescence due to FITC-doped lipid bilayer, and d) overlay of NCP and lipid bilayer fluorescences showing co-localization.

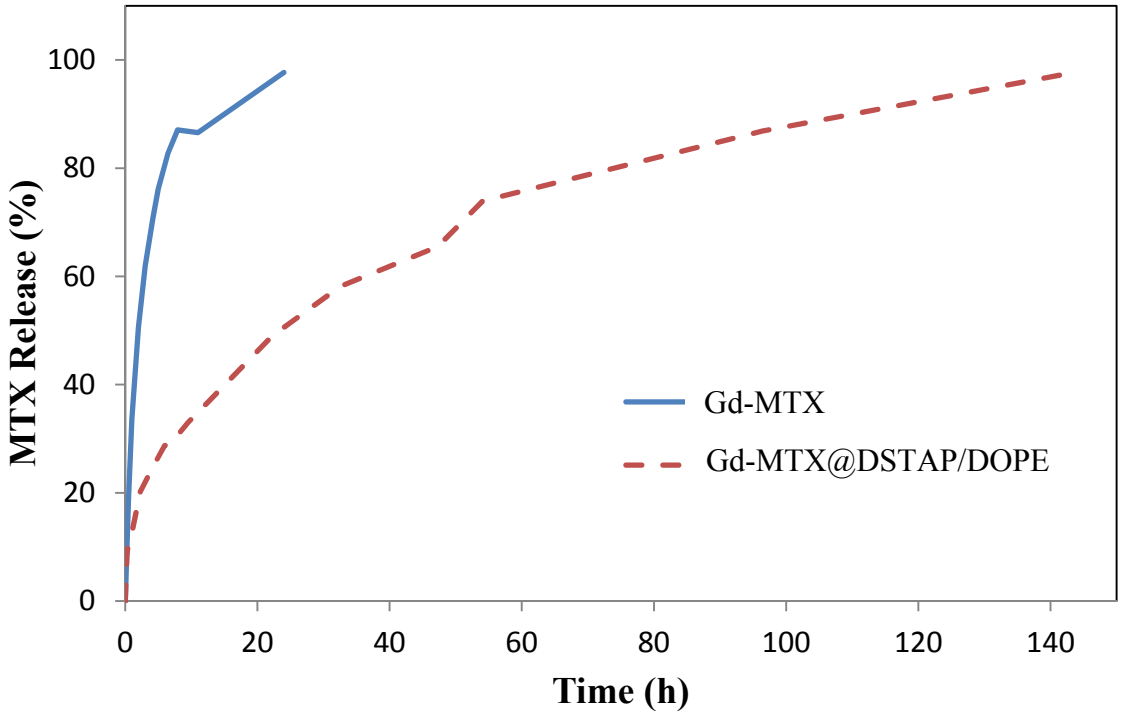

Figure 2.19. Release profile for Gd-MTX@Lipid in 8 mM PBS at 37°C and using 10K mwco dialysis tubing. $t_{1/2}$: free MTX = 1.5 h, Gd-MTX = 2 h, Gd-MTX@Lipid = 23 h. Complete MTX release from Gd-MTX@Lipid was observed at 143 h.

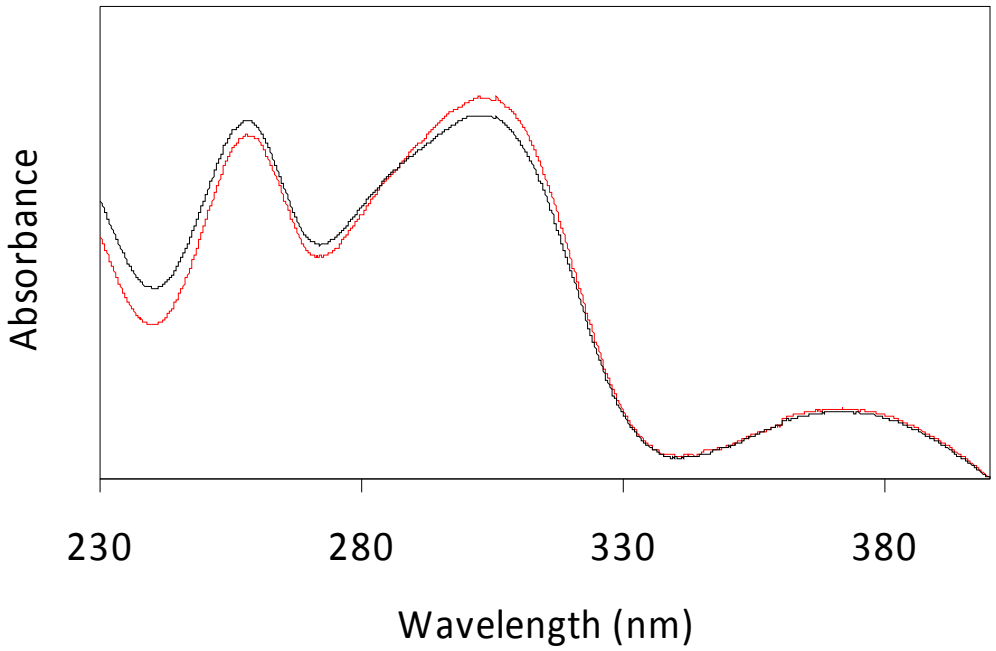

Figure 2.20. An absorption spectrum for MTX (black), compared to an absorption spectrum for a release profile aliquot from dialysis of Zn-MTX (red). The absorption profile does not change significantly, indicating that MTX remains unchanged under the synthetic conditions used.

The Gd-MTX@Lipid NCPs were rendered an active tumor targeting agent by doping the 1:1 (by mol) DSTAP/DOPE liposomes with 10 mol% of an anisamide (AA)-lipid conjugate, DOPE-AA. Anisamide is a small molecule targeting ligand that is known to target sigma receptors which are overexpressed on a number of epithelial cancer cell lines.[19-24] Addition of AA to the liposome formulation did not significantly alter the size of the particles, as Gd-MTX@Lipid-AA has a number average diameter of 76.8 nm, PDI of 0.150, and a ζ potential of 25.3 mV.

2.2.5. Synthesis and Characterization of Gd-Folate NCP

Control vehicles, NCPs that do not contain any cytotoxic agent, were prepared using folic acid, an essential nutrient, instead of MTX. These particles were prepared by a solvothermal method in which $GdNO_3 \cdot 6H_2O$ and folic acid were heated in DMF at 80 °C,

producing particles that were between 200-300 nm by SEM with a number average diameter of 262 nm by DLS (Figure 2.21). These control vehicles were used to show that *in vitro* cytotoxicity arises from MTX, not Gd(III) or the lipid formulation.

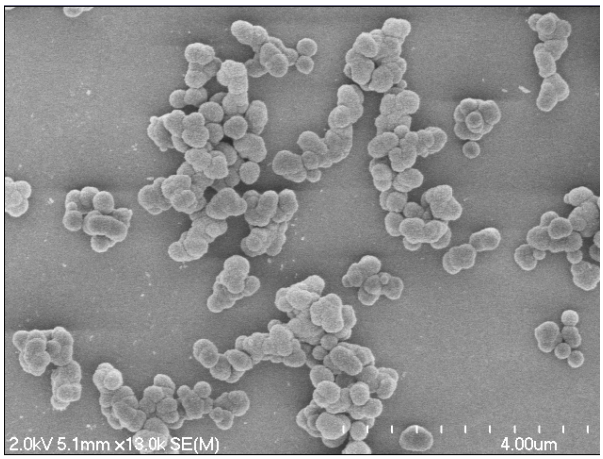

Figure 2.21. SEM micrograph of Gd-Folate NCPs.

2.2.6. In Vitro Cytotoxicity and Viability Assays

A minimal amount of *in vitro* cytotoxicity assays were performed on Zr-MTX using the acute lymphoblastic leukemia cell line, CCRF-CEM. A 3 h cytotoxicity assay was performed in which concentrations of free MTX, Zr-MTX, and Zr-MTX@SiO_2 were tested. Viability was determined by the trypan blue exclusion assay (Figure 2.22). The results show that free MTX and Zr-MTX exhibit similar IC_{50} values, 20 μM and 18 μM, respectively. The similarity in efficacy can be explained by the instability of Zr-MTX; Zr-MTX would dissolve rapidly and essentially become free MTX in the cell medium. Additionally, the efficacies of free MTX and Zr-MTX were equivalent when tested over 48 h, with an IC_{50} value of ~1 μM (Figure 2.23).

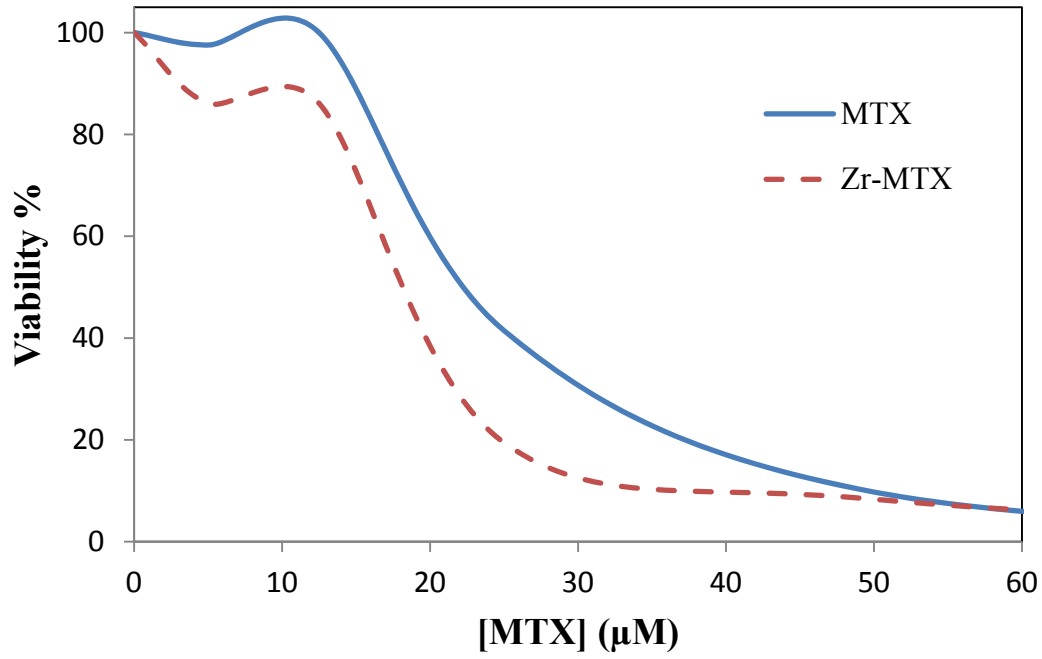

Figure 2.22. *In vitro* viability curves of MTX and Zr-MTX against the CCRF-CEM acute lymphoblastic leukemia cell line over 3 h.

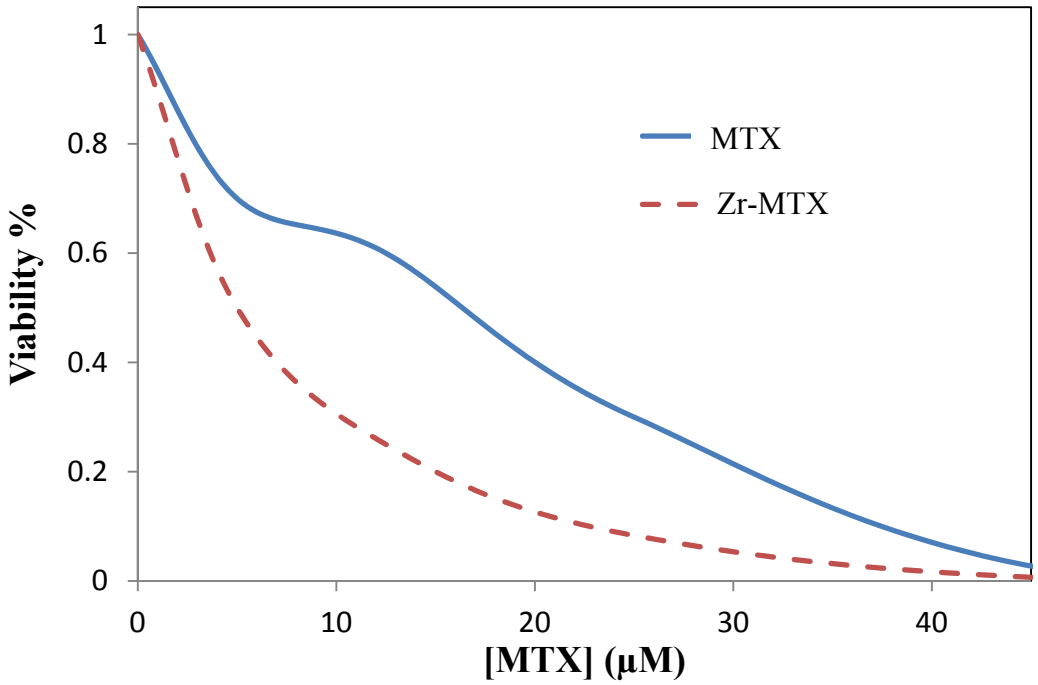

Figure 2.23. *In vitro* viability curves of MTX and Zr-MTX against the CCRF-CEM acute lymphoblastic leukemia cell line for 48 h.

All Gd-MTX formulations were tested against Jurkat cells, an ALL cell line that is known to overexpress sigma receptors.[23] This assay was completed over 72 h, and cytotoxicity was determined by the trypan blue exclusion assay (Figures 2.24 and 2.25). As-synthesized Gd-MTX was slightly less cytotoxic than free MTX (IC_{50} = 34.7 ± 2.5 nM) with an IC_{50} value of 54.7 ± 2.3 nM. The efficacy of Gd-MTX is not expected to be an improvement over the free drug due to rapid degradation of these unstable NCPs. The lipid-coated formulation showed enhanced efficacy over free MTX with an IC_{50} = 28.3 ± 0.6 nM, but the AA-modified particles showed an even more, statistically significant, increase in efficacy (IC_{50} = 23.7 ± 1.5 nM). The enhancement in efficacy of the lipid-coated particles is attributed to the known affinity of cationic lipid bilayers for cell membranes.

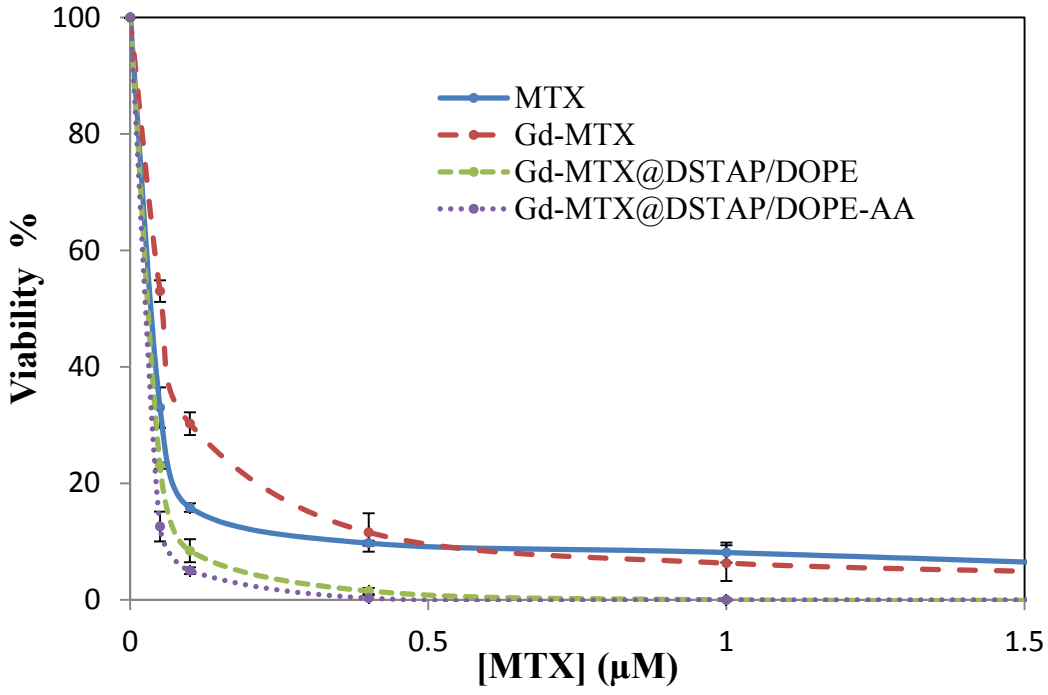

Figure 2.24. *In vitro* cytotoxicity curves for MTX-containing NCPs against Jurkat acute lymphoblastic leukemia cells.

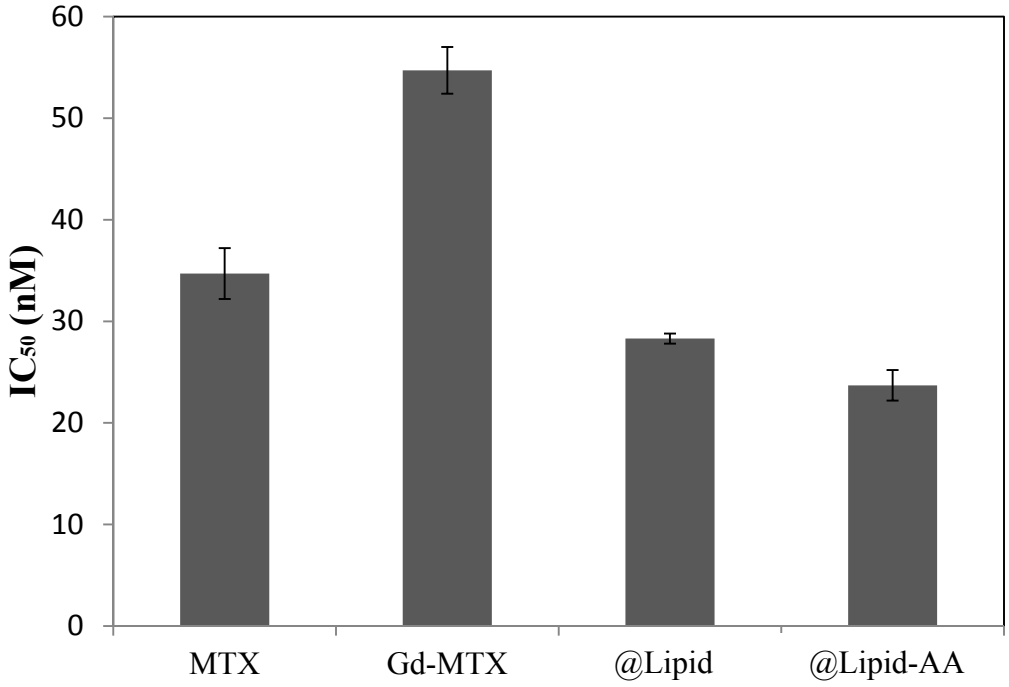

Figure 2.25. IC_{50} plot of MTX-containing NCPs for a 72 h *in vitro* cytotoxicity assay against Jurkat ALL cells.

Viability assays testing the effect of Gd-Folate NCPs or free Gd(III) salt was conducted to ensure that the cytotoxicity of Gd-MTX can be attributed to MTX, not the Gd(III) ions or lipid bilayers. Free $Gd(NO_3)_3$ salt as well as Gd-Folate and the lipid-coated formulations of Gd-Folate were tested, and no cytotoxic effect was observed (Figure 2.26).

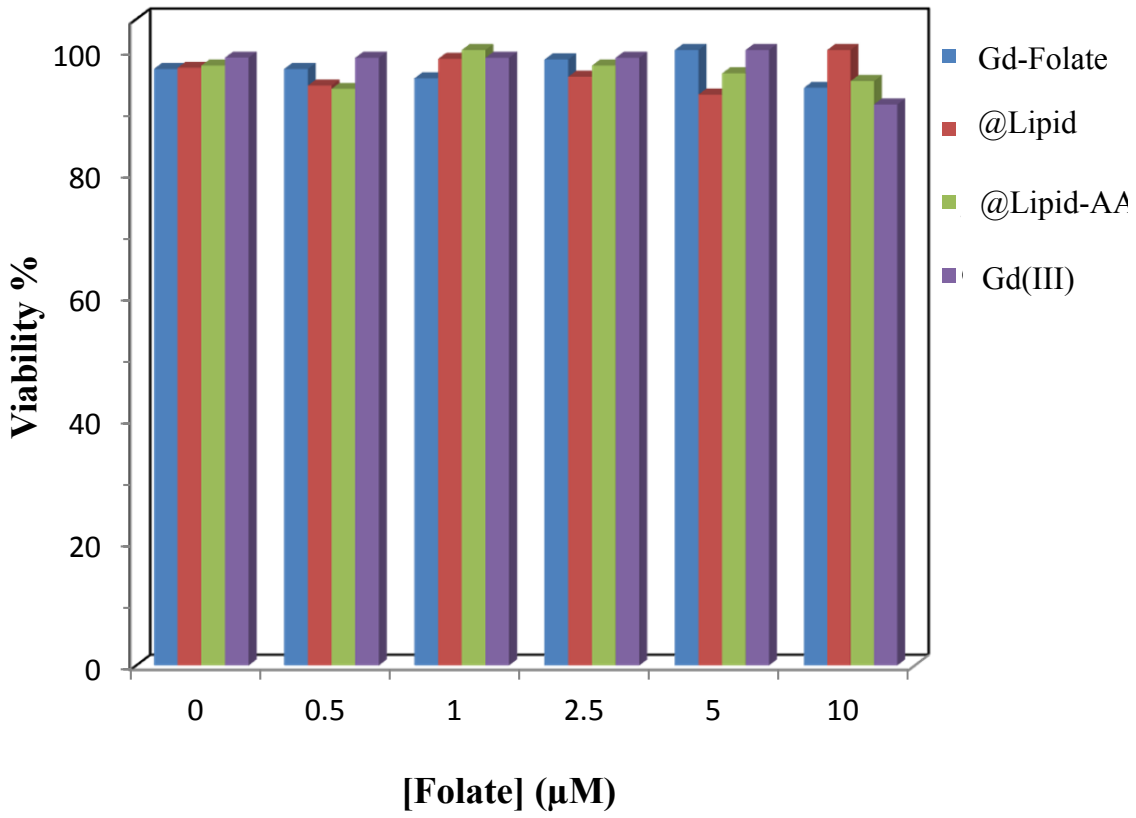

Figure 2.26. *In vitro* viability assay testing free Gd(III) and Gd-Folate NCPs, displaying that no cytotoxic effect was observed due to free Gd(III) or the control vehicles. This experiment confirms that the cytotoxicity observed for MTX-containing NCPs is due solely to MTX and no other agent.

2.2.7. Synthesis and Characterization of $Ru(bpy)_3^{2+}$-Doped Gd-MTX NCP

Gd-MTX doped with 2.5, 5, or 10 mol% $Ru(bpy)_3^{2+}$ were prepared by a similar solvothermal method in which the undoped nanoparticles were prepared. Our previous work has shown that $Ru(bpy)_2^{3+}$ is an efficient optical imaging agent,[25] and these doped NCPs were prepared for confocal microscopy studies. All doped NCPs were between 100-200 nm in diameter by SEM and TEM (Figure 2.27). No additional weight loss is observed by TGA, presumably because the addition of $Ru(bpy)_2^{3+}$ was too low to be detected (Figure 2.28). Gd-MTX doped with 10 mol% $Ru(bpy)_2^{3+}$ was used for confocal microscopy. These particles

have a number average diameter of 119.5 nm with a PDI of 0.154 and a ζ potential of -20.6 mV. These particles are 9.6 mol% Ru by ICP-MS, and the presence of $Ru(bpy)_2^{3+}$ is evident by fluorescence in which a broad emission peak at ~620 nm is present (Figure 2.29).

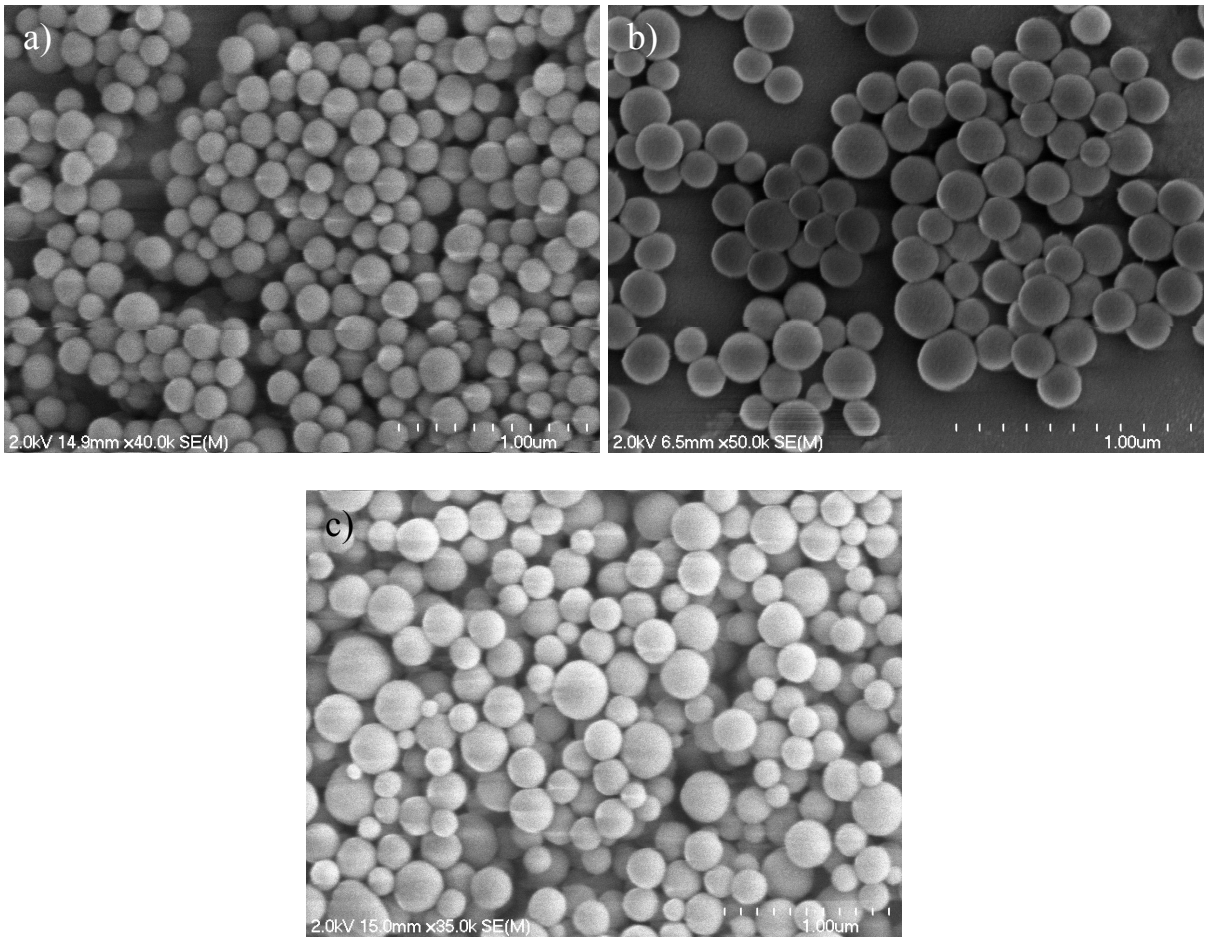

Figure 2.27. SEM micrographs of $Ru(bpy)_3^{2+}$-doped Gd-MTX with different doping amounts: (a) 2.5 mol%, (b) 5 mol%, (c) 10 mol%.

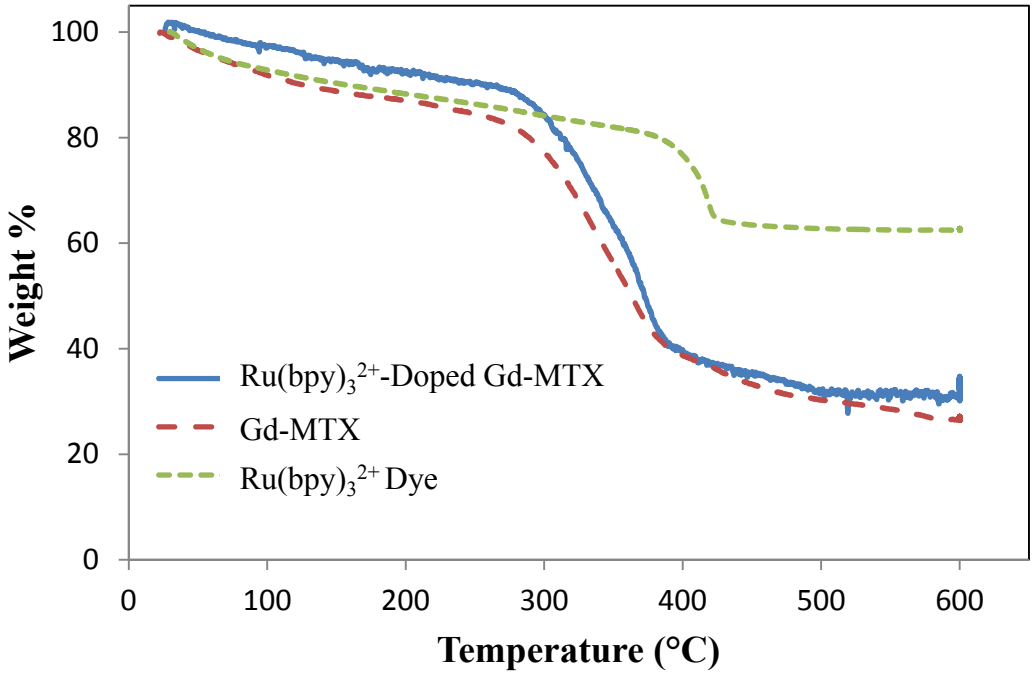

Figure 2.28. TGA plot of Gd-MTX doped with 5 mol% $Ru(bpy)_3^{2+}$ showing organic weight loss attributed to bpy ligands and MTX.

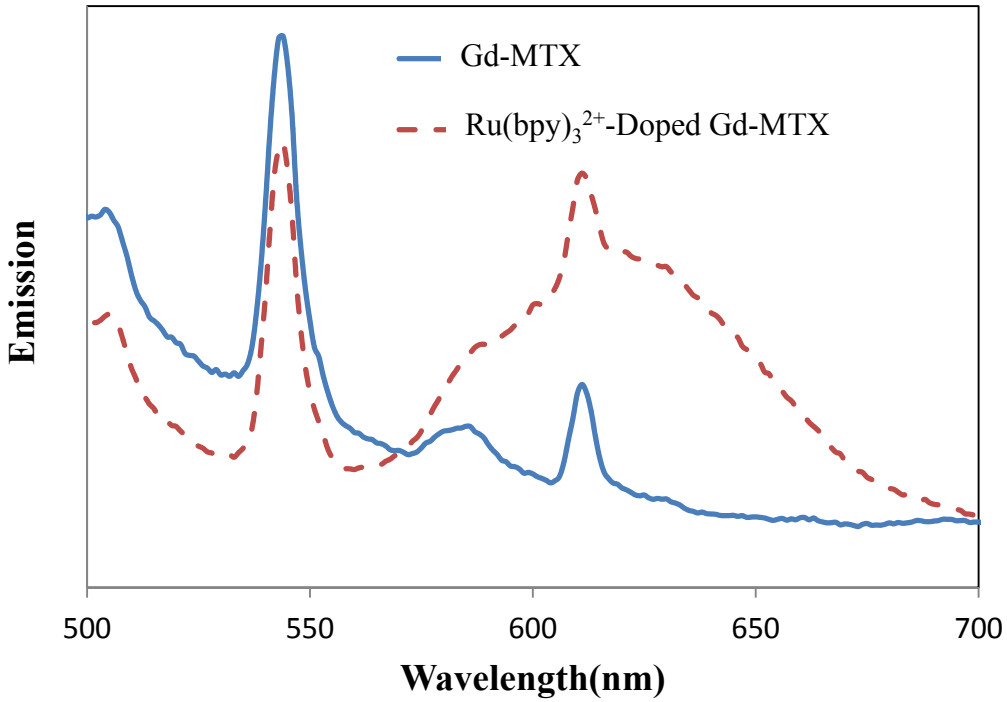

Figure 2.29. Fluorescence spectrum of $Ru(bpy)_3^{2+}$-doped Gd-MTX showing emission from the presence of $Ru(bpy)_3^{2+}$ (~620 nm).

$Ru(bpy)_3^{2+}$-doped Gd-Folate NCPs were also prepared by a solvothermal synthesis in DMF at 80 °C. These particles fluoresce under a UV lamp and are 150-200 nm by SEM (Figure 2.30). This size is also observed by DLS with a number average diameter of 160.6 nm, PDI of 0.365, and ζ potential of -16.1 mV in 1 mM aq. KCl. These particles are 13.4 mol% Ru by ICP-MS.

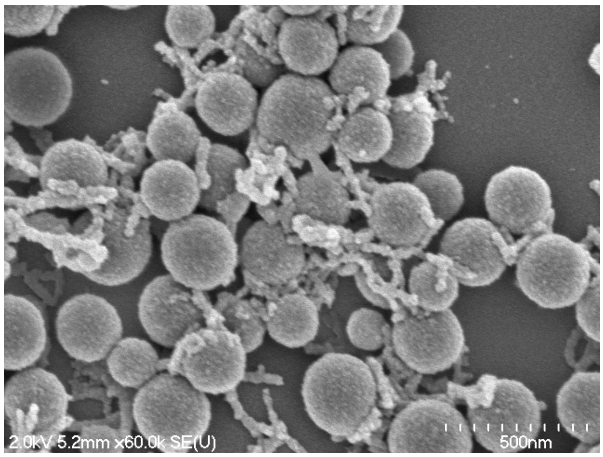

Figure 2.30. SEM micrograph of $Ru(bpy)_3^{2+}$-doped Gd-Folate NCPs.

2.2.8. Confocal Microscopy

$Ru(bpy)_3^{2+}$-doped Gd-MTX NCPs were used to show that this system can be used as a dual optical imaging and chemotherapeutic agent. Amounts of Gd-MTX and lipid-coated formulations were incubated with Jurkat ALL cells for 1 h, followed by incubation with an AnnexinV-FITC conjugate, which is a fluorescent indicator for early apoptosis. These samples were visualized using a confocal microscope (Figure 2.31). No red (particles) or green (apoptosis) fluorescence is observed for the as-synthesized Gd-MTX NCPs, likely due to rapid degradation of these particles. The as-synthesized particles do not have a mechanism for cell internalization. Co-localized fluorescence of the $Ru(bpy)_3^{2+}$-doped Gd-MTX particles

and green (FITC) fluorescence is observed for lipid-coated Gd-MTX, but this signal is greatly enhanced in the AA-targeted particles, indicating increased uptake and efficacy of this formulation.

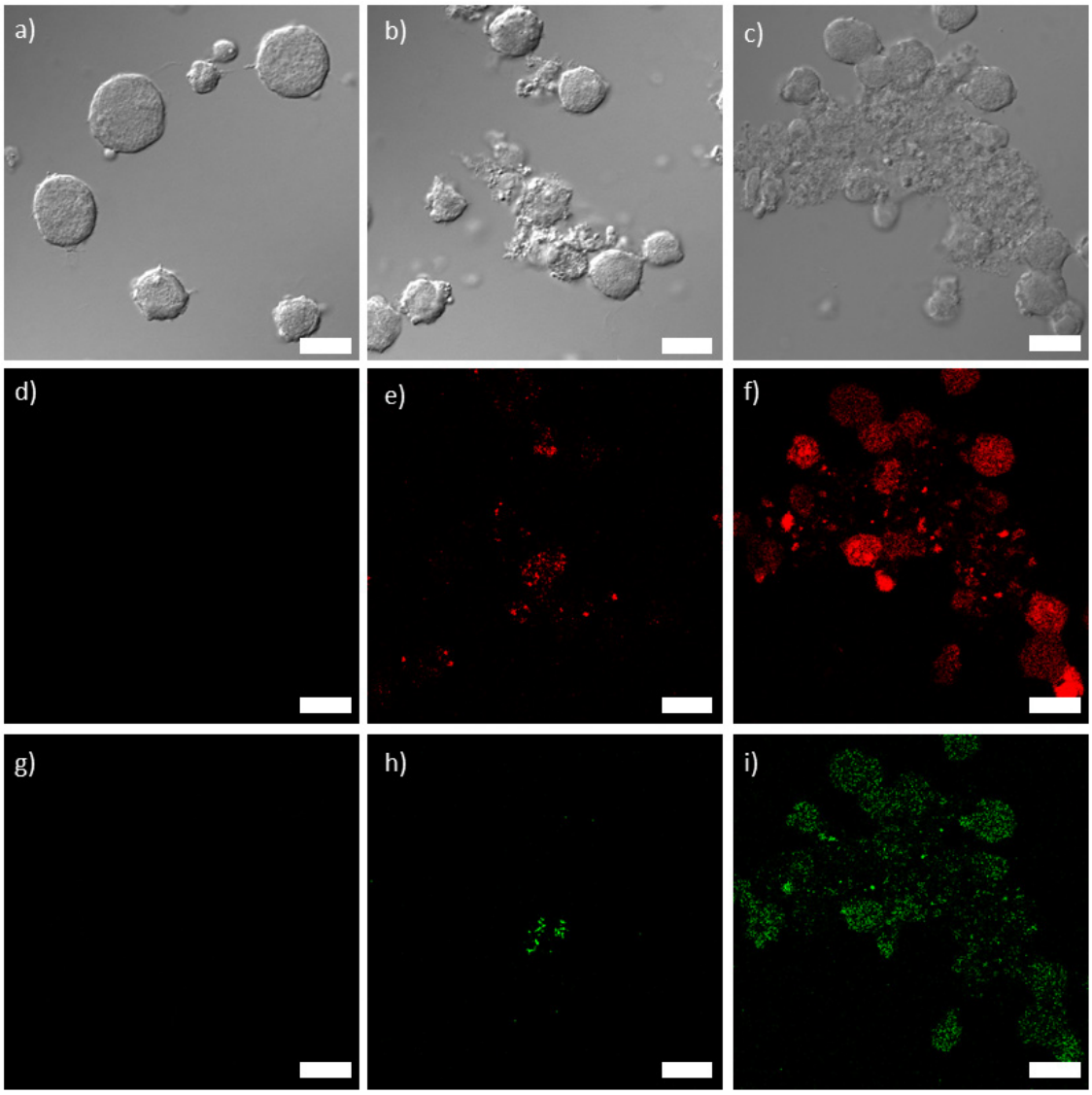

Figure 2.31. (a-c) Differential interference contrast (DIC) images and (d-i) fluorescence images of Jurkat cells incubated with Gd-MTX (d,g), Gd-MTX@DSTAP/DOPE (e,h), and Gd-MTX@DSTAP/DOPE-AA (f,i). Red fluorescence (d-f) is from the $Ru(bpy)_3^{2+}$-doped particles and green fluorescence (g-i) is from the Annexin V FITC conjugate early apoptosis stain. Scale bars represent 25 μm.

When Jurkat cells are incubated with $Ru(bpy)_3^{2+}$-doped Gd-Folate NCPs and stained with the AnnexinV-FITC conjugate, red fluorescence is observed, but no green fluorescence from the early apoptosis indicator is observed (Figure 2.32). This control experiment emphasizes that cytotoxicity of this formulation is due to MTX, not Gd^{3+} or the lipid coating.

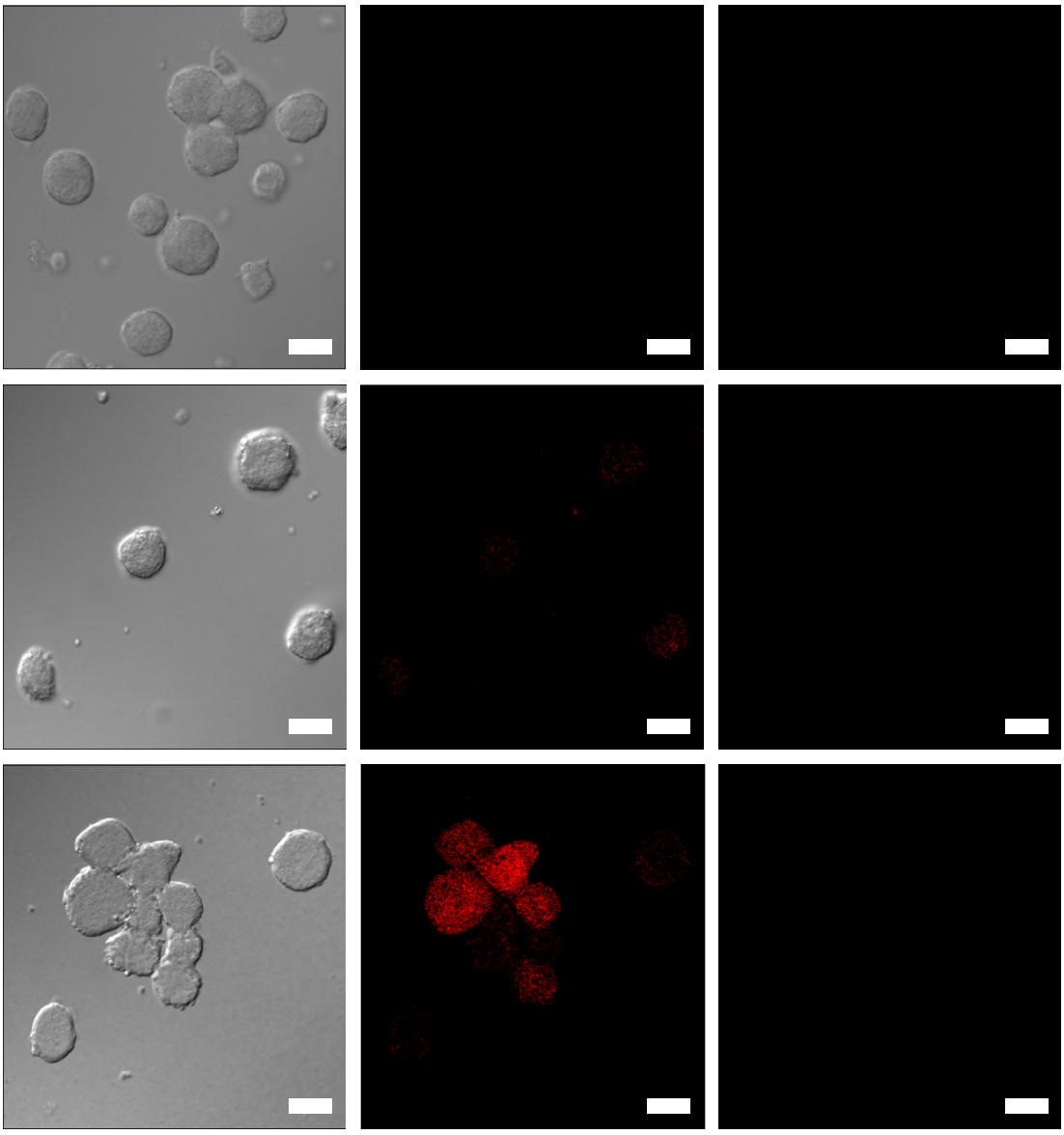

Figure 2.32. Confocal images of Jurkat cells incubated with Gd-Folate (a-c), Gd-Folate@DSTAP/DOPE (d-f), and Gd-Folate@DSTAP/DOPE-AA (g-i). Cells incubated with the AA-targeted formulation shows enhanced uptake, but no apoptosis is apparent. Channels are: a,d,g) DIC, b,e,h) red from particles, c,f,i) green from AnnexinV FITC apoptotic stain. Scale bars are 25 μm.

2.2.9. MR Relaxivities of Gd-MTX NCPs

Gd-MTX and the lipid-coated formulations were probed as potential theranostic agents by taking advantage of the use of Gd(III) as a MRI contrast enhancement agent. Samples of the NCPs were prepared and redispersed in H_2O then analyzed on a 3T MR scanner. MR relaxivities (r_1 and r_2) were analyzed (Figures 2.33, 2.34, 2.35, and 2.36). These values are acceptable for MR contrast agents, as many agents display r_1 values between 4-5 $mM^{-1}s^{-1}$. T_1- and T_2-weighted images of these formulations show increased contrast with increased concentration of NCPs suspended in H_2O. It is likely that the as-synthesized Gd-MTX nanoparticles display higher relaxivities because H_2O exchange is impeded by the lipid coatings.

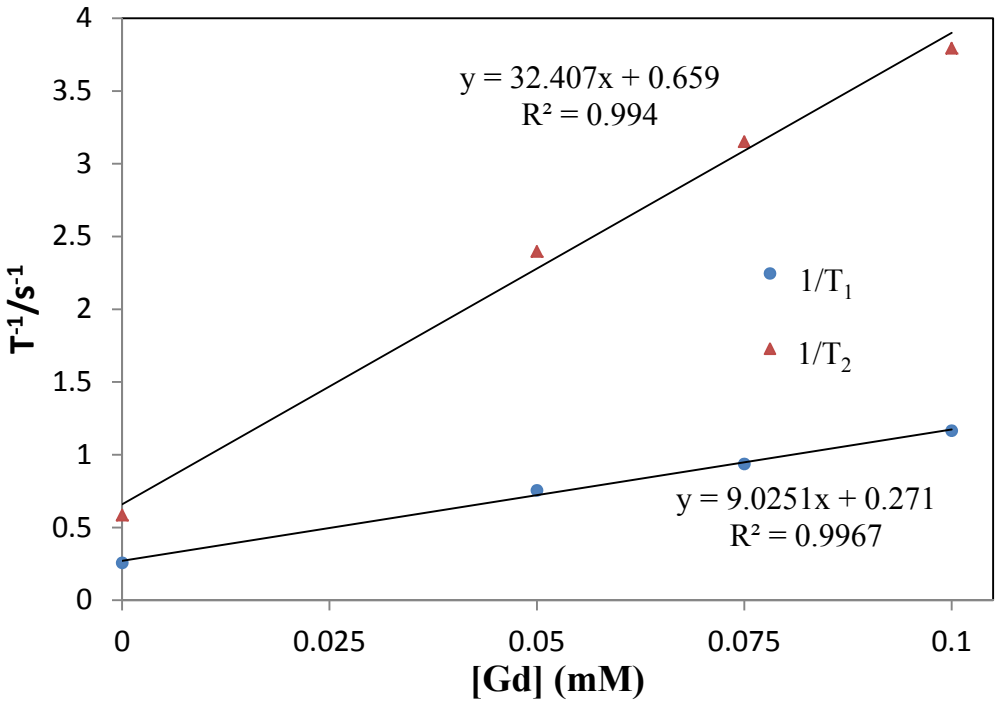

Figure 2.33. MR relaxivity plots for Gd-MTX showing values for r_1 and r_2.

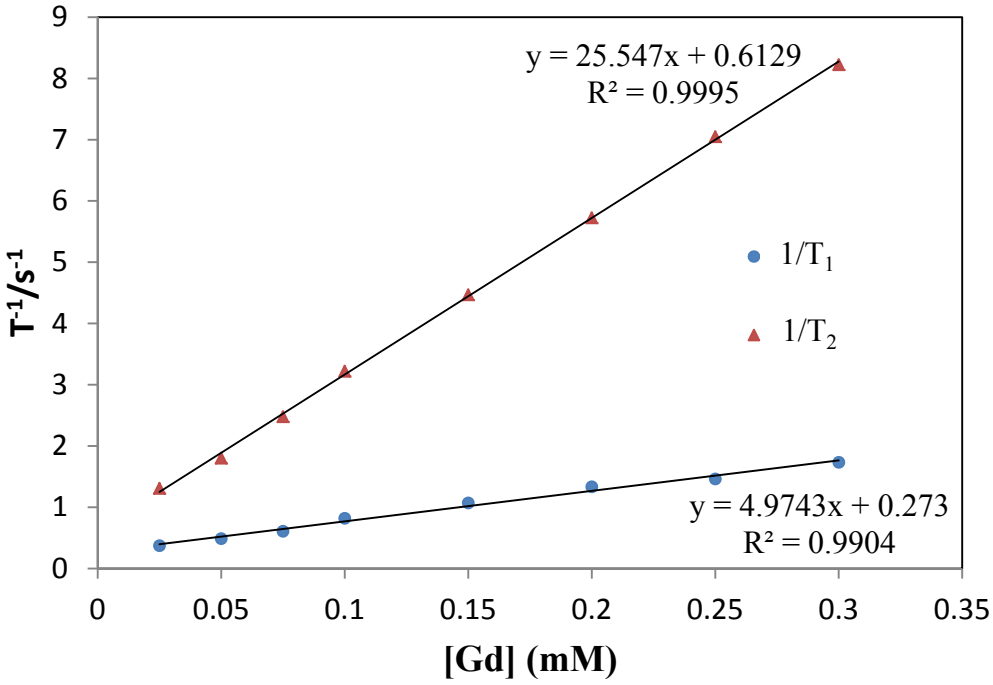

Figure 2.34. MR relaxivity plots for Gd-MTX@Lipid showing values for r_1 and r_2.

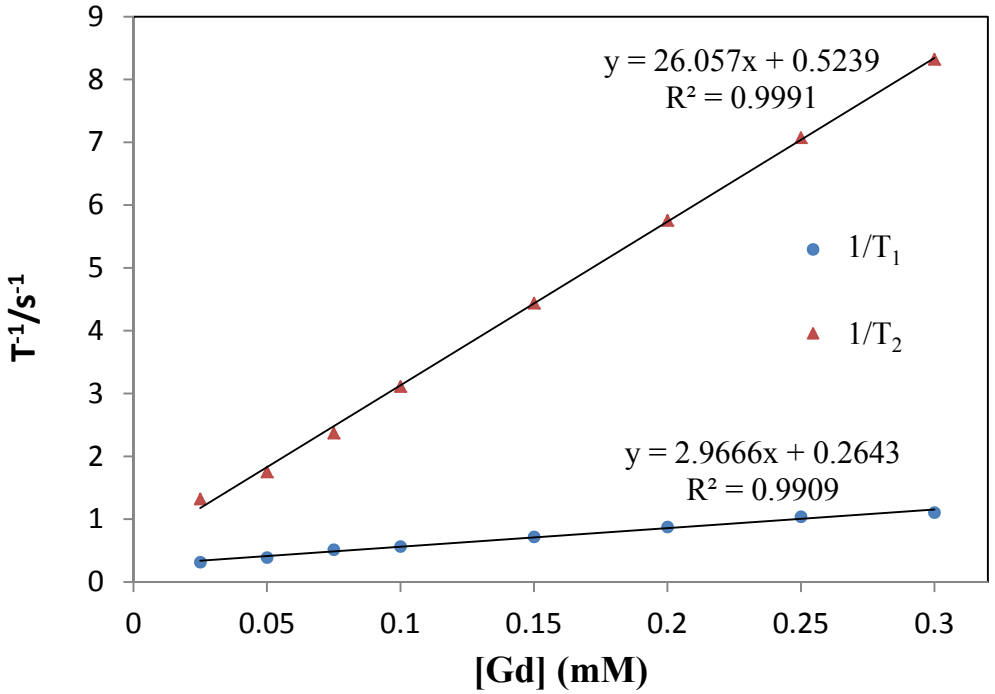

Figure 2.35. MR relaxivity plots for Gd-MTX@Lipid-AA showing values for r_1 and r_2.

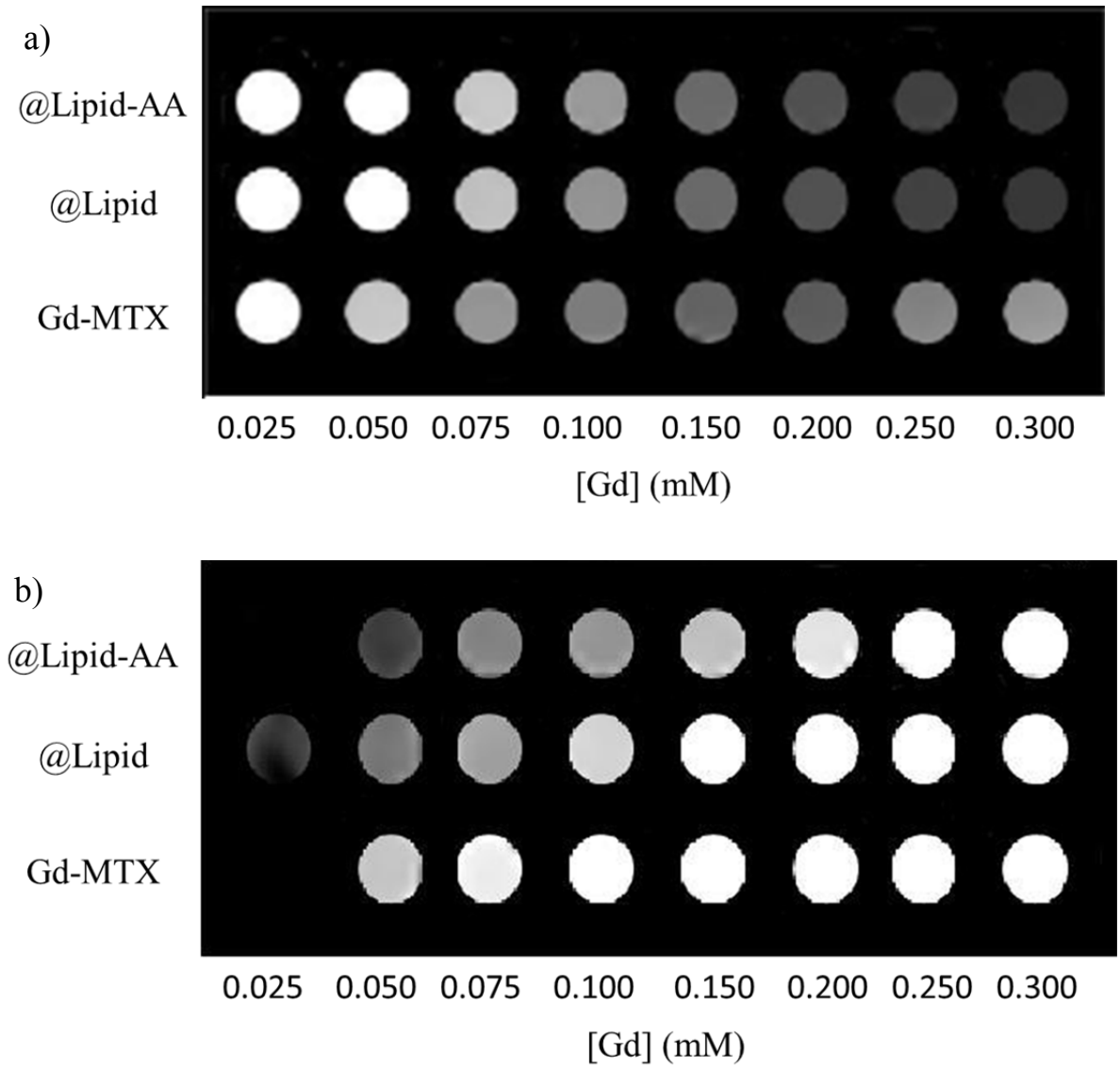

Figure 2.36. T_2- (a) and T_1- (b) weighted images for Gd-MTX, Gd-MTX@DSTAP/DOPE, and Gd-MTX@DSTAP/DOPE-AA. Varying concentrations increase from left to right.

2.2.10. PEGylation of Gd-MTX NCP

Attempts were made to PEGylate the lipid bilayers of the Gd-MTX formulations as PEGylation is known to enhance circulation of nanomaterials in biological systems.[26-30] Two methods were done: post-insertion (in which PEG-lipid is added after lipid coating) and pre-insertion (in which PEG-lipid is added during lipid coating).[31] Post-insertion was attempted

by lipid-coating Gd-MTX by the established procedure and then adding amounts of PEG-DOPE micelles to result in varying mol% PEG-DOPE in the bilayer. Monitoring the ζ potential of the various samples in 1 mM aq. KCl can indicate if PEGylation was successful. Lipid-coated Gd-MTX has a cationic ζ potential (30.5 mV), and the ζ potential becomes more neutral with increased amounts of PEG-DOPE (Figure 2.37). This shift toward neutral ζ potentials is likely due to shielding by the bulky PEG-DOPE lipid. SEM shows that the particle size and morphology does not differ from the as-synthesized particles (Figure 2.38). Additionally, the number average diameters by DLS of the PEGylated particles are larger than the lipid-coated particles, likely due to increased bulk by addition of PEG (Figure 2.39).

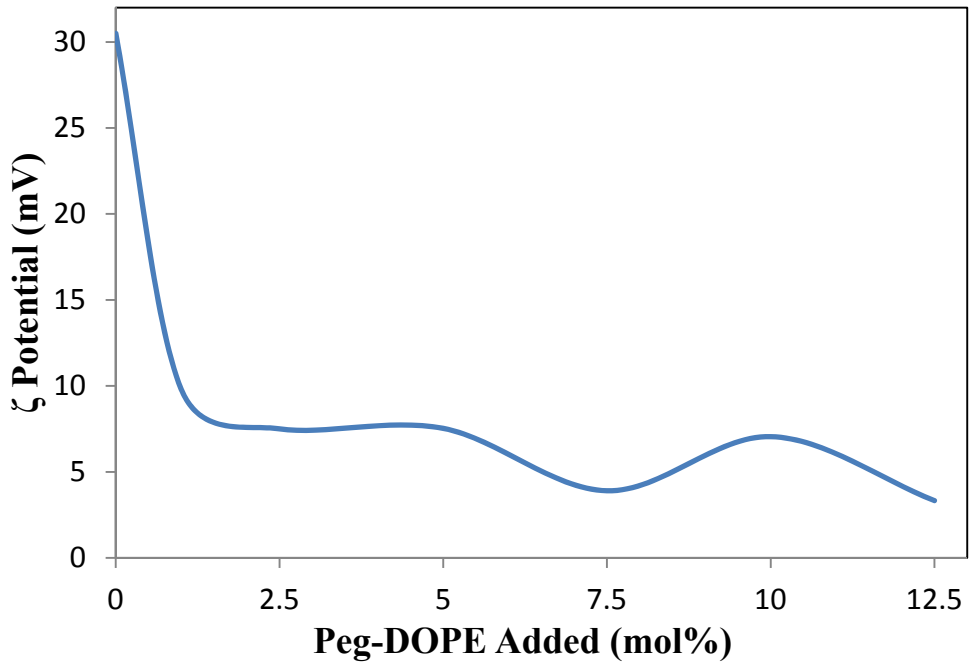

Figure 2.37. ζ potential plot of PEGylated Gd-MTX@Lipid that shows the decrease in ζ potential with increasing amounts of DOPE-PEG added to the formulation.

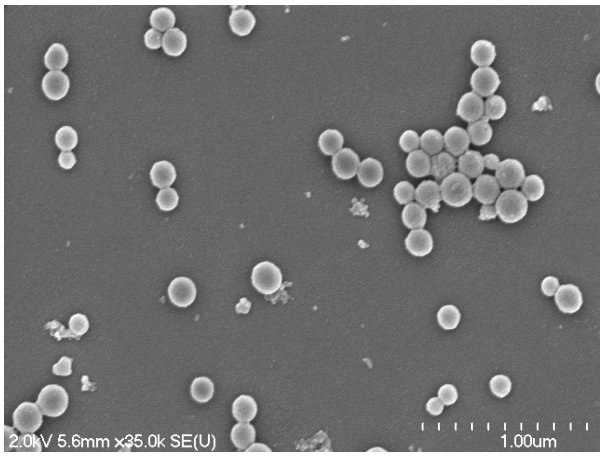

Figure 2.38. SEM micrograph of Gd-MTX PEGylated with DOPE-PEG by post-insertion.

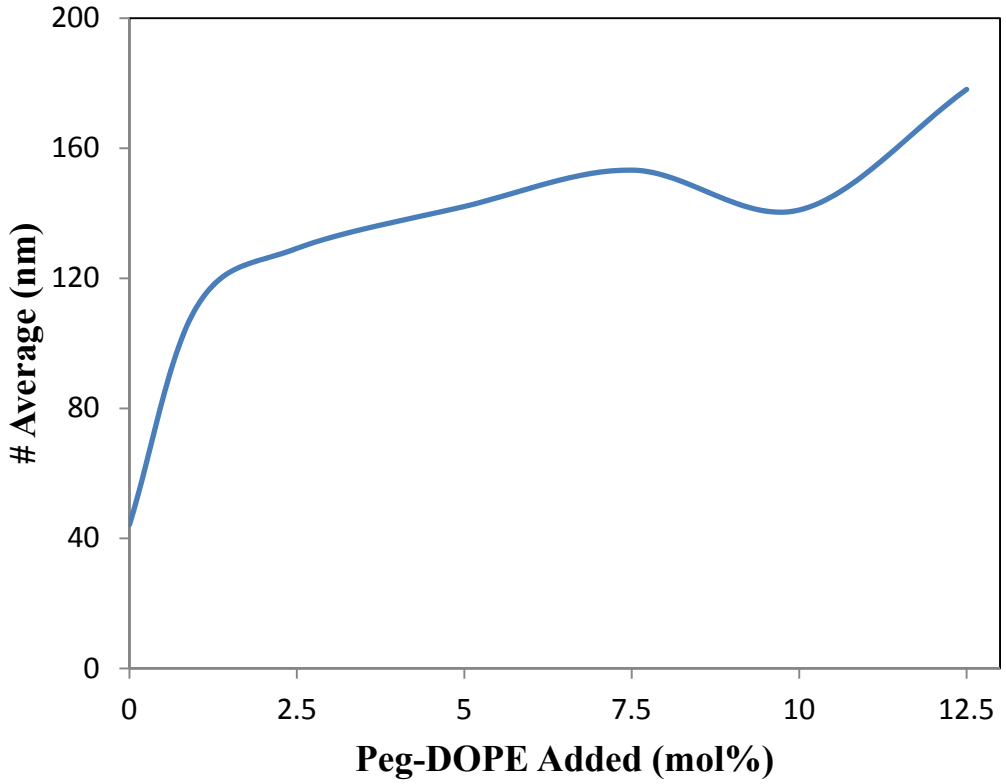

Figure 2.39. DLS plot showing the increase of number average diameter with increased additions of DOPE-PEG.

PEGylated nanoparticles are often characterized by their PEG surface coverage. When the wt% PEG is obtained (either by TGA or an iodine assay), the surface coverage in

nm^2/PEG can be theoretically calculated (section 2.4.4.). The optimum PEG surface coverage was found for lipid-coated Gd-MTX with 15 mol% PEG added (Table 2.1), a PEG surface coverage of 2.3 nm^2/PEG.

Table 2.1. DOPE-PEG coverages of Gd-MTX NCPs PEGylated by post-insertion.

DOPE-PEG (mol%)	DOPE-PEG (wt%)	DOPE-PEG (molecules/particle)	PEG Coverage (nm^2/PEG)
5	2.3	6054	8.1
10	4.5	9871	5.0
15	8.2	18032	2.7

The post-insertion method for PEGylating lipid-coated Gd-MTX NCPs was abandoned because there were concerns as to whether this approach compromised the stability of the lipid-coated formulation. It is known that increased amounts of PEG in a formulation can lead in instability because of the surfactant-nature of PEG lipids.[32] Control experiments monitoring the change in number average diameter of PEGylated particles after subsequent washes and centrifugations showed that even after three washes, liposomes were prevalent in the supernatant, as indicated by a cationic ζ potential, indicating instability of the formulation. The pre-insertion method of liposomal PEGylation was also probed. This procedure is done by preparing PEG-containing liposomes followed by lipid encapsulation of the NCPs. Liposomes containing different amounts of PEG were prepared and analyzed for PEG content. Particles do not differ from the as-synthesized Gd-MTX by SEM (Figure 2.40), but an increase in number average diameter is observed by DLS, presumably due to addition of the bulky PEG lipid (Figure 2.41). PEG lipids and other organic molecules are not typically visible by SEM.

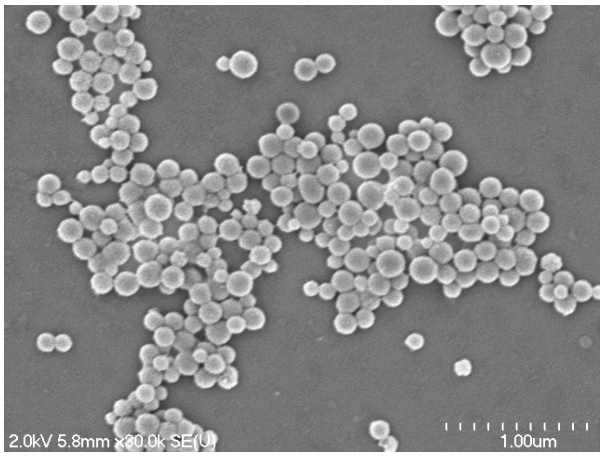

Figure 2.40. SEM micrograph of Gd-MTX@Lipid PEGylated with 5 mol% DOPE-PEG.

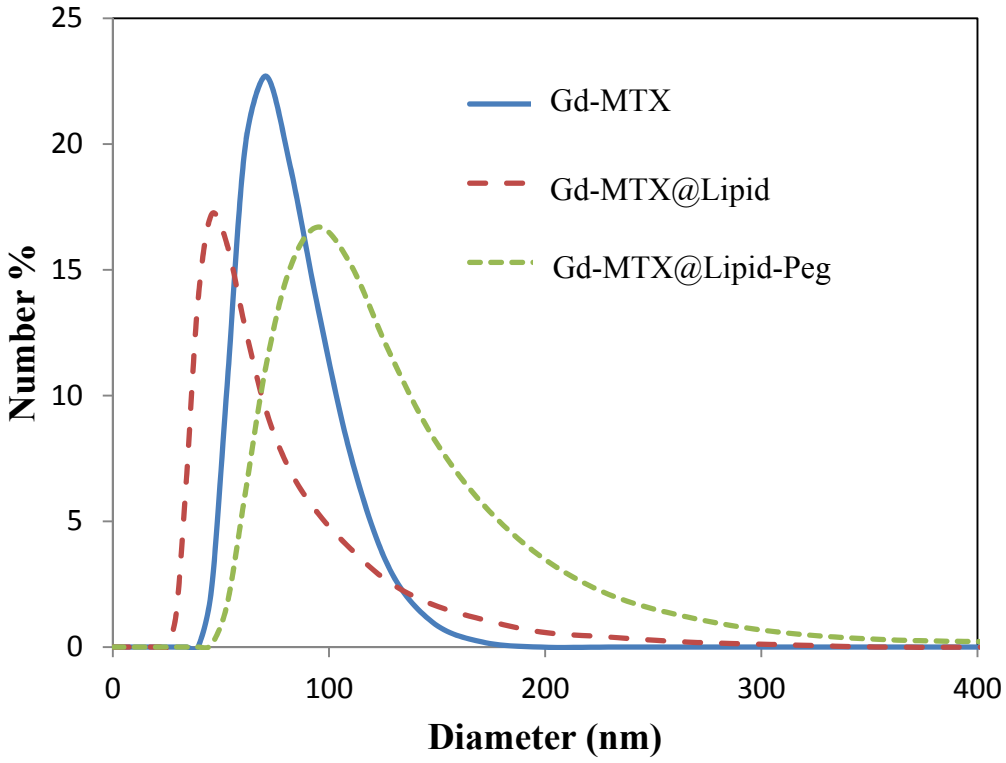

Figure 2.41. DLS number average plots of Gd-MTX, Gd-MTX@Lipid, and PEGylated (5 mol%) Gd-MTX@Lipid.

Particles PEGylated with 5, 10, and 15 mol% pre-inserted liposomes were analyzed for PEG surface coverage using an iodine assay (Table 2.2). The optimum PEG coverage

(3.0 nm^2/PEG) is obtained using 10 mol% PEG-containing liposomes. PEG content decreases with 15 mol% PEG (4.9 nm^2/PEG) likely due to destabilization of the lipid bilayer by the addition of excess PEG-DOPE. TGA comparing Gd-MTX, lipid-coated Gd-MTX, and PEGylated Gd-MTX shows that both lipid-coated formulations exhibit less organic weight loss (Figure 2.42). This observation disputes our hypothesis that lipid-coated formulations should possess more organic weight. Our conclusion is that lipid coating of this system, as well as with pre-inserted PEG liposomes, results in loss of some MTX drug loading.

Table 2.2. DOPE-PEG coverages of Gd-MTX NCPs PEGylated by pre-insertion.

DOPE-PEG (mol%)	DOPE-PEG (wt%)	DOPE-PEG (molecules/particle)	PEG Coverage (nm^2/PEG)
5	5.0	10908	4.5
10	7.5	6544	3.0
15	4.6	10017	4.9

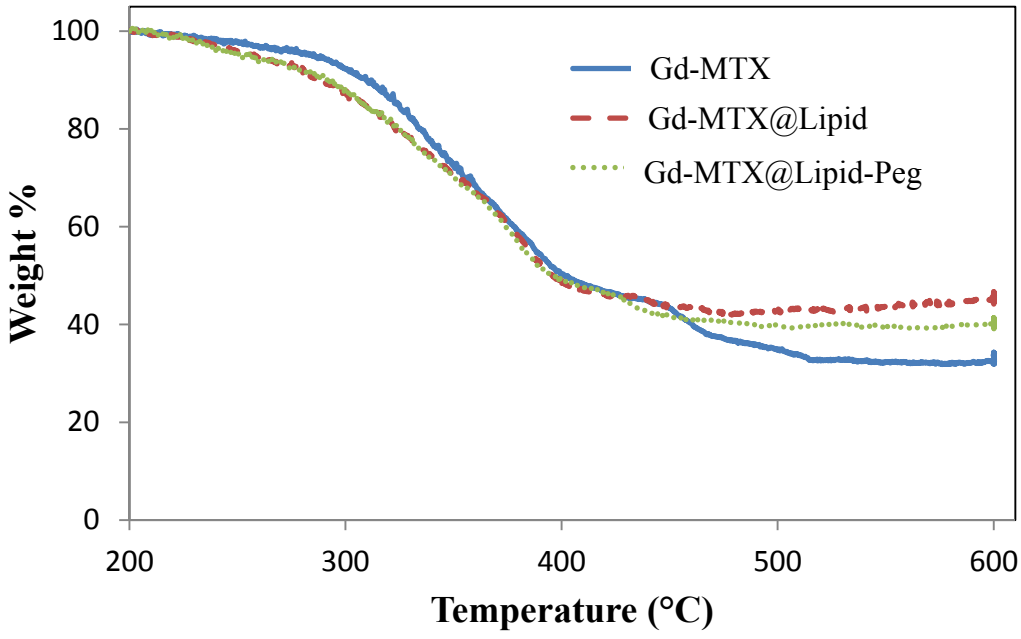

Figure 2.42. TGA plots of Gd-MTX, Gd-MTX@Lipid, and PEGylated Gd-MTX@Lipid with 5 mol% DOPE-PEG by pre-insertion.

2.3. Conclusion

After unsuccessful stabilization of previously-synthesized Zr-MTX NCPs, Gd-MTX NCPs with an extremely high MTX drug loading (71.6 wt%) were synthesized by a solvothermal method and stabilized by encapsulation with a 1:1 (by mol) DSTAP/DOPE lipid bilayer. The formulation was rendered an active targeting agent by addition of an anisamide-DOPE conjugate which targets sigma receptors. Encapsulation of the NCP in a functionalized lipid bilayer allows for targeted delivery and controlled release to cancer cells, as shown by enhanced efficacy of the targeted formulation against Jurkat acute lymphoblastic leukemia cells. The NCPs were doped with the phosphor $Ru(bpy)_3^{2+}$, and the resulting formulation was utilized as an optical imaging agent. Confocal microscopy exhibited enhanced uptake of the targeted NCPs. The lipid-coated Gd-MTX NCPs can be PEGylated using either a post- or pre-insertion method, but there is the possibility that addition of PEG to the lipid membrane using this procedure compromises the stability imparted by the membrane.

2.4. Experimental Details

2.4.1. Materials and Methods

All chemicals, unless otherwise noted, were purchased from Fisher or Sigma Aldrich and used without further purification. Methotrexate was purchased from TCI America. 1,2-dioleoyl-3-trimethylammonium propane, chloride salt (DOTAP) and 1,2-stearoyl-3-trimethylammonium propane, chloride salt (DSTAP) were purchased from Avanti Polar Lipids. L-α-phosphatidylethanolamine, dioleoyl (DOPE) was a gift from Sigma Aldrich. Cell culture supplies: fetal bovine serum (Sigma), RPMI-1640 growth medium (Gibco), penicillin-streptomycin (Sigma), and phosphate buffered saline (Gibco) were purchased from

the Tissue Culture Facility in the Lineberger Cancer Center at UNC-Chapel Hill. AnnexinV FITC conjugate was purchased from Invitrogen.

Microwave reactions were carried out in a CEM Discovery microwave or a CEM MARS 5 microwave. Scanning electron microscopy (SEM) was performed with a Hitachi 4700 Field Emission Scanning Electron Microscope, and transmission electron microscopy (TEM) was performed with a JEM 100CX-II Transmission Electron Microscope. A Cressington 108 Auto Sputter Coater equipped with a Au/Pd (80/20) target and MTM-10 thickness monitor was used to coat samples before SEM imaging. SEM micrographs were obtained on glass slides, and TEM micrographs were obtained on carbon-coated copper grids. Thermogravimetric analysis (TGA) was done on a Shimadzu TGA-50 equipped with a platinum pan, and samples were heated at a rate of 3°C/min under air. Powder x-ray diffraction (PXRD) data was gathered on a Bruker SMART APEX II diffractometer using Cu radiation, and powder patterns were analyzed with the APEX II package using the phase ID plugin. UV-Vis absorption spectra were obtained using a Shimadzu UV-2401 PC UV-Vis recording spectrophotometer. Size and zeta potential information was obtained on a Malvern ZetaSizer dynamic light scattering instrument. A Varian 820-MS Inductively-Coupled Plasma Mass Spectrometer was used to determine metal contents. Confocal microscopic images were obtained on glass slides and imaged on the Olympus FlowView500 confocal microscope at the UNC-CH Microscope and Imaging Facility. Images were analyzed using ImageJ (with the UCSD plugin) and PhotoShop.

MR images were acquired on a Siemens 3T Allegra (Siemens Medical Systems, Erlagen, Germany) with a CP coil. A 3D FLASH sequence was utilized to compute T_1 maps with seven different flip angles (2, 5, 10, 20, 30, 40, and 60). Imaging parameters were

FOV=190 x 190 x 64 mm^3, matrix size= 128 x 128 x 32, TR/TE= 40/1.64 ms, total data acquisition time was 30 min. The net magnetization from the region of interest of each sample was fit using a Marquardt-Levenberg algorithm for multiparametric nonlinear regression analysis using MATLAB program. Longitudinal relaxivity, T_1 was calculated from these data, and r_1 was determined from the slope of $1/T_1$ versus $[Gd^{3+}]$ plot. A 2-D multiple echo spin echo sequence was used to estimate T_2 maps. In total, 32 echoes with an echo spacing of 6.2 ms (the first echo time) were obtained; TR was 3000 ms. FOV and matrix size were set to 190 x 190 mm^2 and 128 x 128. The slice thickness was 2 mm. The total data acquisition time was about 6 minutes and 29 seconds. Transverse relaxivity, r_2, was determined from the slope of $1/T_2$ versus $[Gd^{3+}]$ plot. All images were acquired on a 9.4T Bruker BioSpec system with a 35 mm quadrature RF transmit and receive coil.

2.4.2. Synthesis of Reagents

Synthesis of $[Ru(5,5'\text{-}CO_2H\text{-}bpy)(bpy)_2](PF_6)_2$ (carboxylated $Ru(bpy)_3^{2+}$ derivative). 5,5'-CO_2(Et-bpy) and $Ru(bpy)_2Cl_2$ were prepared according to a literature method.[25] $Ru(bpy)_2Cl_2$ (1.16g, 2.39 mmol) and 1.45 equivalents of 5,5'-CO_2(Et-bpy) (1.04g, 3.46 mmol) were refluxed under argon in 160 mL of H_2O:EtOH (1:1 v/v) for 8 h. After the removal of ethanol by rotary evaporation, the complex was precipitated by the addition of 5 mL of saturated aqueous ammonium hexafluorophosphate. This crude product was filtered and washed with ether, then hydrolyzed by reflux under argon in 100 mL of 4M HCl overnight. Precipitation was achieved by the addition of 5 mL of saturated aqueous ammonium hexafluorophosphate. The product was filtered and washed with water to remove excess HCl and washed with ether. Yield: 1.79 g (80%). ^{1}H NMR (DMSO-d_6): 8.99 (d, 2H),

8.89 (m, 4H), 8.53 (d, 2H), 8.20 (m, 4H), 7.99 (s, 2H), 7.84 (d, 2H), 7.78 (d, 2H), 7.59 (t, 2H), 7.49 (t, 2H).

Synthesis of DOPE-AA. DOPE (50 mg, 0.067 mmol) was reacted with 4-methoxybenzoic acid (103.5 mg, 0.672 mmol) in dichloromethane (10 mL, anhydrous), in the presence of N,N'-dicyclohexylcarbodiimide (27.2 mg, 0.134 mmol) and 4-dimethylaminopyridine (16.42 mg, 0.134 mmol) under nitrogen. The reaction was stirred at room temperature for 24 h in the dark. After the removal of dichloromethane by rotary evaporation, the crude product was dissolved in chloroform, and the solution was washed with 4% Na_2CO_3, 0.2M HCl, water, and then dried over $MgSO_4$. The resulting crude product was purified by column chromatography using silica gel and 5:1 chloroform/methanol (v/v) as the eluent. The product was obtained after removal of the solvents. Yield: 30 mg (51%). ^{1}H NMR ($CDCl_3$): δ 7.82 (d, J =7.6 Hz, 2H); 6.78 (s, 2H); 5.31 (m, 4H); 3.76 (s, 3H); 2.15 (s, 4); 1.97 (s, 6H); 1.62 (s, 10H); 1.46 (s, 4H); 1.21 (t, J= 14 Hz, 30H); 0.85 (t, J = 6 Hz, 6H).

Synthesis of Liposomes. 1:1 (by mol) DSTAP/DOPE liposomes were prepared by combining DSTAP (5 mg, 0.007117 mmol) and DOPE (5.295 mg, 0.07117 mmol) in chloroform. The solvent was removed under vacuum by rotary evaporation. The resulting lipid film was further dried under vacuum then hydrated with 1 mM aq. KCl. The dispersion was extruded three times through a 0.6 μm polycarbonate filter membrane and ten times through a 0.1 μm polycarbonate filter membrane. The resulting liposome formulation can be stored up to 1 week at 4 °C. Liposomes were made to contain DOPE-AA by incorporating 10 mol% DOPE-AA in the initial chloroform solution.

Synthesis of DOPE-FITC. Fluorescein isothiocyanate (FITC, 27.3 mg, 0.07 mmol) was added to a small round-bottom flask and dried under high vacuum for 1 h. Anhydrous methanol (10 mL) and triethylamine (6.2 μL) were added to the round-bottom flask, followed by 0.5 mL DOPE (100 mg/mL, 0.067 mmol in anhydrous dichloromethane). The reaction was magnetically stirred under nitrogen gas at room temperature for 5 h in the dark. After the removal of solvent by rotary evaporation, the product was redissolved in methanol (77 mg, 25 mg/mL, 100% yield).

2.4.3. Synthesis of MTX and Folate-Containing NCPs

Synthesis of La-MTX NCP. Both $LaCl_3 \cdot 7H_2O$ (22.15 mg, 0.0600 mmol) and MTX (13.65 mg, 0.0300 mmol) were dissolved in 6 mL DMF containing 5 μL 6M (0.0300 mmol, 1 eq.) HCl aq. The solution was heated in a sealed microwave vessel at 80 °C for 10 min without stirring. The product was isolated from the resulting yellow dispersion by centrifugation at 13,000 rpm for 15 min, washed by subsequent sonication and centrifugation, with DMF and EtOH, and dispersed in EtOH.

Synthesis of Pr-MTX NCP. Both $Pr(NO_3)_3 \cdot 6H_2O$ (13.36 mg, 0.0300 mmol) and MTX (13.65 mg, 0.0300 mmol) were dissolved in 6 mL DMF and heated in a sealed microwave vessel at 80 °C for 5 min without stirring. The product was isolated from the resulting yellow dispersion by centrifugation at 13,000 rpm for 15 min, washed by subsequent sonication and centrifugation, with EtOH, and dispersed in EtOH.

Synthesis of Gd-MTX NCP. Both $Gd(NO_3)_3 \cdot 6H_2O$ (13.54 mg, 0.0300 mmol) and MTX (13.63 mg, 0.0300 mmol) were dissolved in 6 mL DMF and the solution was heated in a sealed microwave vessel at 80 °C for 5 min without stirring. The product was isolated from the resulting yellow dispersion by centrifugation at 13,000 rpm for 15 min, washed by

sonication and centrifugation, with DMF then EtOH, and dispersed in EtOH. Yield: 15.6 mg (85%).

Synthesis of Gd-Folate NCP. 22.5 mg (0.0498 mmol) $Gd(NO_3)_3 \cdot 6H_2O$ was dissolved in 3 mL DMF, and 22.2 mg (0.0503 mmol) folic acid was dissolved in 7 mL DMF by heating at 50 °C. The solution was heated in a sealed microwave vessel at 80 °C for 5 min without stirring. The product was isolated from the resulting yellow dispersion by centrifugation at 13,000 rpm for 15 min, washed by sonication and centrifugation, with DMF then EtOH, and dispersed in EtOH. Yield: 7.5 mg (25.2%).

Synthesis of [Ru(5,5'-CO_2-bpy)(bpy)$_2$]-doped analogs of Gd-MTX and Gd-Folate. 10 mol% [Ru(5,5'-CO_2-bpy)(bpy)$_2$]-doped Gd-MTX was synthesized by the same procedure as Gd-MTX, but with the addition of 2.02 mg (0.00308 mmol, 10 mol%) [Ru(5,5'-CO_2H-bpy)(bpy)$_2$]$(PF_6)_2$ to the DMF solution. Particles were isolated in a yield of 20.9 mg (72%). 10 mol% [Ru(5,5'-CO_2-bpy)(bpy)$_2$]-doped Gd-Folate was synthesized by the same procedure as Gd-Folate, but with the addition of 3.3 mg (0.0050 mmol, 10 mol%) Ru(bpy)$_2$(bby-CO_2H) to the DMF solution. Particles were isolated in a yield of 9.45 mg (29%). Synthesis of lipid-coated versions of doped Gd-MTX and Gd-Folate were carried out by the same methods described above.

2.4.4. Lipid-Coating Procedures

Synthesis of DOTAP/Cholesterol-coated Zr-MTX. Particle dispersions of Zr-MTX and 1:1 (by mol) DOTAP/cholesterol liposomes in 1 mM aq. KCl were combined and the sample was vortexed and sonicated then isolated by centrifugation at 6,000 rpm for 10 min to remove excess liposomes. The lipid-coated sample was dispersed in 1 mM aq. KCl.

Synthesis of DSTAP/DOPE-coated Gd-MTX or Gd-Folate. Particle dispersions of

Gd-MTX (or Gd-Folate) and 1:1 (by mol) DSTAP/DOPE liposomes in 1 mM aq. KCl were heated to 70 °C and mixed together. The dispersion was vortexed and was allowed to sit at room temperature for 30 minutes. Empty liposomes were removed by centrifugation at 6,000 rpm for 10 minutes, and the resulting particles were dispersed in 1 mM aq. KCl by sonication.

Synthesis of DSTAP/DOPE-AA-coated Gd-MTX or Gd-Folate. These lipid-coated NCPs were produced by the same technique as above, but using 1:1 (by mol) DSTAP/DOPE liposomes, incorporating 10 mol% DOPE-AA.

Release Profiles. An amount of testing material was isolated by centrifugation and redispersed in 1 mM aq. KCl. The material was placed in a length of 10K molecular weight cutoff cellulose dialysis tubing and submerged in 250 mL 8 mM PBS (pH = 7.4, 37 °C). At designated time intervals, 1 mL aliquots were removed from the dialysate and analyzed by UV-Vis spectroscopy at 305 nm.

PEGylation of Lipid-Coated Gd-MTX By Post-Insertion. PEG_{2K}-DOPE micelles were prepared by dissolving PEG-DOPE in 1 mM aq. KCl. Lipid-coated Gd-MTX was prepared as described above. The lipid-coated particles were isolated by centrifugation at 6,000 rpm for 10 min and dispersed in 1 mM aq.KCl. Volumes of DOPE-PEG micelles were added resulting in varying mol% PEG-DOPE amounts, and the samples were mixed by vortexing. The particles were isolated by centrifugation at 6,000 rpm for 10 min and dispersed in 1 mM aq. KCl.

PEGylation of Lipid-Coated Gd-MTX By Pre-Insertion. 1:1 (by mol) DSTAP/DOPE liposomes containing 5 mol% (or another amount) PEG-DOPE were prepared using the procedure described for non-PEGylated liposomes. Gd-MTX nanoparticles were

isolated by centrifugation, dispersed in 1 mM aq. KCl, and heated to 70 °C. PEGylated liposomes were added to the particles and the dispersion was vortexed and heated at 70 °C for 15 min. The lipid-coated particles were centrifuged at 6,000 rpm for 10 min to remove empty liposomes, and dispersed in 1 mM aq. KCl.

Determination of PEG Coverage By Iodine Assay. It is known that solutions of I_2/KI react with PEG, resulting in colored I-PEG species that can be assayed by UV-Vis spectrometry.[33-35] A standard curve of different concentrations (µg/mL) DOPE-PEG_{2K} was assembled by dissolving different amounts of DOPE-PEG_{2K} in aqueous solution containing 5 % (w/v) $BaCl_2$ in 1 N HCl and amounts of 10 g/L I_2 and 20 g/L KI. A maximum absorbance is observed at 500 nm (Figure 2.43) and is converted into a standard curve (Figure 2.44): $Abs_{500\ nm}$ = 0.0507(DOPE-Peg_{2K}, µg/mL)-0.0383.

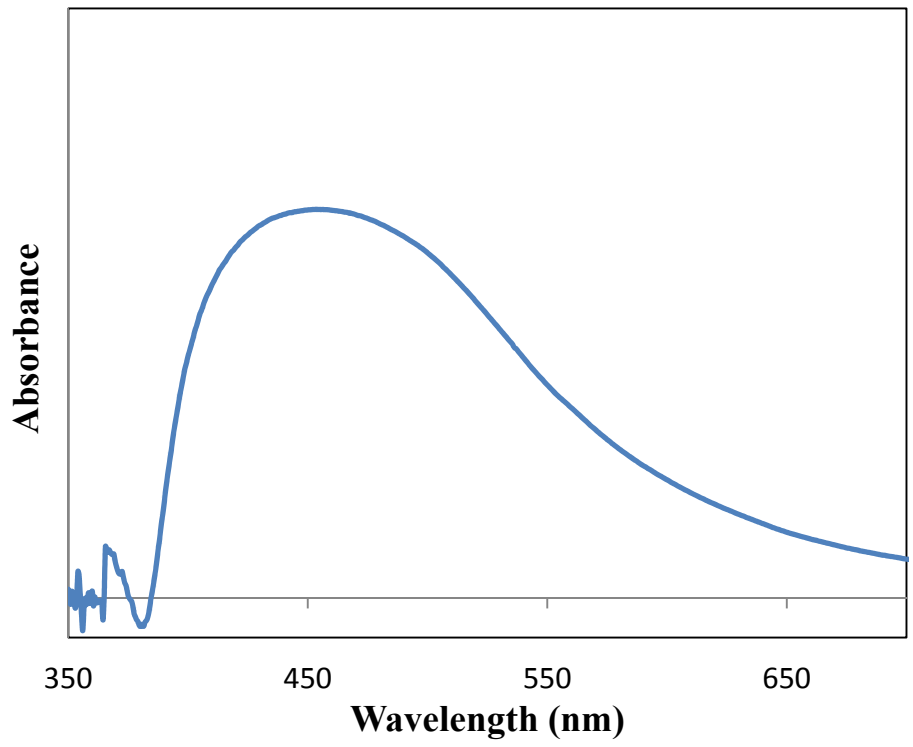

Figure 2.43. UV-Vis spectrum of DOPE-Peg_{2K} in a solution of I_2/KI, showing a maximum absorbance at ~460 nm. 500 nm was used as the standard curve absorbance to reduce any interference from other species in solution.

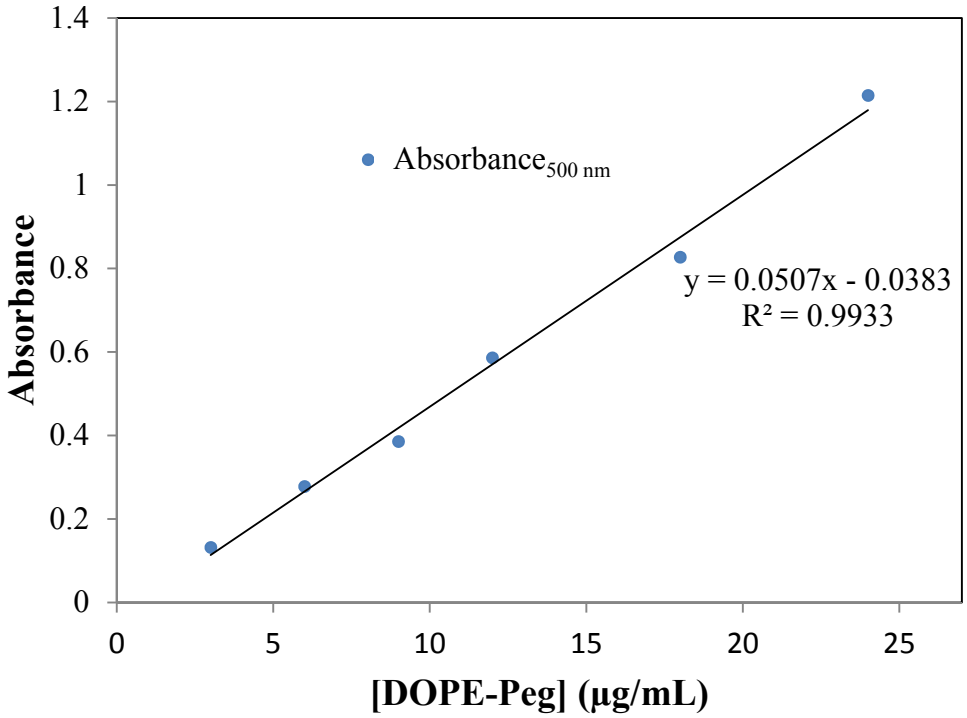

Figure 2.44. Standard curve at 500 nm for different concentrations of DOPE-Peg_{2K} in I_2/KI, $BaCl_2$ in 1 N HCl.

Samples of PEGylated Gd-MTX@Lipid for PEG content analysis were prepared by adding 0.5 mL of NCP dispersion to 1.5 mL H_2O, 0.5 mL $BaCl_2$ in 1 N HCl, and 37.5 µL aq. 10 g/L I_2 and 20 g/L KI. The samples were assayed by UV-Vis, and the absorbance at 500 nm was converted to µg/mL DOPE-Peg_{2K}. The concentration of DOPE-Peg_{2K} was converted into wt% DOPE-Peg_{2K} and PEG coverage in nm^2/PEG by the following theoretical calculation, assuming 5 wt% lipid bilayer, NCP diameter = 120 nm, NCP density (D) = 1 g/cm^3, molecular weight (mw) DOPE-PEG_{2K} = 2800 g/mol:

$$\frac{\mu g\ PEG}{\mu g\ PEG + \ \mu g\ NCP} = wt\ fraction\ (W)\ PEG$$

$$Surface\ Area\ (SA) = 4\pi r^2\ and\ Volume\ (V) = \frac{4}{3}\pi r^3$$

$$Where\ r = radius\ of\ NCP$$

$$Mass\ NCP\ (m) = V \times D$$

$$wt\ PEG\ per\ NCP\ (wt) = m \times W$$

$$Molecules\ PEG\ per\ NCP\ (M) = (wt \div mw) \times A$$

$$Where\ A = Avogadro's\ Number = 6.022\ \times 10^{23} molecules\ per\ mol$$

$$PEG\ Coverage\ (nm^2\ per\ PEG) = SA\ \div M$$

2.4.5. In Vitro Assay Methods

Cell Lines. CCRF-CEM acute lymphoblastic leukemia cells (ATCC# CCL-119) and Jurkat acute lymphoblastic leukemia cells (ATCC# TIB-152) were purchased from the Tissue Culture Facility of Lineberger Comprehensive Cancer Center at the University of North Carolina at Chapel Hill. Both cell lines were maintained as a suspension in RPMI-1640 growth medium (Cellgro) supplemented with 10% fetal bovine serum (Sigma) and 2% penicillin-streptomycin (Sigma).

Cytotoxicity Assays Against CCRF-CEM Cells. For the 3 h assay: confluent CCRF-CEM cells were isolated by centrifugation, dispersed in fresh RPMI-1640 media, and cell density determined by a hemocytometer. Cells were plated in 6-well plates at a cell density of 1 x 10^6 cells/well in 1.5 mL RPMI-1640 medium and incubated overnight at 37 °C and 5% CO_2. Aliquots of MTX or Zr-MTX particles in medium were added to the wells for

MTX concentrations (in μM) of 0, 5, 12.5, 25, 50, and 100. Plates were incubated (37 °C, 5% CO_2) for 3 h. Viability was determined by the trypan blue exclusion assay.

For the 48 h assay: confluent CCRF-CEM cells were isolated by centrifugation, dispersed in fresh RPMI-1640 media, and cell density determined by a hemocytometer. Cells were plated in 6-well plates at a cell density of 5 x 10^4 cells/well in 1.5 mL RPMI-1640 medium and incubated overnight at 37 °C and 5% CO_2. Aliquots of MTX or Zr-MTX particles in medium were added to the wells for MTX concentrations (in μM) of 0, 5, 12.5, 25, 50, and 100. Plates were incubated (37 °C, 5% CO_2) for 48 h. Viability was determined by the trypan blue exclusion assay.

Cytotoxicity Assays Against Jurkat Cells. Confluent Jurkat cells were counted from the culture flask by hemocytometer. Cells were plated in 6-well plates at a cell density of 5 x 10^4 cells/well in 1.5 mL RPMI-1640 complete growth medium. The cells were incubated at 37 °C and 5% CO_2 overnight. MTX and particle dispersions of Gd-MTX and lipid-coated Gd-MTX (16 μM) in RPMI-1640 media and additional media were added to wells, resulting in MTX concentrations (μM) of 0, 0.25, 0.5, 1, 2, and 4. Cells were incubated (37 °C, 5% CO_2) with free MTX or particle for 48 h or for 72 h. Viability was determined by the trypan blue exclusion assay.

Viability Control Assays with Jurkat Cells. This assay was conducted to show that MTX is the only contributor to cytotoxicity and that Gd(III) has no bearing on the cytotoxicity. $Gd(NO_3)_3$, Gd-Folate, and lipid-coated Gd-Folate formulations were tested against Jurkat acute lymphoblastic leukemia cells. Confluent Jurkat cells were counted from the culture flask by hemocytometer. Cells were plated in 6-well plates at a cell density of 5 x 10^4 cells/well in 1.5 mL RPMI-1640 complete growth medium. The cells were incubated at

37 °C and 5% CO_2 overnight. Free Gd(III) and particle dispersions (200 μM) in RPMI-1640 media and additional media were added to wells, resulting in folate concentrations (μM) of 0, 0.5, 1, 2.5, 5, and 10. Cells were incubated (37 °C, 5% CO_2) with free Gd(III) salt or particles for 48 h. Viability was determined by the trypan blue exclusion assay.

Confocal Microscopy of [Ru(5,5'-CO_2-bpy)(bpy)$_2$]-doped Analogs of Gd-MTX and Gd-Folate. Wells in 6-well plates were seeded with 500,000 cells and 2 mL total of RPMI-1640 media (10% FBS, 2% penicillin-streptomycin). The plates were incubated for 24 h at 37 °C and 5% CO_2. Particle dispersions were prepared in RPMI-1640 medium, and aliquots of particle dispersions/additional media were added to the wells, resulting in a concentration of 0.04 mg/well for each particle. The cells were incubated with particles for 1 h, and cell suspensions were centrifuged. Cell pellets were re-suspended in PBS, 15 μL AnnexinV FITC conjugate was added, and the cells were allowed to sit at room temperature for 10 min. The cells were centrifuged and redispersed in 20μL of media. The entire cell suspension was placed on glass coverslips, adhered on glass slides with antifade mounting medium, and imaged at the UNC-CH Microscope and Imaging Facility.

2.5. References

(1) Davis, M. E.; Chen, Z.; Shin, D. M. *Nat. Rev. Drug Discov.* **2008**, *7*, 771.

(2) Krajinovic, M.; Moghrabi, A. *Pharmacogenomics* **2004**, *5*, 819.

(3) Chen, Y.-H.; Tsai, C.-Y.; Huang, P.-Y.; Chang, M.-Y.; Cheng, P.-C.; Chou, C.-H.; Chen, D.-H.; Wang, C.-R.; Shiau, A.-L.; Wu, C.-L. *Mol. Pharmaceutics* **2007**, *4*, 713.

(4) Dhanikula, R. S.; Argaw, A.; Bouchard, J.-F.; Hildgen, P. *Mol. Pharmaceutics* **2008**, *5*, 105.

(5) Kohler, N.; Sun, C.; Wang, J.; Zhnag, M. *Langmuir* **2005**, *21*, 8858.

(6) Kohler, N.; Sun, C.; Fichtenholtz, A.; Gunn, J.; Fang, C.; Zhang, M. *Small* **2006**, *21*, 785.

(7) Wosikowski, K.; Biedermann, E.; Rattel, B.; Breiter, N.; Jank, P.; Loser, R.; Jansen, G.; Peters, G. J. *Clin. Cancer Res.* **2003**, *9*, 1917.

(8) Yang, X.; Zhang, Q.; Wang, H.; Chen, H.; Zhang, F.; Gao, F.; Liu, L. *Colloids Surf. B* **2008**, *61*, 125.

(9) deKrafft, K. E., *Nanoscale Coordination Polymers for Biomedical Applications and Hybrid Materials for Solar Fuel Catalysis*. Ph.D. Dissertation, University of North Carolina, Chapel Hill, **2012**.

(10) Cavka, J. H.; Jakobsen, S.; Olsbye, U.; Guillou, N. L.; Bordiga, C. S.; Lillerud, K. P. *J. Am. Chem. Soc.* **2008**, *130*, 13850.

(11) Stathopoulos, G. P. *Anticancer Drugs* **2010**, *21*, 732.

(12) Li, J.; Chen, Y.-C.; Tseng, Y.-C.; Mozumdar, S.; Huang, L. *J. Controlled Release* **2010**, *142*, 416.

(13) Liu, D.; Kramer, S. A.; Huxford-Phillips, R. C.; Wang, S.; Della Rocca, J.; Lin, W. *Chem. Commun.* **2012**, *48*, 2668.

(14) van Schooneveld, M. M.; Vucic, E.; Koole, R.; Zhou, Y.; Stocks, J.; Cormode, D. P.; Tang, C. Y.; Gordon, R. E.; Nicolay, K.; Meijerink, A.; Fayad, Z. A.; Mulder, W. J. M. *Nano Lett.* **2008**, *8*, 2517.

(15) Troutier, A.-L.; Delair, T.; Pichot, C.; Ladavire, C. *Langmuir* **2005**, *21*, 1305.

(16) Olson, F.; Hunt, C. A.; Szoka, F. C.; Vail, W. J.; Papahadjopoulos, D. *Biochim. Biophys. Acta* **1979**, *557*, 9.

(17) Ashley, C. E.; Carnes, E. C.; Phillips, G. K.; Padilla, D.; Durfee, P. N.; Brown, P. A.; Hanna, T. N.; Liu, J.; Phillips, B.; Carter, M. B.; Carroll, N. J.; Jiang, X.; Dunphy, D. R.; Willman, C. L.; Petsev, D. N.; Evans, D. G.; Parikh, A. N.; Chackerian, B. W.; Peabody, D. S.; Brinker, C. J. *Nat. Mater.* **2011**, *10*, 389.

(18) Liu, J.; Stace-Naughton, A.; Jiang, X.; Brinker, C. J. *J. Am. Chem. Soc*. **2009**, *131*, 1354.

(19) Vilner, B. J.; John, C. S.; Bowen, W. D. *Cancer Res.* **1995**, *55*, 408.

(20) Aydar, E.; Palmer, C. P.; Djamgoz, B. A. *Cancer Res.* **2004**, *64*, 5029.

(21) Banerjee, R.; Tyagi, P.; Li, S.; Huang, L. *Int. J. Cancer* **2004**, *112*, 693.

(22) John, C. S.; Vilner, B. J.; Geyer, B. C.; Moody, T.; Bowen, W. D. *Cancer Res.* **1999**, *59*, 4578.

(23) Ganapathy, M. E.; Prasad, P. D.; Huang, W.; Seth, P.; Leibach, F. H.; Ganapathy, V. *J. Pharmacol. Exp. Ther.* **1999**, *289*, 251.

(24) Cobos, E. J.; Entrena, J. M.; Nieto, F. R.; Cendan, C. M.; Del Pozo, E. *Curr. Neuropharmacol.* **2008**, *6*, 344.

(25) Liu, D.; Huxford, R. C.; Lin, W. *Angew. Chem. Int. Ed.* **2011**, *50*, 3696.

(26) Papahadjopoulous, D.; Allen, T. M.; Gabizon, A.; Mayhew, E.; Matthay, K.; Huang, S. K.; Lee, K. D.; Woodle, M. C.; Lasic, D. D.; Redemann, C.; Martin, F. J. *Proc. Natl. Acad. Sci. USA* **1991**, *88*, 11460.

(27) Woodle, M. C.; Lasic, D. D. *Biochim. Biophys. Acta* **1992**, *1113*, 171.

(28) Gabizon, A.; Catane, R.; Uziely, B.; Kaufman, B.; Safra, T.; Cohen, R.; Martin, F.; Huang, A.; Barenholz, Y. *Cancer Res.* **1994**, *54*, 987.

(29) Lasic, D.; Martin, F. *Stealth Liposomes*; CRC Press: Boca Raton, FL, 1995.

(30) Klibanov, A. L.; Maruyama, K.; Torchilin, V. P.; Huang, L. *FEBS Lett.* **1990**, *268*, 235.

(31) Uster, P. S.; Allen, T. M.; Daniel, B. E.; Mendez, C. J.; Newman, M. S.; Zhu, G. Z. *FEBS Lett.* **1996**, *386*, 243.

(32) Li, S.-D.; Huang, L. *Biochim. Biophys. Acta* **2009**, *1788*, 2259.

(33) Sims, G. E. C.; Snape, T. J. *Anal. Biochem.* **1980**, *107*, 60.

(34) Guttman, D. E.; Higuchi, T. *J. Am. Pharm. Assoc.* **1956**, *45*, 668.

(35) Chang, J.-H.; Ohno, M.; Esumi, K.; Meguro, K. *J. Am .Oil Chem. Soc.* **1988**, *65*, 1664.

CHAPTER 3

Hafnium-Based Nanoscale Coordination Polymers for Delivery of Pemetrexed

3.1. Introduction

3.1.1. Pemetrexed

Pemetrexed (PMX) is an antifolate chemotherapeutic (Figure 3.1) that works by inhibiting multiple enzyme targets in the folic acid pathway and ultimately aiding in apoptotic cell death.[1,2] This antifolate is used alone or in combination with cisplatin for treatment of non-small cell lung cancer (NSCLC) and is currently being surveyed for use in the treatment of other tumor types.[3-5] Even though PMX is a very potent chemotherapeutic, this efficacy comes packaged with a multitude of side effects resulting from high doses such as mucositis, hematological toxicity, and increased risk of infection.[2,5] Considering the drawbacks that come with all small molecule chemotherapy drugs, PMX is an ideal candidate for incorporation into an NCP. Similarly to methotrexate, PMX possesses two carboxylate groups that can be used for coordination to a binding metal. To the best of our knowledge, no nanoscale drug delivery vehicles for the delivery of PMX have been reported.

This chapter presents the synthesis and characterization of PMX-containing NCPs. Hf-PMX particles (19.7 wt% PMX) were stabilized by addition of a lipid bilayer and rendered an active targeting agent via incorporation of an anisamide-lipid conjugate. This formulation was shown to have greater efficacy against free PMX in *in vitro* cytotoxicity assays against two NSCLC cell lines.

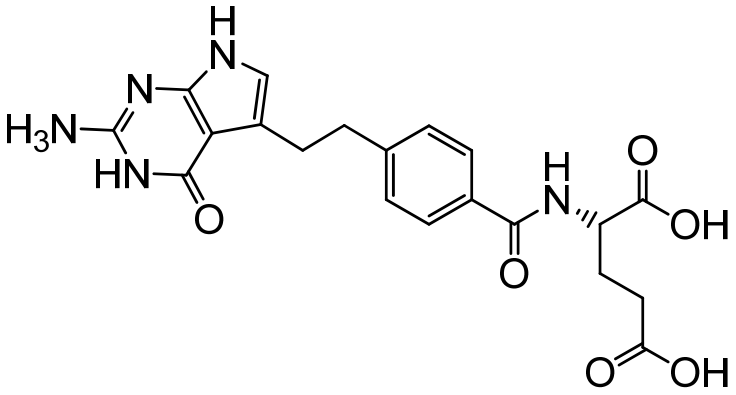

Figure 3.1. Structure of the antifolate pemetrexed (PMX).

3.2. Results and Discussion

3.2.1. UV-Visible Analysis – Pemetrexed

Like methotrexate, PMX can be detected by UV-Vis spectroscopy (Figure 3.2); the UV-Vis spectrum of PMX is however highly pH dependent.[6] Two standard curves were prepared: one using 8 mM PBS for Zr- or Gd-PMX NCP analysis ($Absorbance_{225\ nm}$ = 0.0155(μM PMX) – 0.0007) and another using 0.1 M H_3PO_4 for Hf-PMX analysis ($Absorbance_{285\ nm}$ = 0.0053(μM PMX) + 0.0049). These UV-Vis standard equations were used for analysis of PMX for drug loading data and release profiles.

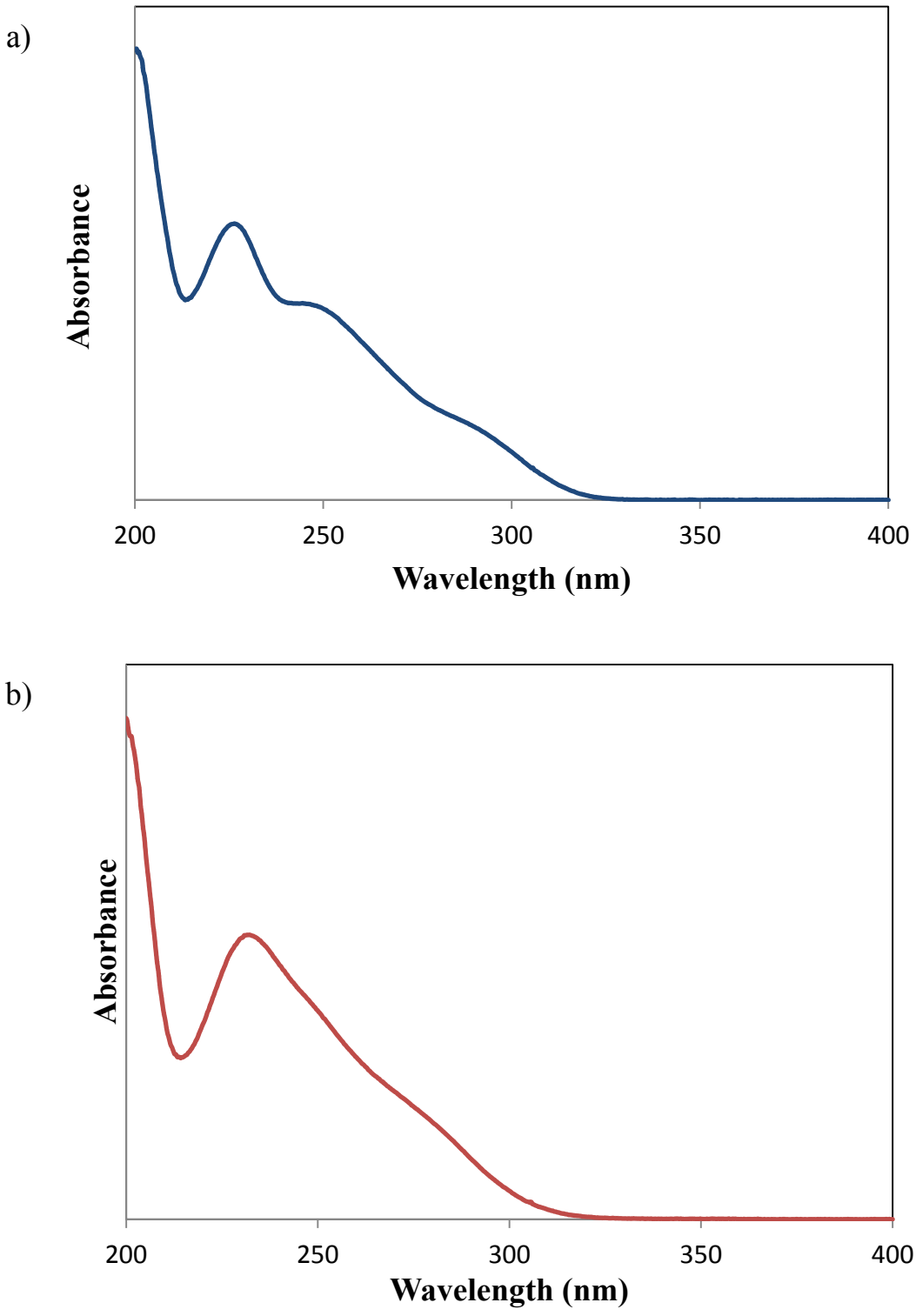

Figure 3.2. UV-Vis plots of PMX in (a) 8 mM PBS and (b) 0.1 M H_3PO_4, both media used for generating standard curves for PMX concentrations.

3.2.2. Synthesis and Characterization of Mn-PMX NCP

Crystalline particles of Mn-PMX were prepared by a surfactant-templated heating method in which $MnCl_2 \cdot 4H_2O$ and Na_2PMX were reacted in a reverse microemulsion (W = 15) with 0.1 M CTAB/0.5 M 1-hexanol in isooctanes at 80 °C for 20 min. Rod-like particles ~1 μm long and ~200 nm wide by SEM (Figure 3.3) were produced. These particles have a ζ potential of -22.3 mV, indicating that these NCPs are carboxylate-terminated and can potentially be lipid-coated by mixing with cationic liposomes. Mn-PMX possesses crystalline attributes by PXRD (Figure 3.4). Attempts to synthesize a single crystal for determination of a structure by X-ray diffraction were unsuccessful. These particles have a very high PMX drug loading by TGA, 69.9 wt%, and Mn-PMX has a 3:1 Mn:PMX molar ratio (Figure 3.5). These particles aggregate heavily in aqueous media, thus precluding their stabilization by lipid coating.

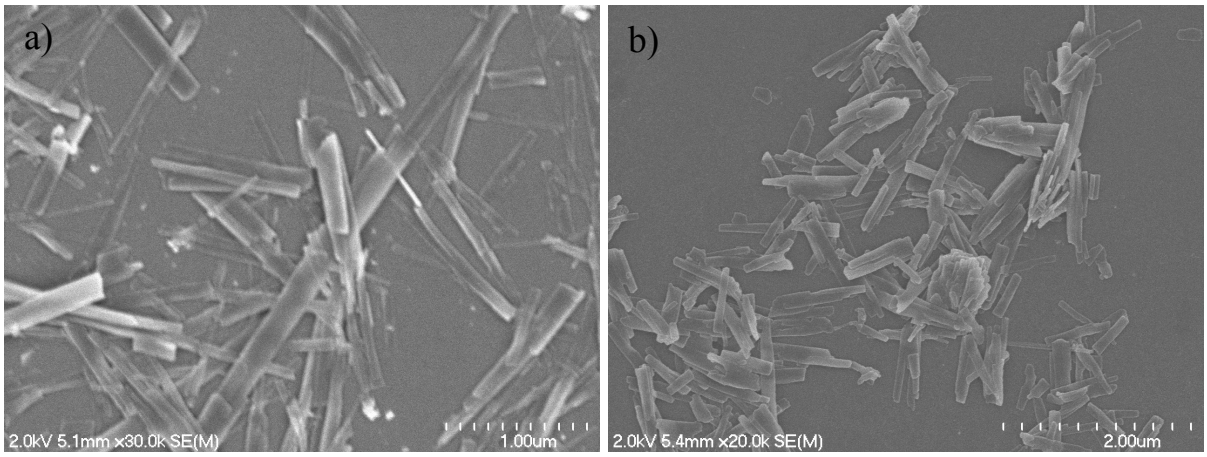

Figure 3.3. SEM micrographs of crystalline, rod-like Mn-PMX NCPs.

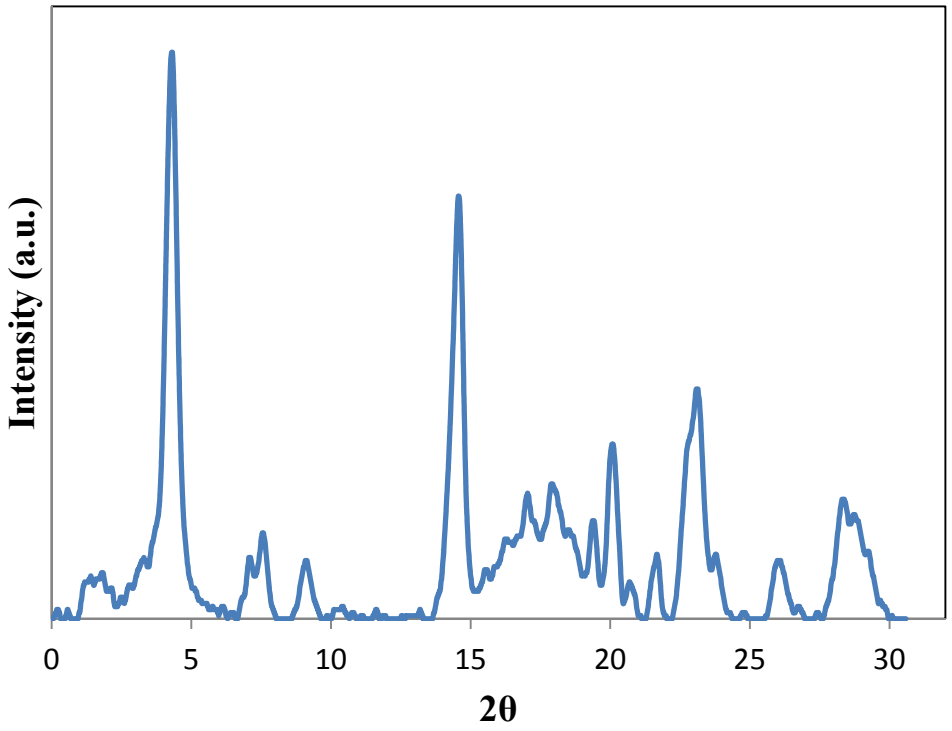

Figure 3.4. PXRD pattern of Mn-PMX nanorods.

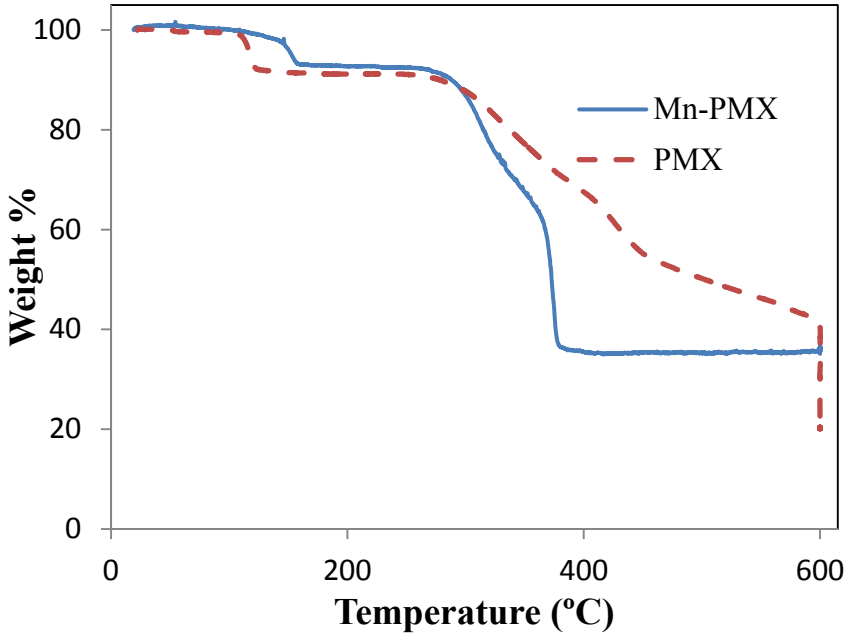

Figure 3.5. TGA of Mn-PMX showing PMX organic weight loss (69.9 wt% PMX) between 275 and 400 °C. TGA of PMX is shown for comparison.

3.2.3. Synthesis and Characterization of Zr-PMX NCP

Amorphous particles of Zr-PMX were synthesized by a solvothermal synthesis in which anhydrous $ZrCl_4$ and Na_2PMX were heated in 5 % v/v H_2O in DMF at 60 °C for 5 min. The resulting blue particles (yield = 85.8 %) are between 250-300 nm by SEM (Figure 3.6) and 273.3 nm (Z average diameter) with a PDI of 0.069 by DLS. Zr-PMX possesses an extremely high PMX drug loading of 60.0 wt% by TGA (Figure 3.7). This drug loading is further supported by the low Zr content of the particles by ICP-MS. Several attempts were made to decrease the size of Zr-PMX, but without success. Additionally, considering the previous issues experienced with stabilization of Zr-MTX, it was decided to pursue synthesis of PMX-containing NCPs using a trivalent lanthanide as the binding metal.

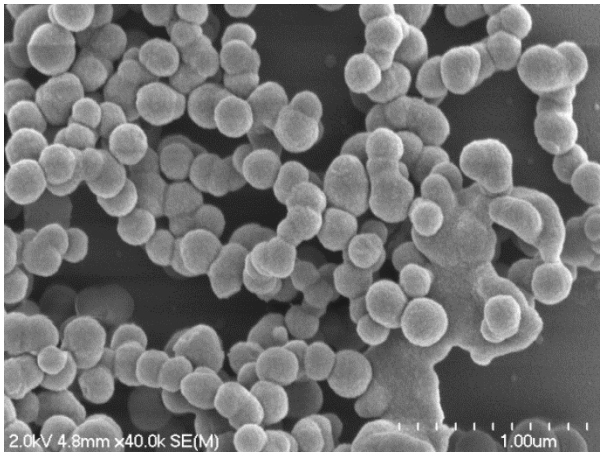

Figure 3.6. SEM micrograph of Zr-PMX NCPs.

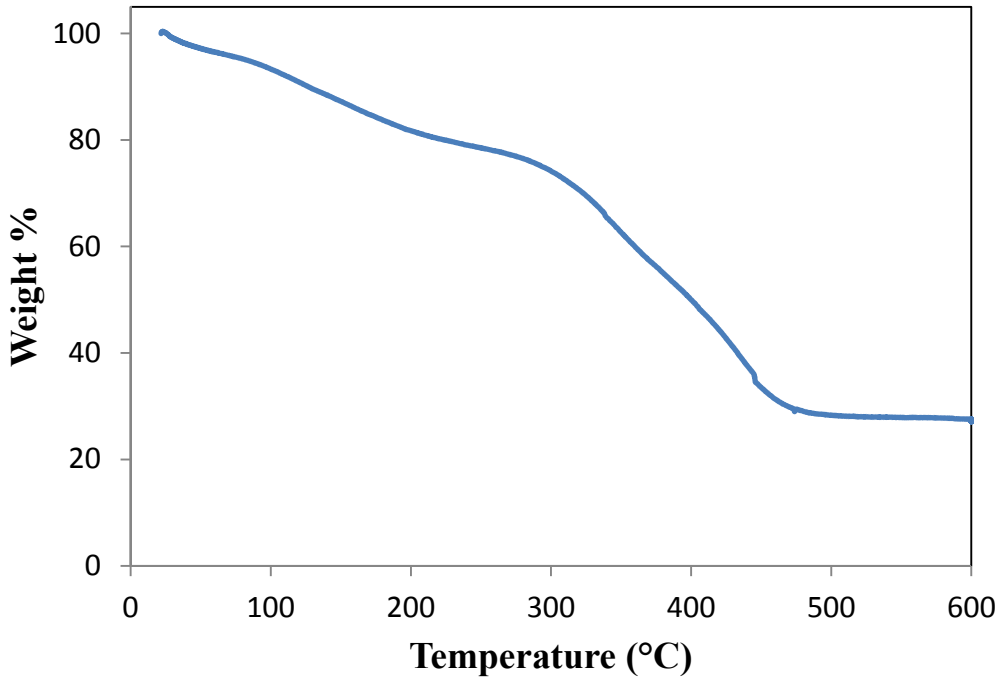

Figure 3.7. TGA plot of Zr-PMX NCPs where the organic weight loss yields high PMX loading of 60.0 wt% between 275 and 450 °C.

3.2.4. Synthesis and Characterization of Gd-PMX NCP

Gd-PMX Synthesized by a Solvothermal Method. Particles of Gd-PMX were prepared using PMX instead of Na_2PMX. PMX was prepared by acidifying Na_2PMX by dissolving in H_2O, precipitating with 1 M aq. HCl, isolating by centrifugation then drying under vacuum. Gd-PMX was synthesized by a solvothermal technique in which $Gd(NO_3)_3 \cdot 6H_2O$ and PMX were dissolved in DMF and heated at 80 °C for 5 min to afford a brown product. Particles are spherical and between 100-200 nm in diameter by SEM (Figure 3.8) with a Z average diameter of 126.9 nm and PDI of 0.027 by DLS. With a ζ potential of -8.37 mV in 1 mM aq. KCl, these particles are ideal for further stabilization by use of liposome encapsulation. Gd-PMX is 65.0 wt% PMX by TGA with a 3:2 Gd:PMX molar ratio (Figure 3.9). This data is further supported by 13.3 wt% Gd by ICP-MS. Digestion of these

Gd-PMX NCPs in 15 mg/mL Na_2EDTA shows that the UV-Vis spectrum has been altered significantly from free PMX (Figure 3.10). We speculate that the oxidizing power of lanthanide nitrates (like $Gd(NO_3)_3$ used in the synthesis of Gd-PMX) may degrade PMX under these synthetic conditions. Thus, we sought to synthesize Gd-PMX NCPs using milder conditions, such as a surfactant-templated technique.

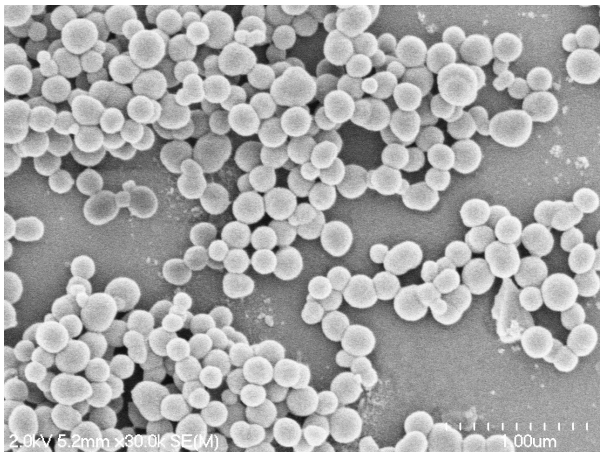

Figure 3.8. SEM micrograph of Gd-MTX NCPs formed by solvothermal synthesis.

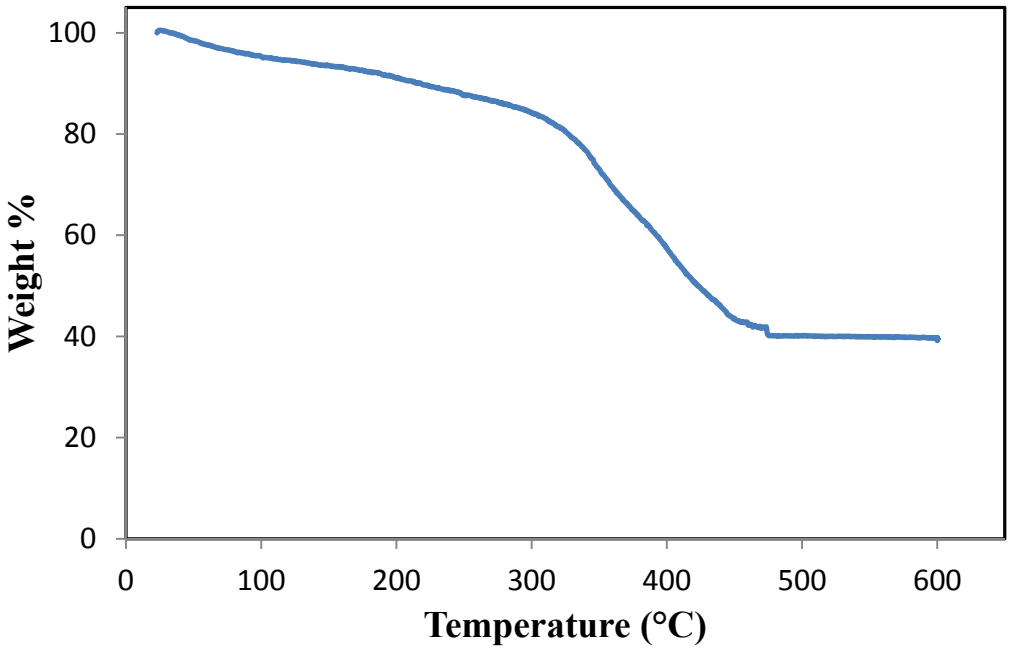

Figure 3.9. TGA plot of Gd-PMX NCPs synthesized by solvothermal synthesis showing weight loss corresponding to 65.0 wt% PMX drug loading between 300 and 450 °C.

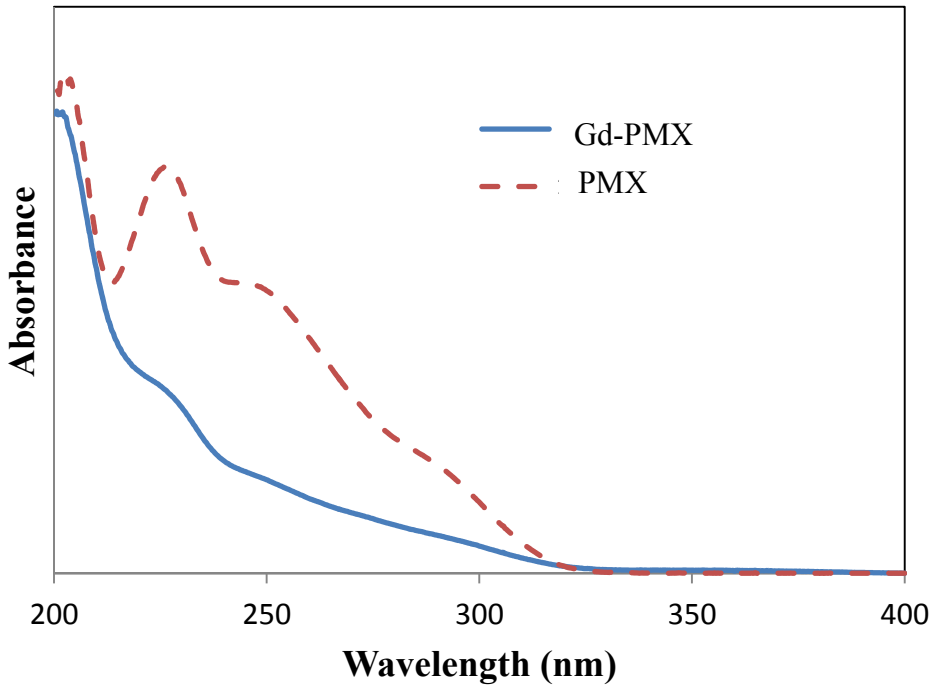

Figure 3.10. UV-Vis plot of digested Gd-PMX NCPs synthesized by a solvothermal synthesis, compared to free PMX at the same pH.

Smaller particles of Gd-PMX were prepared by a surfactant-assisted method ($W = 15$) in which aqueous nanodroplets of $Gd(NO_3)_3 \cdot 6H_2O$ and Na_2PMX in a 0.1 M CTAB/0.5 M 1-hexanol in isooctanes organic phase were heated at 80 °C for 20 min. The resulting white product was between 20-50 nm in diameter by SEM and TEM (Figure 3.11) with a Z average diameter of 88.9 nm and a PDI of 0.158 in EtOH. The Gd-PMX particles have a ζ potential of -5.68 mV in 1 mM aq. KCl, and are not as anionic as previous NCP systems. The particles have a high PMX loading of 72.3 wt% by TGA (Figure 3.12), a drug loading that is supported by the low Gd content obtained by ICP-MS (11.7 wt%).

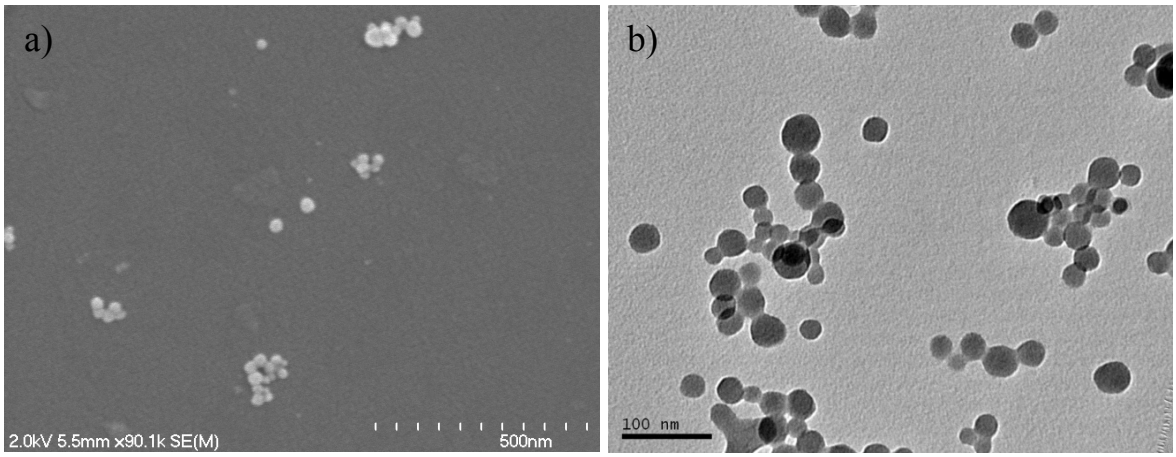

Figure 3.11. SEM (a) and TEM (b) micrographs of Gd-PMX NCPs synthesized by a surfactant-assisted heating technique.

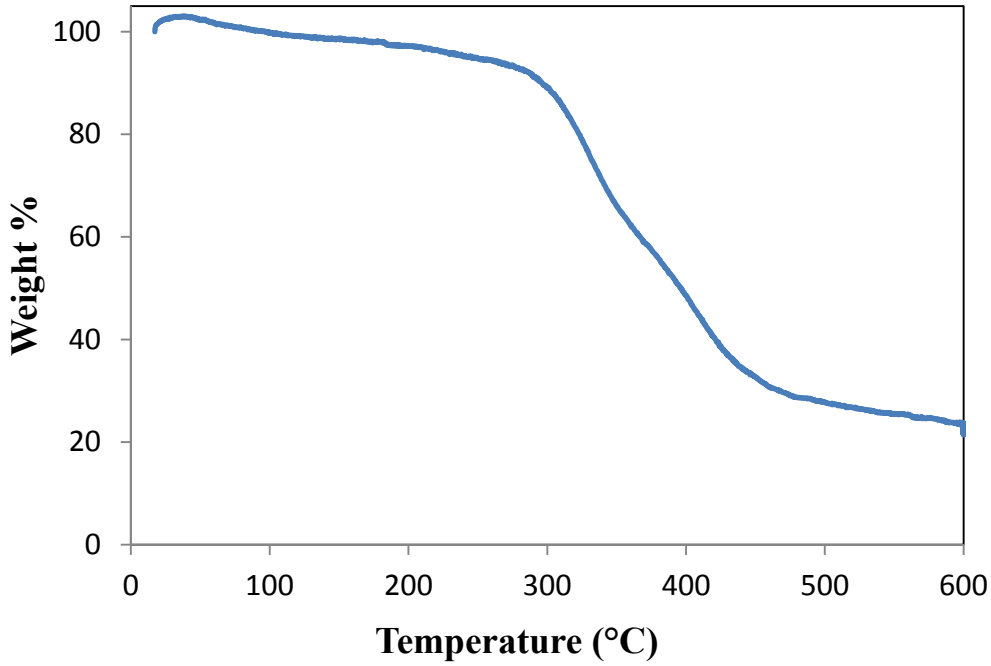

Figure 3.12. TGA plot of Gd-PMX synthesized by a surfactant-templated synthesis showing organic weight loss corresponding to 72.3 wt% PMX drug loading between 300 and 450 °C.

Digestion of these particles in 15 mg/mL Na_2EDTA aq. and analysis by UV-Vis shows that the spectrum for the digested particles matches that of free PMX (Figure 3.13). This indicates that the PMX drug does not degrade during NCP synthesis. The use of Gd(III)

ions in this material makes this material a good candidate as a MRI contrast enhancement agent. As shown in Figure 3.14, Gd-PMX has moderate r_1 and r_2 values, 4.254 $mM^{-1}s^{-1}$ and 13.943 $mM^{-1}s^{-1}$, respectively.

Stabilization of these NCPs was attempted by encapsulation within a 1:1 (by mol) DSTAP/DOPE lipid bilayer. Addition of increasing amounts of liposomes in 1 mM aq. KCl shows alleviation in aggregation as well as a shift from neutral to highly cationic ζ potentials (Figure 3.15). Despite these promising results, the PDI values remain large (indicating a polydisperse sample) and the lipid coating procedure could not be replicated.

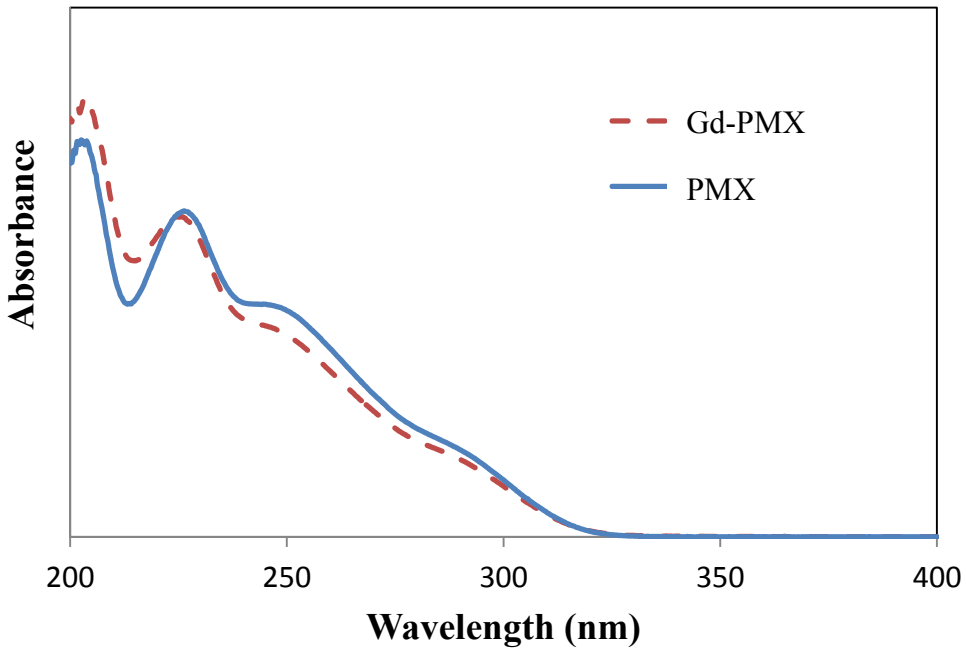

Figure 3.13. UV-Vis plot of Gd-PMX NCPs synthesized by the surfactant-assisted heating method, compared to free PMX showing that the PMX incorporated in the NCP has not degraded.

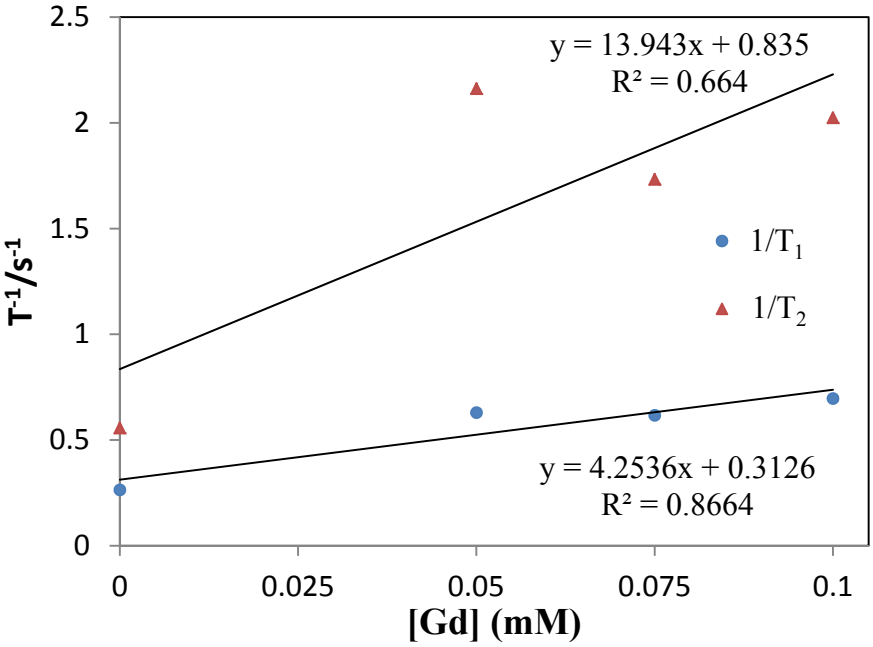

Figure 3.14. MR relaxivity plot for Gd-PMX (surfactant-templated) showing values for r_1 and r_2.

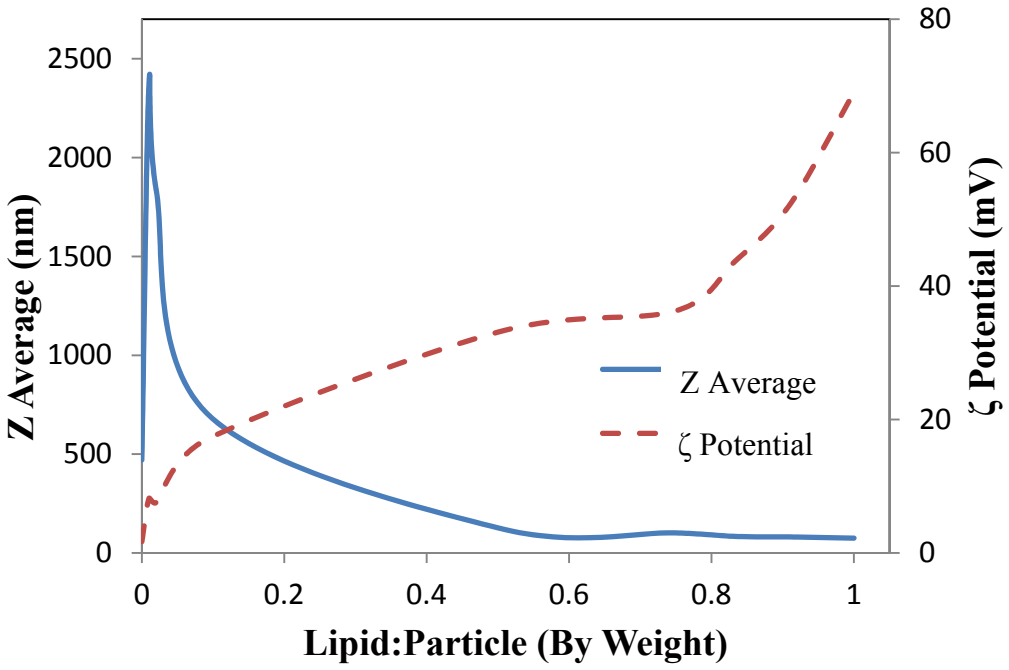

Figure 3.15. DLS Z average and ζ potential plots of Gd-PMX coated with increasing amounts of 1:1 (by mol) DSTAP/DOPE liposomes showing decreased particle aggregation and cationic ζ potentials with increased liposome volumes.

3.2.5. Synthesis and Characterization of Hf-PMX NCP

We sought to use Hf(IV) as the binding metal for PMX-containing NCPs as hafnium oxide is known to be an efficient radiotherapy agent.[7] The combination of PMX and Hf(IV) in an NCP would render this material a dual therapy: a radiotherapeutic with use of Hf(IV) and a chemotherapeutic with incorporation of PMX.

Particles of Hf-PMX were prepared by a solvothermal synthesis in which $HfCl_4$, Na_2PMX, and DOPA (a lipid-based capping agent) were heated in DMF at 80 °C for 10 min. These particles are slightly fused and between 200-400 nm in diameter by SEM (Figure 3.16) with a number average diameter of 563.5 nm and PDI of 0.585 by DLS in THF.

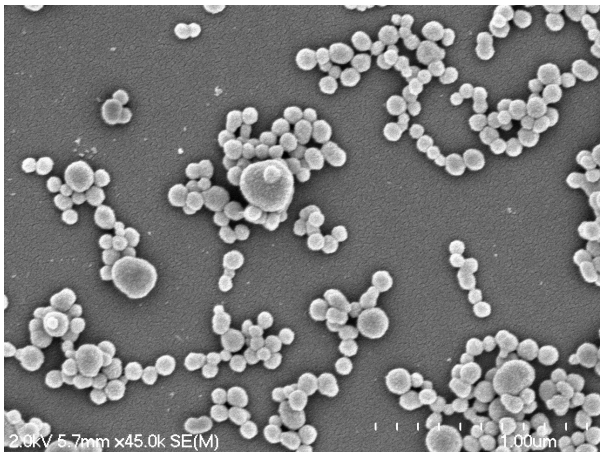

Figure 3.16. SEM micrograph of Hf-PMX NCPs synthesized by a solvothermal method.

TGA gives a PMX drug loading of 40.0 wt% (Figure 3.17). The large amount of inorganic weight remaining indicates that it is likely that these particles contain a large amount of hafnium oxide. Due to the large size of these particles and lack of dispersibility in THF (dispersibility in an organic solvent allows for stabilization by addition of a lipid layer incorporated in the DOPA surface capping agent), we moved to formulate smaller DOPA-capped Hf-PMX NCPs that are dispersible in organic solvent. Smaller particles of DOPA-

capped Hf-PMX were prepared by a reverse microemulsion (W = 7.4) using aqueous solutions of $HfOCl_2 \cdot 8H_2O$ and Na_2PMX dispersed in 0.3 M TritonX-100/1.5 M 1-hexanol in cyclohexane, with the addition of DOPA after 1 h of stirring at room temperature. The particles are spherical and <50 nm by TEM (Figure 3.18) with a Z average diameter of 92.6 nm and PDI of 0.114 in THF, indicating successful capping with DOPA.

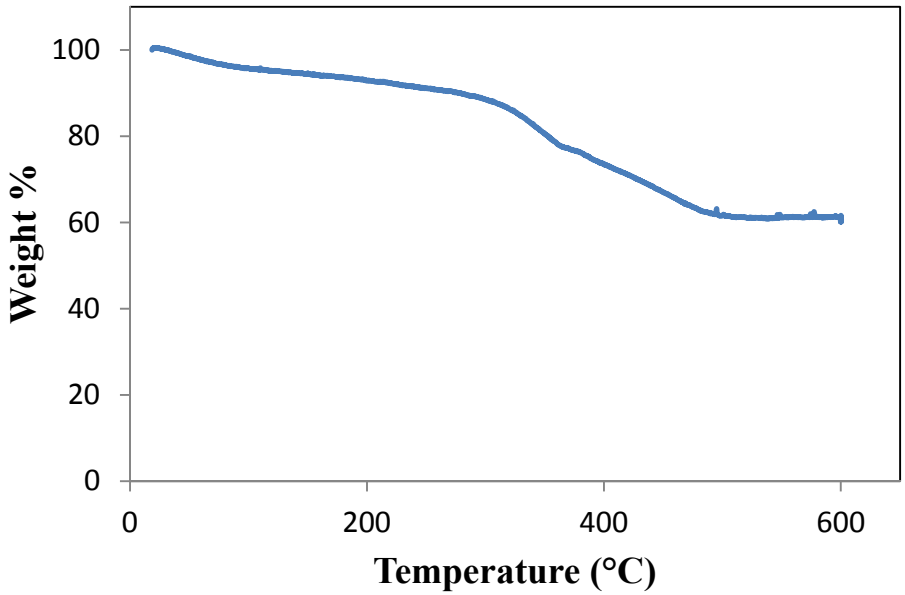

Figure 3.17. TGA plot of Hf-PMX synthesized by a solvothermal synthesis showing 40.0 wt% PMX drug loading.

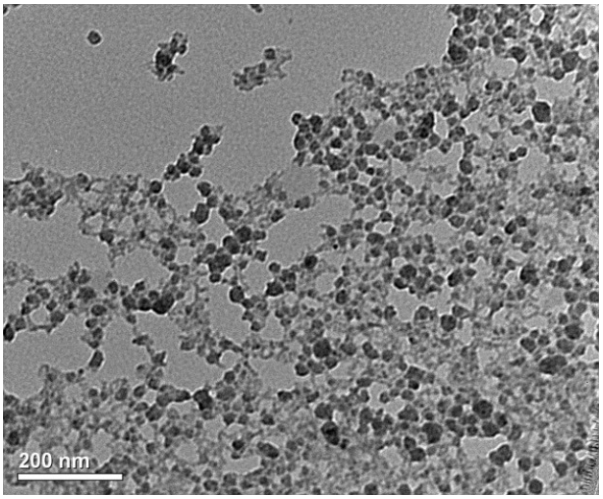

Figure 3.18. TEM micrograph of DOPA-capped Hf-PMX NCPs.

PMX drug loading of these particles is 19.7 wt% as determined by UV-Vis analysis of digested particles in 0.1 M H_3PO_4 ($Absorbance_{285\ nm}$ = 0.0053(μM PMX) + 0.0049); though this loading may be low when compared to other NCP materials, 19.7 wt% PMX is reasonable as PMX is a very potent anticancer agent. TGA of DOPA-capped Hf-PMX shows a large amount of organic weight which can be attributed to DOPA incorporated with the particles (Figure 3.19). It is assumed that all of the DOPA is bound to the NCP as the particles are subsequently washed and centrifuged with cyclohexane and THF. A release profile of Hf-PMX in 5 mM PBS at 37 °C reveals that the particles are unstable in phosphate buffer with a $t_{1/2}$ ~ 15 min. This experiment shows that need for this material to be further stabilized with addition of a lipid layer.

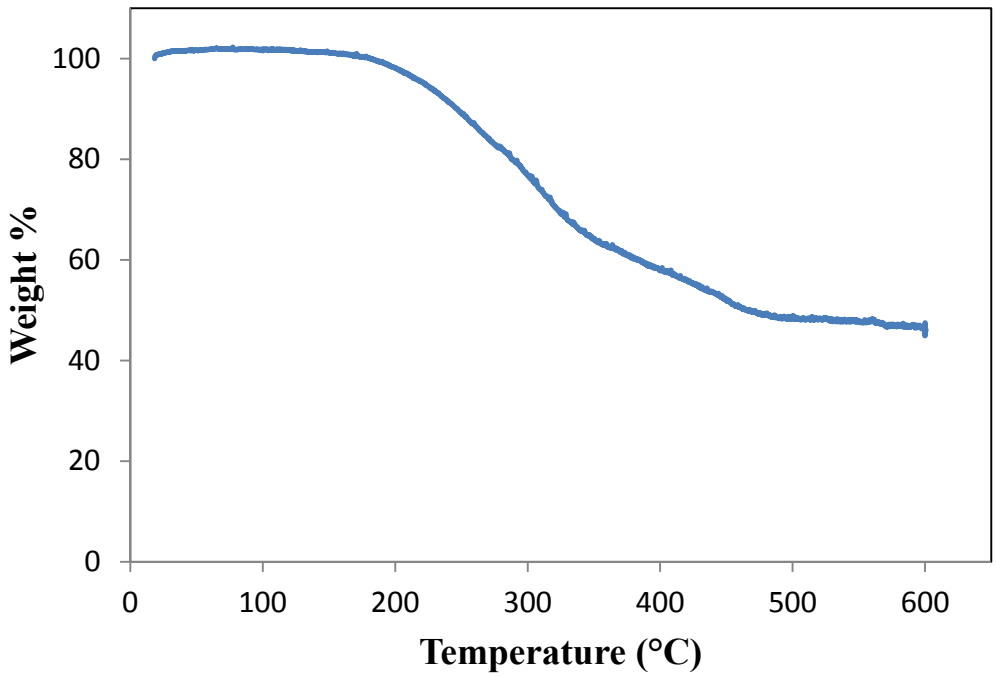

Figure 3.19. TGA plot of DOPA-capped Hf-PMX NCPs, showing organic weight loss attributed to DOPA and PMX.

3.2.6. Lipid Coating of Hf-PMX NCP

A simultaneous lipid coating and PEGylation procedure was done to try to stabilize the DOPA-capped Hf-PMX NCPs based on a previously-reported method.[8] The first attempt involved forming a dispersion of Hf-PMX particles with cholesterol, DOPC, and DSPE-Peg_{2K} in THF. This dispersion was added dropwise to a stirring volume of H_2O at 50 °C, and the THF was removed with a N_2 stream. The resulting lipid-coated NCPs had a Z average diameter of 120.4 nm and a PDI of 0.159 by DLS. Despite these promising results, this procedure did not enhance stability of the NCP nor could it be replicated consistently. However, when the lipid-coated formulation was prepared in 30 % v/v EtOH/H_2O instead of only H_2O, the resulting NCPs were more stable than the as-synthesized ones. These lipid-coated Hf-PMX particles did not differ in size or morphology from the as-synthesized NCPs by TEM (Figure 3.20) and had a Z average diameter of 135.9 nm with a PDI of 0.199. A release profile in 5 mM PBS at 37 °C showed that Hf-PMX lipid-coated with the procedure had a $t_{1/2}$ ~ 3 h compared to 15 min for the as-synthesized particles (Figure 3.21). We believe that more stable NCPs result from using 30 % v/v EtOH/H_2O because EtOH is important to ensure dispersibility of the as-synthesized particles as lipid coating occurs.

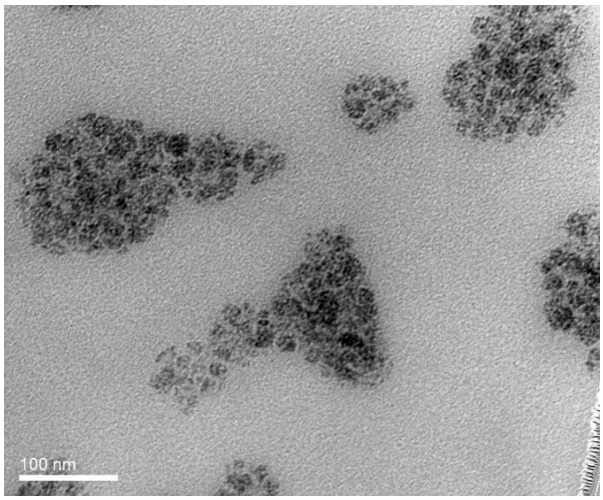

Figure 3.20. TEM micrograph of lipid-coated Hf-PMX NCPs.

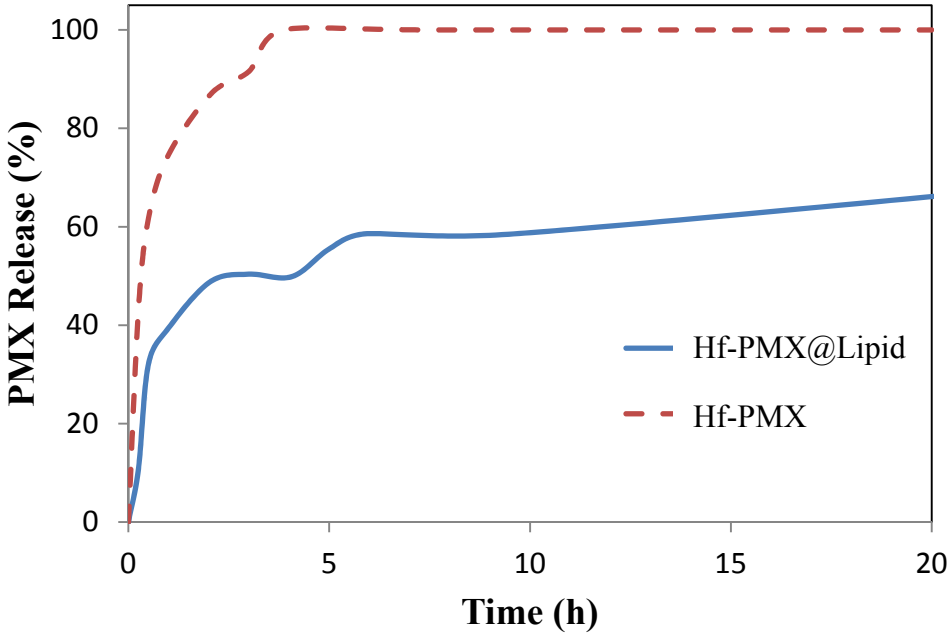

Figure 3.21. Release profile of DOPA-capped Hf-PMX ($t_{1/2}$ ~ 15 min) and Lipid-coated Hf-PMX ($t_{1/2}$ ~ 3 h) in 8 mM PBS at 37 °C showing stabilization with a lipid bilayer.

Stability was also demonstrated by observing the changes in diameter and PDI over 18 h in 5 mg/mL bovine serum albumin (BSA) in 5 mM PBS. Albumin is a blood protein used known to bind and aggregate poorly-PEGylated particles in the bloodstream. Stability is

assessed by observing little to no change of particle diameter as the particles are exposed to BSA over several hours. Over ~18 h, a 20 nm decrease in Z average is observed, likely due to the eventual settling out of larger particles (Figure 3.22). No aggregation or increase in particle diameter or PDI is observed, further establishing that the lipid-coated particles are stable under these conditions.

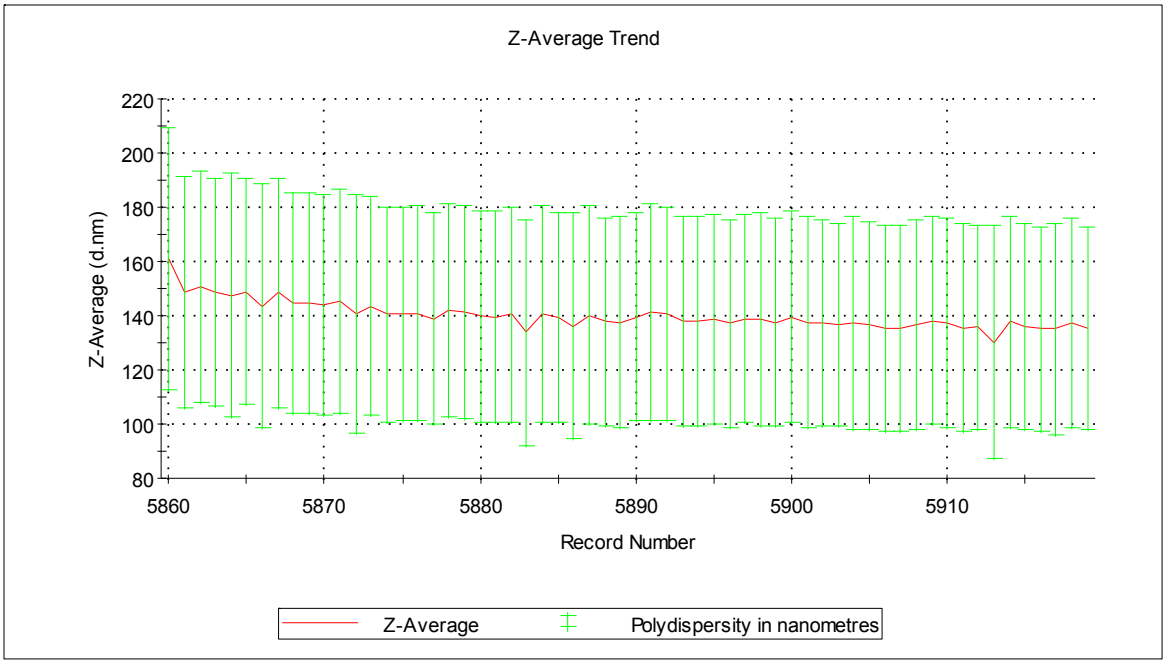

Figure 3.22. BSA assay testing the stability of lipid-coated Hf-PMX for 18 h.

Lipid-coated Hf-PMX was doped with a small amount (10 mol% of DSPE-Peg_{2K}) of DSPE-Peg_{2K}-AA, to afford a formulation that actively targets sigma receptors which are overexpressed in a number of epithelial cancer tissues.[9-13] This formulation was prepared by the same method as the non-targeted particles, but with the addition of both DSPE-Peg_{2K} and DSPE-Peg_{2K}-AA instead of only DSPE-Peg_{2K} in the lipid formulation. The resulting particles are the same size and morphology as the non-targeted formulation by TEM (Figure 3.23) with a Z average diameter of 134.5 nm and PDI of 0.334.

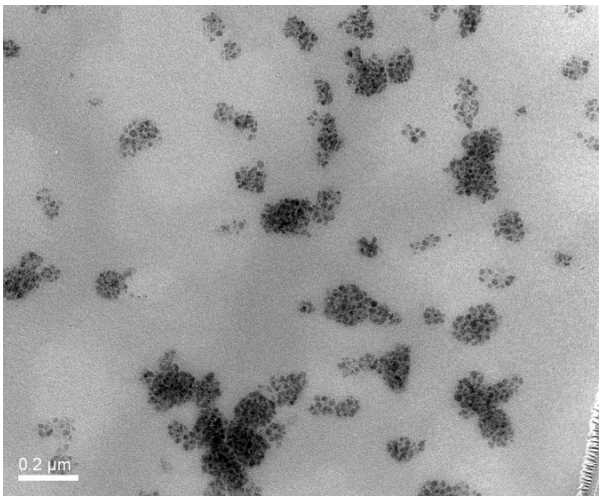

Figure 3.23. TEM micrograph of Hf-PMX@Lipid-AA NCPs.

3.2.7. Synthesis and Characterization of Hf-Folate NCP

Control vehicles using folic acid as the ligand instead of cytotoxic PMX were prepared by a solvothermal synthesis in which folic acid and $HfOCl_2 \cdot 8H_2O$ were heated at 80 °C in DMF in the presence of H_3PO_4 aq. The resulting particles have a Z average diameter of 128.6 nm and PDI of 0.136 in EtOH and are between 50 and 150 nm by TEM (Figure 3.24). These NCPs, Hf-Folate, are ~34 wt% folic acid by TGA (Figure 3.25).

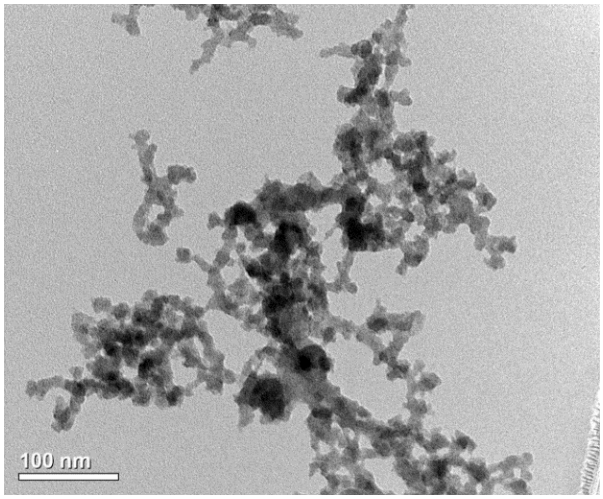

Figure 3.24. TEM micrograph of Hf-Folate control vehicles.

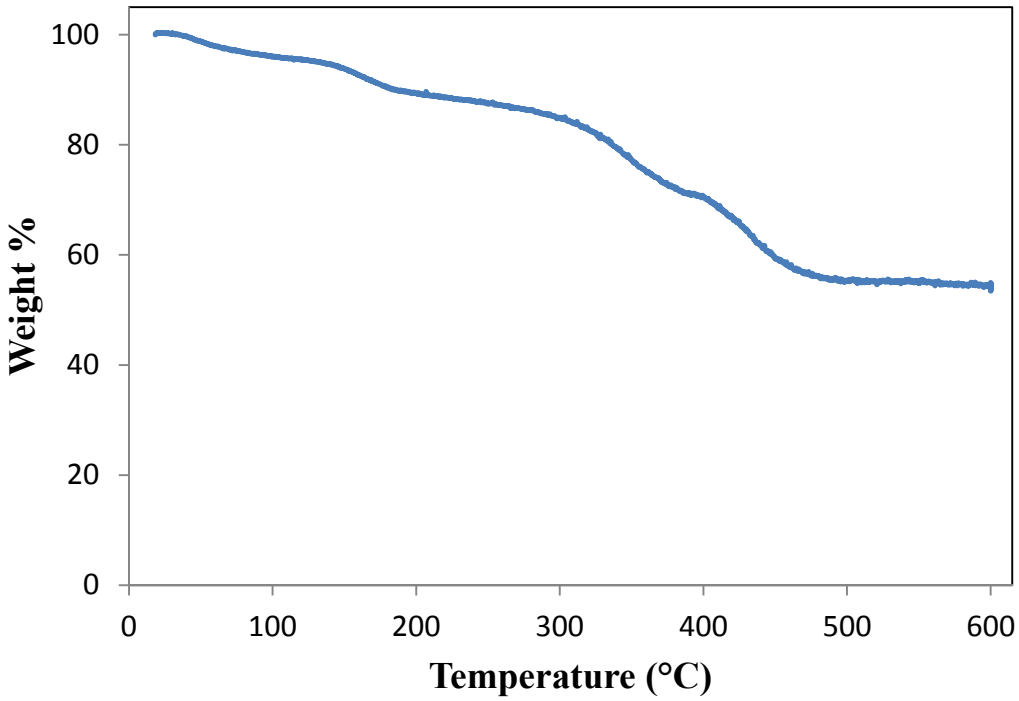

Figure 3.25. TGA of Hf-Folate NCPs showing 34 wt% folic acid organic weight loss between 300 and 500 °C.

The Hf-Folate NCPs were capped with DOPA by stirring a suspension of NCPs in an EtOH/$CHCl_3$ mixture with DOPA for 2 h at room temperature. The resulting DOPA-capped NCPs do not differ in size or morphology from the as-synthesized particles by SEM (Figure 3.26) or DLS (Z average diameter of 144.7 nm and PDI of 0.095 in THF). The DOPA-capped Hf-Folate control vehicles can be encapsulated in a lipid layer with cholesterol/DOPC/DSPE-Peg_{2K} by the same method used for lipid coating of Hf-PMX. The resulting Hf-Folate@Lipid NCPs have a Z average diameter of 135.6 nm and PDI of 0.299 in 5 mM PBS. Additionally, the Hf-Folate control vehicles were targeted with DSPE-Peg_{2K}-AA using the same procedure for Hf-PMX. These particles have a Z average diameter of 116.7 nm and PDI of 0.276.

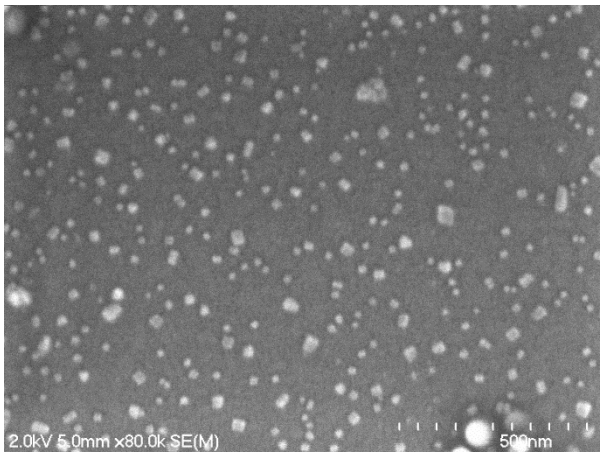

Figure 3.26. SEM micrograph of DOPA-capped Hf-Folate NCPs.

3.2.8. In Vitro Cytotoxicity Assays

Gd-PMX particles formed by the surfactant-templated method were tested *in vitro* against A549 non-small cell lung cancer cells and compared to the efficacy of free PMX. Cells were incubated with Gd-PMX or free PMX for 48 h and viability was determined by the trypan blue exclusion assay. IC_{50} values of both free PMX and the NCPs were similar with values of 0.75 μM and 1.0 μM, respectively (Figure 3.27). This means that the Gd-PMX particles degrade in cell medium and essentially are the equivalent of free PMX.

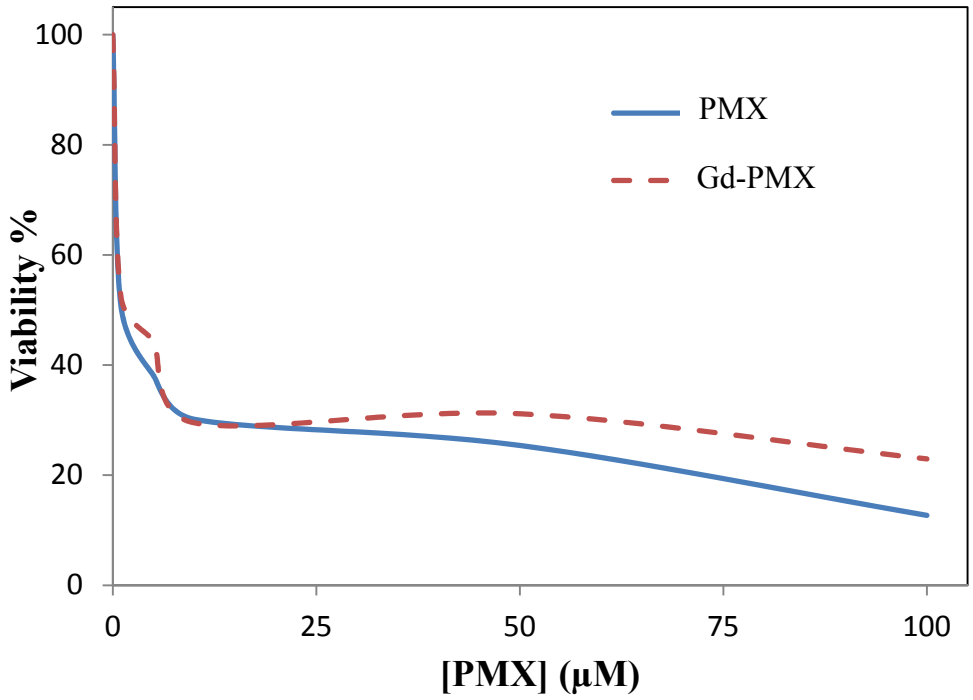

Figure 3.27. *In vitro* cytotoxicity curves of free PMX and Gd-PMX (by surfactant-assisted synthesis) showing equal cytotoxicity over 48 h for both agents.

Hf-PMX and the lipid-coated formulations of these NCPs were tested *in vitro* against two NSCLC cell lines. The NCI-H460 line, which overexpresses sigma receptors were tested to delve into the cytotoxic effect of this formulation as well as the efficiency of the AA targeting ligand. Over 48 h, enhanced efficacy from the targeted formulation was observed (Figure 3.28) compared to both the other formulations as well as free PMX. IC_{50} values were free PMX = 170 ± 10 nM, Hf-PMX = 200 ± 14 nM, Hf-PMX@Lipid = 195 ± 7 nM, and Hf-PMX@Lipid-AA = 63 ± 5 nM. The t test shows that there is a statistically significant difference between the IC_{50} values for Hf-PMX@Lipid and Hf-PMX@Lipid-AA with $\alpha = 0.087$ (≤ 0.1).

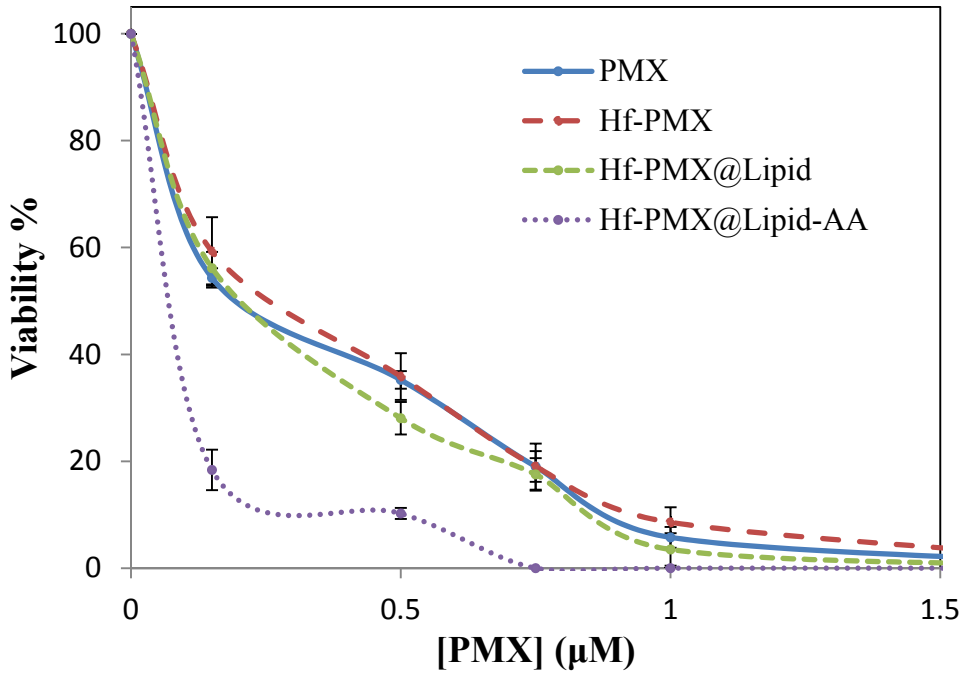

Figure 3.28. IC_{50} curves of Hf-PMX formulations against the NCI-H460 NSCLC cell line, showing enhanced efficacy from the AA-targeted formulation.

Additionally, the Hf-PMX formulations were tested *in vitro* against the A549 NSCLC cell line. This cell line expresses sigma receptors in very low amounts, so this 48 h assay was used as a control to show that efficacy of the AA-targeted formulation is not enhanced (Figure 3.29). The AA-targeted formulation and the nontargeted formulation possess similar IC_{50} values of 467 ± 58 nM and 497 ± 12 nM, respectively. The as-synthesized Hf-PMX (IC_{50} = 400 ± 44 nM) and free PMX (IC_{50} = 503 ± 25 nM) had similar cytotoxicity to the other formulations. The t test shows that there is not a statistically significant difference between the IC_{50} values for Hf-PMX@Lipid and Hf-PMX@Lipid-AA with $\alpha = 0.20$ (>0.05).

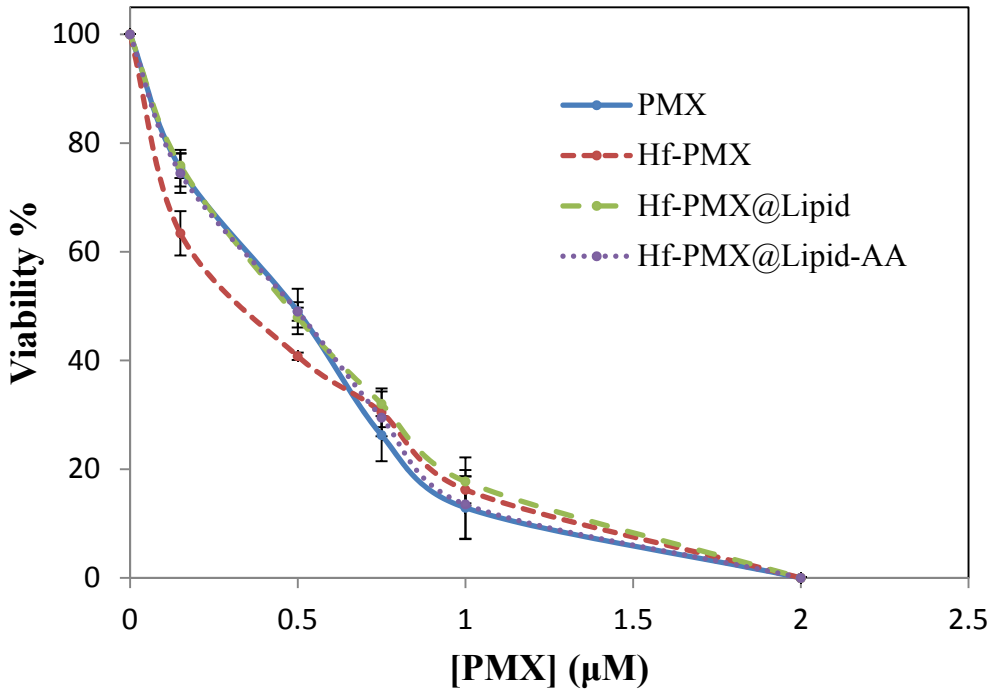

Figure 3.29. IC_{50} curves of Hf-PMX formulations against the A549 NSCLC cell line, showing the same efficacy for both lipid-coated formulations.

3.3. Conclusion

NCPs containing the antifolate chemotherapeutic agent PMX were synthesized using different binding metals. Zr-based materials could not be stabilized by the addition of a lipid bilayer, and Gd-based materials showed that PMX had degraded during synthesis, thus compromising its efficacy. However, Hf-based NCPs containing 19.7 wt% PMX could be further stabilized by a lipid coating and showed improved *in vitro* efficacy against two NSCLC cell lines. Enhanced efficacy was observed for formulations containing the sigma receptor target, anisamide.

3.4. Experimental Details

3.4.1. Materials and Methods

All chemicals, unless otherwise noted, were purchased from Fisher or Sigma Aldrich and used without further purification. Pemetrexed was purchased from Shanghai Sunny Chemicals (China). 1,2-stearoyl-3-trimethylammonium propane, chloride salt (DSTAP), 1,2-dioleoyl-*sn*-glycero-3-phosphate (DOPA), 1,2-dioleoyl-*sn*-glycero-3-phosphocholine (DOPC), and 1,2-distearoyl-*sn*-glycero-3-phosphoethanolamine-N-(polyethylene glycol) (DSPE-Peg_{2K}) were purchased from Avanti Polar Lipids. L-α-phosphatidylethanolamine, dioleoyl (DOPE) was a gift from Sigma Aldrich. Cell culture supplies, fetal bovine serum (Sigma), RPMI-1640 growth medium (Gibco), penicillin-streptomycin (Sigma), and phosphate buffered saline (Gibco) were purchased from the Tissue Culture Facility in the Lineberger Cancer Center at UNC-Chapel Hill.

Microwave reactions were carried out in a CEM Discovery or CEM MARS 5 microwave. Scanning electron microscopy (SEM) was performed with a Hitachi 4700 Field Emission Scanning Electron Microscope, and transmission electron microscopy (TEM) was performed with a JEM 100CX-II Transmission Electron Microscope. A Cressington 108 Auto Sputter Coater equipped with a Au/Pd (80/20) target and MTM-10 thickness monitor was used to coat samples before SEM imaging. SEM micrographs were obtained on glass slides, and TEM micrographs were obtained on carbon-coated copper grids. Thermogravimetric analysis (TGA) was done on a Shimadzu TGA-50 equipped with a platinum pan, and samples were heated at a rate of 3°C/min under air. Powder x-ray diffraction (PXRD) data was gathered on a Bruker SMART APEX II diffractometer using Cu radiation, and powder patterns were analyzed with the APEX II package using the phase ID

plugin. UV-Vis absorption spectra were obtained using a Shimadzu UV-2401 PC UV-Vis recording spectrophotometer. Size and zeta potential information was obtained on a Malvern ZetaSizer dynamic light scattering instrument. A Varian 820-MS Inductively-Coupled Plasma Mass Spectrometer was used to determine metal contents.

MR images were acquired on a Siemens 3T Allegra (Siemens Medical Systems, Erlagen, Germany) with a CP coil. A 3D FLASH sequence was utilized to compute T_1 maps with seven different flip angles (2, 5, 10, 20, 30, 40, and 60). Imaging parameters were FOV=190 x 190 x 64 mm^3, matrix size= 128 x 128 x 32, TR/TE= 40/1.64 ms, total data acquisition time was 30 min. The net magnetization from the region of interest of each sample was fit using a Marquardt-Levenberg algorithm for multiparametric nonlinear regression analysis using MATLAB program. Longitudinal relaxivity, T_1 was calculated from these data, and r_1 was determined from the slope of $1/T_1$ versus $[Gd^{3+}]$ plot. A 2-D multiple echo spin echo sequence was used to estimate T_2 maps. In total, 32 echoes with an echo spacing of 6.2 ms (the first echo time) were obtained; TR was 3000 ms. FOV and matrix size were set to 190 x 190 mm^2 and 128 x 128. The slice thickness was 2 mm. The total data acquisition time was about 6 minutes and 29 seconds. Transverse relaxivity, r_2, was determined from the slope of $1/T_2$ versus $[Gd^{3+}]$ plot. All images were acquired on a 9.4T Bruker BioSpec system with a 35 mm quadrature RF transmit and receive coil.

3.4.2. Synthesis of Reagents

Synthesis of DSPE-Peg_{2K}-AA. 4-methoxybenzoic acid (3 g, 20 mmol) in 10 mL thionyl chloride was refluxed for 2 h. Remaining thionyl chloride was removed in vacuo to give 4-methoxybenzoyl chloride. Under Ar gas, a solution of 4-methoxybenzoyl chloride

(1.000 g, 5.862 mmol) in 10 mL CH_2Cl_2 was slowly added to a solution of diethylenetriamine (0.588 mL, 5.862 mmol) and 2 mL TEA in 10 mL CH_2Cl_2 at 0 °C. The reaction mixture was stirred for 2 h, and the slurry was diluted with additional CH_2Cl_2 and washed with 1 M NaOH. The organic layer was dried with Na_2SO_4, and the solvent was concentrated under reduced pressure. The residue was purified by silica gel column chromatography with CH_2Cl_2/methanol (5:1, v/v) with 1-2% TEA as the eluent to yield N-(2-((2-aminoethyl)amino)ethyl)-4-methoxybenzamide. Yield: 20%. ^{1}H NMR ($CDCl_3$): δ 7.79 (d, 2H), 6.90 (d, 2H), 3.82 (s, 3H), 3.91 (s, 24H), 3.27 (m, 2H), 2.90 (m, 4H), 2.75 (m, 2H). N-(2-((2-aminoethyl)amino)ethyl)-4-methoxybenzamide (130 mg, 0.55 mmol) was reacted with PEG_{2K}-bis-carboxylate (1.2 g, 0.55 mmol) in 80 mL anhydrous CH_2Cl_2 in the presence of N,N'-dicyclohexylcarbodiimide (230 mg, 1.1 mmol) and 4-dimethylaminopyridine (135 mg, 1.1 mmol) under N_2 for 48 h. After solvent concentration, 300 mL diethyl ether was added to the mixture, and the crude product precipitated out and was isolated by centrifugation. The product was purified by silica gel column chromatography with CH_2Cl_2/methanol (10:1 v/v) as the eluent to afford AA-PEG_{2K}-mono-carboxylate. Yield: 35%.^{1}H NMR ($CDCl_3$): δ 7.77 (m, 2H), 6.89 (d, 2H), 4.20 (m, 2H), 3.95 (s, 3H), 3.81 (t,4H), 3.61 (s,180H)3.44 (m, 2H). AA-PEG_{2K}-mono-carboxylate (300 mg, 0.13 mmol) was reacted with DSPE (115 mg, 0.15 mmol) in 25 mL anhydrous CH_2Cl_2 in the presence of N,N'-dicyclohexylcarbodiimide (53 mg, 0.26mmol) and 4-dimethylaminopyridine (31.3 mg, 0.26 mmol) under N_2 for 48 h. After solvent concentration, 50 mL diethyl ether was added to the mixture, and the crude product precipitated out and was isolated by centrifugation. The product was then purified by silica gel column chromatography with CH_2Cl_2/methanol (10:1 v/v) as the eluent to afford AA-PEG_{2K}-DSPE. Yield: 30%.^{1}H NMR ($CDCl_3$): δ 7.78 (m, 2H),

6.88 (d, 2H), 4.22 (m, 4H), 3.81 (s, 3H), 3.62 (s, 180H), 2.25 (s, 6H), 1.57 (s, 10H), 1.23 (S, 30H), 0.85 (t, 6H).

3.4.3. Synthesis of PMX- and Folate-Containing NCPs

Synthesis of Mn-PMX NCP. Particles of Mn-PMX were prepared by a surfactant-assisted heating method. Two reverse (water in oil) microemulsions were prepared by two 50 mL round bottom flasks receiving 10 mL 0.3 M 0.5 M 1-hexanol in isooctanes and 365 mg CTAB (for 0.1 M CTAB). One flask was given (while stirring) 270 µL 0.1 M (4.7 mg, 0.027 mmol) aq. $MnCl_2 \cdot 4H_2O$. The other flask was given 270 µL 0.1 M (11.5 mg, 0.027 mmol) aq. Na_2PMX pH = 7.5. Both reverse microemulsions (W = 15) became clear instantly, were combined in a microwave vessel, and microwaved at 80 ºC for 20 min using 400 W, 100% power, and a 1 min ramping time. The white product was isolated by centrifugation, subsequently washed and centrifuged twice with EtOH, and dispersed in EtOH. Yield: 10.2 mg (86.6 %).

Synthesis of Zr-PMX NCP. Both $ZrCl_4$ (6.98 mg, 0.0300 mmol) and Na_2PMX (12.90 mg, 0.0300 mmol) were dissolved in 5.7 mL DMF containing 0.3 mL H_2O, and the solution was heated in a sealed microwave vessel at 60 °C for 5 min without stirring. The product was isolated from the resulting blue dispersion by centrifugation at 13,000 rpm for 15 min, washed by sonication and centrifugation with H_2O then EtOH, and dispersed in EtOH.

Synthesis of Gd-PMX NCP by Solvothermal Method. Na_2PMX was acidified by dissolving 100 mg (0.2433 mmol) in 0.5 mL H_2O and adding dilute HCl until a precipitate formed (PMX). The white precipitate was isolated by centrifugation, washed with Et_2O and allowed to dry under vacuum for 18 h. This PMX was used in the solvothermal synthesis of

Gd-PMX. Both $Gd(NO_3)_3 \cdot 6H_2O$ (13.7 mg, 0.0300 mmol) and PMX (11.4 mg, 0.0300 mmol) were dissolved in 5.5 mL DMF, and the solution was heated in a sealed microwave vessel at 80 °C for 5 min without stirring. The product was isolated from the resulting brown dispersion by centrifugation at 13,000 rpm for 15 min, washed by sonication and centrifugation with DMF then EtOH, and dispersed in EtOH.

Synthesis of Gd-PMX by Surfactant-Templated Procedure. Particles of Gd-PMX were prepared by a surfactant-assisted heating method. Two reverse (water in oil) microemulsions were prepared by two 25 mL round bottom flasks receiving 10 mL 0.3 M 0.5 M 1-hexanol in isooctanes and 365 mg CTAB (for 0.1 M CTAB). One flask was given (while stirring) 270 μL 0.1 M (11.9 mg, 0.027 mmol) aq. $Gd(NO_3)_3 \cdot 6H_2O$. The other flask was given 270 μL 0.1 M (10.3 mg, 0.027 mmol) aq. Na_2PMX pH = 7.5. Both reverse microemulsions (W = 15) became clear instantly, were combined in a microwave vessel, and microwaved at 80 ºC for 20 min using 400 W, 100% power, and a 2 min ramping time. The white product was isolated by centrifugation, subsequently washed/centrifuged twice with EtOH, and dispersed in EtOH. Yield: 6.97 mg (48.0 %).

Synthesis of Hf-PMX by Solvothermal Method. $HfOCl_2 \cdot 8H_2O$ (9.0 mg, 0.022 mmol) and Na_2PMX (5 mg, 0.0106 mmol) were dissolved in 10 mL DMF, and the solution was heated in a sealed microwave vessel at 80 °C for 10 min without stirring. The product was isolated from the resulting blue dispersion by centrifugation at 13,000 rpm for 15 min, washed by sonication and centrifugation in EtOH, and dispersed in EtOH.

Synthesis of Hf-PMX by Reverse Microemulsion Method. Particles of Hf-PMX were prepared by a reverse microemulsion method. Two reverse (water in oil) microemulsions were prepared by two 20 mL glass vials receiving 5 mL 0.3 M TritonX-

100/1.5 M 1-hexanol in cyclohexane. One flask was given (while stirring) 200 μL 25 mg/mL (5 mg, 0.0122 mmol) aq. $HfOCl_2 \cdot 8H_2O$. The other flask was given 200 μL 25 mg/mL (5 mg, 0.0106 mmol) aq. Na_2PMX pH = 7.5. Both reverse microemulsions (W = 7.4) became clear instantly, were combined and stirred for 1 h. 15 μL 200 mg/mL (3 mg, 0.00414 mmol) DOPA in $CHCl_3$ was added, and the reverse microemulsion was stirred for another hour; the reaction was quenched with the addition of 10 mL EtOH and stirred for 1 h. The white product was isolated by centrifugation, subsequently washed/centrifuged once with cyclohexane and twice with THF, and dispersed in THF. Yield: 1.86 mg (30.0 %).

Synthesis of Hf-Folate NCP. $HfOCl_2 \cdot 8H_2O$ (20.4 mg, 0.0498 mmol) and folic acid (22.2 mg, 0.0503 mmol) were dissolved in 10 mL DMF, followed by the addition of 400 μL 0.1 M (0.04 mmol) H_3PO_4 aq. The solution was heated in a sealed microwave vessel at 80 °C for 5 min without stirring. The product was isolated from the resulting orange dispersion by centrifugation at 13,000 rpm for 15 min, washed by sonication and centrifugation twice with EtOH, and dispersed in EtOH. Yield: 22.3 mg (72.0 %).

Synthesis of DOPA-Capped Hf-Folate NCP. Hf-folate NCPs (10 mg) were isolated by centrifugation and dispersed in a 1:7 v/v EtOH/$CHCl_3$ solution. While stirring, 75 μL 200 mg/mL (15 mg, 0.0207 mmol) DOPA in $CHCl_3$ was added, and the dispersion was stirred at room temperature for 2 h. Particles were isolated by centrifugation, washed by sonication and centrifugation with THF, and dispersed in THF.

3.4.4. Lipid Coating Procedure

Lipid Coating of Gd-PMX with 1:1 DSTAP/DOPE. Particle dispersions of Gd-PMX and various amounts of 1:1 (by mol) DSTAP/DOPE liposomes in 1 mM aq. KCl were combined and the sample was vortexed and sonicated then analyzed by DLS in 1 mM KCl.

Lipid Coating of Hf-PMX with cholesterol/DOPC/DSPE-Peg_{2K}. Particles of Hf-PMX (0.5 mg) were isolated by centrifugation and dispersed in 100 µL THF. All lipid solutions (5 mg/mL in THF) and the particle dispersion were heated to 50 ºC in a water bath. The following lipids were added to the particle dispersion: 42 µL (0.21 mg, 0.543 µmol) cholesterol, 84 µL (0.42 mg, 0.543 µmol) DOPC, and 150 µL (0.75 mg, 0.273 µmol, 20 mol%) DSPE-Peg_{2K}. A solution of EtOH/H_2O (30 % v/v, 500 µL) was heated to 50 ºC, and, while stirring at the maximum rate, the particle dispersion was added dropwise. THF was removed by an N_2 stream.

Lipid Coating and Anisamide Targeting of Hf-PMX. Particles of Hf-PMX (0.5 mg) were isolated by centrifugation and dispersed in 100 µL THF. All lipid solutions (5 mg/mL in THF) and the particle dispersion were heated to 50 ºC in a water bath. The following lipids were added to the particle dispersion: 42 µL (0.21 mg, 0.543 µmol) cholesterol, 84 µL (0.42 mg, 0.543 µmol) DOPC, 135 µL (0.675 mg, 0.245 µmol) DSPE-Peg_{2K}, and 15 µL (0.075 mg, 0.025 µmol) DSPE-Peg_{2K}-AA. A solution of EtOH/H_2O (30 % v/v, 500 µL) was heated to 50 ºC, and, while stirring, the particle dispersion was added dropwise. THF was removed by an N_2 stream.

Lipid Coating of Hf-Folate. Particles of Hf-Folate (0.7 mg) were isolated by centrifugation and dispersed in 100 µL THF. All lipid solutions (5 mg/mL in THF) and the particle dispersion were heated to 50 ºC in a water bath. The following lipids were added to the particle dispersion: 42 µL (0.21 mg, 0.543 µmol) cholesterol, 84 µL (0.42 mg, 0.543 µmol) DOPC, and 150 µL (0.75 mg, 0.273 µmol, 20 mol%) DSPE-Peg_{2K}. A solution of EtOH/H_2O (30 % v/v, 500 µL) was heated to 50 ºC, and, while stirring, the particle dispersion was added dropwise. THF was removed by an N_2 stream.

Lipid Coating and Anisamide-Targeting of Hf-Folate. Particles of Hf-Folate (0.7 mg) were isolated by centrifugation and dispersed in 100 μL THF. All lipid solutions (5 mg/mL in THF) and the particle dispersion were heated to 50 ºC in a water bath. The following lipids were added to the particle dispersion: 42 μL (0.21 mg, 0.543 μmol) cholesterol, 84 μL (0.42 mg, 0.543 μmol) DOPC, 135 μL (0.675 mg, 0.245 μmol) DSPE-Peg_{2K}, and 15 μL (0.075 mg, 0.025 μmol) DSPE-Peg_{2K}-AA. A solution of EtOH/H_2O (30 % v/v, 500 μL) was heated to 50 ºC, and, while stirring, the particle dispersion was added dropwise. THF was removed by an N_2 stream.

Release Profiles. All release profiles were carried out in 5 mM PBS at 37 ºC. A 1 L solution of 5 mM PBS was prepared by dissolving 8.528 g (0.146 mol) NaCl and 680 mg (5 mmol) KH_2PO_4 in 500 mL MilliQ H_2O. The pH was adjusted to 7.4 with NaOH, and the solution was brought to 1 L with MilliQ H_2O. Between 2-4 mg PMX-containing NCPs were prepared in 500 μL PBS or 30 % v/v EtOH/H_2O and added to a length of 10K molecular weight cutoff dialysis tubing. The dialysis tubing was submerged in a beaker containing 400 mL 5 mM PBS stirring at 37 ºC. Aliquots of 1 mL each were removed from the beaker at designated time intervals, and the volumes were replaced with fresh PBS. Samples were digested in 0.5 mL 0.3 M H_3PO_4, filtered through a 0.2 μM PTFE syringe filter, and analyzed by UV-Vis for PMX content. PMX content (in μM) was converted to % drug released.

DLS Stability Assays in PBS with Bovine Serum Album (BSA). Lipid-coated Hf-PMX was prepared in 500 μL 30% v/v EtOH/H_2O and added to 500 μL 5 mM PBS. BSA (5 mg) was dissolved in the particle dispersion, and Z average diameter, PDI, and count rate were monitored for 18 h.

Lipid Coating and AA Targeting of Hf-PMX. These lipid-coated particles were produced by the same technique as the non-targeted formulation, but using the same amount of cholesterol and DOPC, 135 μL 5 mg/mL (0.675 mg, 2.45 x 10^{-4} mmol) DSPE-Peg_{2K} and 15 μL 5 mg/mL (0.075 mg, 2.5 x 10^{-5} mmol) DSPE-Peg_{2K}-AA in THF.

3.4.5. In Vitro Assay Methods

Cell Lines. NCI-H460 non-small cell lung cancer cells (ATCC# HTB-177) and A549 non-small cell lung cancer cells (ATCC# CCL-185) were purchased from the Tissue Culture Facility of Lineberger Comprehensive Cancer Center at the University of North Carolina at Chapel Hill. Both cell lines were maintained in RPMI-1640 growth medium supplemented with 10% FBS and 2% penicillin-streptomycin.

Cytotoxicity Assays Against A549 NSCLC Cells. For the Gd-PMX Assay: Confluent A549 cells were trypsinized and a cell density was obtained from a hemocytometer. Six-well plates were seeded with 5.0x10^4 cells/well and a total of 2 mL media. Plates were incubated at 37°C and 5% CO_2 overnight. Amounts of PMX or NCP suspension in RPMI-1640 medium were added to wells, along with additional media, resulting in PMX concentrations (μM) of 0, 1, 5, 10, 50, and 100. Plates were incubated at 37°C and 5% CO_2 for 48 h and viability was determined via the trypan blue exclusion assay.

For the Hf-PMX Assay: Confluent A549 cells were trypsinized and a cell density was obtained from a hemocytometer. Six-well plates were seeded with 5.0x10^4 cells/well and a total of 2 mL media. Plates were incubated at 37°C and 5% CO_2 overnight. Amounts of PMX or Hf-PMX dispersions in RPMI-1640 medium were added to wells, along with additional media, resulting in PMX concentrations (μM) of 0, 0.15, 0.5, 0.75, 1, and 2. Plates were

incubated at 37°C and 5% CO_2 for 48 h and viability was determined via the trypan blue exclusion assay.

Cytotoxicity Assay Against NCI-H460 NSCLC Cells. Confluent NCI-H460 cells were trypsinized and a cell density was obtained from a hemocytometer. Six-well plates were seeded with $5.0x10^4$ cells/well and a total of 2 mL media. Plates were incubated at 37°C and 5% CO_2 overnight. Amounts of PMX or Hf-PMX dispersions in RPMI-1640 medium were added to wells, along with additional media, resulting in PMX concentrations (μM) of 0, 0.15, 0.5, 0.75, 1, and 2. Plates were incubated at 37°C and 5% CO_2 for 48 h and viability was determined via the trypan blue exclusion assay.

3.5. References

(1) Calvert, A. H. *Oncology* **2004**, *18*.

(2) Villela, L. R.; Stanford, B. L.; Shah, S. R. *Pharmacotherapy* **2006**, *26*, 641.

(3) Li, B.-S.; Gong, H.-Y.; Huang, W.; Yi, Y.; Yu, J.-M.; Wang, Z.-T.; Zhang, Z.-C.; Sun, H.-F.; Li, H.-S.; Wang, L.-Y. *Am. J. Clin. Oncol.* **2011**, *35*, 115.

(4) Dickgreber, N. J.; Fink, T. H.; Latz, J. E.; Hossain, A. M.; Musib, L. C.; Thomas, M. *Clin. Cancer Res.* **2009**, *15*, 382.

(5) Fuld, A. D.; Dragnev, K. H.; Rigas, J. R. *Expert Opin. Pharmacother.* **2010**, *11*, 1387.

(6) Min, T.; Ye, T.; Zhang, P.; Liu, J.; Zhang, C.; Shen, W.; Wang, W.; Shen, L. *J. App. Poly. Sci.* **2009**, *111*, 444.

(7) Levy, L.; Pottier, A.; Rouet, A.; Marill, J.; Devaux, C. 2009; Vol. 081567686.0, p 32.

(8) Li, J.; Yang, Y.; Huang, L. *J. Controlled Release* **2012**, *158*, 108.

(9) Cobos, E. J.; Entrena, J. M.; Nieto, F. R.; Cendan, C. M.; Del Pozo, E. *Curr. Neuropharmacol.* **2008**, *6*, 344.

(10) Ganapathy, M. E.; Prasad, P. D.; Huang, W.; Seth, P.; Leibach, F. H.; Ganapathy, V. *J. Pharmacol. Exp. Ther.* **1999**, *289*, 251.

(11) John, C. S.; Vilner, B. J.; Geyer, B. C.; Moody, T.; Bowen, W. D. *Cancer Res.* **1999**, *59*, 4578.

(12) Vilner, B. J.; John, C. S.; Bowen, W. D. *Cancer Res.* **1995**, *55*, 408.

(13) Maurice, T.; Su, T.-P. *Pharmacol. Ther.* **2009**, *124*, 195.

CHAPTER 4

Nanoscale Coorination Polymers for Targeted Delivery of Cisplatin

4.1. Introduction

4.1.1. Platinum Complexes for Cancer Chemotherapy - Cisplatin

Cancer treatment was revolutionized by the serendipitous discovery of the biological properties of cisplatin in 1965 by Rosenberg and co-workers.[1] Since this discovery, there have been three FDA-approved Pt-based anticancer agents: cisplatin, oxaliplatin, and carboplatin. This chapter will focus on the delivery of cisplatin (Figure 4.1); NCPs for the delivery of oxaliplatin will be discussed in Chapter 5. These drugs, as with all small molecule chemotherapeutics, are used to treat various cancers, are vastly limited by their poor pharmacokinetics, low selectivity, and detrimental side effects. These agents, with their short half-lives in the body, diffuse through all tissues, resulting in high systemic toxicity.[2-4] Nephrotoxicity and neurotoxicity are not uncommon for patients treated specifically with Pt-based therapeutics.

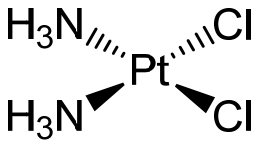

Figure 4.1. Structure of cisplatin, one of the three FDA-approved platin-based chemotherapeutics.

Cisplatin has a defined mechanism of action against cancer (Figure 4.2).[5,6] Upon entry into a cell, cisplatin becomes aquated by loss of the two chloro ligands, as a result of

the lower chloride concentration inside the cell (3-20 mM) than outside of the cell (~100 mM). The resulting diaquo cisplatin (or the mono-aquated form) is the active drug, which forms adducts with the strands of DNA, inhibiting repair and replication. These adducts bend and twist DNA, triggering many signal-transduction pathways that ultimately result in apoptosis.

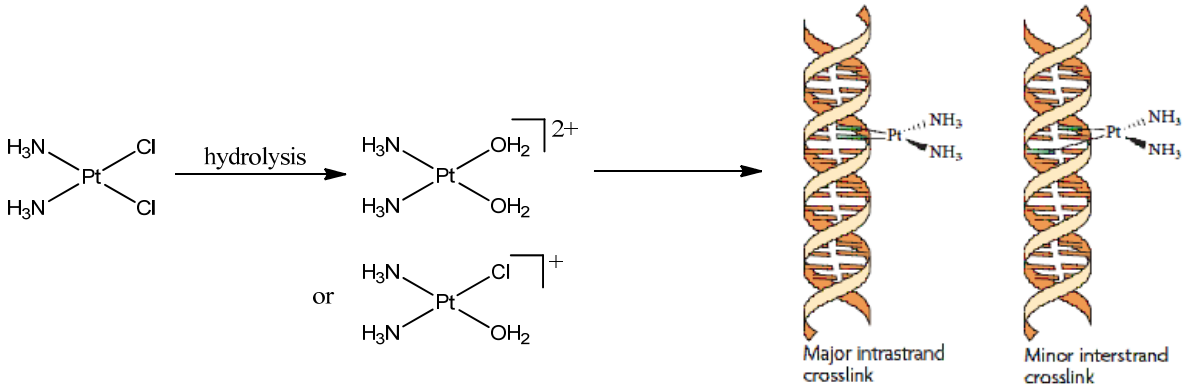

Figure 4.2. Mechanism of cisplatin in apoptotic cell death.

This mechanism of action seems rather straightforward and effective; however, many cancers develop resistance to cisplatin.[2] Resistance, as well as other drawbacks of cisplatin therapy, can be much alleviated by the incorporation of a cisplatin prodrug into an NCP. Other nanoparticle carriers have been utilized for the delivery of cisplatin,[7-10] but the Lin group is the only group to use an NCP platform for delivery of this chemotherapeutic. Although an earlier silica-coated NCP formulation was developed in the Lin lab to deliver cisplatin at very high drug loadings, this system suffers from the burst release of significant amounts of drug from the particles.[11] Herein is reported the synthesis and characterization of new cisplatin-containing NCPs which have been stabilized by lipid coatings and functionalized with the small molecule targeting ligand, anisamide (AA), which displays an

affinity for sigma receptors (Figure 4.3). The present NCP system shows enhanced efficacy compared to cisplatin in non-small cell lung cancer (NSCLC) cell lines; increased uptake is further demonstrated by confocal microscopy imaging and competitive binding assays.

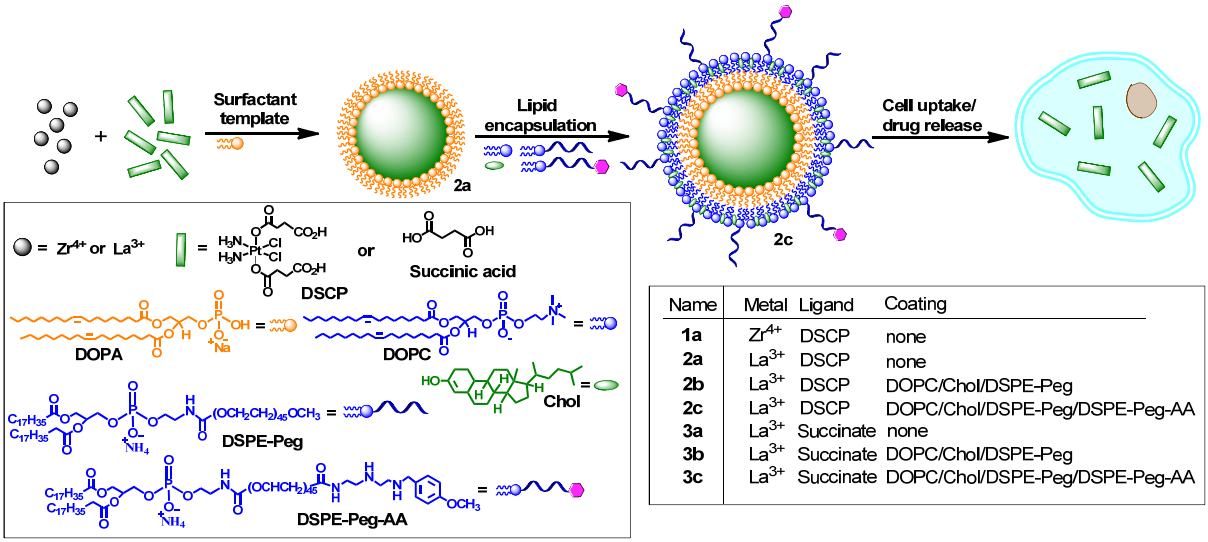

Name	Metal	Ligand	Coating
1a	Zr^{4+}	DSCP	none
2a	La^{3+}	DSCP	none
2b	La^{3+}	DSCP	DOPC/Chol/DSPE-Peg
2c	La^{3+}	DSCP	DOPC/Chol/DSPE-Peg/DSPE-Peg-AA
3a	La^{3+}	Succinate	none
3b	La^{3+}	Succinate	DOPC/Chol/DSPE-Peg
3c	La^{3+}	Succinate	DOPC/Chol/DSPE-Peg/DSPE-Peg-AA

Figure 4.3. Schematic showing the synthesis of La-DSCP NCPs, stabilization with a lipid bilayer, and uptake into lung cancer cells.

4.2. Results and Discussion

4.2.1. Synthesis and Characterization of Mg-DSCP NCP

NCPs of Mg-DSCP were prepared by a nanoprecipitation technique in which the methylammonium salt of disuccinatocisplatin (DSCP) and $MgCl_2 \cdot 6H_2O$ were dissolved in H_2O and the formation of NCPs was induced by the rapid addition of MeOH. These particles are slightly fused and between 100-150 nm in diameter by SEM (Figure 4.4). However, these particles were not stable and degraded shortly after their storage in EtOH.

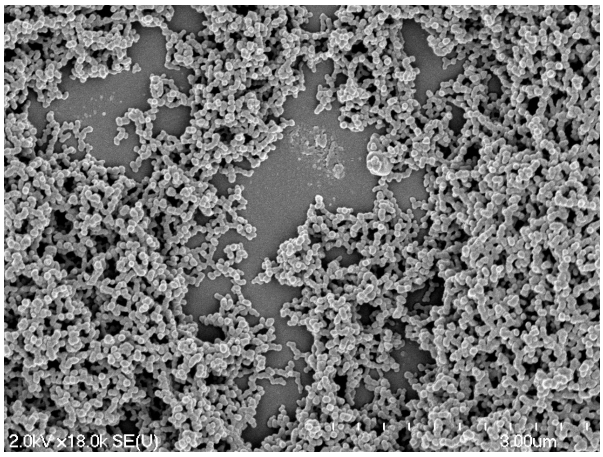

Figure 4.4. SEM micrograph of Mg-DSCP NCPs.

4.2.2. Synthesis and Characterization of Mn-DSCP NCP

Two formulations of Mn-DSCP NCPs were prepared. First, NCPs were synthesized by a nanoprecipitation technique in which the methylammonium salt of DSCP and $MnCl_2 \cdot 4H_2O$ were dissolved in H_2O and the formation of NCPs was induced by the rapid addition of MeOH. These particles are slightly fused and between 100-200 nm in diameter by SEM (Figure 4.5). The particles possess a moderate DSCP loading, 31.8 wt% by TGA (Figure 4.6). The ICP-MS analysis for Pt content yields 10.6 wt% Pt which translates to ~30 wt% DSCP, a drug loading that agrees well with the TGA data. These particles were slightly fused, which hindered their further development as a drug delivery vehicle.

Another version of Mn-DSCP NCPs were prepared by a surfactant-assisted heating method in which reverse microemulsions (W = 10) containing aqueous phase methylammonium DSCP salt and $MnCl_2 \cdot 4H_2O$ were stabilized in the organic phase 0.1 M CTAB/0.5 M 1-hexanol in isoocatnes and heated to 120 °C for 10 min. The resulting spherical particles were between 50-200 nm in diameter by SEM (Figure 4.7). However, the inability to reproduce this synthesis precluded its use in further studies.

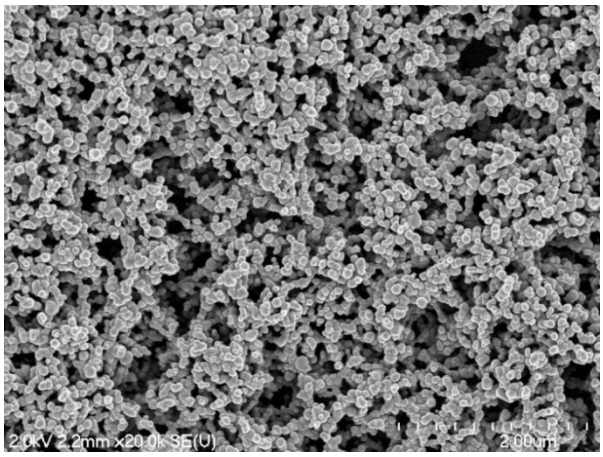

Figure 4.5. SEM micrograph of Mn-DSCP NCPs.

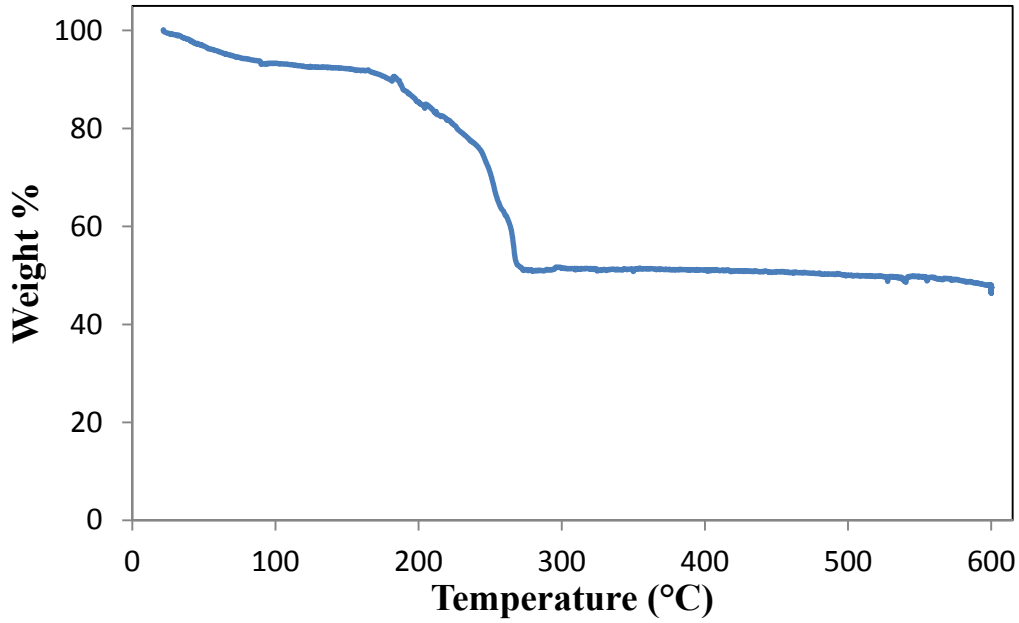

Figure 4.6. TGA plot of Mn-DSCP showing organic weight loss corresponding to 31.8 wt% DSCP drug loading. DSCP organic weight loss is observed between 150 and 275 °C.

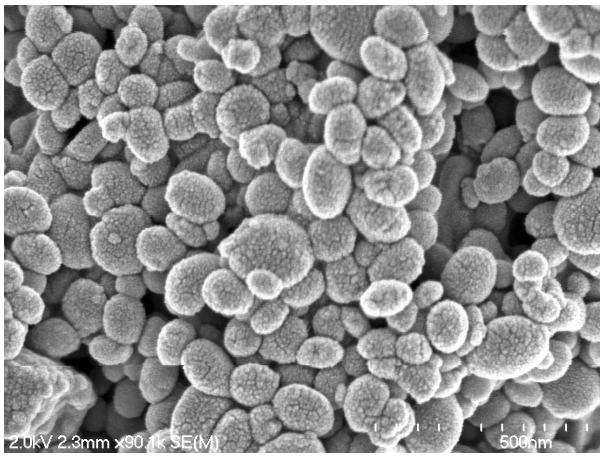

Figure 4.7. SEM micrograph of Mn-DSCP synthesized by a surfactant-assisted heating synthesis.

4.2.3. Synthesis and Characterization of Zr-DSCP NCP

We sought to synthesize NCPs of Zr-DSCP because a Zr-carboxylate MOF was reported to have high stability[12] (note: this work was done concurrently with MTX-containing NCPs (Chapter 2) so conclusions about the stability of Zr-based NCPs had not been made). The first generation of Zr-DSCP was made by a solvothermal method in which $ZrCl_4$, DSCP, and 5 eq. acetic acid were combined in DMF and heated in an oven at 60 °C for 18 h. The resulting amorphous NCPs were ~400 nm in diameter by both SEM and TEM (Figure 4.8). This size correlates well with the Z average diameter of 432.1 nm and PDI of 0.106 by DLS. These nanoparticles display a high drug loading of DSCP, 41.1 wt% by TGA (Figure 4.9). These larger Zr-DSCP NCPs are too large for drug delivery applications, so attempts were made to produce smaller (less than 200 nm diameter) Zr-DSCP particles. Smaller Zr-DSCP particles were prepared by a solvothermal reaction in which $ZrCl_4$, DSCP, and acetic acid were heated in a microwave in DMF at 60 °C for 5 min. The resulting white particles were ~50 nm and slightly fused by SEM (Figure 4.10). The fused particles are evident from DLS, with a Z average diameter of 204.9 nm and PDI of 0.194 in EtOH.

Particles of Zr-DSCP that were not fused were prepared by the acetone-induced nano-precipitation of a solution of $ZrCl_4$, DSCP, and 5 eq. acetic acid in DMF. Smaller particles were achieved by the acetone-induced nanoprecipitation of a solution of $ZrCl_4$, DSCP, and acetic acid in DMF. The particles resulting from this reaction were between 100-200 nm in diameter by SEM and TEM (Figure 4.11) with a Z average diameter of 190.0 nm with a PDI of 0.080 by DLS. TGA gives a DSCP drug loading of 27.1 wt% (Figure 4.12). This drug loading value matches that obtained by ICP-MS analysis of Pt content, 28.1 wt%. These particles dissolve instantly in 5 mM PBS at 37 °C with a $t_{1/2} \sim 10$ min, indicating the need for further stabilization (Figure 4.13).

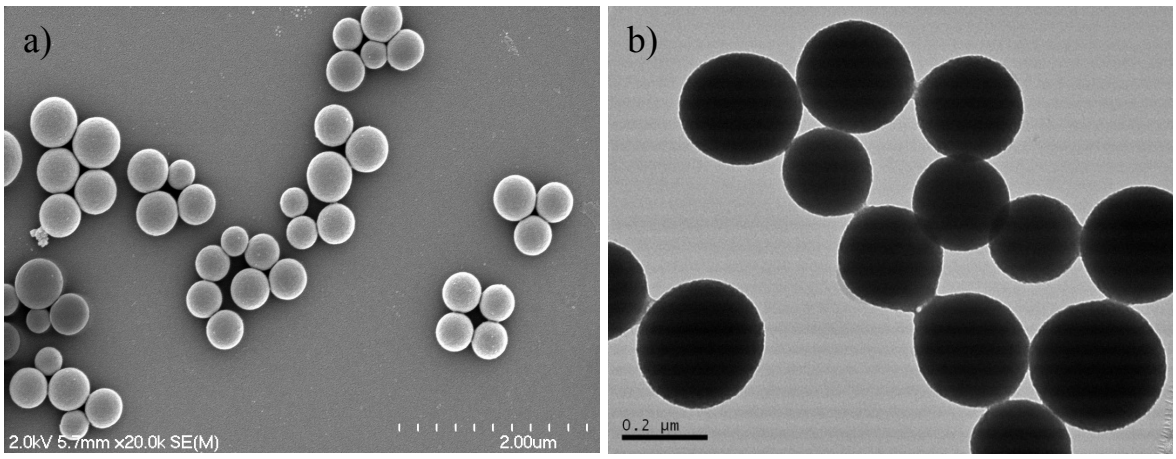

Figure 4.8. SEM (a) and TEM (b) micrographs of larger Zr-DSCP.

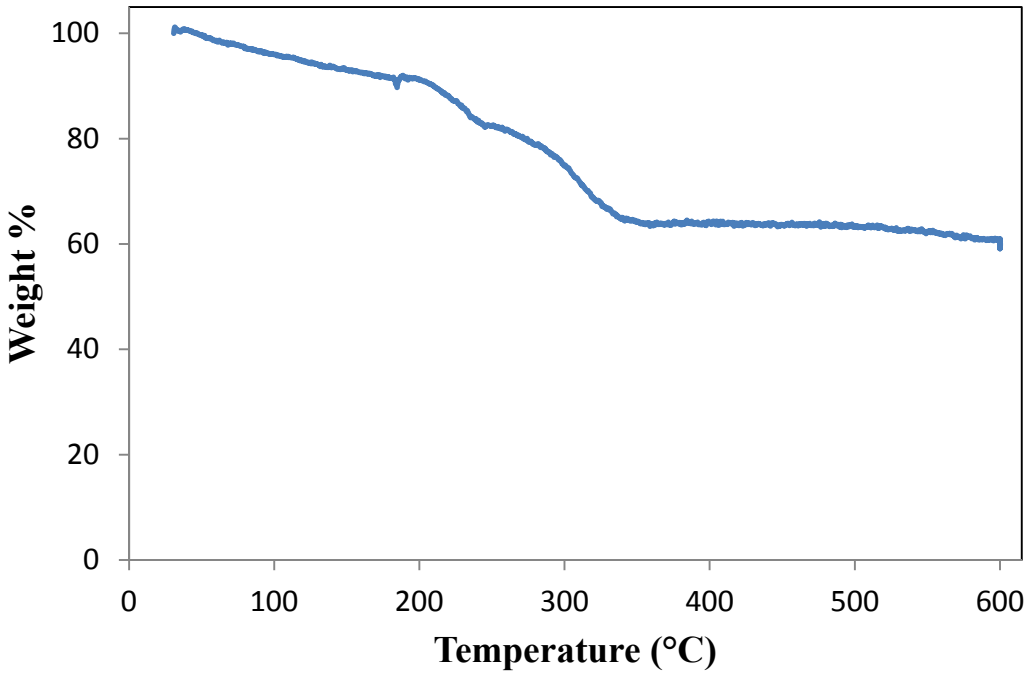

Figure 4.9. TGA plot of larger Zr-DSCP NCPs showing organic weight loss corresponding to 41.1 wt% DSCP between 150 and 300 °C.

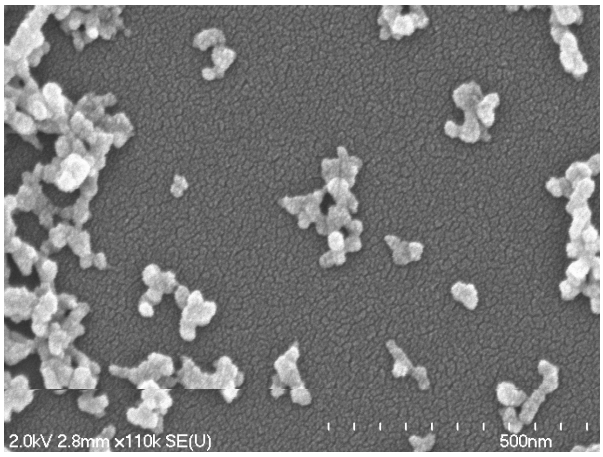

Figure 4.10. SEM micrograph of Zr-DSCP NCPs synthesized by solvothermal synthesis.

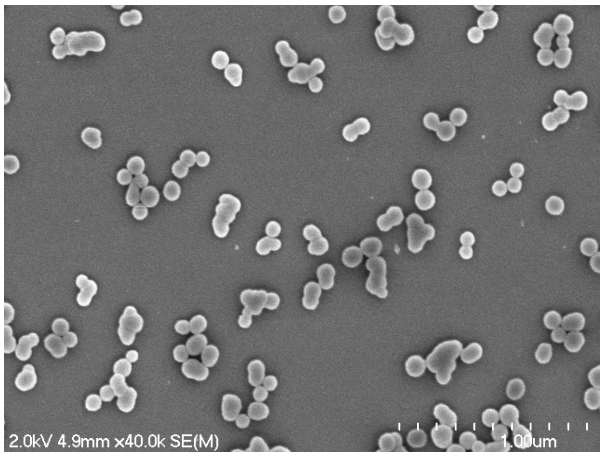

Figure 4.11. SEM micrograph of Zr-DSCP NCPs by acetone-induced rapid precipitation.

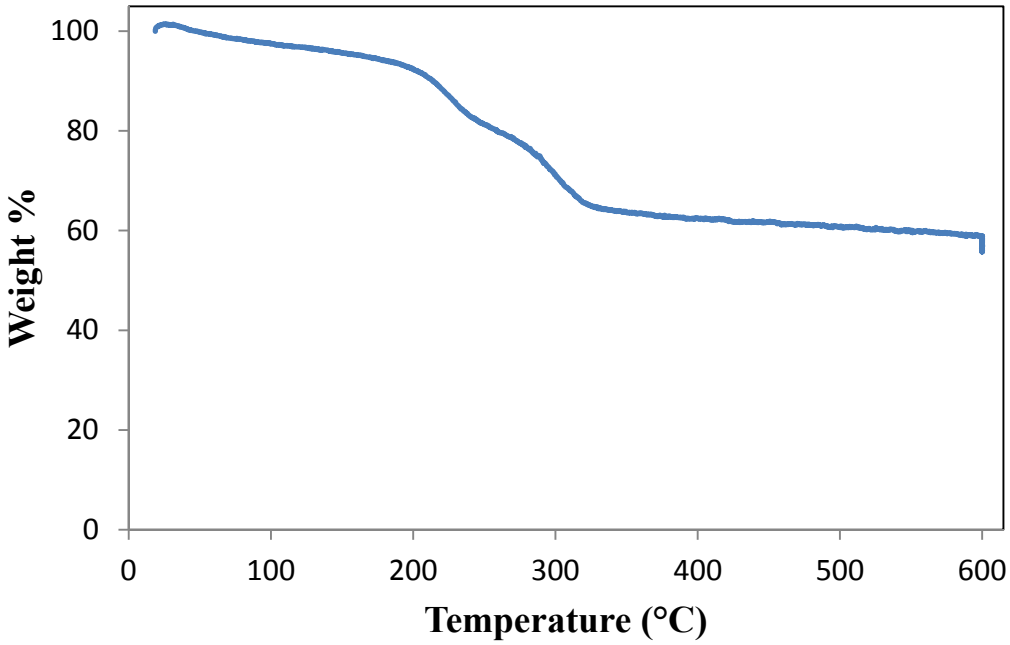

Figure 4.12. TGA plot of Zr-DSCP where organic weight loss corresponds to 27.1 wt% DSCP between 150 and 300 °C.

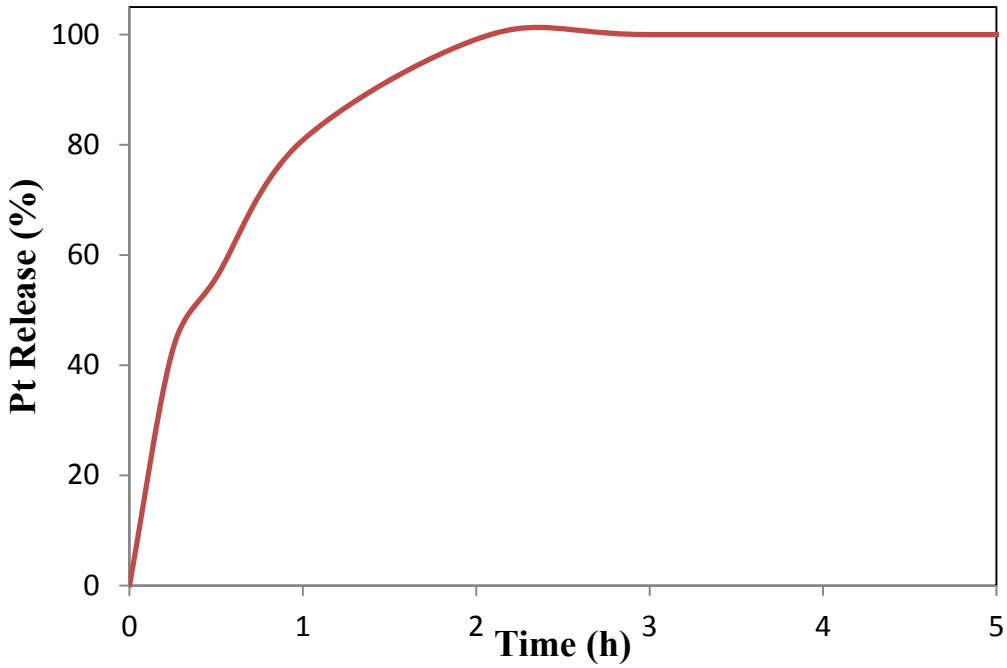

Figure 4.13. Release profile of Zr-DSCP in 8 mM PBS at 37 °C.

Additionally, a Zr-DSCP NCP formulation in which the particles are capped with a hydrophobic capping agent (DOPA) was made to perhaps have these particles stabilized by a different lipid coating method.[13] These particles were made by the chloroform-induced nano-precipitation of a solution of $ZrCl_4$, DSCP, DOPA, and acetic acid in DMF. These particles, called Zr-DSCP@DOPA, are between 100-200 nm in diameter by SEM and TEM (Figure 4.14). The size in THF by DLS is a Z average diameter of 224.8 nm with a PDI of 0.116. TGA of this material shows more organic weight loss than the uncapped Zr-DSCP, indicating the addition of the DOPA capping agent (Figure 4.15). ICP-MS of Pt content gives 32.9 wt% DSCP. A release profile of these particles in 5 mM PBS at 37 °C gives a $t_{1/2}$ ~30 min (Figure 4.16). Attempts to stabilize this material by lipid coating are described in a later section.

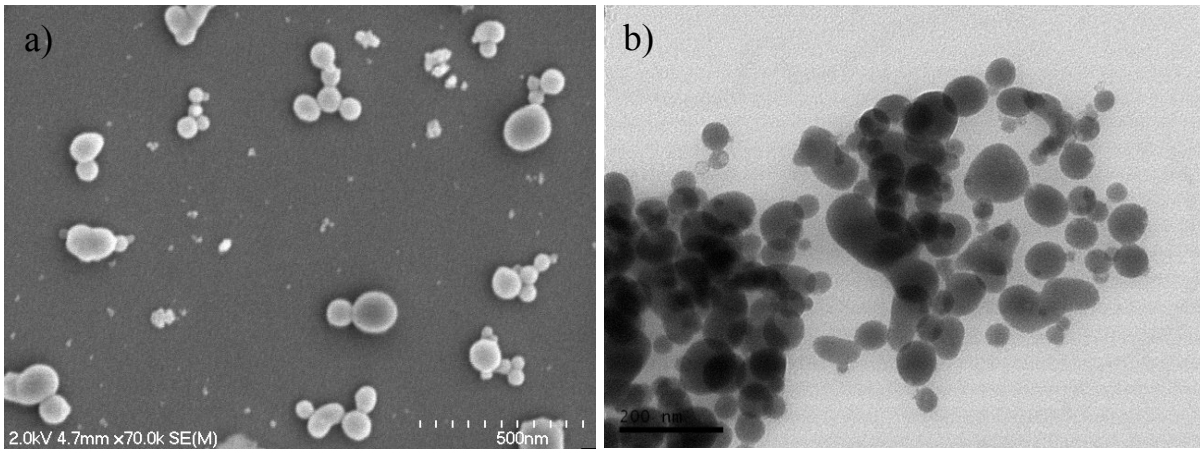

Figure 4.14. SEM (a) and TEM (b) micrographs of DOPA-capped Zr-DSCP.

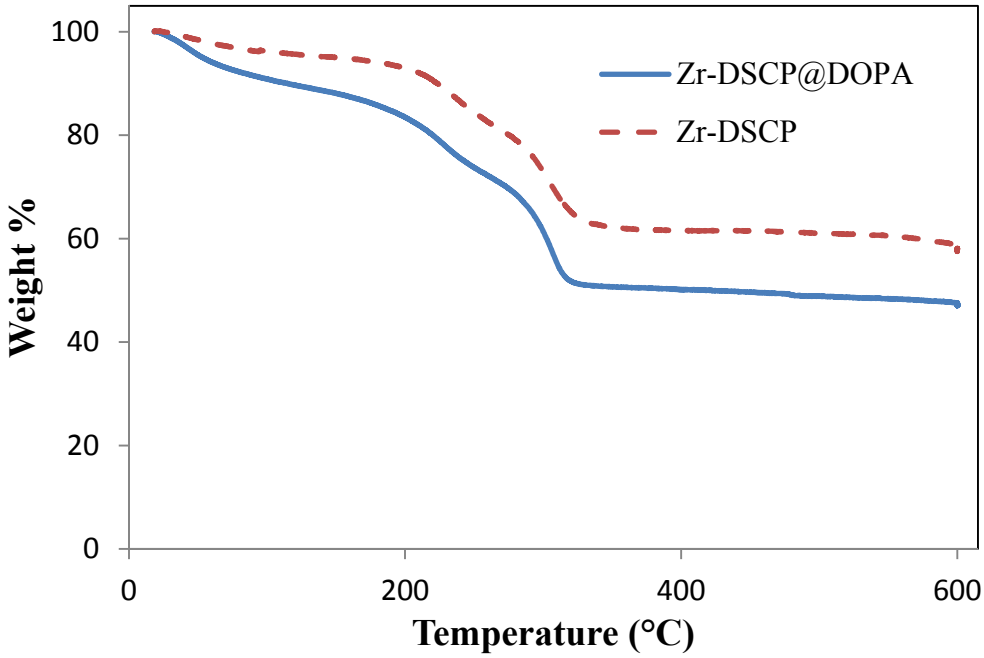

Figure 4.15. TGA plot of DOPA-capped Zr-DSCP, showing more organic weight loss (due to the addition of DOPA) than Zr-DSCP.

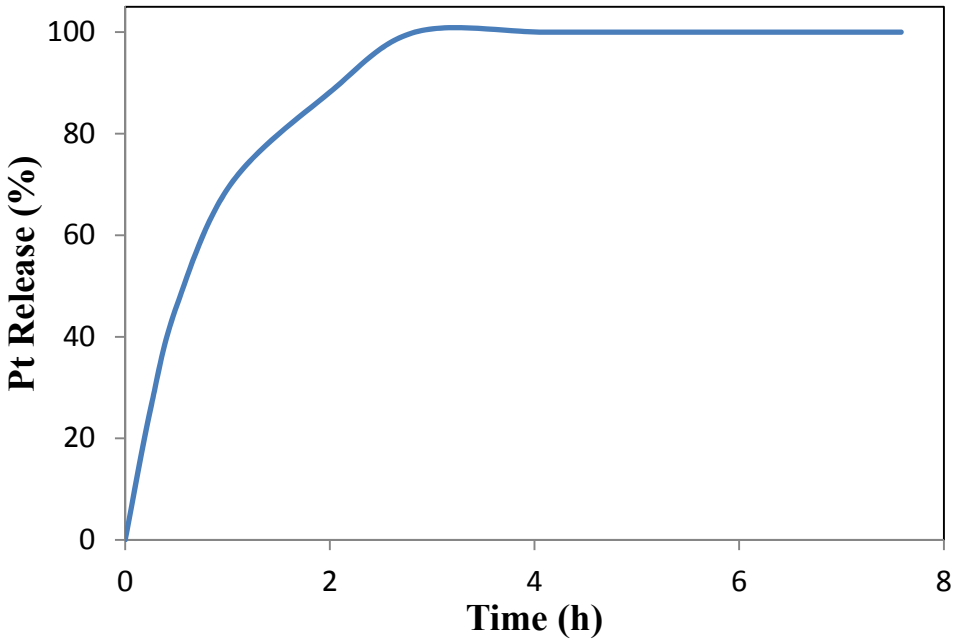

Figure 4.16. Release profile of Zr-DSCP@DOPA in 8 mM PBS at 37 °C.

4.2.4. Stabilization Attempts of Zr-DSCP NCP

It has been previously reported that NCPs can be stabilized by the subsequent coating with polyvinylpyrollidone (PVP) and silica.[11] Zr-DSCP NCPs were coated with PVP by stirring a dispersion of Zr-DSCP in EtOH containing PVP for 18 h. Coating the particles with PVP before silica coating make the particles more dispersible so that more efficient silica coating can be achieved. The resulting particles do not differ in size from the as-synthesized particles, but appear more dispersible on the SEM or TEM slide (Figure 4.17). These particles appear smaller by DLS with a Z average diameter of 158.3 nm and a PDI of 0.155, indicating that the particles are more dispersible in EtOH. An increase in organic weight loss between Zr-DSCP and Zr-DSCP@PVP by TGA indicates the added amount of PVP, 12.0 wt% (Figure 4.18). After successful coating of Zr-DSCP with PVP, the particles were coated with silica to afford Zr-DSCP@PVP@SiO_2. Silica coating was achieved by stirring Zr-

DSCP@PVP in a basic ethanol solution containing tetraethyl orthosilicate for 2 h. The resulting particles do not differ in size from the as-synthesized particles by SEM or TEM (Figure 4.19).

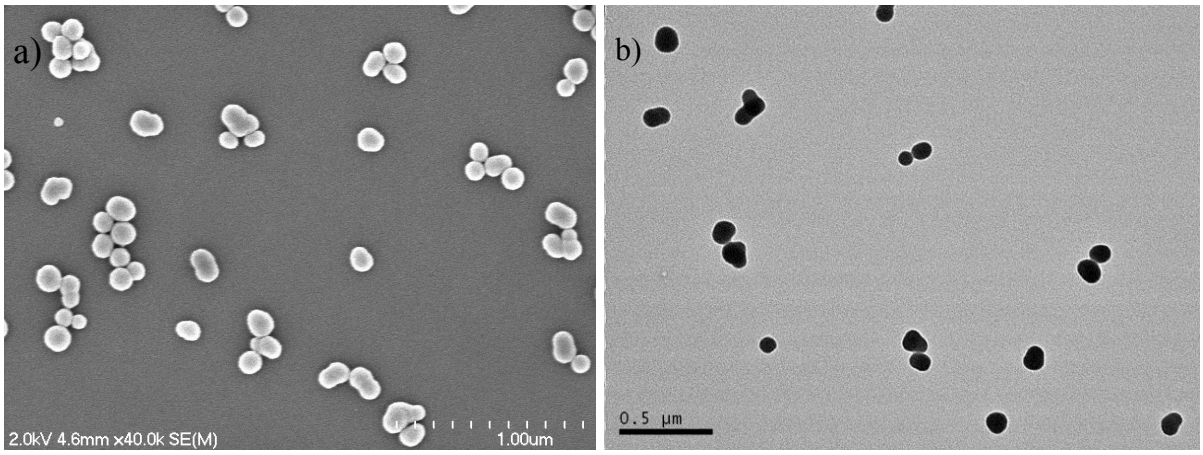

Figure 4.17. SEM (a) and TEM (b) micrographs of Zr-DSCP@PVP.

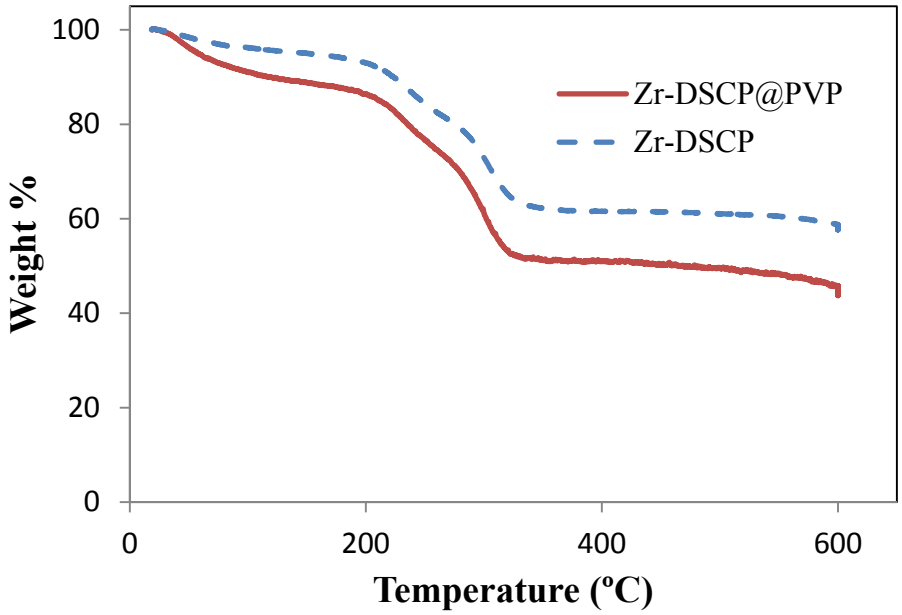

Figure 4.18. TGA plot of Zr-DSCP@PVP, compared to Zr-DSCP, showing increased organic weight loss due to the presence of DOPA. DSCP weight loss is observed between 175 and 350 °C.

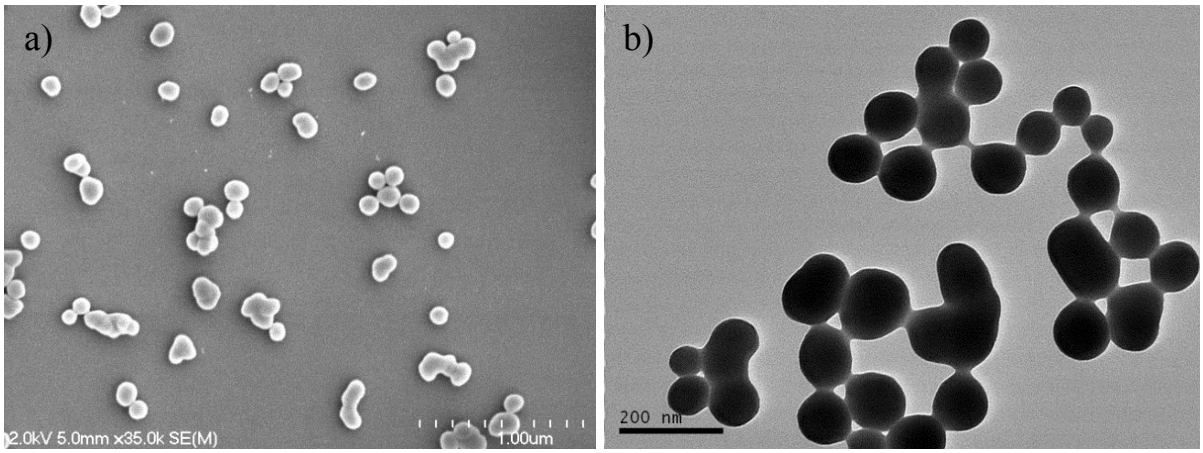

Figure 4.19. SEM (a) and TEM (b) micrographs of Zr-DSCP@PVP@SiO_2.

Zr-DSCP@PVP@SiO_2 NCPs increase in size from the PVP-coated NCPs by DLS with a Z average diameter of 209.3 nm and PDI of 0.123. EDS shows the presence of Pt, Zr, and Si, which indicates successful silica coating (Figure 4.20); however, ICP-MS analysis of Pt gives the same DSCP drug loading as the as-synthesized particles, 32.9 wt%. TGA shows that the weight loss characteristics are the same for Zr-DSCP and the silica-coated particles, indicating that all PVP may have been lost and the amount of silica coating is minimal. Unfortunately, silica coating of Zr-DSCP@PVP did not enhance stability of the NCPs.

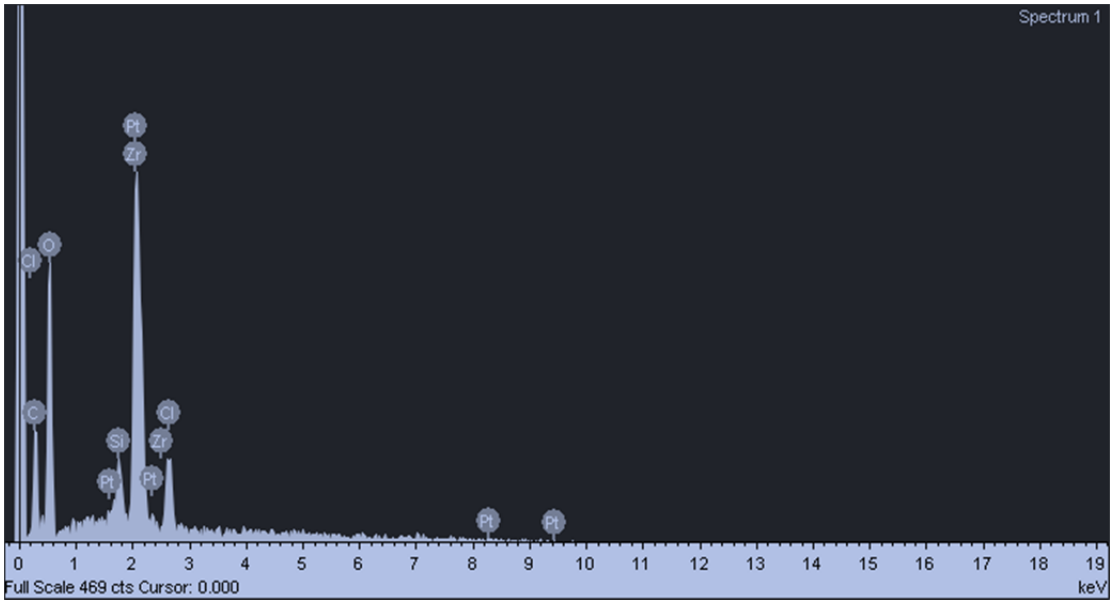

Figure 4.20. EDS plot of Zr-DSCP@PVP@SiO_2 showing the presence of Zr, Pt, and Si.

We also attempted to induce stability by lipid-coating Zr-DSCP@DOPA by injecting a dispersion of particles and cholesterol, DOPC, and DSPE-Peg_{2K} in THF into 30 % v/v EtOH/H_2O and removing the THF by a N_2 stream. These particles do not differ from the as-synthesized particles by TEM (Figure 4.21) or DLS (Z average diameter = 200.0 nm, PDI = 0.141). Unfortunately, these lipid-coated Zr-DSCP@DOPA NCPs did not lead to any stabilization by a release profile in 5 mM PBS at 37 °C ($t_{1/2}$ ~ 25 min). The inability to stabilize any of the Zr-DSCP NCPs is likely due to the tendency of Zr-carboxylate materials to rapidly form phosphate salts in the presence of phosphates, as demonstrated in the case of Zr-MTX.[14]

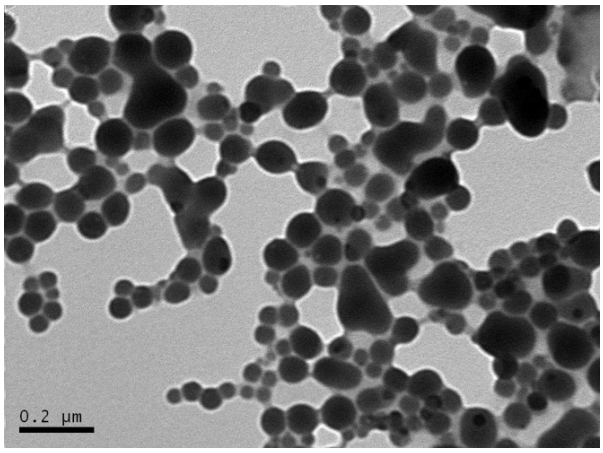

Figure 4.21. TEM micrograph of lipid-coated Zr-DSCP@DOPA NCPs.

4.2.5. Synthesis and Characterization of La-DSCP NCP

Knowing that trivalent lanthanides have a reduced tendency to form phosphate salts, we sought to prepare a DSCP-containing NCP with La(III) as the binding metal. This system differs from that of the previously reported Tb-DSCP material as we had hoped that lipid-coating a hydrophobic NCP would lead to less burst release and an overall more stable formulation. DOPA-capped NCPs of La-DSCP were produced by a surfactant-assisted heating technique in which reverse microemulsions (W = 7.4) containing aqueous droplets of $LaCl_3 \cdot 7H_2O$ and DSCP (containing DOPA in $CHCl_3$) in the organic phase 0.3 M TritonX-100/1.5 M 1-hexanol in cyclohexane were heated at 70 °C for 10 min. The resulting NCPs were irregularly-shaped and between 50-150 nm by SEM and TEM (Figure 4.22). DLS analysis in THF shows that the particles are dispersible in organic solvent (Z average diameter = 133.0 nm, PDI = 0.120), indicating successful capping with the hydrophobic capping agent.

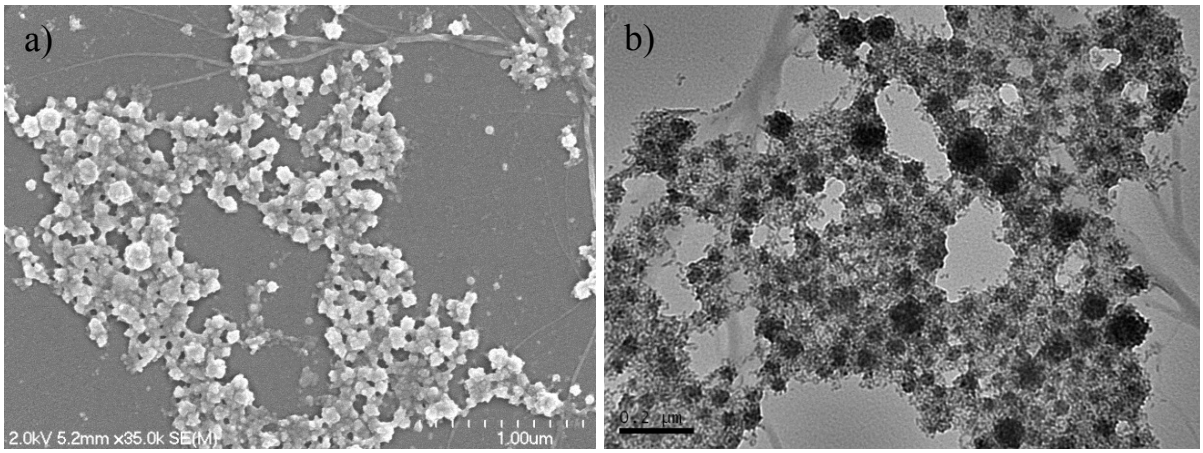

Figure 4.22. SEM (a) and TEM (b) micrographs of La-DSCP NCP.

ICP-MS analysis for Pt content reveals that these particles are 8.2 wt% DSCP (20 wt% La). Even though this drug loading is considered low for NCP formulations, cisplatin is a very potent chemotherapeutic agent and when delivered selectively and specifically to cancer tissue, the dose required is quite low. TGA shows a large amount of organic weight, presumably due to a significant amount of DOPA associated with the formulation (Figure 4.23). A release profile in 5 mM PBS at 37 °C shows that the formulation degrades almost immediately (Figure 4.24, $t_{1/2}$ ~ 35 min), emphasizing the requirement to stabilize this material.

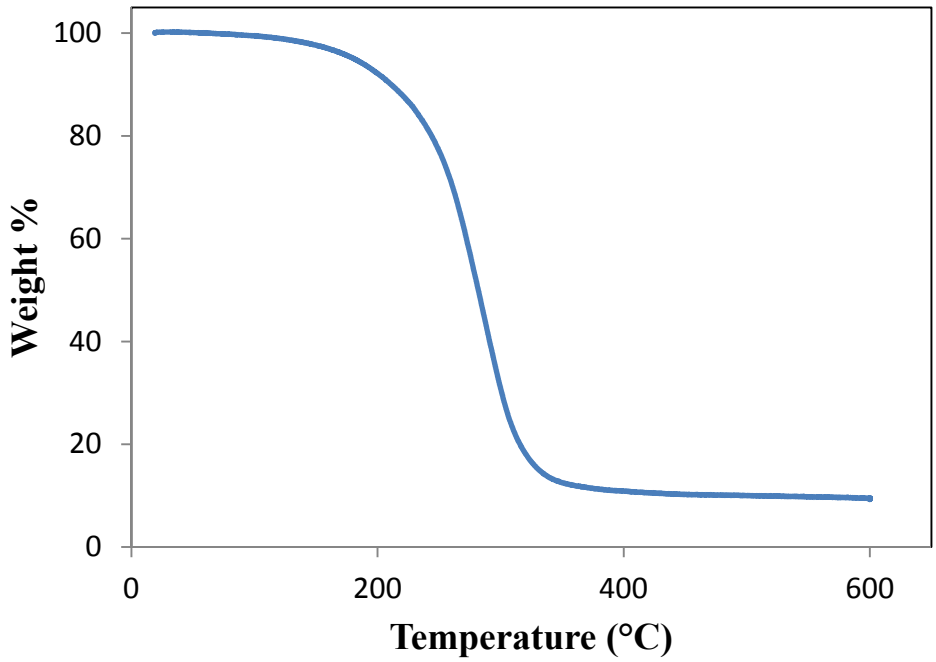

Figure 4.23. TGA plot of La-DSCP showing a large amount of organic weight loss attributed mostly to the presence of DOPA.

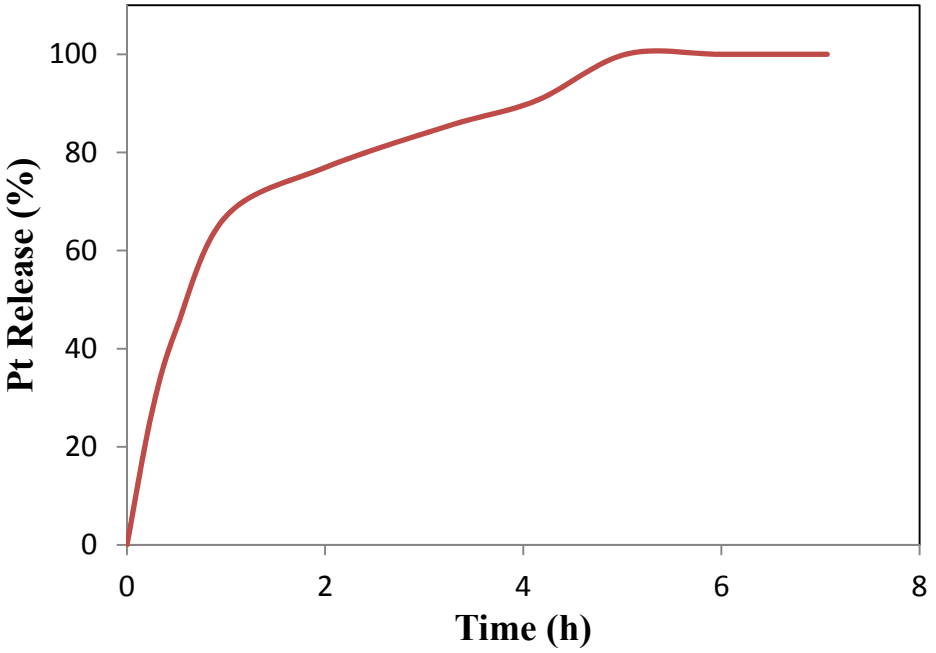

Figure 4.24. Release profile of La-DSCP in 8 mM PBS at 37 °C.

4.2.6. Lipid Coating of La-DSCP NCP

La-DSCP NCPs were stabilized by addition of a lipid coating by encapsulation in a lipid layer of cholesterol, DOPC, and DSPE-Peg_{2K} in a 2:2:1 molar ratio following a reported protocol.[13] A dispersion of La-DSCP and lipids in THF was added dropwise to a solution of 30 % v/v EtOH/H_2O stirring at 50 °C. These particles are not any different in morphology from the as-synthesized particles by TEM (Figure 4.25). An increase in Z average diameter (163.0 nm with a PDI of 0.140) is observed by DLS in PBS. Increased stability is observed compared to the as-synthesized La-DSCP NCPs in a release profile in 5 mM PBS at 37 °C (Figure 4.26). Over the first hour, ~25% drug release is observed, with no more Pt release observed by ICP-MS up to 192 h. This type of release profile is desired as the remaining DSCP loading would be released inside the cell environment via the pH-labile Pt-O bonds in the Pt(IV) prodrug. This enhanced stability is quite an improvement from the previously reported Tb-DSCP system ($t_{1/2}$ ~ 9 h with complete release at 42 h).[11]

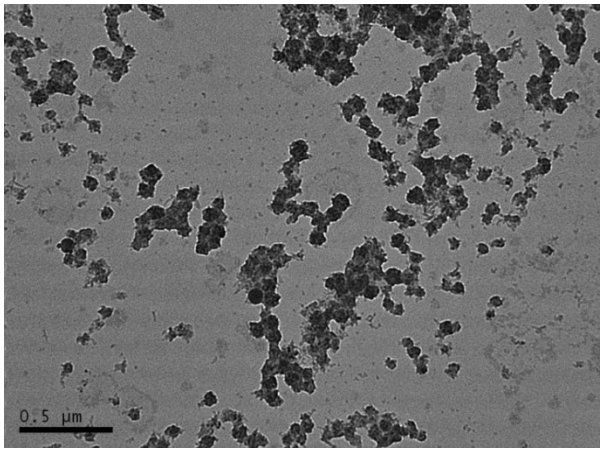

Figure 4.25. TEM micrograph of La-DSCP@Lipid.

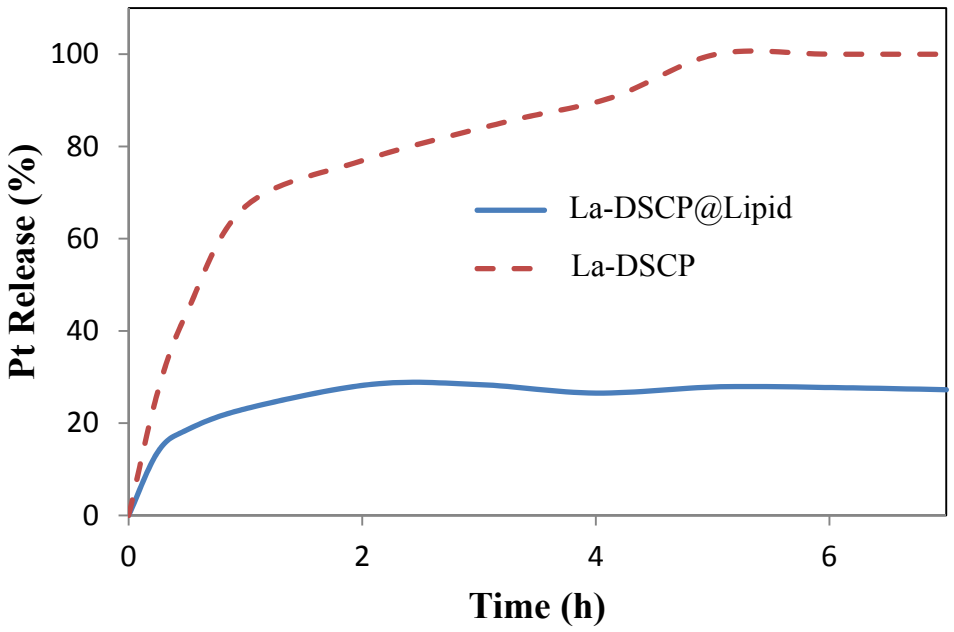

Figure 4.26. Release profile of La-DSCP@Lipid in 8 mM PBS at 37 °C, showing enhanced stability over the as-synthesized NCPs.

Further stability tests were conducted on the lipid-coated La-DSCP NCPs. First, the Z average diameter was monitored in 5 mM PBS for 18 h to show that the diameter remains the same over this time period (Figure 4.27a). Additionally, this same experiment was conducted in 5 mM PBS containing 5 mg/mL bovine serum albumin (Figure 4.27b, BSA). BSA is a blood protein that is used to assess the potential stability of the NCP formulation in blood circulation. Poorly PEGylated particles would aggregate significantly in the presence of BSA as PEG creates a water layer that impedes blood proteins from attaching to the material. When the particle diameter is monitored over 18 h in 5 mg/mL BSA, no aggregation is observed (the PDI remains the same) and a ~20 nm decrease in Z average is observed, likely due to the settling out of larger particles overnight.

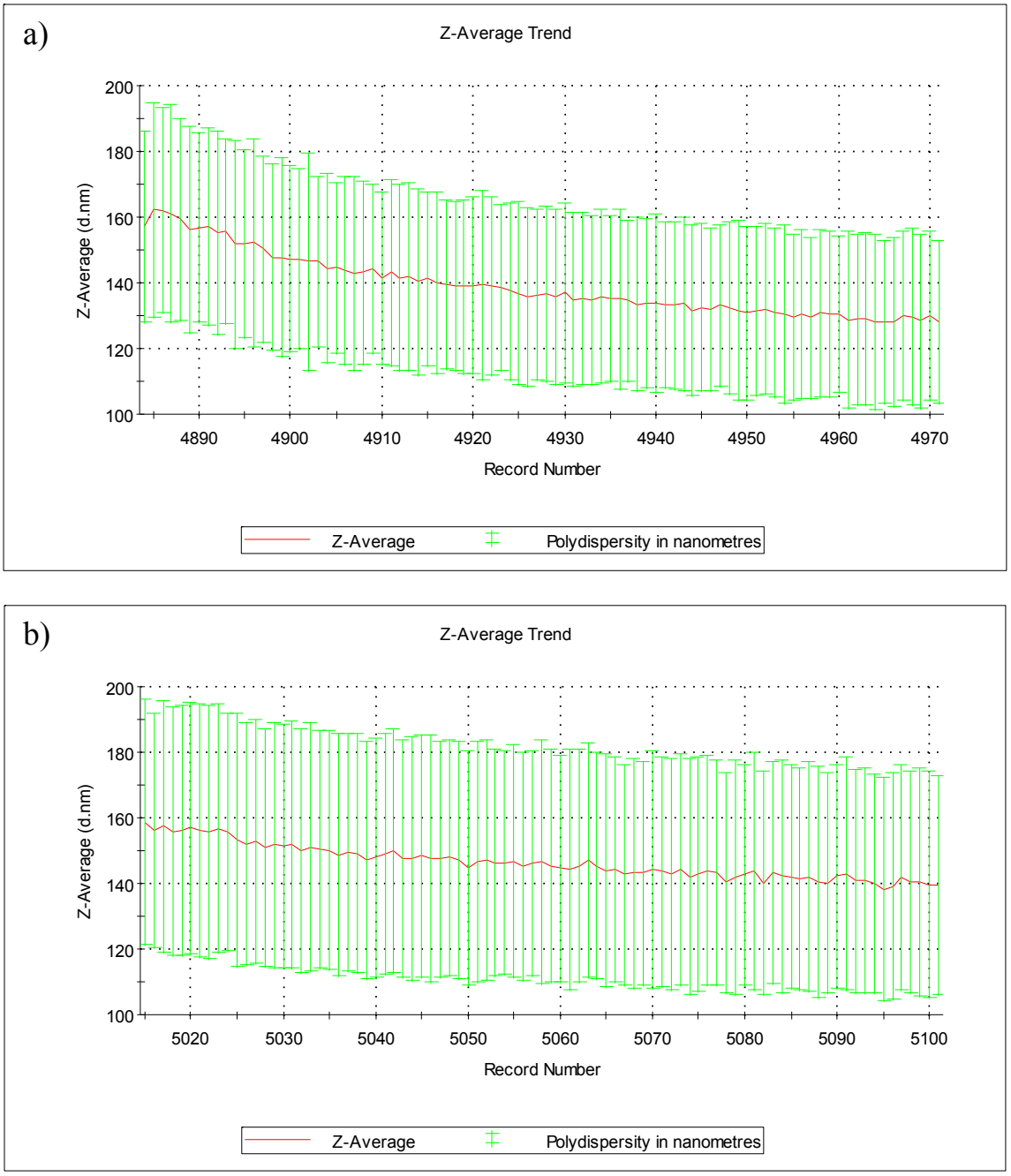

Figure 4.27. (a) DLS stability of La-DSCP@DOPA@Lipid in PBS overnight. The Z average diameter slowly stabilizes to 130 nm, which may indicate a small population of larger particles settles out. Zavg = 139.2 ± 9.3 nm, PDI = 0.153 ± 0.013, and count rate = 330.4 ± 27.3 kcps. (b) DLS stability of La-DSCP@DOPA@Lipid in 5 mM PBS with 5 mg/mL BSA. Zavg = 146.5 ± 5.1 nm, PDI = 0.238 ± 0.010, and count rate = 325.1 ± 16.2 kcps.

The lipid-coated La-DSCP NCPs were modified with DSPE-Peg_{2K}-AA to be rendered cancer specific as AA is known to target sigma receptors that are overexpressed on epithelial cancer tissues.[15-20] AA-modified NCPs were prepared by replacing DSPE-Peg_{2K} with both DSPE-Peg_{2K} and DSPE-Peg_{2K}-AA in a 9:1 molar ratio during the lipid coating procedure. These particles are the same size and morphology as the non-targeted formulation and display similar DLS stability characteristics in an abbreviated BSA assay (Figure 4.28).

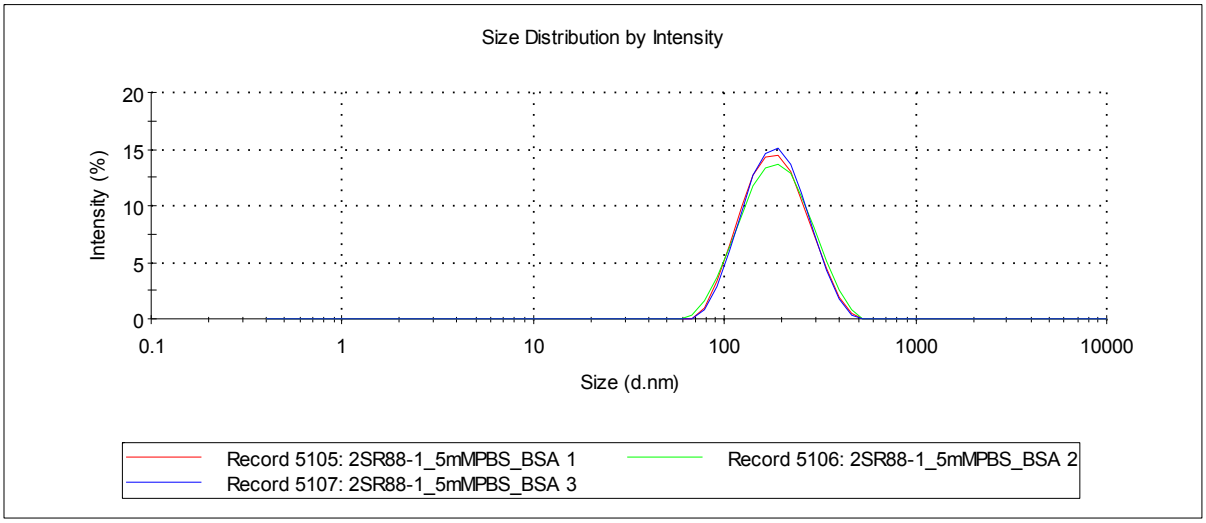

Figure 4.28. DLS stability of La-DSCP@DOPA@Lipid-AA in 5 mM PBS with 5 mg/mL BSA over 1 h.

4.2.7. Synthesis and Characterization of La-Suc NCP

Control vehicles, La(III) NCP formulations that do not contain the cisplatin prodrug, were prepared for *in vitro* viability assays. Succinic acid (Suc) was used as the ligand instead of the cytotoxic prodrug, and particles of La-Suc were prepared by a similar surfactant-templated heating method as the La-DSCP NCP. Lipid-coated and AA-targeted versions of these control vehicles were prepared using the same lipid coating strategies described above for La-DSCP. Particles of La-Suc were the same size and morphology as the La-DSCP NCPs by both SEM and TEM (Figure 4.29). La-Suc has a Z average diameter similar to La-DSCP

as well (141.0 nm with a PDI of 0.137). The Z average diameters for the lipid-coated non-targeted and targeted La-Suc NCPs are 227.6 nm (PDI of 0.211) and 185.6 nm (PDI of 0.282), respectively. These formulations were used in *in vitro* viability assays with NSCLC cell lines.

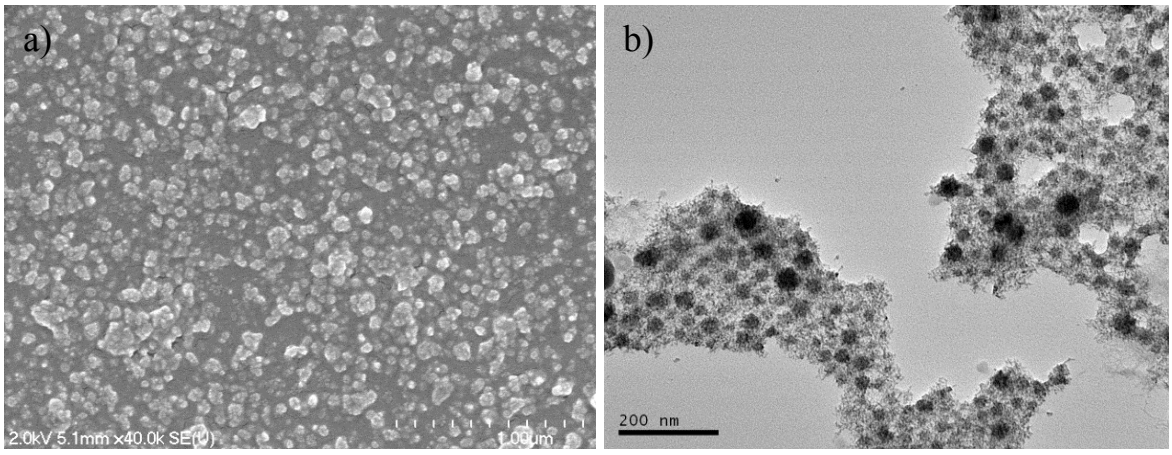

Figure 4.29. SEM (a) and TEM (b) micrographs of La-Suc control vehicle NCPs.

4.2.8. In Vitro Cytotoxicity and Viability Assays

Larger Zr-DSCP NCPs were tested in a 72 h *in vitro* cytotoxicity assay against NCI-H460 NSCLC cells (Figure 4.30). Compared to free cisplatin, both cisplatin and Zr-DSCP have the same IC_{50} value of ~ 1 μM. This is expected because as-synthesized Zr-DSCP will degrade in the cell medium and will essentially become the equivalent of free cisplatin. La-DSCP formulations were tested in a 48 h trypan blue exclusion assay against NCI-H460 cells (Figure 4.31). NCI-H460 cells are known to overexpress sigma receptors. IC_{50} values (μM) were: cisplatin = 0.53 ± 0.14, La-DSCP = 5.57 ± 0.40, La-DSCP@Lipid = 0.67 ± 0.06, and La-DSCP@Lipid-AA = 0.32 ± 0.03. There is a statistically significant difference between the IC_{50} values for the non-targeted and AA-targeted NCPs by the t test ($\alpha \leq 0.05$). Thus, it can be concluded that targeting with AA leads to a significant improvement in efficacy.

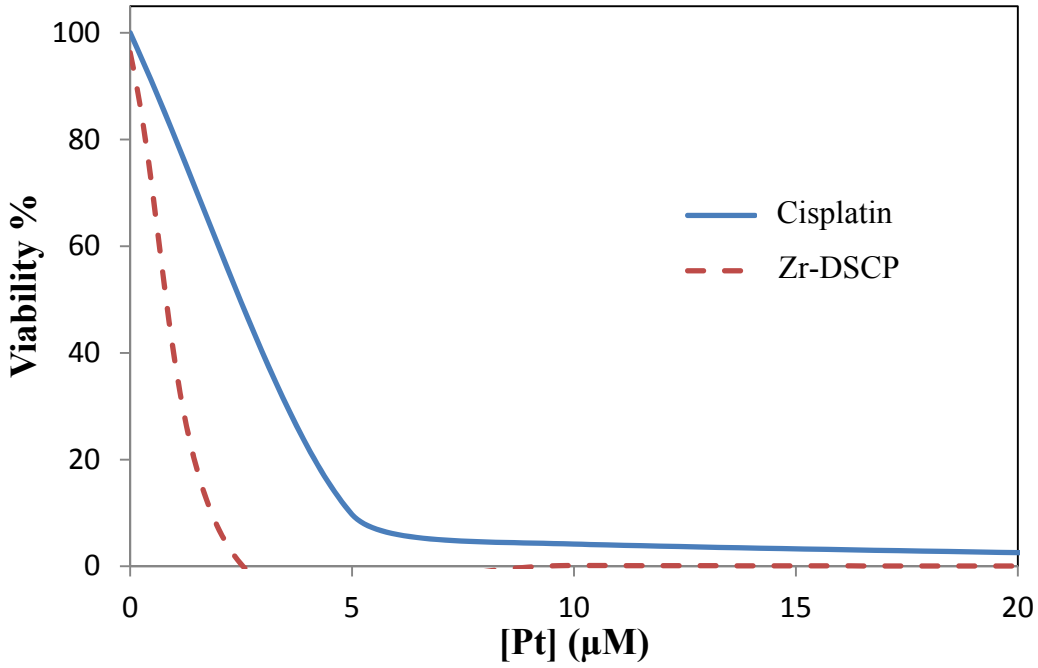

Figure 4.30. *In vitro* cytotoxicity curves for cisplatin and large Zr-DSCP against NCI-H460 NSCLC cells over 72 h.

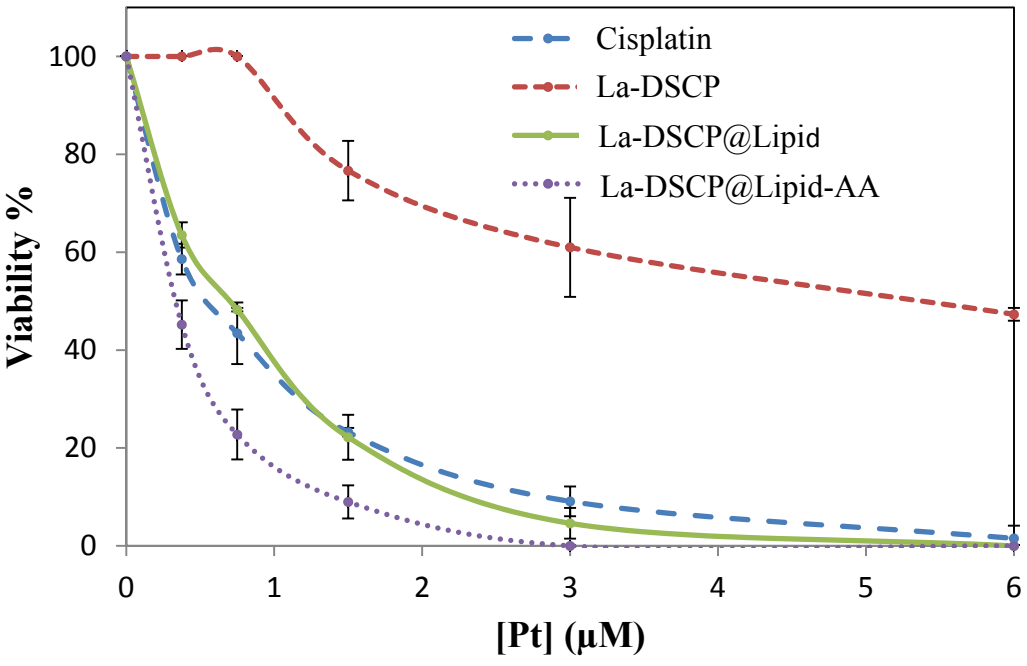

Figure 4.31. *In vitro* cytotoxicity curves for cisplatin and La-DSCP formulations against NCI-H460 cells for 48 h.

The La-DSCP formulations were also tested for efficacy in the A549 NSCLC cell line, a cell line that has very minimal expression of sigma receptors. For a 48 h trypan blue exclusion assay, IC_{50} values (μM) were: cisplatin = 2.20 ± 0.17, La-DSCP = 5.90 ± 1.03, La-DSCP@Lipid = 1.20 ± 0.53, and La-DSCP@Lipid-AA = 1.33 ± 0.32 (Figure 4.32). There was not a statistically significant difference between IC_{50} values of the non-targeted and AA-targeted La-DSCP formulations by the t test ($\alpha = 0.32$), likely due to lack of expression of sigma receptors for this cell line.

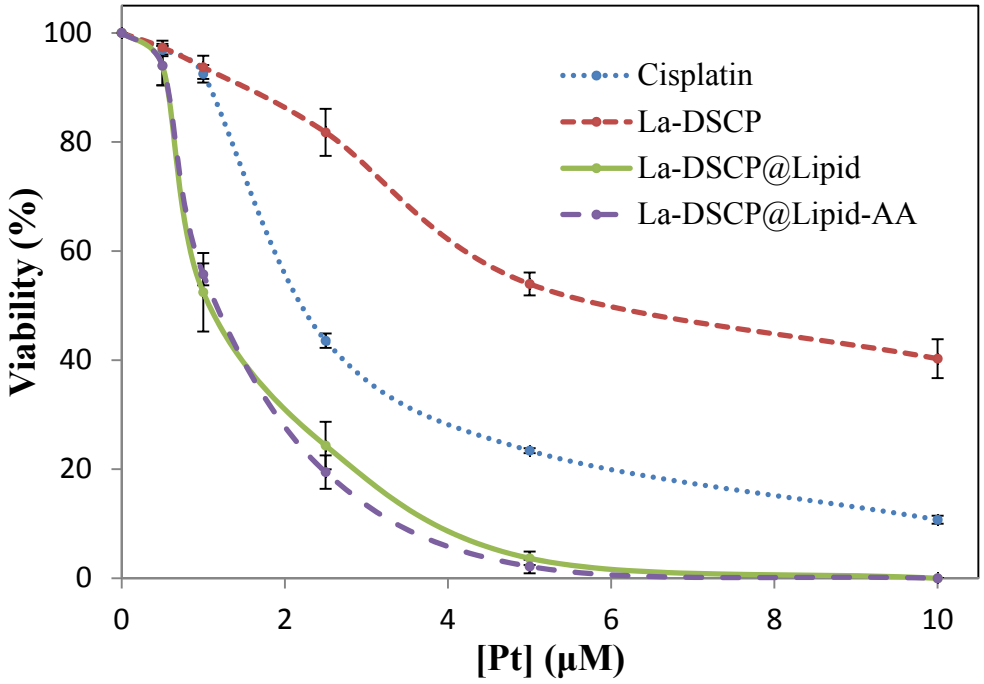

Figure 4.32. *In vitro* cytotoxicity assay testing cisplatin and La-DSCP formulations against A549 NSCLC cells for 48 h.

A viability assay was conducted using the same conditions for the cytotoxicity assay. In the relevant concentration range, no cytotoxicity was observed for the La-Suc formulations in NCI-H460 cells (Figure 4.33) or A549 cells (Figure 4.34). This result means that any observed cytotoxicity for La-DSCP formulations is from the DSCP prodrug, not

from La(III) or the lipid coating formulation. Additionally, a viability test was done to test from $LaCl_3$ salt to observe any cytotoxic effects from the amount of La(III) that would be released from La-DSCP during the assay. This amount was determined by the ICP-MS analysis for La content (La-DSCP = 20 wt% La). No cytotoxic effects were observed for NCI-H460 cells (Figure 4.35) or A549 cells (Figure 4.36).

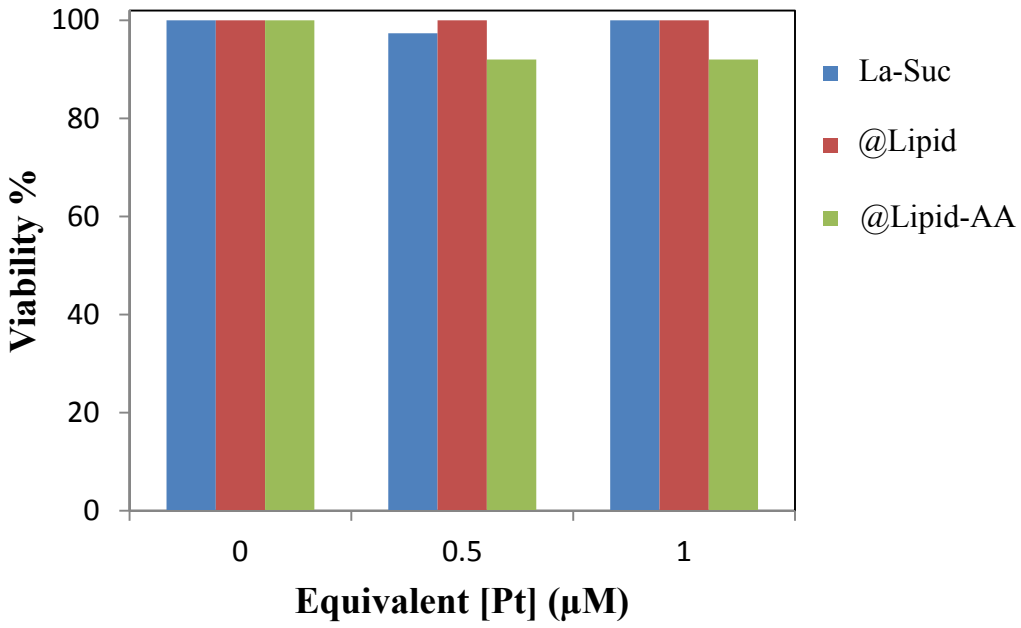

Figure 4.33. *In vitro* viability assay testing La-Suc formulations against NCI-H460 NSCLC cells for 48 h, showing no cytotoxic effects.

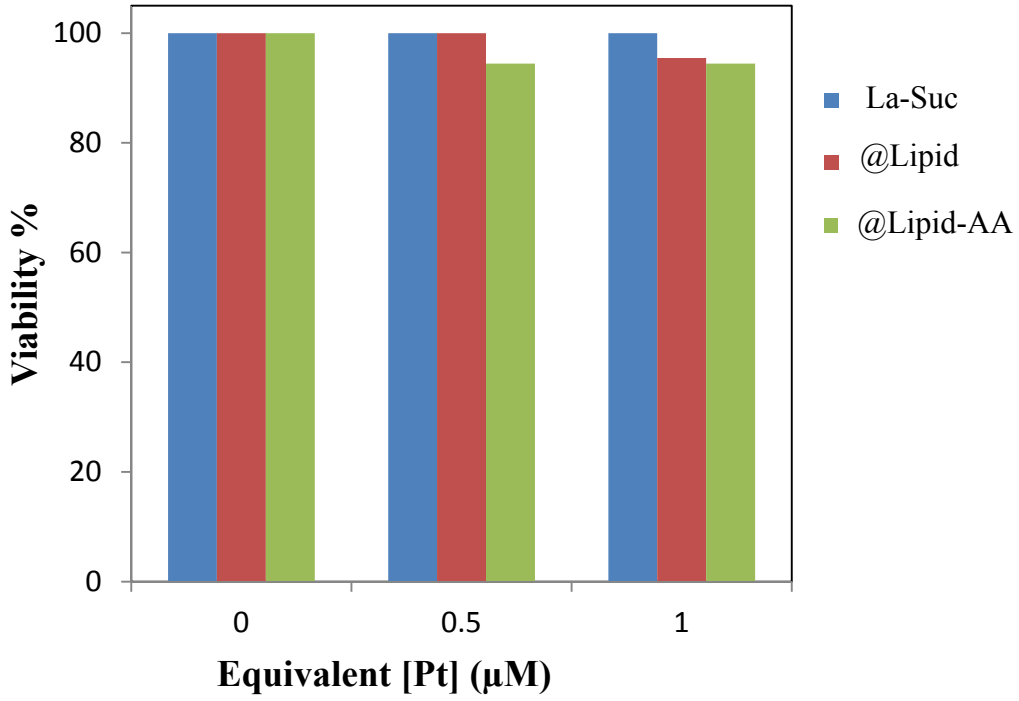

Figure 4.34. *In vitro* viability assay testing La-Suc formulations against A549 NSCLC cells for 48 h, showing no cytotoxic effects.

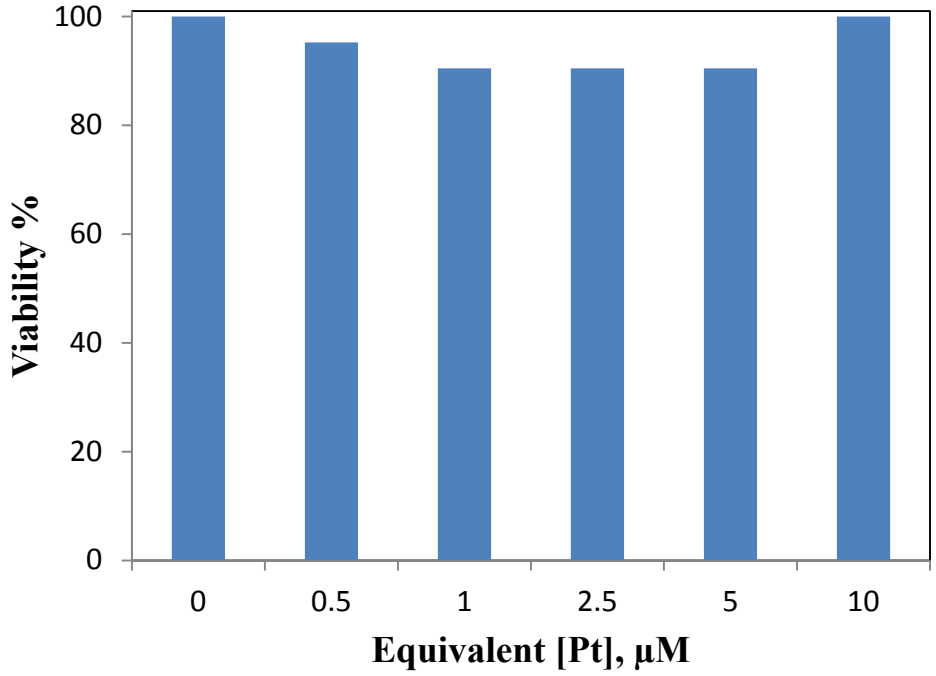

Figure 4.35. *In vitro* viability assay testing $LaCl_3$ salt against NCI-H460 NSCLC cells for 48 h, showing no cytotoxic effects.

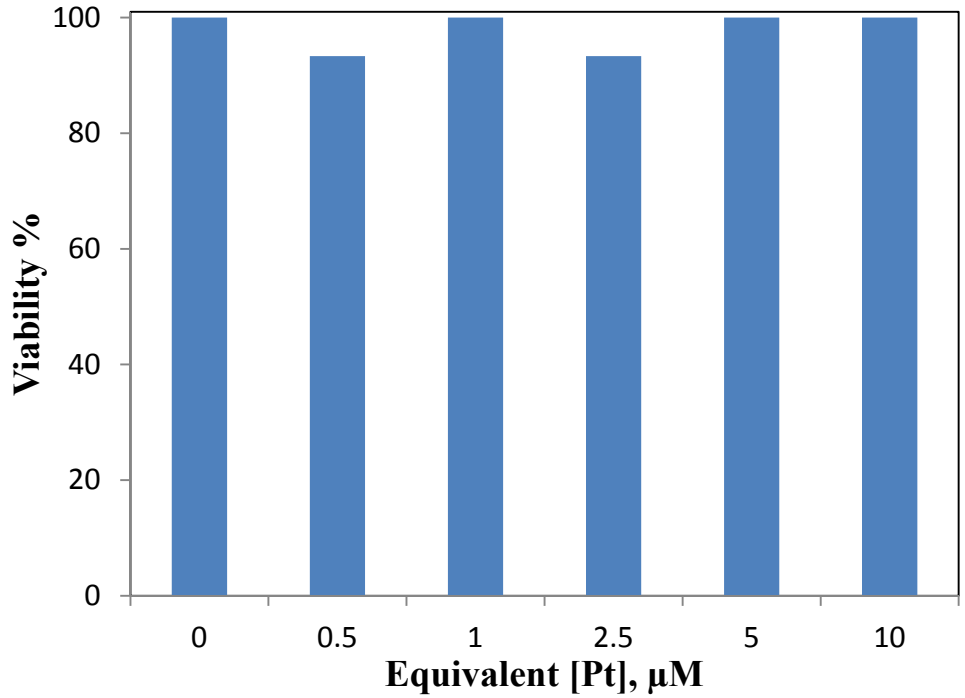

Figure 4.36. *In vitro* viability assay testing $LaCl_3$ salt against A549 NSCLC cells for 48 h, showing no cytotoxic effects.

4.2.9. Synthesis and Characterization of $Ru(bpy)_3^{2+}$-Containing NCPs

La-Suc NCPs doped with the optical imaging agent $Ru(bpy)_3^{2+}$ were prepared by a similar surfactant-templated heating method in which ~10 mol% [Ru(5,5'-CO_2H-bpy)$(bpy)_2$]$(PF_6)_2$ was added to the reverse microemulsion containing Suc. These particles were used in laser scanning confocal microscopy studies. Particles are between 50-200 nm by SEM and TEM (Figure 4.37) and have a Z average diameter of 187.3 nm with a PDI of 0.238. Like their non-doped counterparts, these particles possess a large amount of organic weight by TGA (Figure 4.38), presumably due to the large amount of DOPA associated with these particles. The presence of Ru was confirmed by ICP-MS (0.5 wt%). The presence of $Ru(bpy)_3^{2+}$ in these doped La-Suc NCPs was also confirmed by fluorescence spectroscopy (Figure 4.39). A broad emission characteristic of $Ru(bpy)_3^{2+}$ is observed at ~ 620 nm.

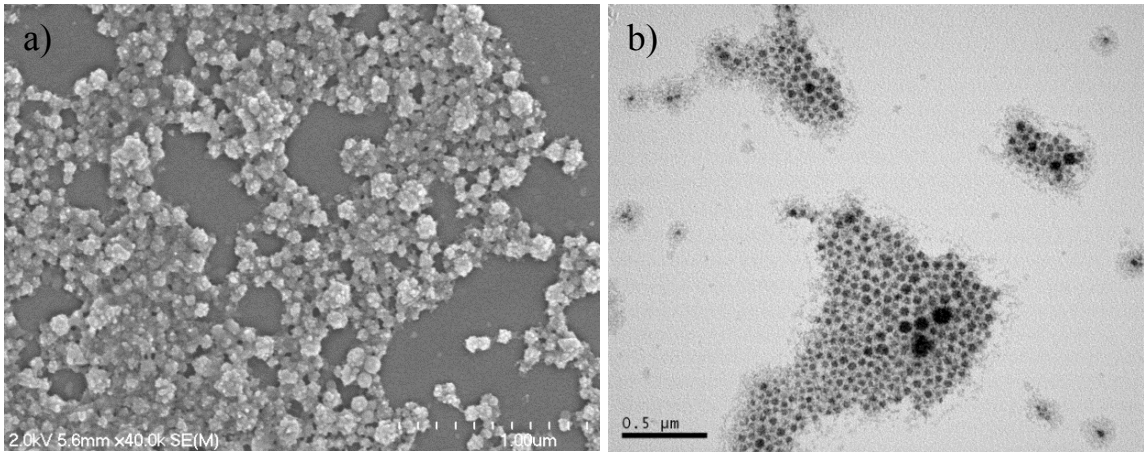

Figure 4.37. SEM (a) and TEM (b) micrographs of $Ru(bpy)_3^{2+}$-doped La-Suc NCPs.

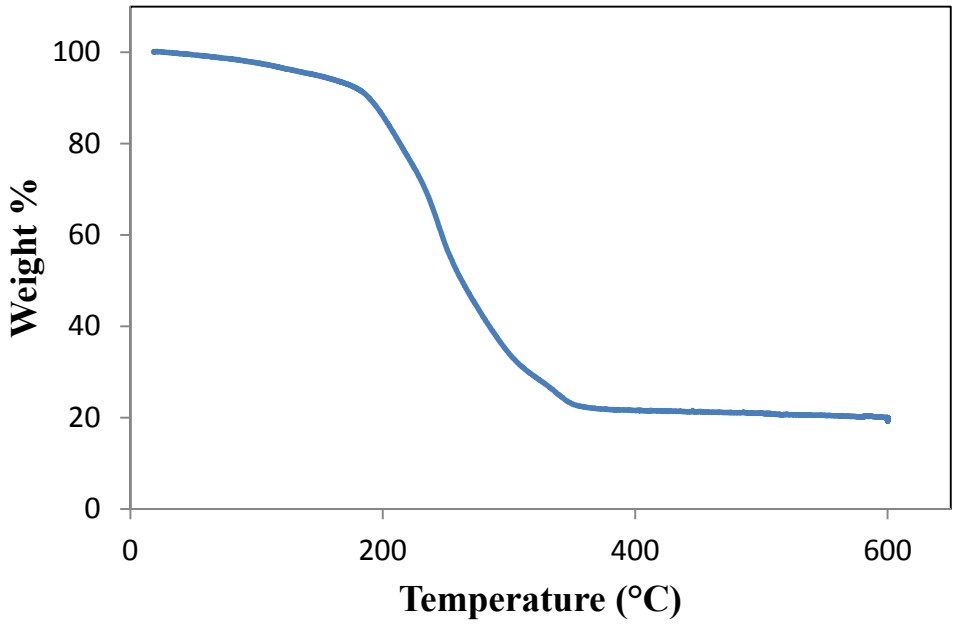

Figure 4.38. TGA plot of $Ru(bpy)_3^{2+}$-doped La-DSCP showing a large amount of organic weight loss, presumably due to DOPA associated with the particles.

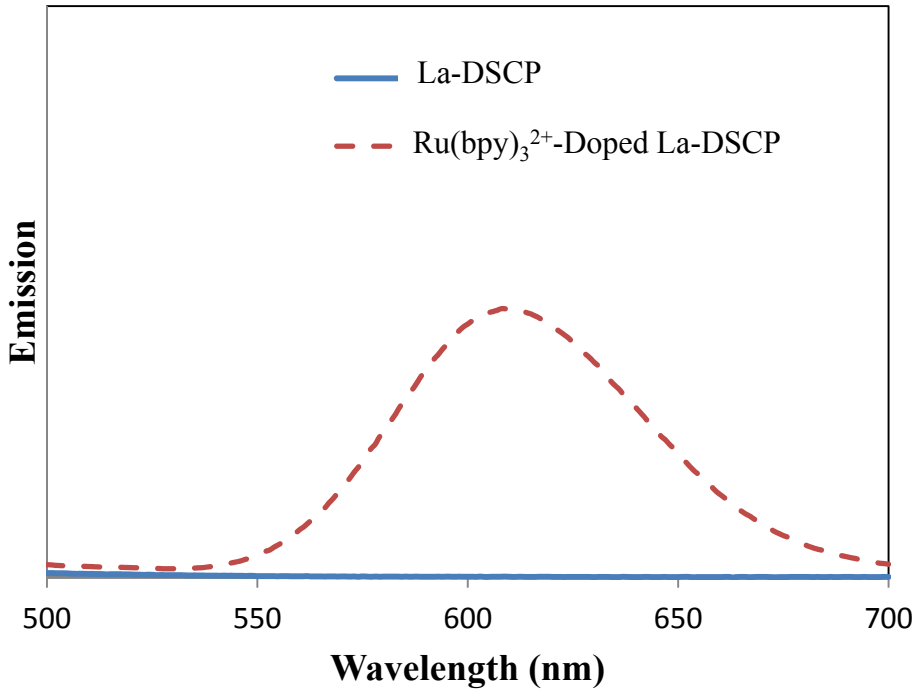

Figure 4.39. Florescence spectra of La-DSCP and $Ru(bpy)_3^{2+}$-doped La-DSCP, showing emission of $Ru(bpy)_3^{2+}$ at ~620 nm (excitation 450 nm).

4.2.10. Confocal Microscopy

Enhanced uptake of the AA-targeted La-DSCP formulation was confirmed by laser scanning confocal microscopy. Particles of $Ru(bpy)_3^{2+}$-doped La-Suc were incubated with NCI-H460 cells for 30 min and imaged on a confocal microscope (Figure 4.40). Images show almost no fluorescence for La-Suc, likely due to rapid degradation of the as-synthesized particles. Slightly more fluorescence is observed for La-Suc@Lipid, but intense fluorescence from La-Suc@Lipid-AA is observed, indicating enhanced uptake due to active targeting of these targeted particles.

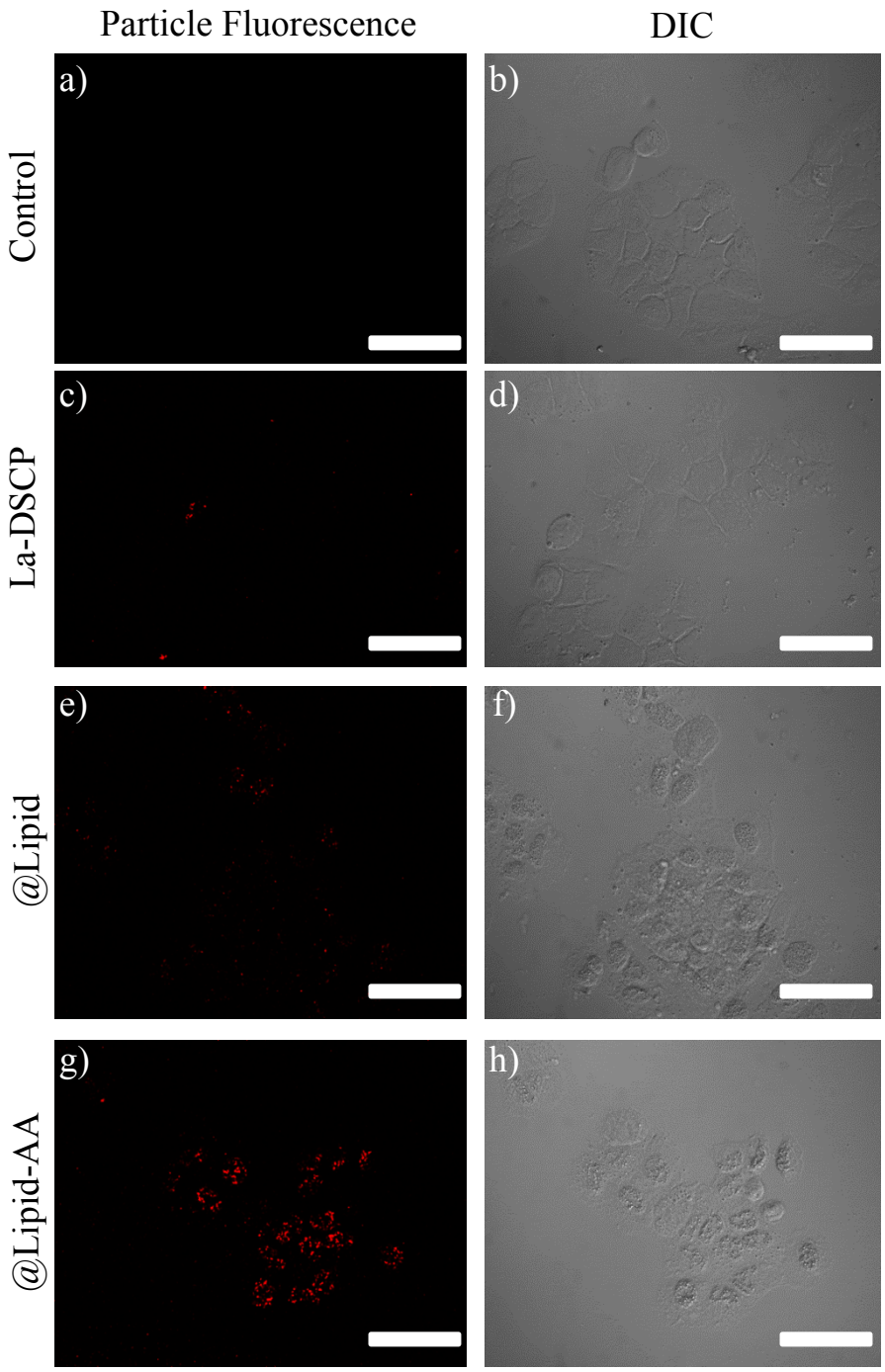

Figure 4.40. Laser scanning confocal microscopy images showing DIC (b, d, f, h) and red fluorescence (a, c, e, g) attributed to particle fluorescence from $Ru(bpy)_3^{2+}$: (a, b) control (no particles), (c, d) La-Suc, (e, f) La-Suc@Lipid, and (g, h) La-Suc@Lipid-AA. Scale bars = 20 μm.

4.2.11. Competitive Binding Assays

In order to further confirm enhanced uptake due to active targeting of the AA-targeted La-Suc formulation, competitive binding assays were conducted in which the sigma receptors of NCI-H460 cells were saturated with NH_3-Peg_{5K}-AA, then incubated with either La-DSCP@Lipid or La-DSCP@Lipid-AA. The amount of La and Pt internalized by the cells was determined by ICP-MS. As shown in Figures 4.41 and 4.42, the uptakes of both formulations are the same when the cells have been incubated with an equal amount of NH_3-Peg_{5K}-AA, which means that the active targeting ability of La-DSCP@Lipid-AA has been silenced. Additionally, less uptake of the AA-targeted formulation is observed when the amount of NH_3-Peg_{5K}-AA is increased.

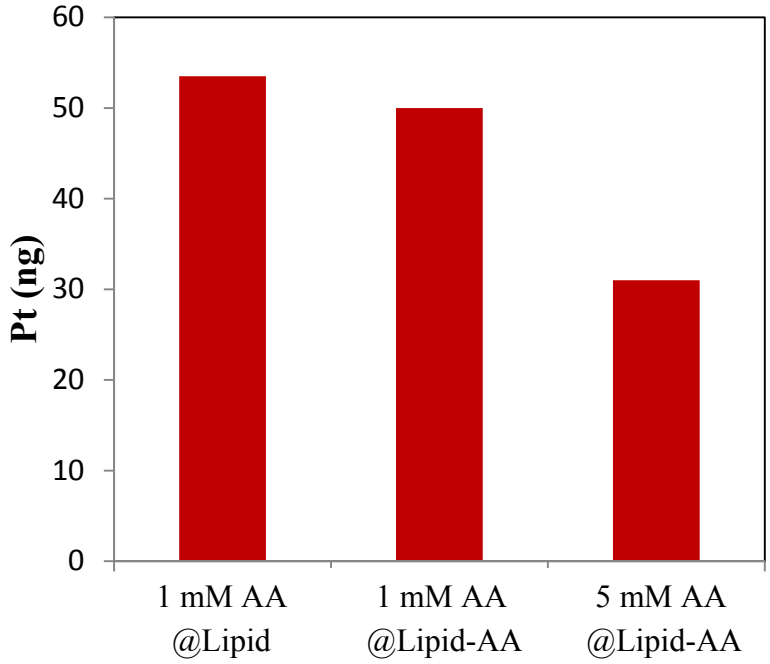

Figure 4.41. Competitive binding assay showing amount of Pt uptake in NCI-H460 cells treated subsequently with amounts of NH_2-PEG_{5K}-AA and either La-DSCP@Lipid or La-DSCP@Lipid-AA.

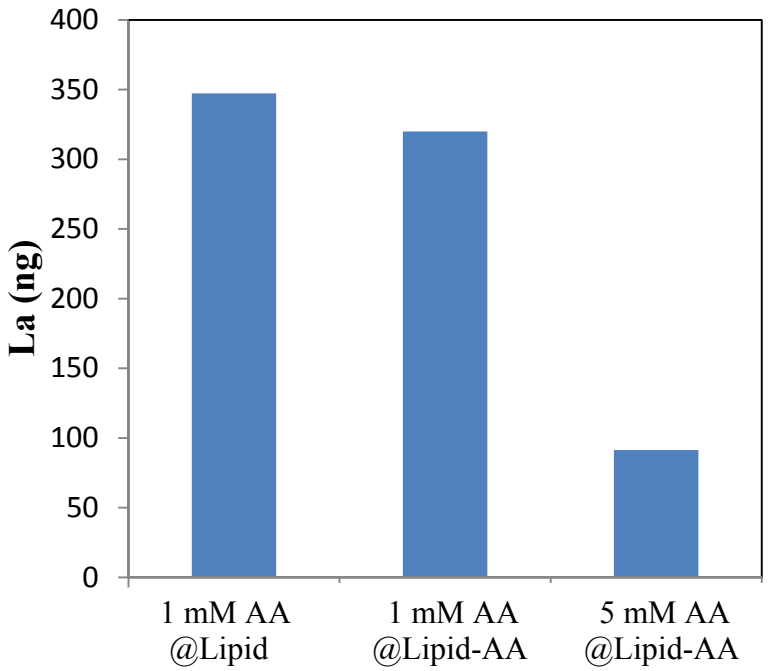

Figure 4.42. Competitive binding assay showing amount of La uptake in NCI-H460 cells treated subsequently with amounts of NH_2-PEG_{5K}-AA and either La-DSCP@Lipid or La-DSCP@Lipid-AA.

4.3. Conclusion

In summary, several NCP formulations containing the cisplatin prodrug DSCP were prepared using different binding metals; however only one of these formulations could be stabilized with encapsulation with a lipid bilayer, La-DSCP. Coating with a cholesterol/DOPC/DSPE-Peg_{2K} lipid layer doped with DSPE-Peg_{2K}-AA rendered this formulation an active targeting agent for sigma receptors. The resulting formulation proved more potent than free cisplatin in NSCLC cell lines; enhanced uptake was demonstrated by both confocal microscopy and competitive binding assays.

4.4. Experimental Details

4.4.1. Materials and Methods

All chemicals, unless otherwise noted, were purchased from Fisher Scientific or Sigma Aldrich and used without further purification. Cisplatin (for synthesis of disuccinatocisplatin, DSCP) was purchased from AK Scientific. DSCP was prepared by an established procedure.[11] 1,2-dioleoyl-*sn*-glycero-3-phosphate (DOPA), 1,2-dioleoyl-*sn*-glycero-3-phosphocholine (DOPC), and 1,2-distearoyl-*sn*-glycero-3-phosphoethanolamine-N-(polyethylene glycol) (DSPE-Peg_{2K}) were purchased from Avanti Polar Lipids. Cell culturing supplies, fetal bovine serum (FBS), RPMI-1640 growth medium, phosphate buffered saline (PBS), penicillin-streptomycin, and trypsin-EDTA were purchased from Fisher Scientific. Microwave reactions were carried out in a CEM MARS 5 digestion microwave system. Scanning electron microscopy (SEM) was obtained on a Hitachi 4700 Field Emission Scanning Electron Microscope, and transmission electron microscopy (TEM) was obtained on a JEM 100CX-II Transmission Electron Microscope. A Cressington 108 Auto Sputter Coater equipped with a Au/Pd (80/20) target and MTM-10 thickness monitor was used to coat samples before SEM imaging. SEM micrographs were obtained on glass slides, and TEM micrographs were obtained on carbon-coated copper grids. Thermogravimetric analysis (TGA) was performed on a Shimadzu TGA-50 equipped with a platinum pan, and samples were heated at a rate of 3°C/min under air. Size and zeta potential information was obtained on a Malvern ZetaSizer dynamic light scattering instrument. Fluorescence spectra were obtained on a Shimadzu RF-530PC spectrofluorophotometer. Confocal microscopic images were obtained on glass slides and imaged on the Olympus

FlowView500 confocal microscope at the UNC-CH Microscope and Imaging Facility. Images were analyzed using ImageJ (with the UCSD plugin) and PhotoShop.

4.4.2. Synthesis of Reagents

Synthesis of DSPE-Peg$_{2K}$-AA. 4-methoxybenzoic acid (3 g, 20 mmol) in 10 mL thionyl chloride was refluxed for 2 h. Remaining thionyl chloride was removed in vacuo to give 4-methoxybenzoyl chloride. Under Ar gas, a solution of 4-methoxybenzoyl chloride (1.000 g, 5.862 mmol) in 10 mL CH_2Cl_2 was slowly added to a solution of diethylenetriamine (0.588 mL, 5.862 mmol) and 2 mL TEA in 10 mL CH_2Cl_2 at 0 °C. The reaction mixture was stirred for 2 h, and the slurry was diluted with additional CH_2Cl_2 and washed with 1 M NaOH. The organic layer was dried with Na_2SO_4, and the solvent was concentrated under reduced pressure. The residue was purified by silica gel column chromatography with CH_2Cl_2/methanol (5:1, v/v) with 1-2% TEA as the eluent to yield N-(2-((2-aminoethyl)amino)ethyl)-4-methoxybenzamide. Yield: 20%. ^{1}H NMR ($CDCl_3$): δ 7.79 (d, 2H), 6.90 (d, 2H), 3.82 (s, 3H), 3.91 (s, 24H), 3.27 (m, 2H), 2.90 (m, 4H), 2.75 (m, 2H). N-(2-((2-aminoethyl)amino)ethyl)-4-methoxybenzamide (130 mg, 0.55 mmol) was reacted with PEG$_{2K}$-bis-carboxylate (1.2 g, 0.55 mmol) in 80 mL anhydrous CH_2Cl_2 in the presence of N,N'-dicyclohexylcarbodiimide (230 mg, 1.1 mmol) and 4-dimethylaminopyridine (135 mg, 1.1 mmol) under N_2 for 48 h. After solvent concentration, 300 mL diethyl ether was added to the mixture, and the crude product precipitated out and was isolated by centrifugation. The product was purified by silica gel column chromatography with CH_2Cl_2/methanol (10:1 v/v) as the eluent to afford AA-PEG$_{2K}$-mono-carboxylate. Yield: 35%.^{1}H NMR ($CDCl_3$): δ 7.77 (m, 2H), 6.89 (d, 2H), 4.20 (m, 2H), 3.95 (s, 3H), 3.81 (t,4H), 3.61 (s,180H)3.44 (m, 2H). AA-PEG$_{2K}$-mono-carboxylate (300 mg, 0.13 mmol) was reacted

with DSPE (115 mg, 0.15 mmol) in 25 mL anhydrous CH_2Cl_2 in the presence of N,N'-dicyclohexylcarbodiimide (53 mg, 0.26mmol) and 4-dimethylaminopyridine (31.3 mg, 0.26 mmol) under N_2 for 48 h. After solvent concentration, 50 mL diethyl ether was added to the mixture, and the crude product precipitated out and was isolated by centrifugation. The product was then purified by silica gel column chromatography with CH_2Cl_2/methanol (10:1 v/v) as the eluent to afford AA-PEG_{2K}-DSPE. Yield: 30%.^{1}H NMR ($CDCl_3$): δ 7.78 (m, 2H), 6.88 (d, 2H), 4.22 (m, 4H), 3.81 (s, 3H), 3.62 (s, 180H), 2.25 (s, 6H), 1.57 (s, 10H), 1.23 (S, 30H), 0.85 (t, 6H).

4.4.3. Synthesis of DSCP- and Suc-Containing NCPs

Synthesis of Mg-DSCP NCP. Particles of Mg-DSCP were prepared by a methanol-induced nanoprecipitation technique. In a 50 mL round bottom flask, 125 μL 0.25 M methyl ammonium DSCP (18.6 mg, 0.0313 mmol) and 188 μL 0.2 M $MgCl_2 \cdot 6H_2O$ (7.64 mg, 0.0376 mmol) were combined in 4.685 mL H_2O. Stirring rapidly, ~30 mL methanol was poured into the H_2O solution, resulting in a white dispersion which was stirred at room temperature for 1 h, in the dark. The particles were isolated by centrifugation at 13,000 rpm for 15 min, washed and centrifuged once with EtOH, and dispersed in EtOH. Yield = 3.5 mg (43.0 %).

Synthesis of Mn-DSCP NCPs. Particles of Mn-DSCP were first prepared by a methanol-induced nanoprecipitation technique. In a 50 mL round bottom flask, 125 μL 0.25 M aq. methyl ammonium DSCP (18.6 mg, 0.0313 mmol) and 188 μL 0.2 M aq. $MnCl_2 \cdot 4H_2O$ (7.44 mg, 0.0376 mmol) were combined in 4.685 mL H_2O. Stirring rapidly, ~30 mL methanol was poured into the H_2O solution, resulting in a white dispersion which was stirred at room temperature for 1 h, in the dark. The particles were isolated by centrifugation at 13,000 rpm for 15 min, washed and centrifuged twice with EtOH, and dispersed in EtOH.

Additionally, a surfactant-templated heating technique resulted in particles of Mn-DSCP. Two reverse (water in oil) microemulsions were prepared by two 50 mL round bottom flasks receiving 10 mL 0.5 M 1-hexanol in isooctanes and 365 mg CTAB (for 0.1 M CTAB). One flask was given (while stirring) 90 μL 0.2 M (9.58 mg, 0.018 mmol) aq. methylammonium DSCP. The other flask was given 90 μL 0.2 M (4.21 mg, 0.018 mmol) aq. $MnCl_2 \cdot 6H_2O$. Both reverse microemulsions (W = 10) became clear instantly, were combined in a microwave vessel, and microwaved at 120 ºC for 10 min using 400 W and 100% power. The product was isolated by centrifugation, subsequently washed and centrifuged once with EtOH, and dispersed in EtOH.

Synthesis of Larger Zr-DSCP NCP. Larger NCPs of Zr-DSCP were synthesized by a solvothermal method. In a 20 mL glass vial, 59.6 mg (0.1116 mmol) DSCP and 26.7 mg (0.1146 mmol) $ZrCl_4$ were dissolved in 10 mL DMF containing 200 μL 3M (0.6 mmol, 5 eq.) acetic acid. The vial was capped and placed in a 60 ºC oven overnight (18 h). The resulting white dispersion was isolated by centrifugation and were subsequently washed (by sonication) and centrifuged twice with ethanol. The particles were dispersed in ethanol Yield: 30 mg (34.8 %).

Solvothermal Microwave Synthesis of Smaller Zr-DSCP NCP. $ZrCl_4$ (12.56 mg, 0.0539 mmol) and DSCP (26.95 mg, 0.0505 mmol) were dissolved in 10 mL DMF with the addition of 83 μL 3 M (0.25 mmol) acetic acid aq., and the solution was heated in a sealed microwave vessel at 60 °C for 20 min without stirring. The product was isolated from the resulting white dispersion by centrifugation at 13,000 rpm for 15 min, washed by sonication and centrifugation once each with DMF and H_2O, and dispersed in EtOH.

Synthesis of Smaller Zr-DSCP NCP. NCPs of DOPA-capped Zr-DSCP were prepared by an acetone-induced precipitation technique. In a 150 mL beaker, 34.8 mg (0.1493 mmol) $ZrCl_4$ was dissolved in 13.5 mL DMF, followed by the addition of 80.4 mg (0.1505 mmol) DSCP and 270 μL 3M (0.75 mmol, 5 eq.) acetic acid. Stirring rapidly, ~100 mL acetone was poured into the DMF solution, resulting in a white dispersion which was stirred at room temperature for 1 h, in the dark. The particles were isolated by centrifugation and underwent subsequent washes/centrifugation once with acetone and once with ethanol. The particles were dispersed in ethanol. Yield: 24 mg (21.0 %).

Synthesis of DOPA-Capped Zr-DSCP NCP. Particles of DOPA-capped Zr-DSCP NCP were prepared by a chloroform-induced precipitation technique. $ZrCl_4$ (17.4 mg, 0.0747 mmol) was dissolved in 6.25 mL DMF, followed by the addition of 40.2 mg (0.0753 mmol) DSCP and 135 μL 3M (0.405 mmol, 5 eq.) acetic acid. A separate solution of $CHCl_3$ containing 2.4 mg (3.32 μmol) DOPA was prepared. Stirring rapidly, the reaction slurry was precipitated with the DOPA solution, resulting in a white dispersion which was stirred at room temperature for 1 h, in the dark. The particles were isolated by centrifugation, subsequently washed/centrifuged twice with ethanol, and dispersed in ethanol. Yield: 22 mg (38.1 %).

Synthesis of La-DSCP NCP. Particles of La-DSCP NCP were prepared by a surfactant-assisted heating method. Two reverse (water in oil) microemulsions were prepared by two 25 mL round bottom flasks receiving 5 mL 0.3 M TritonX-100/1.5 M 1-hexanol in cyclohexane. One flask was given (while stirring) 200 μL 25 mg/mL (5 mg, 0.0135 mmol) aq. $LaCl_3 \cdot 7H_2O$ pH = 5.5. The other flask was given 200 μL 25 mg/mL (5 mg, 0.00936 mmol) aq. DSCP pH = 4 and 30 μL 200 mg/mL (6 mg, 0.0083 mmol) DOPA in $CHCl_3$. Both

reverse microemulsions (W = 7.4) became clear instantly, were combined in a microwave vessel, and microwaved at 70 ºC for 10 min using 400 W, 100% power, and a 5 min ramping time. The white product was isolated by centrifugation, subsequently washed/centrifuged once with THF, and dispersed in THF. Yield: 13.5 mg (84.4 %).

Synthesis of La-Suc NCP. Particles of La-Suc were prepared by a surfactant-assisted heating method. Two reverse (water in oil) microemulsions were prepared by two 25 mL round bottom flasks receiving 5 mL 0.3 M TritonX-100/1.5 M 1-hexanol in cyclohexane. One flask was given (while stirring) 200 µL 25 mg/mL (5 mg, 0.0135 mmol) aq. $LaCl_3 \cdot 7H_2O$ pH = 5.5. The other flask was given 200 µL 50 mg/mL (10 mg, 0.037 mmol) aq. succinic acid ($Na_2(suc) \cdot 6H_2O$) pH = 6 and 30 µL 200 mg/mL (6 mg, 0.0083 mmol) DOPA in $CHCl_3$. Both reverse microemulsions (W = 7.4) were combined in a microwave vessel, and microwaved at 70 ºC for 10 min using 400 W, 100% power, and a 5 min ramping time. The white product was isolated by centrifugation, subsequently washed and centrifuged once with THF, and dispersed in THF. Yield: 13.5 mg (64.3 %).

Synthesis of $Ru(bpy)_3^{2+}$-doped La-DSCP. Particles of La-Suc doped with $Ru(bpy)_3^{2+}$ were prepared by a surfactant-templated method in which two reverse (water in oil) microemulsions were made by two 25 mL round bottom flasks receiving 5 mL 0.3 M TritonX-100/1.5 M 1-hexanol in cyclohexane. One flask was given (while stirring) 200 µL 25 mg/mL (5 mg, 0.0135 mmol) aq. $LaCl_3 \cdot 7H_2O$ pH = 5.5. The other flask was given 200 µL 50 mg/mL (10 mg, 0.037 mmol) aq. succinic acid ($Na_2(suc) \cdot 6H_2O$) pH = 6, 30 µL 200 mg/mL (6 mg, 0.0083 mmol) DOPA in $CHCl_3$, and 48 µL 50 mg/mL (2.4 mg, 0.0037 mmol) $[Ru(5,5'\text{-}CO_2H\text{-}bpy)(bpy)_2](PF_6)_2$. The $Ru(bpy)_3^{2+}$ derivative was synthesized by a previous method.[1] Both reverse microemulsions (W = 7.4) became clear instantly, were combined in a

microwave vessel, and microwaved at 70 ºC for 10 min using 400 W, 100% power, and a 5 min ramping time. The orange product was isolated by centrifugation, subsequently washed/centrifuged once with THF, and dispersed in THF. Yield: 1.7 mg (8.5 %).

4.4.4. Surface Modifications of Zr-DSCP NCP

Synthesis of PVP-Coated Zr-DSCP NCP. A total of 8 mg of Zr-DSCP was isolated by centrifugation and dispersed by sonication in 8 mL ethanol (for 1 mg/mL particles). Molecular weight 23K polyvinylpyrollidone (PVP) (8.5 mg, 0.37 μmol) was added and the dispersion was stirred at room temperature 18 h, in the dark. The resulting particles of Zr-DSCP@PVP were isolated by centrifugation, subsequently washed and centrifuged twice with ethanol, and redispersed in ethanol. Yield: 5 mg (62.5 %).

Silica Coating of PVP-Coated Zr-DSCP NCP. Silica coating of Zr-DSCP@PVP was carried out by isolating 6.6 mg Zr-DSCP@PVP by centrifugation and dispersing in 3.025 mL ethanol. A basic ethanol solution was prepared by adding 275 μL concentrated NH_4OH to 13.2 mL ethanol. While stirring, the particle dispersion was added to the basic ethanol solution, followed by the addition of 26.5 μL tetraethyl orthosilicate (TEOS). The dispersion was stirred at room temperature for 4 h, in the dark. This procedure was carried out such that there was 0.4 mg/mL Zr-DSCP@PVP, 0.25 M NH_4OH, and 4 μL TEOS per mg Zr-DSCP@PVP. The resulting particles were isolated by centrifugation, subsequently washed/centrifuged twice with ethanol, and dispersed in ethanol. Yield: 5.8 mg (87.5 %).

4.4.5. Lipid Coating Procedures

Lipid Coating of Zr-DSCP or La-DSCP NCP. Particles of Zr-DSCP or La-DSCP (0.5 mg) were isolated by centrifugation and dispersed in 100 μL THF. All lipid solutions (5

mg/mL in THF) and the particle dispersion were heated to 50 ºC in a water bath. The following lipids were added to the particle dispersion: 42 µL (0.21 mg, 0.543 µmol) cholesterol, 84 µL (0.42 mg, 0.543 µmol) DOPC, and 150 µL (0.75 mg, 0.273 µmol, 20 mol%) DSPE-Peg_{2K}. A solution of EtOH/H_2O (30 % v/v, 500 µL) was heated to 50 ºC, and, while stirring, the particle dispersion was added dropwise. THF was removed by an N_2 stream.

Lipid Coating and Anisamide-Targeting of La-DSCP or La-Suc NCP. Particles of La-DSCP or La-Suc (0.5 mg) were isolated by centrifugation and dispersed in 100 µL THF. All lipid solutions (5 mg/mL in THF) and the particle dispersion were heated to 50 ºC in a water bath. The following lipids were added to the particle dispersion: 42 µL (0.21 mg, 0.543 µmol) cholesterol, 84 µL (0.42 mg, 0.543 µmol) DOPC, 135 µL (0.675 mg, 0.245 µmol) DSPE-Peg_{2K}, and 15 µL (0.075 mg, 0.025 µmol) DSPE-Peg_{2K}-AA. A solution of EtOH/H_2O (30 % v/v, 500 µL) was heated to 50 ºC, and, while stirring, the particle dispersion was added dropwise. THF was removed by an N_2 stream.

Release Profiles. All release profiles were carried out in 5 mM PBS at 37 ºC. A 1 L solution of 5 mM PBS was prepared by dissolving 8.528 g (0.146 mol) NaCl and 680 mg (5 mmol) KH_2PO_4 in 500 mL MilliQ H_2O. The pH was adjusted to 7.4 with NaOH, and the solution was brought to 1 L with MilliQ H_2O. Between 2-4 mg DSCP-containing NCPs were prepared in 500 µL PBS or 30 % v/v EtOH/H_2O and added to a length of 10K molecular weight cutoff dialysis tubing. The dialysis tubing was submerged in a beaker containing 400 mL 5 mM PBS stirring at 37 ºC. Aliquots of 1 mL each were removed from the beaker at designated time intervals, and the volumes were replaced with fresh PBS. Samples were

digested in 115 μL concentrated HNO_3, filtered through a 0.2 μM PTFE syringe filter, and analyzed by ICP-MS for Pt content. Pt content (in ppb) was converted to % drug released.

4.4.6. In Vitro Assay Methods

Cell Lines. NCI-H460 non-small cell lung cancer cells (ATCC# HTB-177) and A549 non-small cell lung cancer cells (ATCC# CCL-185) were purchased from the Tissue Culture Facility of Lineberger Comprehensive Cancer Center at the University of North Carolina at Chapel Hill. Both cell lines were maintained in RPMI-1640 growth medium supplemented with 10% FBS and 2% penicillin-streptomycin.

Cytotoxicity Assays of Zr-DSCP NCPs Against NCI-H460 Cells. Confluent NCI-H460 cells were trypsinized and counted by hemocytometer. Cells were plated in 6-well plates at a cell density of 5 x 10^4 cells/well in 3 mL RPMI-1640 complete growth medium. The cells were incubated at 37 °C and 5% CO_2 overnight. Cisplatin and a particle dispersion of large Zr-DSCP in RPMI-1640 media and additional media were added to wells, resulting in cisplatin concentrations (μM) of 0, 2.5, 5, 10, 30, and 80. Cells were incubated (37 °C, 5% CO_2) for 72 h. Viability was determined by the trypan blue exclusion assay.

Cytotoxicity Assay of La-DSCP NCPs Against NCI-H460 Cells. Confluent NCI-H460 cells were trypsinized and a cell density was obtained from a hemocytometer. Six-well plates were seeded with 5.0x10^4 cells/well and a total of 3 mL media. Plates were incubated at 37°C and 5% CO_2 overnight. Amounts of cisplatin or NCP suspensions in RPMI-1640 medium were added to wells, along with additional media, resulting in various cisplatin concentrations (μM). Plates were incubated at 37°C and 5% CO_2 for 48 h and viability was determined via the trypan blue exclusion assay.

Cytotoxicity Assay of La-DSCP Against A549 Cells. Confluent A549 cells were trypsinized and a cell density was obtained from a hemocytometer. Six-well plates were seeded with $5.0x10^4$ cells/well and a total of 3 mL media. Plates were incubated at 37°C and 5% CO_2 overnight. Amounts of cisplatin or NCP suspensions in RPMI-1640 medium were added to wells, along with additional media, resulting in various cisplatin concentrations (μM). Plates were incubated at 37°C and 5% CO_2 for 48 h and viability was determined via the trypan blue exclusion assay.

Viability Assay of La-Suc NCPs Against NCI-H460 Cells. Confluent NCI-H460 cells were trypsinized and a cell density was obtained from a hemocytometer. Six-well plates were seeded with $5.0x10^4$ cells/well and a total of 3 mL media. Plates were incubated at 37°C and 5% CO_2 overnight. Amounts of NCP suspensions in RPMI-1640 medium were added to wells, along with additional media, resulting in various amounts equivalent to μM cisplatin concentrations tested in the cytotoxicity assays. Plates were incubated at 37°C and 5% CO_2 for 24 h and viability was determined via the trypan blue exclusion assay.

Viability Assay of La-Suc NCPs Against A549 Cells. Confluent A549 cells were trypsinized and a cell density was obtained from a hemocytometer. Six-well plates were seeded with $5.0x10^4$ cells/well and a total of 3 mL media. Plates were incubated at 37°C and 5% CO_2 overnight. Media was removed from wells, and each well was washed with 2 mL PBS. Amounts of NCP suspensions in RPMI-1640 medium were added to wells, along with additional media, resulting in various amounts equivalent to μM cisplatin concentrations tested in the cytotoxicity assays. Plates were incubated at 37°C and 5% CO_2 for 24 h and viability was determined via the trypan blue exclusion assay.

Viability Assay of $LaCl_3$ Salt Against NCI-H460 and A549 Cells. Either confluent NCI-H460 or A549 cells were trypsinized and counted with a hemocytometer. Six-well plates were seeded with $5.0x10^4$ cells/well and a total of 3 mL media/well. Plates were incubated at 37 °C and 5 % CO_2 overnight. Media was removed from wells, and each well was washed with 2 mL PBS. Amounts of $LaCl_3 \cdot 7H_2O$ dissolved in media were added to the wells, followed by additional media, resulting in amounts equivalent to that given with La contained in NCP in cytotoxicity assays. Plates were incubated at 37 °C with 5 % CO_2 for 48 h, and viability was determined via the trypan blue exclusion assay.

Confocal Microscopy Using NCI-H460 Cells. Confluent NCI-H460 cells were trypsinized and counted with a hemocytometer. Glass coverslips were placed in the wells of six-well plates, followed by $2.0x10^5$ cells/well and a total of 3 mL media/well. Plates were incubated at 37 °C and 5 % CO_2 overnight. Media was removed from wells, and each well was washed with 2 mL PBS. Amounts of $Ru(bpy)_3^{2+}$-doped La-Suc NCPs (0.2 mg/well) were added with a total of 2 mL media/well. Wells were incubated at 37 °C and 5 % CO_2 for 30 min, media removed, wells washed with 1 mL PBS, and coverslips adhered onto glass slides with antifade mounting medium. Images were obtained on an Olympus FlowView500 confocal microscope.

Competitive Binding Assays Using NCI-H460 Cells. Confluent NCI-H460 cells were trypsinized and counted with a hemocytometer. Five T25 culture flasks were seeded with $1x10^6$ cells/flask and 6 mL of complete growth medium. The flasks were incubated at 37 °C and 5 % CO_2 for three days, changing the media once during this time. Media was removed from the flasks, and each flask was washed with 2 mL PBS. The flasks were given 3 mL media containing different amounts of NH_3-PEG_{5K}-AA and incubated for 30 min. The

media was removed, each flask washed with 2 mL PBS, and 0.5 mg La-DSCP NCPs were added to each flask with a total of 6 mL media. The flasks were incubated for 30 min, trypsinized, and cell pellets were digested in concentrated HNO_3 for 2 days. Samples were diluted with H_2O for a total of 4 mL 2% HNO_3 and analyzed by ICP-MS for La and Pt content.

4.5. References

(1) Rosenberg, B.; VanCamp, L.; Krigas, T. *Nature* **1965**, *205*, 698.

(2) Haag, R.; Kratz, F. *Angew. Chem. Int. Ed.* **2006**, *45*, 1198.

(3) Davis, M. E.; Chen, Z.; Shin, D. M. *Nat. Rev. Drug Discov.* **2008**, *7*, 771.

(4) Hall, M. D.; Hambley, T. W. *Coord. Chem. Rev.* **2002**, *232*, 49.

(5) Kelland, L. *Nat. Rev. Cancer* **2007**, *7*, 573.

(6) Jordan, P.; Carmo-Fonesca, M. *Cell. Mol. Life Sci.* **2000**, *57*, 1229.

(7) Feazell, R. P.; Nakayama-Ratchford, N.; Dai, H.; Lippard, S. J. *J. Am. Chem. Soc.* **2007**, *129*, 8438.

(8) Dhar, S.; Liu, Z.; Thomale, J.; Dai, H.; Lippard, S. J. *J. Am. Chem. Soc.* **2008**, *130*, 11467.

(9) Dhar, S.; Gu, F. X.; Langer, R.; Farokhzad, O. C.; Lippard, S. J. *Proc. Natl. Acad. Sci. USA* **2008**, *105*, 17356.

(10) Harper, B. W.; Krause-Heuer, A. M.; Grant, M. P.; Manohar, M.; Garbutcheon-Singh, K. B.; Aldrich-Wright, J. R. *Chem. Eur. J.* **2010**, *16*, 7064.

(11) Rieter, W. J.; Pott, K. M.; Taylor, K. M. L.; Lin, W. *J. Am. Chem. Soc.* **2008**, *130*, 11584.

(12) Cavka, J. H.; Jakobsen, S.; Olsbye, U.; Guillou, N. L.; Bordiga, C. S.; Lillerud, K. P. *J. Am. Chem. Soc.* **2008**, *130*, 13850.

(13) Li, J.; Yang, Y.; Huang, L. *J. Controlled Release* **2012**, *158*, 108.

(14) Huxford, R. C.; deKrafft, K. E.; Boyle, W. S.; Liu, D.; Lin, W. *Chem. Sci.* **2012**, *3*, 198.

(15) Kashiwagi, H.; McDunn, J. E.; Simon, P. O.; Goedegebuure, P. S.; Xu, J.; Jones, L.; Chang, K.; Johnston, F.; Trinkhaus, K.; Hotchkiss, R. S.; Mach, R. H.; Hawkins, W. G. *Mol. Cancer* **2007**, *6*, 48.

(16) Vilner, B. J.; John, C. S.; Bowen, W. D. *Cancer Res.* **1995**, *55*, 408.

(17) Ganapathy, M. E.; Prasad, P. D.; Huang, W.; Seth, P.; Leibach, F. H.; Ganapathy, V. *J. Pharmacol. Exp. Ther.* **1999**, *289*, 251.

(18) Cobos, E. J.; Entrena, J. M.; Nieto, F. R.; Cendan, C. M.; Del Pozo, E. *Curr. Neuropharmacol.* **2008**, *6*, 344.

(19) Maurice, T.; Su, T.-P. *Pharmacol. Ther.* **2009**, *124*, 195.

(20) Walker, J. M.; Bowen, W. D.; Walker, F. O.; Matsumoto, R. R.; de Costa, B.; Rice, K. C. *Pharmacol. Rev.* **1990**, *42*, 355.

CHAPTER 5

Nanoscale Coorination Polymers for Delivery of an Oxaliplatin Analog

5.1. Introduction

5.1.1. Platinum Complexes for Cancer Chemotherapy - Oxaliplatin

Platinum-based drugs have played an important role in cancer treatment. Oxaliplatin (Figure 5.1) is one of the three FDA-approved platin-based cancer chemotherapeutics (approved in 2004) and was approved for the treatment of colorectal cancer alone or in combination with 5-fluorouracil.[1,2] Additionally, oxaliplatin is undergoing clinical trials for the treatment of pancreatic ductal adenocarcinoma, a disease with an extremely low survival rate. Oxaliplatin chemotherapy was originally used to treat cisplatin-resistant cancers and lower the toxicity profile of platin chemotherapeutics.[3-5] Oxaliplatin is adept at treating cisplatin-resistant cancers as this agent forms different DNA adducts that are not routinely recognized by repair proteins and the accumulation of this agent is less-dependent on copper transporters, which contributes to cisplatin resistance.

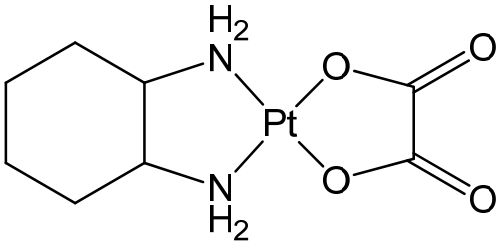

Figure 5.1. Structure of oxaliplatin, one of the three FDA-approved platin-based chemotherapeutics.

Even though oxaliplatin therapy does not lead to nephrotoxicity like cisplatin treatment, oxaliplatin suffers from the myriad of drawbacks characteristic of conventional anticancer agents such as low selectivity, high systemic toxicity, poor pharmacokinetics, and narrow therapeutic windows.[3] Non-specific distribution of oxaliplatin leads to serious side effects such as neurotoxicity and hematologic toxicity. In order to alleviate these drawbacks, we propose incorporation of a Pt(IV) oxaliplatin prodrug within an NCP material. Nanocarriers for the delivery of oxaliplatin have been reported previously,[6,7] but an NCP platform for delivery of this agent has never been reported.

Herein this chapter, synthesis and characterization of NCPs containing an oxaliplatin prodrug are discussed. These NCPs are constructed with different binding metals and the oxaliplatin prodrug *c*,*c*,*t*-[$PtCl_2$(DACH)($O_2CCH_2CH_2CO_2H)_2$] (Figure 5.2, DSOX for disuccinato oxaliplatin). Synthesis and characterization of all oxaliplatin prodrugs and associated complexes is described in the experimental section in their entirety.

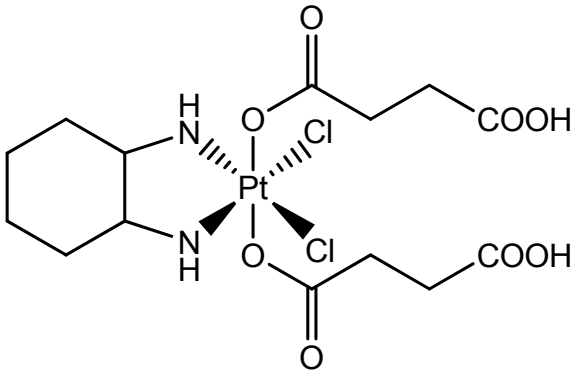

Figure 5.2. Structure of disuccinato oxaliplatin (DSOX), an oxaliplatin prodrug.

5.2. Results and Discussion

5.2.1. Synthesis and Characterization of La-DSOX NCP

NCPs of La-DSOX were prepared by a methanol-induced nanoprecipitation of a solution of the methylammonium salt of DSOX and $LaCl_3 \cdot 7H_2O$ in H_2O adjusted to pH = 7.25 with NaOH. The resulting material is irregularly-shaped and ~50 nm by SEM (Figure 5.3). These particles are 5.3 wt% Pt (16.7 wt% DSOX) and 42.7 wt% La by ICP-MS. This low drug loading suggests that these particles are primarily La_2O_3, indicating the need for a different synthetic strategy. A reverse microemulsion technique yielded NCPs of La-DSOX as well. Aqueous solutions of DSOX and $LaCl_3 \cdot 7H_2O$ were placed in a reverse microemulsion with the organic phase 0.3 M TritonX-100/1.5 M 1-hexanol in cyclohexane and stirred at room temperature for 24 h. The resulting particles are between 150-300 nm by SEM (Figure 5.4).

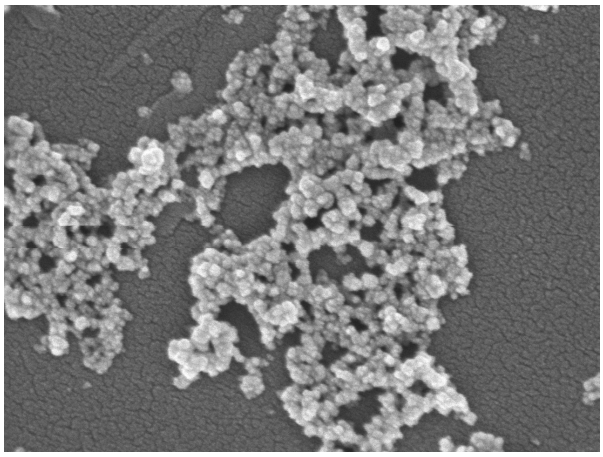

Figure 5.3. SEM micrograph of La-DSOX NCP synthesized by a rapid precipitation technique.

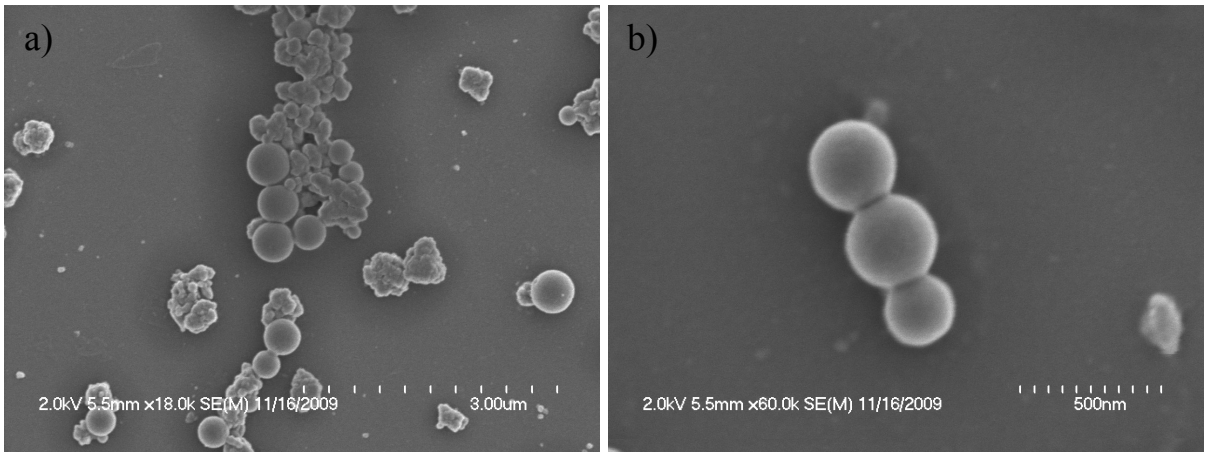

Figure 5.4. SEM micrographs of La-DSOX synthesized by a reverse microemulsion technique.

5.2.2. Synthesis and Characterization of Nd-DSOX NCP

NCPs of Nd-DSOX were prepared by a methanol-induced nanoprecipitation of a solution of the dimethylammonium salt of DSOX and $Nd(NO_3)_3 \cdot 6H_2O$ in H_2O adjusted to pH = 7.0. The resulting particles are irregularly-shaped and ~100 nm in diameter by SEM (Figure 5.6). EDS shows the presence of both Pt and Nd (Figure 5.5). Nd-DSOX is 5.2 wt% Pt (16.3 wt% DSOX) by ICP-MS. Like with La-DSOX, these NCPs possess lower DSOX drug loading than expected, likely due to the formation of La_2O_3 or Nd_2O_3 with this method.

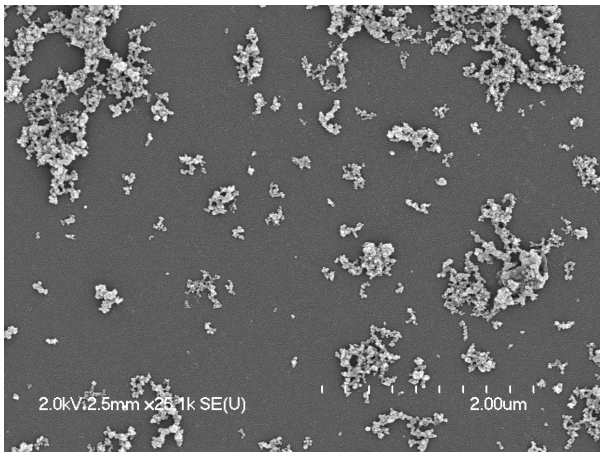

Figure 5.5. SEM micrograph of Nd-DSOX NCPs.

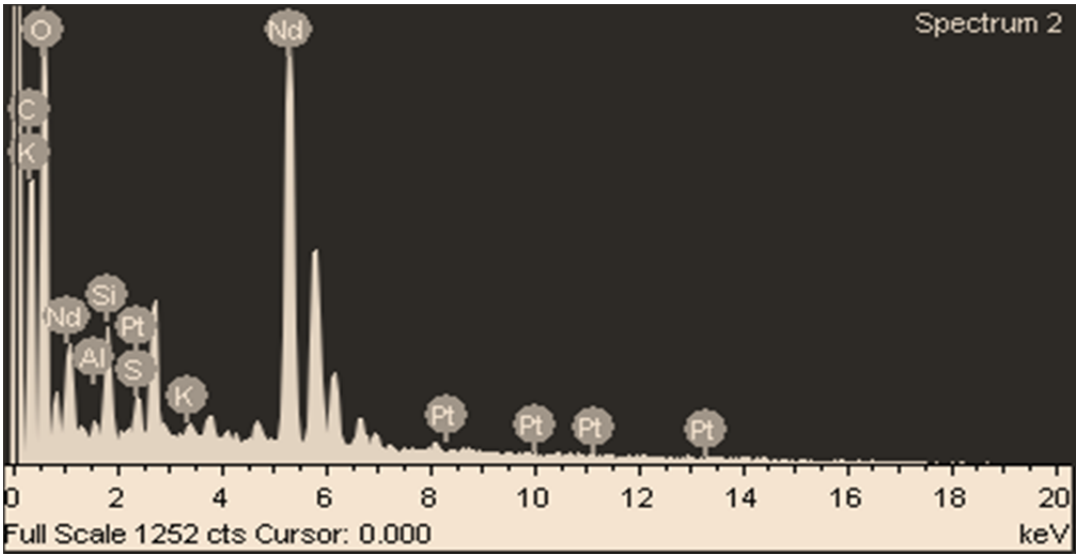

Figure 5.6. EDS plot of Nd-DSOX NCPs showing the presence of Nd and Pt.

5.2.3. Synthesis and Characterization of Zr-DSOX NCP

Particles of Zr-DSOX were prepared by a solvothermal synthesis in which DSOX and $ZrCl_4$ were reacted in DMF and acetic acid at 100 °C for 4 h. The resulting particles were spherical and between 100-150 nm in diameter by SEM and irregular and slightly fused by TEM (Figure 5.7). It is likely that these particles degrade by high energy electrons used in TEM imaging studies. The SEM diameter agrees with size data obtained by DLS in EtOH (Z average = 116 nm, PDI = 0.271) and H_2O (Z average = 121 nm, PDI = 0.260). TGA yields a moderate DSOX drug loading, 44.9 wt% (Figure 5.8).

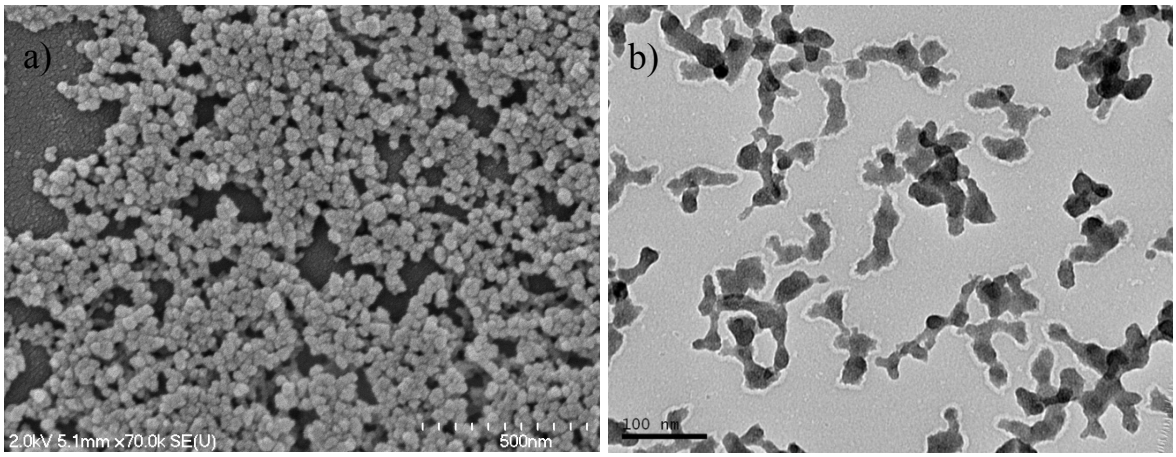

Figure 5.7. SEM (a) and TEM (b) micrographs of Zr-DSOX NCPs.

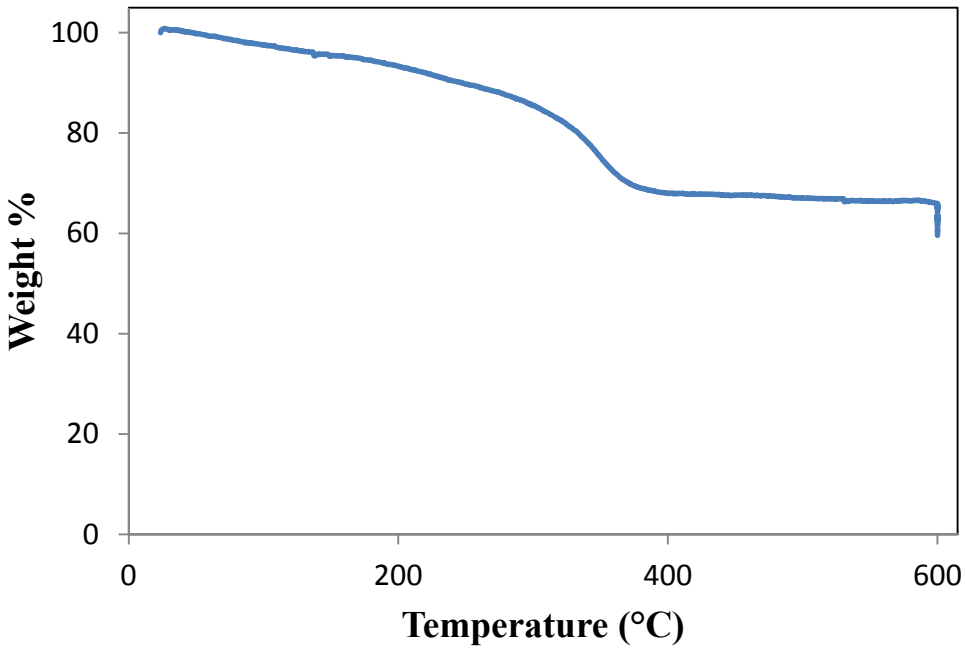

Figure 5.8. TGA plot of Zr-DSOX showing organic weight loss corresponding to 44.9 wt% DSOX drug loading.

5.3. Conclusion

A Pt(IV) oxaliplatin prodrug was synthesized and incorporated in different NCPs using various binding metals. A moderate drug loading was determined for Zr-based NCPs

(44.9 wt%). This drug loading, along with a diameter less than 200 nm, make these particles promising candidates for further stabilization via lipid encapsulation.

5.4. Experimental Details

5.4.1. Materials and Methods

All chemicals, unless otherwise noted, were purchased from Fisher Scientific or Sigma Aldrich and used without further purification. Scanning electron microscopy (SEM) was obtained on a Hitachi 4700 Field Emission Scanning Electron Microscope, and transmission electron microscopy (TEM) was obtained on a JEM 100CX-II Transmission Electron Microscope. A Cressington 108 Auto Sputter Coater equipped with a Au/Pd (80/20) target and MTM-10 thickness monitor was used to coat samples before SEM imaging. SEM micrographs were obtained on glass slides, and TEM micrographs were obtained on carbon-coated copper grids. Thermogravimetric analysis (TGA) was performed on a Shimadzu TGA-50 equipped with a platinum pan, and samples were heated at a rate of 3°C/min under air. Size and zeta potential information was obtained on a Malvern ZetaSizer dynamic light scattering instrument. A Varian 820-MS Inductively Coupled Plasma-Mass Spectrometer was used to determine metal contents. Energy dispersive X-ray spectroscopy (EDS) was conducted using an Oxford 7200 IncaPentaFET-x3 energy dispersive X-ray spectrometer. The EDS data was processed with the Inca Microanalysis Suite. Each EDS sample was prepared by placing a drop of an ethanol suspension of the nanomaterial on a strip of carbon tape affixed to an aluminum sample holder, and the ethanol was allowed to evaporate. ^{1}H NMR spectra were recorded on a Bruker NMR 400 DRX 400 MHz instrument. Infrared spectra were obtained of solid powders using a Shimadzu IR Prestige-21 Fourier Transform Infrared Spectrophotometer.

5.4.2. Synthesis of Pt(IV) Oxaliplatin Prodrugs and Related Complexes

Synthesis of $Pt(DACH)Cl_2$.

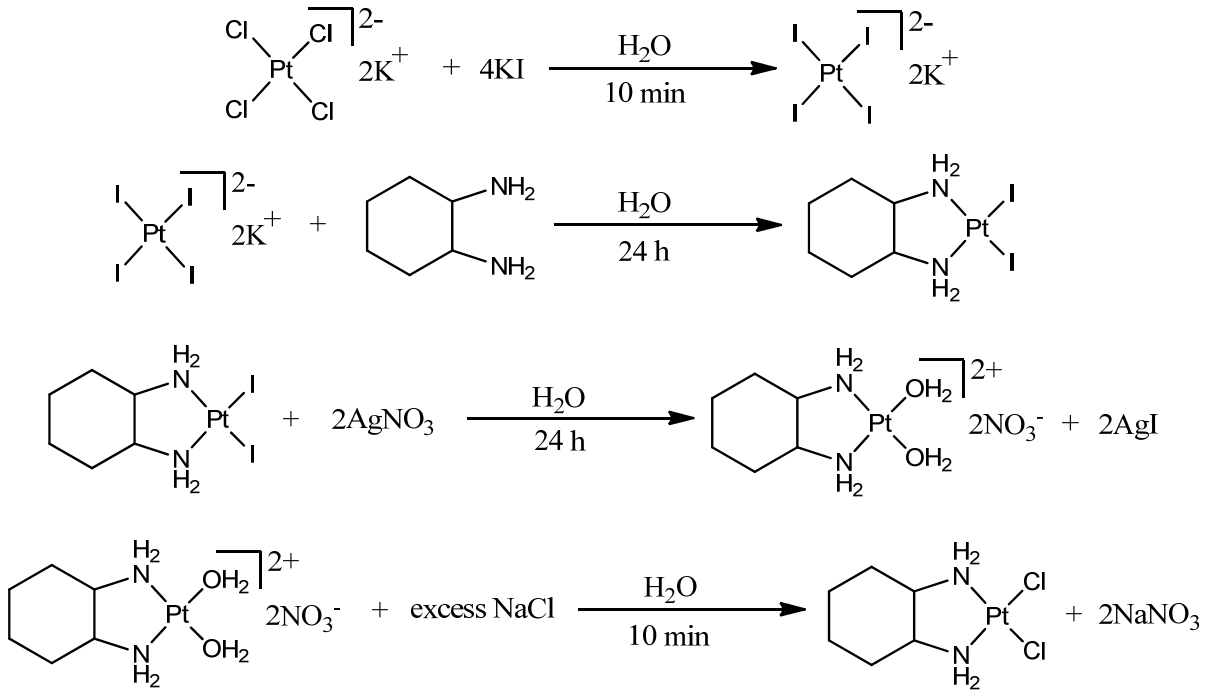

$Pt(DACH)Cl_2$ was synthesized using an established method.[8] Potassium tetrachloroplatinate, K_2PtCl_4, (1 g, 2.4 mmol) was dissolved in 40 mL H_2O, followed by the addition of 1.690 g (10.2 mmol) KI dissolved in 6 mL H_2O which instantly led to the formation of a violet solution. R,R-diamminocyclohexane (DACH, 490 mg, 4.2 mmol) dissolved in 6 mL H_2O was added dropwise, resulting in formation of a yellow precipitate which was stirred at room temperature for 24 h. The precipitate, $Pt(DACH)I_2$, was filtered and washed with H_2O and acetone and dried under vacuum. Yield: 78.2%. ^1H NMR (DMSO-d_6): δ (ppm), 1.030 (m, 2H); 1.241 (m, 2H); 1.467 (m, 2H); 1.934 (m, 2H); 2.354 (m, 2H). IR: $\tilde{\upsilon}$ = 3280, 3200 (υ_{N-H}); 3020, 2960 (υ_{C-H}); 1640 (υ_{C-N}). $Pt(DACH)I_2$ (1 g, 1.9 mmol) was suspended in 30 mL H_2O, followed by the addition of 650 mg (3.9 mmol) $AgNO_3$, which led to the instant formation of $Pt(DACH)(H_2O)_2^{2+}$ and AgI. The dispersion was stirred at room

temperature for 24 h, and AgI removed by filtration. While stirring, excess NaCl was added to the filtrate, resulting in the formation of the bright yellow $Pt(DACH)Cl_2$ product which was filtered, washed with H_2O and acetone, and allowed dried under vacuum. Yield = 91.8%. IR: $\tilde{\upsilon}$ = 3320, 3200 (υ_{N-H}); 2960, 2880 (υ_{C-H}); 1560 (υ_{C-N}). TGA: 46.7 wt% organic loss, theoretical = 48.7 wt%.

Synthesis and Characterization of $Pt(DACH)Cl_2(OH)_2$.

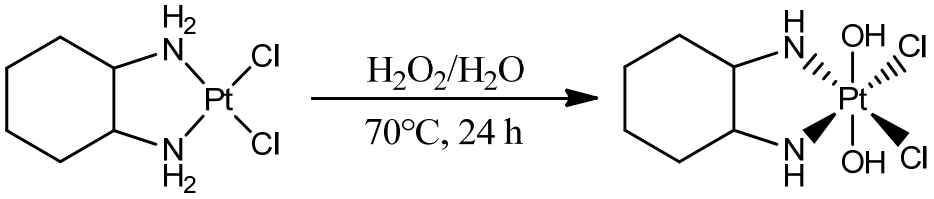

$Pt(DACH)Cl_2$ (730 mg, 1.9 mmol) was suspended in 50 mL H_2O, followed by the addition of 7 mL 30% H_2O_2/H_2O. The slurry was heated to 70 °C and stirred at this temperature for 24 h. The light yellow product, $Pt(DACH)Cl_2(OH)_2$, was filtered and washed with H_2O and acetone. Yield = 64.7%. ^{1}H NMR (DMSO-d_6): δ (ppm), 1.054 (m, 2H); 1.235 (m, 2H); 1.471 (m, 2H); 1.838 (m, 2H); 2.077 (m, 2H). IR: $\tilde{\upsilon}$ = 3495 (υ_{O-H}); 3105 (υ_{N-H}); 2925, 2865 (υ_{C-H}); 1580 (υ_{C-N}).

Synthesis and Characterization of $Pt(DACH)Cl_2(OH)_2(suc)_2$.

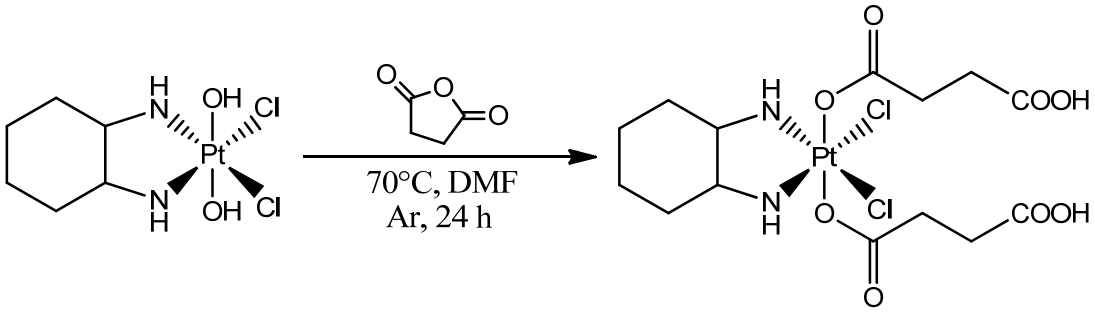

$Pt(DACH)Cl_2(OH)_2$ (100 mg, 0.24 mmol) and succinic anhydride (52 mg, 0.52 mmol) were suspended in 2 mL anhydrous DMSO and heated at 70 °C for 48 h under Ar.

DMSO was removed by lyophilization, and the resulting brown product, $Pt(DACH)Cl_2(OH)_2(suc)_2$, was washed with acetone and Et_2O and dried under vacuum. Yield = 50.3%. ^1H NMR (DMSO-d_6): δ (ppm), 0.896 (m, 2H); 1.233 (m, 2H); 1.421 (m, 2H); 1.838 (m, 2H); 2.073 (m, 2H); 2.382 (m, 2H); 2.495 (m, 2H). IR: $\tilde{\upsilon}$ = 3280 (υ_{N-H}); 2960, 2880 (υ_{C-H}); 1680 ($\upsilon_{C=O}$); 1540 (υ_{C-N}). TGA: step 1 (125-215 °C, $(suc)_2Cl_2$) 50.5 wt%, calculated = 49.6 wt%; step 2 (215-400 °C, DACH) 25.5 wt%, calculated = 18.6 wt%.

Synthesis and Characterization of $Pt(DACH)Cl_2(OH)(OEt)$.

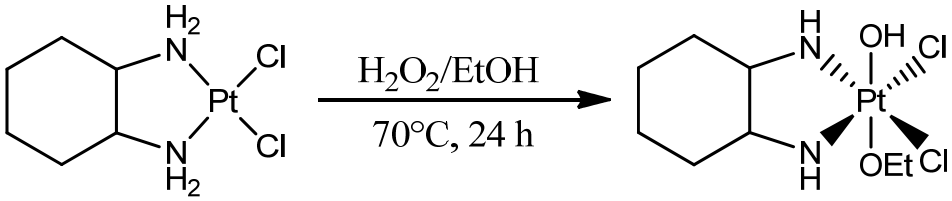

This complex was not used in the synthesis of DSOX-containing NCPs, but may be used for future drug delivery materials. $Pt(DACH)Cl_2$ (200 mg, 0.53 mmol) was suspended in 30 mL EtOH, followed by the addition of 10 mL 30% H_2O_2/H_2O. The slurry was heated at 70 °C for 24 h. The white product, $Pt(DACH)Cl_2(OH)(OEt)$, was filtered and dried under vacuum. Yield = 57.5%. ^1H NMR (DMSO-d_6): δ (ppm), 0.750 (m, 2H); 1.150 (t, 2H); 1.235 (m, 2H); 1.490 (q, 3H); 1.357 (m, 2H); 1.800 (m, 2H); 2.051 (m, 2H). IR: $\tilde{\upsilon}$ = 3480 (υ_{O-H}); 3080 (υ_{N-H}); 2920, 2880 (υ_{C-H}); 1560 (υ_{C-N}); 1040 (υ_{C-O}). TGA: 51.0 wt% organic loss, theoretical = 48.7 wt%

Synthesis and Characterization of $Pt(DACH)Cl_2(OEt)(Suc)$.

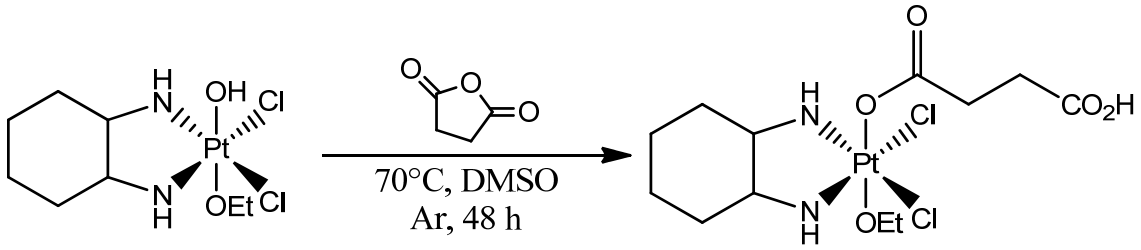

This complex was not used in the synthesis of DSOX-containing NCPs, but may be used for future drug delivery materials. $Pt(DACH)Cl_2(OH)(OEt)$ (125 mg, 0.29 mmol) and succinic anhydride (33 mg, 0.33 mmol) were dissolved in 2.5 mL anhydrous DMSO and reacted at 70 °C for 48 h. DMSO was removed by lyophilization, and the brown product, $Pt(DACH)Cl_2(OEt)(Suc)$, was washed with EtOH and dried under vacuum. Yield = 27.9%. ^1H NMR (DMSO-d_6): δ (ppm), 0.857 (m, 2H); 1.063 (m, 2H); 1.350 (t, 3H); 1.511 (m, 2H); 1.939 (m, 2H); 2.089 (m, 2H); 2.315 (m, 2H); 2.410 (m, 2H).

Synthesis and Characterization of Oxaliplatin.

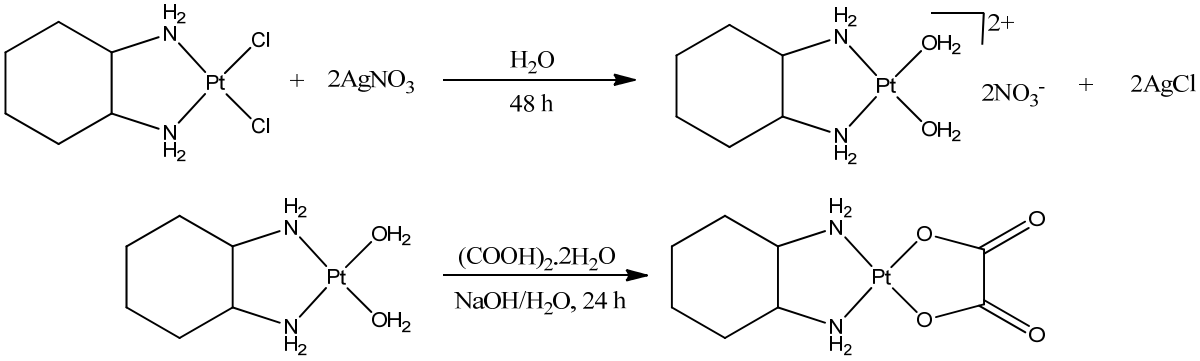

Oxaliplatin was synthesized as the comparison free drug for any *in vitro* cytotoxicity studies. $Pt(DACH)Cl_2$ (60 mg, 0.16 mmol) was suspended in 5 mL H_2O followed by the addition of 52 mg (0.31 mmol) $AgNO_3$, resulting in the formation of $Pt(DACH)(H_2O)_2^{2+}$ and AgCl. The slurry was stirred at room temperature for 24 h. AgCl was removed by filtration, and 13 mg (0.11 mmol) oxalic acid dissolved in 300 µL 1 M NaOH (0.3 mmol) was added to the filtrate and stirred at room temperature for 24 h. The volume was reduced by rotary evaporation and white crystals of oxaliplatin formed upon cooling at 4 °C for several hours. The crystals were washed with H_2O and Et_2O and dried under vacuum. IR: $\tilde{\upsilon}$ = 3120 (υ_{N-H}); 2950, 2915 (υ_{C-H}); 1710, 1670 ($\upsilon_{C=O}$); 1380 (υ_{C-O}).

5.4.3. Synthesis of Oxaliplatin-Based NCPs

Synthesis of La-DSOX NCPs. Particles of La-DSOX were prepared by a methanol-induced nanoprecipitation: 750 μL 10 mM (4.9 mg, 0.0075 mmol) DSOX methylammonium salt and 75 μL 0.2 M (5.6 mg, 0.015 mmol) $LaCl_3 \cdot 7H_2O$ was added to 675 μL H_2O. The pH of the solution was adjusted to 7.25, and, stirring rapidly, 6 mL methanol was added, resulting in the formation of a white dispersion which was stirred for 1 h. The particles were isolated by centrifugation, subsequently washed and centrifuged with MeOH and dispersed in MeOH. Yield = 1.1 mg (15.7%).

A different synthesis of La-DSOX was applied as well using a reverse microemulsion synthesis. Two reverse (water in oil) microemulsions were prepared by two 50 mL round bottom flasks receiving 23.6 mL 0.3 M TritonX-100/1.5 M 1-hexanol in cyclohexane. One flask was given (while stirring) 1.255 H_2O containing 3.2 mg (0.0052 mmol) DSOX pH = 7.5. The other flask was given 12.5 μL 0.2 M (0.9 mg, 0.0025 mmol) aq. $LaCl_3 \cdot 7H_2O$. Both reverse microemulsions became clear instantly, were combined (W = 10) and stirred at room temperature for 24 h. The reaction was quenched with ~15 mL EtOH. The product was isolated by centrifugation, subsequently washed and centrifuged twice with EtOH, and dispersed in EtOH.

Synthesis of Nd-DSOX NCPs. Particles of Nd-DSOX were prepared by a methanol-induced nanoprecipitation: 38 μL 0.2 M (4.9 mg, 0.0075 mmol) DSOX methylammonium salt and 75 μL 0.2 M (6.6 mg, 0.015 mmol) $Nd(NO_3)_3 \cdot 6H_2O$ was added to 1.385 mL H_2O. The pH of the solution was adjusted to 7.0, and, stirring rapidly, 14 mL methanol was added, resulting in the formation of a white dispersion which was stirred for 1 h. The particles were

isolated by centrifugation, subsequently washed and centrifuged with MeOH and dispersed in MeOH. Yield = 6.0 mg (85.0%).

Synthesis of Zr-DSOX NCPs. Particles of Zr-DSOX were synthesized by a solvothermal method. In a 20 mL glass vial, 52.6 mg (0.0856 mmol) DSOX and 22.4 mg (0.0962 mmol) $ZrCl_4$ were dissolved in 10 mL DMF containing 150 μL 3M (0.45 mmol) acetic acid. The vial was capped and placed in a 100 ºC oven for 4 h. The resulting brown dispersion was isolated by centrifugation and were subsequently washed (by sonication) and centrifuged once each with DMF, H_2O, and ethanol. The particles were dispersed in ethanol Yield: 3.1 mg (48.0 %).

5.5. References

(1) Extra, J. M.; Esspie, M.; Calvo, F.; Ferme, C.; Mignot, L.; Marty, M. *Cancer Chemother. Pharmacol* . **1990**, *25*, 299.

(2) Ibrahim, A.; Hirschfeld, S.; Cohen, M. H.; Griebel, D. J.; Williams, G. A.; Pazdur, R. *The Oncologist* **2004**, *9*, 8.

(3) Kelland, L. *Nat. Rev. Cancer* **2007**, *7*, 573.

(4) Mathe, G.; Kidani, Y.; Segiguchi, M.; Eriguchi, M.; Fredj, G.; Peytavin, G.; Misset, J. L.; Brienza, S.; de Vassals, F.; Chenu, E.; Bounit, C. *Biomed. Pharmacother.* **1989**, *43*, 237.

(5) Hall, M. D.; Hambley, T. W. *Coord. Chem. Rev.* **2002**, *232*, 49.

(6) Sood, P.; Thurmond, K. B. I.; Jacob, J. E.; Walker, L. K.; Silva, G. O.; Stewart, D. R.; Nowotnik, D. P. *Bioconj. Chem.* **2006**, *17*, 1270.

(7) Cabral, H.; Nishiyama, N.; Kataoka, K. *J. Controlled Release* **2007**, *121*, 146.

(8) Dhara, C. S. *Indian J. Chem.* **1970**, *8*, 193.